LOEWE center for synthetic microbiology (SYNMIKRO)

Investigating the Function and the Interaction Network of the Flagellar Regulator ATPase FlhG

Untersuchung der Funktion und des Interaktionsnetzwerkes des Flagellaren Regulators FlhG

DOCTORAL THESIS

Submitted in Fulfilment of the Requirements

of a Doctoral Degree in Chemistry

(Dr. rer. nat.)

to the

Department of Chemistry,

Philipps-Universität Marburg

Jan Simon Schuhmacher, M.Sc.

Ulm (Baden-Württemberg)

Marburg an der Lahn, 2015

Vom Fachbereich Chemie

der Philipps-Universität Marburg (Hochschulkennziffer 1180)

als Dissertation am 04.11.2015 angenommen

Erstgutachter: Dr. Gert Bange

(Fachbereich Chemie, Philpps-Universität Marburg)

Zweitgutachter: Prof. Dr. Peter Graumann

(Fachbereich Chemie, Philpps-Universität Marburg)

Tag der Disputation: 06.11.2015

Declaration of authorship

I hereby declare that this submission is entirely of my own and to the best of my knowledge has not been submitted, either in part or whole, for a degree at this or any other educational institution except where due acknowledgement is made in this work. Quotes and paraphrased material are clearly acknowledged and all sources are referenced.

Jan Simon Schuhmacher Marburg, 31st July 2015

…dedicated to my father Martin, who died shortly after receiving his PhD in chemistry.

Acknowledgements

It is a pleasure for me to thank all those who made this work possible.

First and foremost, I would like to express my gratitude to Dr. Gert Bange for offering me the opportunity to carry out my PhD thesis in his research group as his first PhD student, thus sharing with me the experience to build up and organize a research laboratory. It was a pleasure for me to experience the enthusiastic atmosphere of a young group with an excellent supervisor and mentor, who supported and challenged me throughout my entire work and beyond. Exciting scientific discussions and his open-mindedness towards new ideas benefited me immensely. I want to thank Dr. Gert Bange for the freedom to develop my own ideas, to design experiments and to apply new methods and strategies, which allowed me to mature as a scientist. I am also grateful for the opportunity to attend the BACNET 2015 in San Feliu de Guixols (Spain) to present my scientific work.

I am also deeply grateful to Prof. Dr. Peter Graumann for providing me with the opportunity to perform *in vivo* fluorescence microscopy in his research group as well as for his constant support as a member of my thesis advisory committee.

I especially want to thank Prof. Dr. Kai M. Thormann for a productive collaboration as well as an exciting scientific exchange during the preparation of a manuscript and the committee meetings.

My sincere thank goes to Dr. Uwe Linne for an exceptional collaboration to implement hydrogen deuterium exchange mass spectrometry in Marburg as well as for his continuous support and advice during my PhD thesis, not only when I faced challenges during mass spectrometry experiments.

I would like to thank Dr. Felix Dempwolff for patiently introducing me to fluorescence microscopy and to the basics of image processing. I also want to acknowledge his general support whenever I needed it.

I am grateful to Prof. Dr. Uwe G. Maier, Dr. Andreas Klingl und Dr. Kathrin Bolte for providing me with electron micrographs.

I would also like to thank Prof. Daniel B. Kearns for providing plasmids that helped to generate *B. subtilis* strains during my work.

My sincere thanks go to Florian Roßmann and Susanne Brenzinger of the Thormann group for the fruitful collaborative work on several very exciting projects.

I am grateful to Carina Knauer, Florian Altegoer and Wieland Steinchen for their contribution to the FlhG project and for a collaborative atmosphere and work during my time in the lab.

I appreciate the very productive practical course as well as the master thesis that Sabrina Henche completed under my supervision and that she contributed to this PhD thesis at various stages. I also want to acknowledge Sabrina Gies for contributing to my work during a practical course.

I would like to acknowledge Matthew McIntosh and Chris Fage for their corrections and feedback.

I also thank to the whole Bange group including all former members for a nice working atmosphere, many exciting discussions and events in, around and outside the lab. I also want to acknowledge the whole Graumann group for their warm welcome to Marburg when we started the research group as well as for sharing the coffee machine.

Although the fascinating work, done in collaboration with the group of Prof. Dr. Regine Kahmann could not be included in this thesis, I would like to express my gratitude to Prof. Dr. Regine Kahmann for her continuous support. I would also like to thank Dr. Stefanie Reißmann and Xiaowei Han for the close and valueable collaboration.

For the financial support, I thank the Fonds der Chemischen Industrie (FCI).

Most of all, I am deeply indebted to my family and friends and especially to Milena Stephan who always accompanied and supported me.

Abstract

Motility plays a key role for the superior survival strategy of many bacteria. Sophisticated, macromolecular machines, called flagella, serve as bacterial locomotion organelles. These flagella appear in distinct spatial arrangements along the bacterial cell, constituting the flagellation patterns, whose disruption is detrimental to motility. However, the number of flagellation patterns that have arisen in a plethora of bacterial species can be counted by the fingers of one hand. How these patterns are established in the first place, and how they are maintained during cell division, remains a yet unassessed task in the field.

Two nucleotide-binding proteins, FlhF and FlhG, were identified to be crucial for the spatial regulation of flagella in most flagellated bacteria, which exhibit various flagellation patterns. This work presents a structural and biochemical characterization of the flagella regulating ATPase FlhG, which revealed its function as a molecular switch, having a dimeric, membrane-associated state and a mobile, monomeric state in the cytoplasm. This hallmark feature of MinD/ParA ATPases is conserved in FlhG of peritrichous *B. subtilis* as well as monotrichous *S. putrefaciens*. In both organisms FlhG interacts with the flagellar C-ring components FliM and FliN(Y) providing insight into its role as a flagellar C-ring assembly factor, coordinating the assembly of a FliM/FliN(Y) complex to FliG. Differences in the regulatory networks underlying different flagellation patterns were identified in species-specific interaction partners of FlhG, such as the flagellar master regulator FlrA in *S. putrefaciens* or the late divisome component GpsB in *B. subtilis*. These findings led to the hypothesis that the spatial arrangement of flagella is encoded in the structure of the interaction network of FlhF and FlhG. This hypothesis is supported by the occurrence of varying C-ring components in differently flagellated bacteria.

This work also includes the implementation and successful application of $^{1}H/^{2}H$ exchange mass spectrometry in Marburg. Not only does this powerful tool allow the convenient investigation of protein dynamics, but also the rapid mapping of protein-protein and protein-ligand interfaces. Interface mapping, in particular, revealed the power of this method and was applied in various research projects.

Zusammenfassung

Motilität ist ein zentraler Aspekt der Überlebensstrategie von Bakterien. Viele Bakterien bewegen sich mit Hilfe komplexer makromolekularer Motoren, Geißeln oder Flagellen genannt. Diese sind in speziellen Mustern auf der Zelloberfläche verteilt und werden im Folgenden Flagellierungsmuster genannt. Trotz der unglaublichen Vielzahl unterschiedlicher Bakterien finden sich in der Natur nur eine Hand voll dieser flagellaren Muster. Darüber, wie diese Muster nach jeder Zellteilung reproduzierbar und präzise ausgebildet werden, liegen nur spärlich Informationen vor.

Zwei Proteine, FlhF und FlhG, spielen in diesem Zusammenhang eine wichtige Rolle und führen zu unterschiedlichen Mustern in den jeweiligen Bakterien. Diese Arbeit beinhaltet eine biochemische und strukturelle Charakterisierung der ATPase FlhG, die die Funktion von FlhG als molekularen Schalter hervorhebt. FlhG kann einerseits als Dimer in Membran-assoziiertem Zustand vorliegen, andererseits als Monomer frei im Zytoplasma diffundieren. Homologe Proteine in den unterschiedlich flagellierten Bakterien *B. subtilis* und *S. putrefaciens* weisen dieselben charakteristischen Merkmale auf und deuten auf ein einheitliches Funktionsprinzip der ATPase hin. FlhG interagiert in beiden Organismen mit den Proteinen FliM und FliN(Y) des flagellaren C-rings und offenbart dabei seinen Beitrag zum Aufbau des flagellaren C-rings indem es die Interaktion des FliM/FliN(Y)-Komplexes mit FliG ermöglicht. Weitere Untersuchungen des Interaktionsnetzwerkes von FlhG in beiden Organismen zeigten sowohl speziesübergreifende (FliM/FliN(Y)) als auch speziesspezifische Interaktionspartner, darunter das Zellteilungsprotein GpsB in *B. subtilis* und der Hauptregulator der Flagellenbiosynthese FlrA in *S. putrefaciens*. Daraus lässt sich ableiten, dass die unterschiedlichen Flagellierungsmuster nicht direkt durch FlhG bestimmt werden, jedoch in der Struktur des Interaktionsnetzwerkes von FlhG und FlhF kodiert sind. Darüber hinaus deutet die Variabilität des C-ring Proteins FliN(Y) in unterschiedlichen Bakterien, das mit der Ausbildung unterschiedlicher Muster korreliert, in dieselbe Richtung.

Außerdem wurde im Rahmen dieser Arbeit in enger Zusammenarbeit mit der Massenspektrometrie Abteilung der Chemischen Fakultät der Universität Marburg

eine Technik zur Untersuchung von Proteinen mit Hilfe von Wasserstoff/Deuterium Austausch etabliert. Die erfolgreiche Anwendung wird in dieser Arbeit am Beispiel von drei unterschiedlichen Projekten beschrieben und zeigt die Vorteile dieser Methode zur Bestimmung von Portein-Ligand und Protein-Protein Interaktionsoberflächen.

Publications

The majority of the work presented herein has been published in the following articles:

Steinchen W, **Schuhmacher JS**, Altegoer F, Fage CD, Shrinivasan V, Linne U, Marahiel MA, Bange G (2015) Catalytic mechanism and allosteric regulation of an oligomeric (p)ppGpp synthetase by an alarmone, *Proc Natl Acad Sci USA* 112(43):13348-13353. (Equally contributing)

Schuhmacher JS, Thormann KM, Bange G (2015) How bacteria maintain location and number of flagella, *FEMS Microbiol Rev* 39(6):812-822.

Schuhmacher JS, Rossmann F, Dempwolff F, Knauer C, Altegoer F, Steinchen W, Dörrich A, Klingl A, Stephan M, Linne U, Thormann KM, Bange G (2015) The MinD-like ATPase FlhG effects location and number of bacterial flagella during C-ring assembly, *Proc Natl Acad Sci USA* 112(10):3092-3097.

Altegoer F, **Schuhmacher J**, Pausch P, Bange G (2014) From molecular evolution to biobricks and synthetic modules: A lesson by the bacterial flagellum, *Biotechnol Genet Eng* 30(1-2):49-64.

Table of contents

Table of figures

Abbreviations

Standardized abbreviations, such as chemical symbols, SI units as well as the one- and three-letter code for amino acids and x for any amino acid as well as h for hydrophobic amino acid residues are used without further reference. All other abbreviations employed in this work are listed in the following. Bacterial species mentioned in the thesis are listed separately.

Å	Ångström (10^{-10} m)
ADP	adenosine diphosphate
AMPCPP	adenosine-5'-[(α,β)-methyleno]triphosphate
AMPPNP	adenylyl-imidodiphosphate
ARM	Armadillo repeat
ATP	adenosine triphosphate
Au	Absorption unit
au	atomic unit
c-di-GMP	cyclic diguanosine monophosphate
CCW	counter clockwise
CFP	cyan fluorescent protein
CV	column volume
CW	clockwise
Da	Dalton (1.660538 x 10^{-27} kg)
DNA	desoxyribonucleic acid
ESI	electrospray ionisation
ESRF	European Synchrotron Radiation Facility
FP	fluorescent protein
GAP	GTPase-activating protein
GEF	Guanine nucleotide exchange factor
GFP	green fluorescent protein
GST	glutathione S-transferase
GTP	guanosine triphosphate

h	hours
HDX	$^{1}H/^{2}H$ exchange mass spectrometry
HEPES	4-(2-hydroxyethyl)-1-piperazineethanesulfonic acid
HPLC	high performance liquid chromatography
ID	insertion device
IM	inner membrane
IPTG	isopropyl β-D-1-thiogalactopyranoside
JCSG	Joint Center for Structural Genomics
LB broth	lysogeny broth
Lip.	lipid
LUV	large unilamellar vesicle
M	mol/litre
min	minute
MR	molecular replacement
MS	mass spectrometry
MTS	membrane targeting sequence
NA	numerical aperture
NMR	nuclear magnetic resonance
NTA	nitrilotiracetic acid
NTP	nucleotide triphosphate
OD	optical density
OM	outer membrane
PBS	phosphate buffered saline
PCR	polymerase chain reaction
PDB	protein data bank
PE	2-oleoyl-1-palmitoyl-*sn*-glycero-3-phosphoethanolamine
PEG	polyethylene glycol
PG	(1-palmitoyl-2-oleoyl-*sn*-glycero-3-phospho-(1'-rac-glycerol)(sodium salt)
PM	plasma membrane

PMF	proton motive force
ppGpp	guanosine tetraphosphate
pppGpp	guanosine pentaphosphate
RNA	ribonucleic acid
rpm	revelations per minute
rt	room temperature
SD	Shine-Dalgarno sequence
SDS-PAGE	sodium dodecylsulfate polyacrylamide gel electrophoresis
SEC	size exclusion chromatography
SIMIBI	signal recognition particle, MinD, BioD
SRP	signal recognition particle
STED	stimulated emission depletion
T3SS	type III secretion system
TCA	trichloroacetic acid
TRIS	Tris(hydroxymethyl)aminomethane
UV	ultraviolet
YFP	yellow fluorescent protein

Bacterial species:

B. subtilis (*Bs*)	*Bacillus subtilis*
C. jejuni (*Cj*)	*Campylobacter jejuni*
E. coli (*Ec*)	*Escherichia coli*
G. thermodenitrificans (*Gt*)	*Geobacillus thermodenitrificans*
H. pylori (*Hp*)	*Helicobacter pylori*
P. aeruginosa (*Pa*)	*Pseudomonas aeruginosa*
R. shpaeroides (Rs)	*Rhodobacter shpaeroides*
S. putrefaciens (*Sp*)	*Shewanella putrefaciens*
V. alginolytics (*Va*)	*Vibrio alginolyticus*
V. cholerae (*Vc*)	*Vibrio cholerae*

Introduction

Can you imagine any organism that is more successful than bacteria? Bacteria are the most abundant organisms in the world. Rapid adaptation to environmental cues and changes due to fast generation times and horizontal gene transfer is a hallmark of bacterial survival. Bacterial motility not only allows them to directly move towards nutrition sources, but also to avoid toxins and find putative host infection sites, which is an essential feature of the bacterial life style. To fulfil all these tasks, motility is tightly regulated and intimately linked to fundamental cellular processes such as the chemosensory system, gene transcription, translation and the determination of the future cell division site.

The Introduction will give an overview of bacterial locomotion systems, especially the flagellum, and will highlight the occurrence of spatial arrangements of flagella in different bacterial species, the so-called flagellation patterns. Furthermore, cell division and chemotaxis will be discussed as contiguous cellular processes emphasising possible links, similarities and analogous mechanistic features of the regulation that underlies the formation of the flagellation patterns.

1.1 Bacterial motility

Nature invented a plethora of bacterial motility strategies. The majority of motile bacteria move by rotating a long helical filament, the flagellum, which constitutes one of the most powerful and tiniest motors in the biosphere (1). Its power is comparable to the motor of a Ferrari in macromolecular dimensions. Flagellated bacteria propel themselves through liquid media (swimming) or move in rafts or communities on (semi-)solid surfaces (swarming) (**Figure 1AB**) (2, 3). Swarming behaviour plays a key role within microbial communities and biofilms (4, 5). A unique flagella-related movement was observed in spirochetes exhibiting

periplasmic flagella attached to each end of the protoplasmic cylinder. Rotating these periplasmic flagella results in backward-moving waves of the cell body, generating the force for motility (reviewed in: (6)). Besides flagella, some bacteria (*e.g. Myxococcus, Pseudomonas, Neisseria)* also rely on type IV pili to move through their environment by twitching motility (**Figure 1C**; reviewed in: (7, 8)).

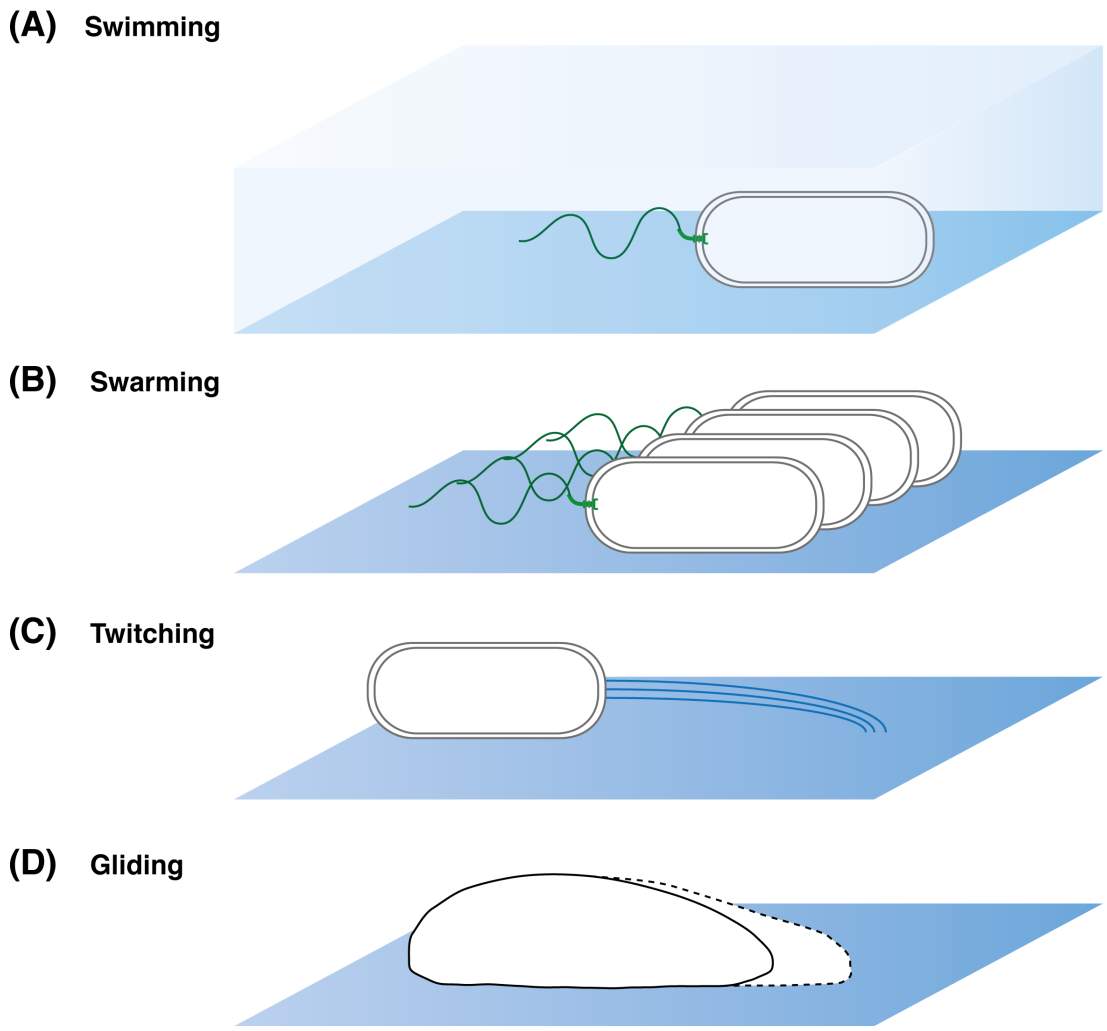

Figure 1. Bacterial motility. Flagella-based motility includes **(A)** swimming of a single cell through liquid medium and **(B)** swarming of microbial communities on surfaces or semisolid surfaces. **(C)** Twitching motility relies on type IV pili that are extended and retracted into the cell upon attachment to the environment, generating a pulling movement. **(D)** A fourth method of motility is called gliding and involves a change in cell shape in order to move in a specific direction. The image was adapted from ref. (4).

Type IV pili have a simpler architecture and can be extended from and retracted into the cell and therefore result in a step-wise pulling movement (review on

type IV pili: (9, 10)). A third way to move is called gliding motility and is independent of flagella or pili (**Figure 1D**). A membrane protrusion is formed at a cell pole and attaches to a solid surface, allowing the bacterium to glide towards it. Large intracellular protein complexes, acting together with cytoskeletal filaments, are responsible to generate the force required for gliding (reviewed in: (11, 12)). Notably, flagella-based motility is approximately one thousand times faster than gliding or twitching motility (13). In accordance with the bacterial flagellum the archaeal locomotion organelle is called the archaellum, although it resembles a rotating type IV pilus rather than a bacterial flagellum (reviewed in: (14, 15)).

1.2 The bacterial flagellum

The flagellum in Gram-positive and Gram-negative bacteria is almost identical.

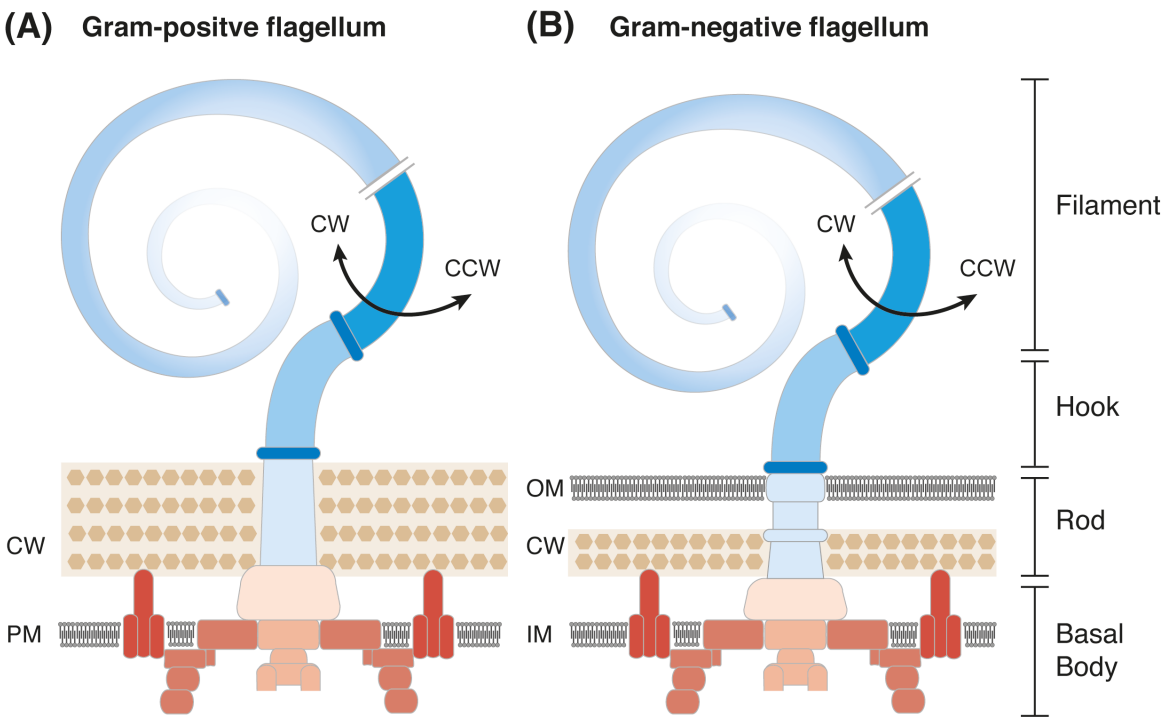

Figure 2. The bacterial flagellum. Scheme of the bacterial flagellum of Gram-positive **(A)** and Gram-negative bacteria **(B)** depicts the main flagellar building blocks: the basal body, the rod, the hook and the filament structures. The major difference between flagella of Gram-positive and Gram-negative organisms is found in the structure of the rod. Most flagella can rotate either CW or CCW. Important cellular components are abbreviated (PM: plasma membrane, CW: cell wall, OM: outer membrane, IM: inner membrane). The figure was slightly adapted from ref. (16).

The bacterial flagellum is an ancient structure with a defined architecture conserved throughout all bacterial clades and families with four major building blocks: the membrane-spanning basal body, an adjacent rod that differs between Gram-positive and Gram-negative bacteria, the extracellular hook as a universal joint and the filament (**Figure 2**; reviewed in: (17-21)). The filament itself is a long, helical tube around 10-15 µm in length and approximately 20 nm in diameter (see chapter on flagella in: (22)). The flagellum therefore resembles a ship's propulsion system with an engine room, the transmission and the Archimedes screw that generates the propulsion. Fuelled by a gradient of protons (proton motive force (PMF)) or sodium ions, it can rotate in a clockwise (CW) or counter clockwise (CCW) direction for straight swimming ('run') or reorientation ('tumble') (23).

1.2.1 Architecture of the flagellum

The core of the basal body is formed by the flagellar type III secretion system (fT3SS), a central pore which is composed of 6 trans-membrane proteins (FlhAB, FliOPQR), mediating the export of flagellar building blocks and thus playing a crucial role for flagellar assembly (**Figure 3**) ((24) reviewed in: (18, 25)). Surrounding this central channel, the membrane spanning protein FliF forms the MS-ring and serves as a scaffold for a cup-like structure in the cytoplasm called the C-ring (26, 27). It is composed of FliG, FliM and FliN (homologue: FliY) and enables bacteria to switch the rotation direction of the flagellum from CW to CCW or *vice versa* upon stimulation of the chemosensory system (reviewed in: (28, 29)). Accordingly, FliM is able to sense the presence of the response regulator CheY in its phosphorylated state (CheY-P) and propagates the signal to FliG, which controls the rotation direction through adopting different conformational states (30, 31). The motor proteins (MotABXY, PomAB: (32, 33)) are assembled around the C-ring in a late stage of the flagellar assembly process and provide the energy for rotation by exploiting a flux of ions (H^+ or Na^+) through the membrane (**Figure 3**; reviewed in: (34)). The actual rotation is generated through the interaction of the motor proteins MotA and FliG of the flagellar rotor (35). The architecture of the rod differs in Gram-positive and Gram-negative bacteria due to

the morphology of the cell wall and the respective arrangement of the bi-layered lipid membranes (**Figure 2**). The extracellular hook is a joint, which connects the filament with the membrane and cell wall embedded parts of the flagellum. The filament is composed of around 20 000 copies of flagellin, assembled into an 11-fold helix and closed by the pentameric cap protein FliD at its distal end (36-38).

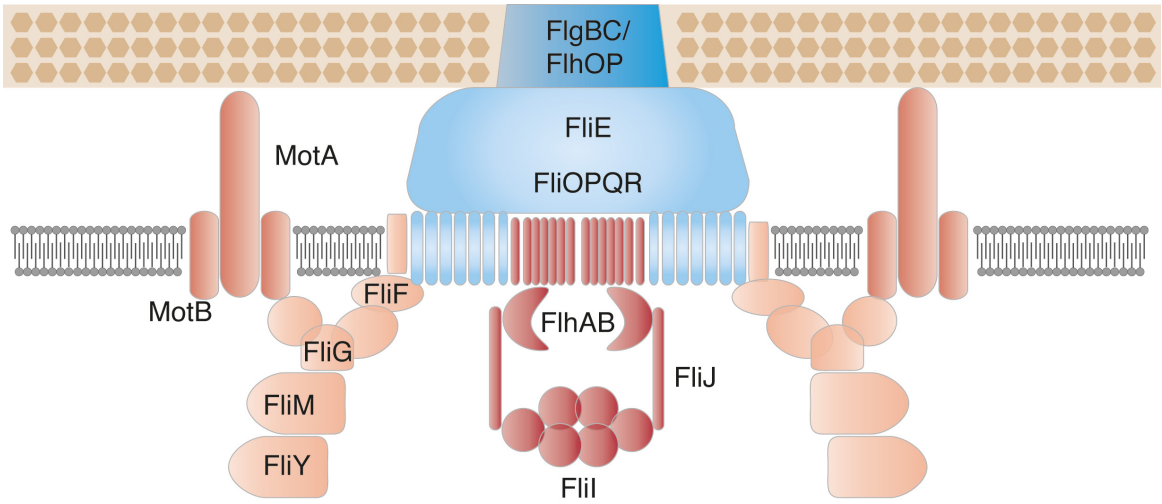

Figure 3. The flagellar basal body. A scheme of the flagellar basal body of *Bacillus subtilis* displays sub-structures of the basal body, including motor components in red (MotAB), the MS-ring (FliF) as well as the C-ring in light red (FliG, FliM and FliY), the export apparatus in dark red (FlhAB, FliJ and FliI) and further integral membrane components of the basal body in light blue (FliE and FliOPQ). The adjacent rod structures are coloured in blue (FlgBC, FlhOP).

1.2.2 The flagellar C-ring

Together with FliF, the flagellar C-ring constitutes the rotor of the flagellum and receives the chemotactic stimuli through its interaction with the final chemotactic response regulator CheY. Upon binding of CheY the C-ring switches the direction of flagellar rotation from CW to CCW or *vice versa* (39). The three C-ring components FliG, FliM and FliN(Y) are arranged in a specific cup-like architecture at the cytoplasmic face of the basal body. The N-terminal domain of FliG ($FliG_N$) interacts with the cytoplasmic C-terminus of the MS-ring constituent FliF connecting the cytoplasmic and the membrane-embedded parts of the rotor (**Figure 4AB**) (27, 40-44). A helix links the N-terminal domain of FliG with its middle domain, which interacts with FliM the second C-ring component (30). The

conserved 'EHPQR' motif of the middle domain of FliG ($FliG_M$) plays a major role for the interaction with FliM (**Figure 4A**) (31, 45, 46). Another helix with an adjacent loop region connects $FliG_M$ with the C-terminal part of FliG ($FliG_C$), which comprises an Armadillo repeat domain (ARM_C) and a helical domain composed of six α-helices (30, 47). While ARM_C interacts with FliM through a hydrophobic patch, three conserved charged residues in helix 5 of the helical domain are responsible for the interaction with the stator protein MotA in *Escherichia coli* and *Salmonella* (**Figure 4A**) (35, 48).

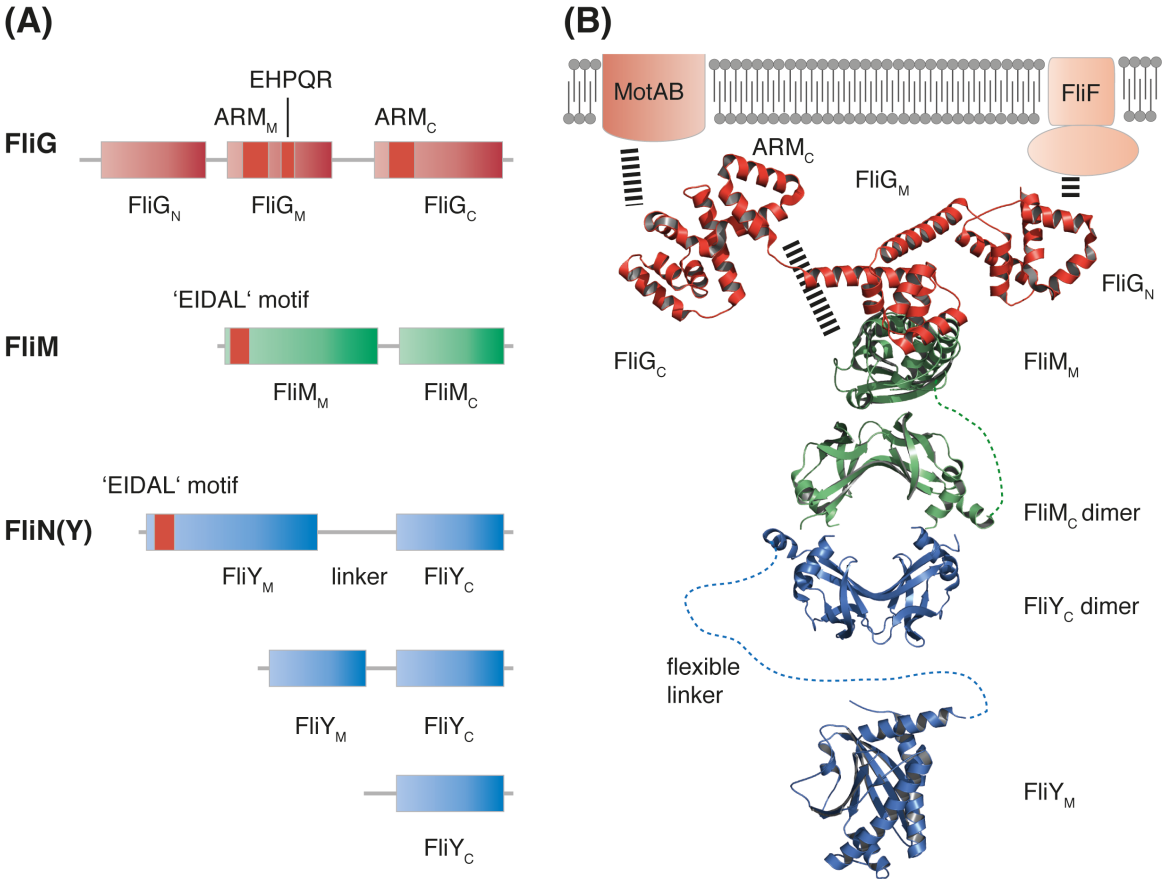

Figure 4. The flagellar C-ring. (A) shows the domain architecture of the C-ring proteins FliG (red), FiM (green) and FliN(Y) (blue). Domains and important motifs are indicated. **(B)** displays a structural model of the flagellar C-ring, with placement of single structures inspired by electron microscopy studies of the basal body (42, 49). The single components are coloured according to (A) and illustrated by FliG (pdb: 3HJL), $FliM_M$ (pdb: 4FQ0), $FliM_C$ (pdb: 1O6A), $FliY_M$ (pdb: 4HYN) and $FliY_C$ (pdb: 1O6A). Dashed lines indicate interactions.

Recent studies propose a mechanistic model for the switching of rotational direction involving conformational rearrangements in $FliG_M$ and $FliG_C$, resulting in

contacts between neighbouring FliG protomers in the C-ring (30, 50). FliM is the second component of the C-ring and interacts through its middle domain ($FliM_M$) with $FliG_M$ and $FliG_C$ (46, 51). The N-terminal part of FliM containing the conserved 'EIDAL' motif binds phosphorylated CheY, whereas the C-terminal domain ($FliM_C$) represents a FliN-homology domain, which forms dimers or larger oligomers (52-54). The third C-ring component FliN(Y) is variable and exclusively comprises a FliN dimerization domain in some bacteria, while in other bacteria it possesses another N-terminal domain or even an additional 'EIDAL' motif (**Figure 4A**). A recent report indicates a role of FliN in the interaction of the C-ring with CheY in *E. coli* (55). Although extensive research has focussed on the reconstruction of the flagellar basal body, the exact location of the C-ring proteins remains elusive (56).

Besides its fundamental role for the implementation of chemotactic signals and the switching of the rotation mode of the flagellum, the C-ring seems to be crucial for flagellar assembly. The C-ring component FliN interacts with the very N-terminus of FliH, a member of the cytoplasmic ATPase complex FliH/FliI, which is involved in cargo export through the type III secretion system (53, 57-62). The FliN-FliH interaction mediates the correct localization of the FliH/FliI complex (57). Therefore, the flagellar C-ring and the cytoplasmic ATPase complex FliH/FliI may provide a sorting platform for type III export cargo (63).

1.2.3 Transcriptional regulation of flagellar genes

Flagellar assembly requires the allocation of more than 50 different proteins in precise order and in definite numbers, giving rise to the idea that the process is highly regulated at the level of transcription as well as translation (64). Flagellar genes are organised in operons on the genome, controlled by sigma factors and transcribed in a hierarchical order. The transcriptional hierarchy has been extensively investigated in the polar flagellated bacteria *Vibrio cholerae*, *Pseudomonas aeruginosa* and *Aeromonas hydrophila* where the σ^{70}-dependent master regulator FleQ/FlrA (class I) activates the transcription of early flagellar genes (class II). These encode proteins involved in basal body and rod formation. Class III genes are under control of FlrC and comprise rod and hook proteins. Both class II and III

genes are additionally regulated by σ^{54}. Late flagellar building blocks including flagellin, the anti-sigma factor FlgM and motor proteins are expressed under the control of σ^{28} factor (**Figure 5**) (65-67).

Flagellar gene regulation in *V. cholerae*

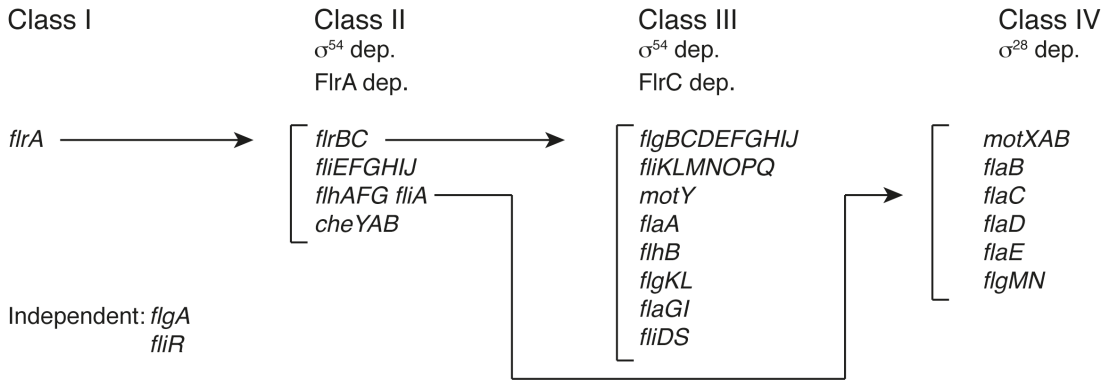

Figure 5. Hierarchy of flagellar gene expression in *V. cholerae.* The hierarchical flagellar gene expression comprises four classes of genes, ordered from early to late flagellar building blocks in flagella biogenesis. Arrows mark regulating proteins of adjacent classes of genes. Figure 5 was adapted from ref. (67).

Notably, a FleQ homologue is missing in the lophotrichously flagellated *H. pylori* and the amphitrichous *C. jejuni* as well as the peritrichously flagellated *B. subtilis*.

During exponential growth *B. subtilis* displays a bistable behaviour growing either as long sessile chains or individual motile cells (68). This heterogeneity in population is under the control of the alternate sigma factor σ^D, which fosters growth as motile individuals (69, 70). SwrA is another flagellar regulator, which enhances bistable behaviour of σ^D and activates the transcription of the *fla*/*che* operon (68, 71, 72). This large operon (27 kb) comprises most of the flagellar genes involved in basal body and rod assembly as well as chemotaxis genes and measures twice the length of a *B. subtilis* cell when fully extended (**Figure 6**). SigD, encoded at the downstream end of the *fla*/*che* operon, feeds back to σ^D and regulates production of late flagellar building blocks (73-75).

Additional factors are involved in the regulation of flagellar gene expression, such as SinR, the master repressor of biofilm formation, as well as SlrA, a small peptide that inhibits transcription of the *fla*/*che* operon (76-78). An anti-sigma

factor, FlgM, is produced in a late stage of flagellar assembly, antagonizing σ^D (79-81)(reviewed in: (82)).

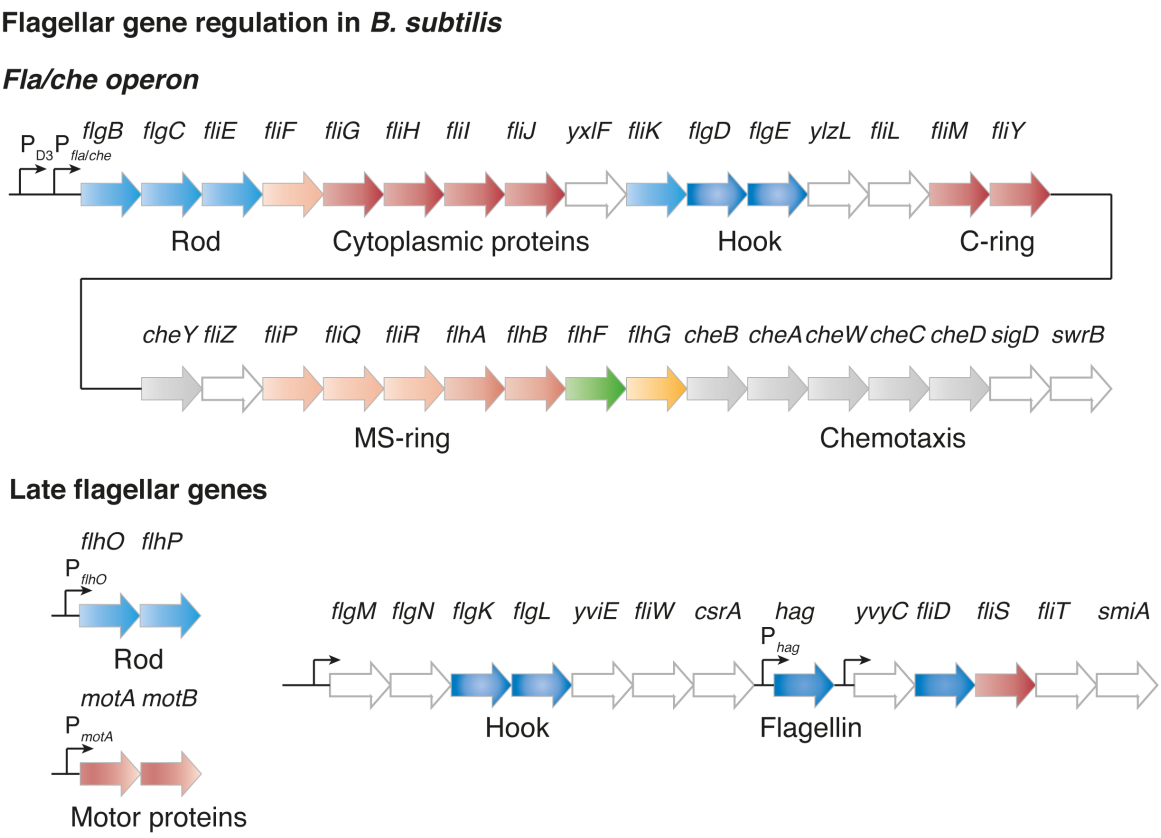

Figure 6. Arrangement of flagellar genes in *B. subtilis*. Relative to the temporal order of flagella biogenesis, early and middle genes are organized in a large transcriptional unit, the *fla/che* operon, which also comprises vital chemotaxis genes (grey). The *fla/che* operon includes many genes essential for basal body formation (red) as well as hook and rod genes (blue) and regulatory genes such as the sigma factor *sigD* as well as *flhF* (green) and *flhG* (orange). Late rod genes (*flhOP*) and the motor components (*motAB*) are encoded separately. Late flagellar building blocks, especially type III export cargo, are encoded on a second gene cluster, including the *hag* gene, which encodes for flagellin, the major component of the flagellar filament. This figure was adapted and modified according to ref. (82).

The regulatory network of flagellar genes in *B. subtilis* seems more sophisticated compared to those of the polar flagella of *Vibrio* and *Pseudomonas species*. Moreover, flagellar regulation is directly coupled to biofilm formation through SinR.

1.3 Flagellation patterns

Flagella appear in species-specific arrangements along the cell body, which differ in number and location and thus constitute flagellation patterns (19).

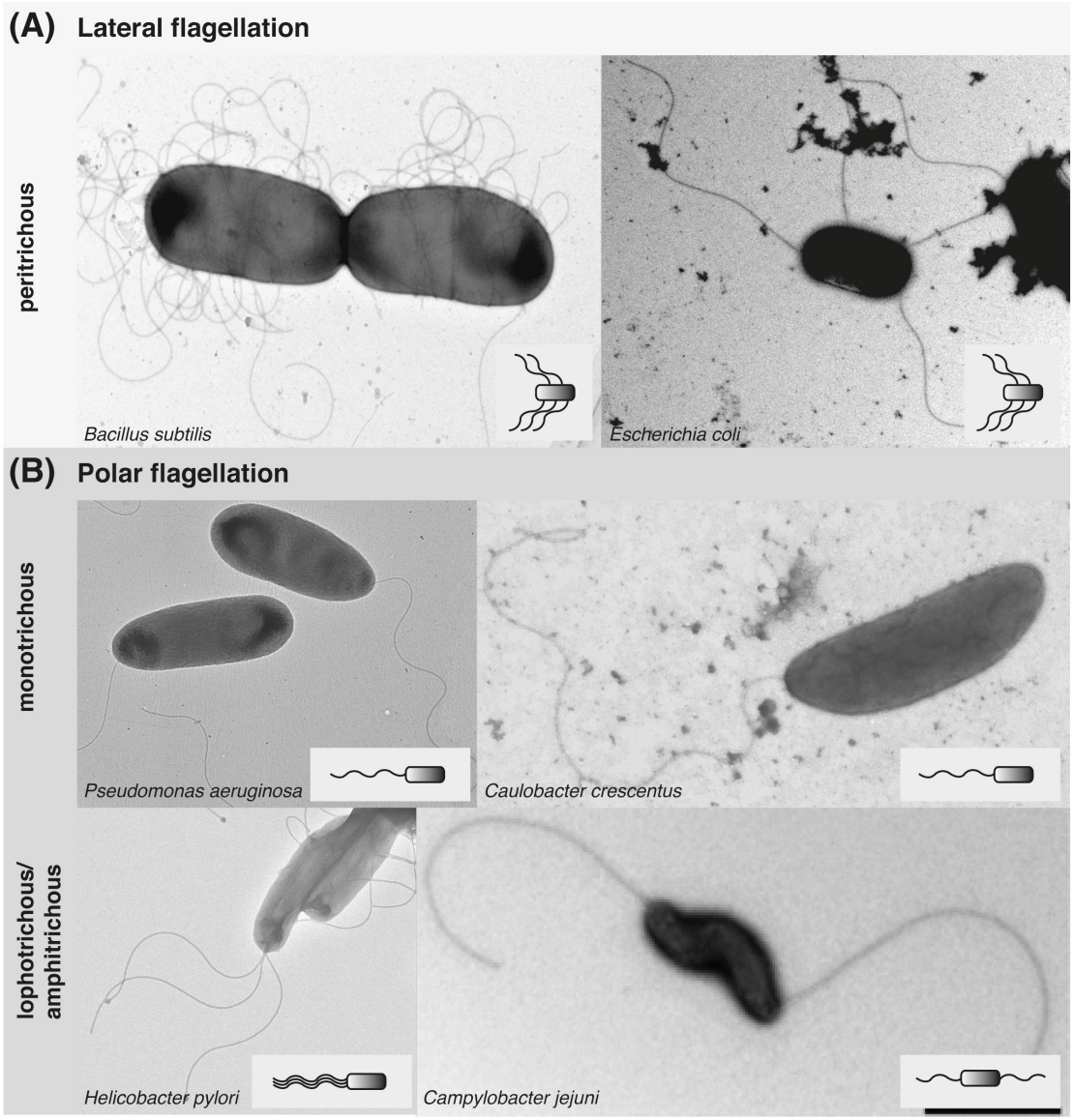

Figure 7. Bacterial flagellation patterns. (A) shows electron micrographs of the peritrichously flagellated bacteria *B. subtilis* and *E. coli*, while **(B)** shows electron micrographs of the monotrichously flagellated *P. aeruginosa* and *C. crescentus*, the lophotrichous *H. pylori* and the amphitrichous *C. jejuni*. A scheme of the respective flagellation pattern is depicted in the bottom right corner of the respective electron micrograph. The electron micrographs were kindly provided by Albert Siryaporn and Yi Shen (Princeton; *P. aeruginosa*), Martin Thanbichler and Kathrin Bolte (Marburg; *C. crescentus*), Dave Hendrixson (Texas; *C. jejuni*) as well as Barbara Waidner (Marburg; *H. pylori*). This figure was adapted from ref. (16).

As readily evident phenotypic characteristics, these patterns were among the earliest taxonomic criteria in microbiology (83). Despite the yet unexplored number of bacterial species showing a plethora of unique structures and features, only a handful flagellation patterns have been observed in microbiology (19). The localization of a flagellum at the cell body can be restricted to the cell pole (polar localization), along the side of the cell (lateral) at midcell or randomly distributed. In addition, bacteria also vary in the number of flagella from 1 to more than 100 flagella per cell, resulting in 5 major flagellation patterns: i) monotrichous, ii) lophotrichous, iii) amphitrichous, iv) peritrichous and v) medial (**Figure 7**).

Monotrichously flagellated bacteria, such as the well-studied model organisms *P. aeruginosa*, *Vibrio species* or *Caulobacter crescentus,* exhibit a single flagellum at one cell pole (84-87). The human pathogenic bacterium *H. pylori* has more than one flagellum at one cell pole and is an example of lophotrichous flagellation (64). One flagellum at each pole, amphitrichous flagellation, is observed for the ε-proteobacterium *C. jejuni* (88). In a large group of bacteria, flagella emerge from the entire side of the cell body, except for the cell poles and midcell. Among these peritrichously flagellated bacteria are three of the most prominent model organisms of microbiology *E. coli*, *Salmonella enterica* and *B. subtilis* (71, 89, 90). Having one flagellum at approximately midcell, *Rhodobacter sphaeroides* displays an exceptional arrangement of flagella and is a representative of the medial-flagellated bacteria (91).

1.3.1 Dual flagellated bacteria

Some bacteria exhibit two independent flagellar systems encoded as separate gene clusters at different locations on the genome (92-95). *V. alginolyticus*, *V. parahaemolyticus*, *Aeromonas sp*ecies, *Rhodosiprillum centenum* and *Azospirillum brasilense*, which are commonly described as polar flagellated, possess one flagellum at the cell pole in liquid medium, (96-100) (reviewed in: (101)). However, in more viscous environments or on surfaces, these bacteria are able to build lateral flagella resulting in a polar-peritrichous pattern (**Figure 8A**). The Gram-negative marine bacterium *Shewanella putrefaciens* also possesses two independent flagellar systems, the primary being a monotrichous arrangement

and the secondary flagella emerging from a lateral position (33). In contrast to *Vibrio species* both flagella systems are constitutively expressed and result in one polar and one or two lateral flagella (**Figure 8B**).

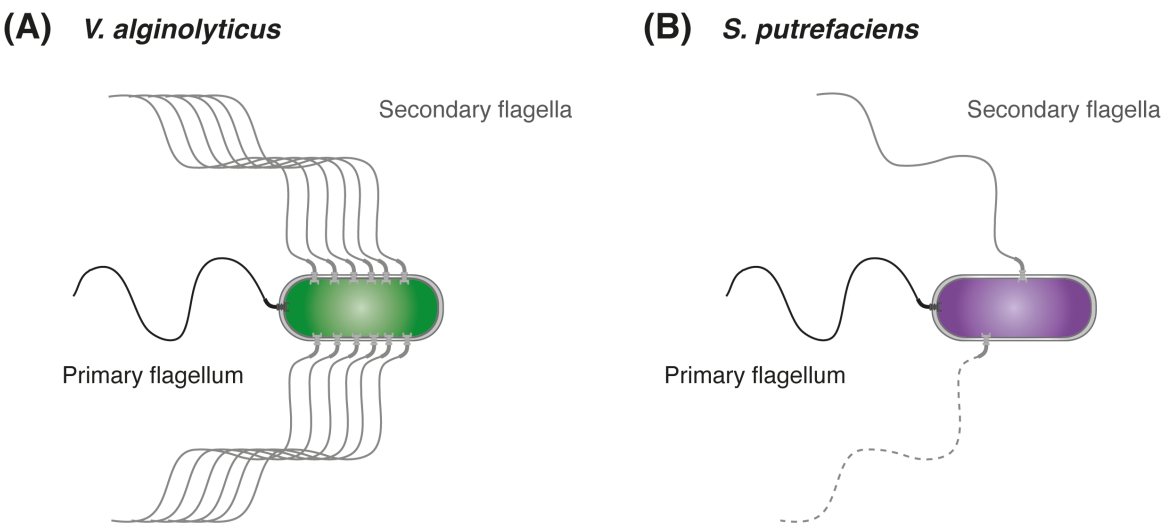

Figure 8. Dual flagellation. (A) *V. alginolyticus* employs a primary polar flagellum to move through liquid environments. On surfaces *V. alginolyticus* is able to build a multitude of lateral flagella. **(B)** *S. putrefaciens* possesses two independent flagella systems, a primary polar flagellum (black) and one or two secondary lateral flagella (grey). The flagella are encoded on different gene clusters in the genome of *S. putrefaciens* and are constitutively expressed.

Recent studies showed that in the case of *S. putrefaciens* the second system provides better navigation and advantages in directed movement rather than favouring swimming behaviour in viscous media. However, the secondary flagellar system does not respond to chemotaxis signals, but leads to realignment angles smaller than 90° upon tumbling, which promotes directed swimming (102). Spatial regulation of the two constitutively produced flagellar systems seems to rely on different mechanisms. While the regulatory genes *flhF* and *flhG* are encoded in the polar flagellar gene cluster, no homologues were found for the lateral system. Indeed, deletion of either *flhF* or *flhG* only affects the number and location of the polar flagellum, but has no influence on the lateral one (103). These unique features render *S. putrefaciens* the ideal model organism to complement the peritrichous Gram-positive *B. subtilis*. This approach not only offers a more general perspective of flagellar regulation mechanisms by comparing different organisms, but also delivers an internal control with the secondary flagellar system that is believed to be unaffected by manipulation of the primary polar system.

1.4 Flagellation pattern regulation

E. coli displays 5-6 flagella in a peritrichously arranged pattern, which until recently was assumed to be generated by random distribution. However, a new study was able to demonstrate that emerging flagella avoid the cell pole and even exhibit an asymmetric distribution with higher numbers of flagella in the 'old' half of the cell (90). This phenomenon does not only occur in *E. coli*, but also in the peritrichous *B. subtilis*, where 20-25 flagella are distributed along the cell body in a grid-like pattern, indicating that tight spatial regulation processes underlie flagella positioning (71). The reproducible polar arrangement of one or more flagella immediately implies an intrinsically spatial regulation of these sophisticated nano machines. All these results demonstrate that positioning of flagella is a process under strict control of diverse regulatory systems, acting on different levels. This raises the question how a bacterium defines or recognizes its cell pole. One approach is the use of so-called 'landmark' proteins, which is a common principle for other processes such as cell division, chromosome segregation and chemotaxis array localization (87, 104-106). 'Landmark' proteins localize to specific regions inside the cell recruiting essential effector proteins for positioning processes.

1.4.1 The 'landmark' system in *C. crescentus*

In the monotrichous α-proteobacterium *C. crescentus,* the flagellum is exclusively formed at the inherited cell pole after cell division. Having a dimorphic life cycle with a non-replicative swarmer cell that transitions into a non-flagellated replication-competent sessile state, it has been a model organism for studying life cycle progression and cell polarity for many decades (reviewed in: (107, 108)). Upon entering the replication-competent state the polar flagellum is replaced by a stalk, a cylindrical extension that serves as an adhesion organelle. Prior to cell division, a flagellum is built at the opposite pole resulting in a motile, flagellated daughter cell and a non-motile, stalked mother cell after asymmetric cell division.

Recent studies on cell polarity identified the coiled-coil membrane protein TipN as 'landmark' protein for the old cell pole. TipN not only plays an essential role for

cell polarity but also is responsible for polar localization of the flagellum. In accordance with cell cycle progression TipN relocates from the stalked to the nascent pole in a late stage of cytokinesis. Deletion of TipN leads to more and mislocalized flagella as well as severe polarity defects (87, 105). Polar localization of the membrane protein TipF strongly depends on the 'landmark' protein TipN and the presence of cyclic diguanosine monophosphate (c-di-GMP) (109). TipF is able to recruit the third flagellar positioning factor PflI to the cell pole (109, 110). TipF not only directs building blocks of the flagellar C-ring (FliG and FliM) to the correct assembly site but also may serve in assembly itself, as a *tipF* deletion results in a non-flagellated phenotype (109). In *C. crescentus*, vital processes such as cell cycle progression, cell division plane positioning, chromosome segregation and spatio-temporal regulation of flagellar assembly are coordinated by the 'landmark' protein system TipN/F (109). How TipN relocates during cytokinesis still remains enigmatic.

1.4.2 FlhF and FlhG affect number and placement of flagella

Besides 'landmark' proteins, bacteria have developed a second mechanism for the spatial regulation of macromolecular structures within the cell (reviewed in: (111)). Based on the dynamic cycle of dimeric ParA/MinD ATPases, bacteria are capable of positioning the cell division plane precisely at midcell (Min system; reviewed in: (112-114)) segregating replicated chromosomes into both daughter cells (ParAB*S*; reviewed in: (115, 116)) and spatially regulating the location of chemotaxis arrays (ParC; (117)). In diverse bacterial species two nucleotide-binding proteins, FlhF and FlhG (synonyms: YlxH, FleN, MotR, MinD2), were identified to maintain the specific arrangement of flagella (19). Interestingly, a close homologue of FlhG is MinD, and both proteins share the conserved ATPase domain (**Figure 9B**) (118).

1.4.2.1 FlhF

FlhF belongs to the Signal recognition particle (SRP), MinD, BioD (SIMIBI) class of nucleotide-binding proteins and constitutes, besides Ffh (also SRP 54 in eu-

karyotes) and FtsY, the third SRP-GTPase (119). While Ffh and FtsY represent the universally conserved core of the SRP-system, which co-translationally inserts membrane proteins into the cognate membrane (reviewed in: (120-122)), FlhF only occurs in bacteria and is involved in flagella regulation (123). All three GTPases share the conserved NG domains, including a regulatory domain (N-domain) and the GTPase (G-domain) (**Figure 9A**).

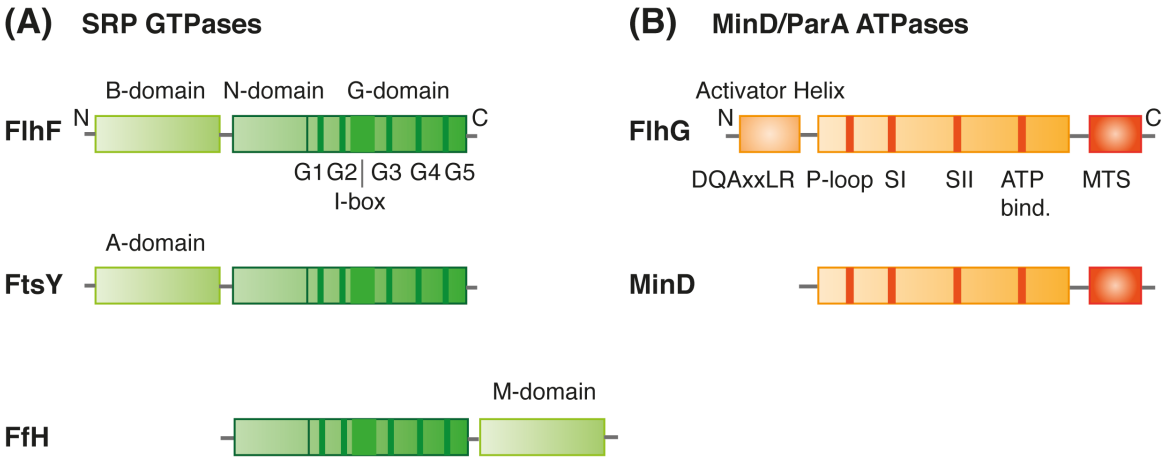

Figure 9. Domain architecture of FlhF and FlhG. **(A)** The domain architecture of the three members of the SRP-GTPase family (FlhF, FtsY and Ffh) shows that they all share the NG domain comprising all essential motifs for GTPase activity (G1 to G5 elements, Insertion box). They differ in the third domain, which serves SRP-specific purposes in FtsY (A-domain) and Ffh (M-domain). The function of the B-domain of FlhF remains elusive. **(B)** A comparison of the MinD/ParA member ATPases MinD and FlhG revealed a shared ATPase domain and an adjacent membrane targeting sequence (MTS). Important motifs are indicated in red (P-loop, SI: Switch I motif, SII: Switch II motif FlhG, ATP bind. residues essential for ATP recognition). FlhG comprises an additional N-terminal domain carrying the conserved DQAxxLR motif that serves as an activator motif of the FlhF GTPase in *B. subtilis*. N- and C-termini are indicated and apply to all proteins below. Figure was modified according to ref. (16).

During membrane protein insertion, Ffh and FtsY form a GTP-dependent heterodimeric complex to target a ribosome nascent chain complex to an available translocon. The complex falls apart upon stimulation of GTP hydrolysis through the SRP-RNA. Upon binding of GTP, FlhF forms a homodimeric complex that structurally resembles the SRP heterodimer (124). In addition to the NG-domain, FlhF comprises of an N-terminal basic and natively unfolded domain (B-domain) (**Figure 9A**). In *V. cholerae,* this domain is involved in recruiting the MS-

ring component FliF to the cell pole as the first building block for a future flagellum (125). Despite extensive research the molecular role and mechanism of FlhF remains elusive and further investigations are required to dissect the function of the individual domains involved in flagellar regulation.

1.4.2.2 The regulatory circuit of FlhF and FlhG

In most bacterial genomes *flhF* and *flhG* form a transcriptional unit with *flhG* being the downstream neighbour of *flhF* embedded into a flagellar gene cluster. Very often FlhA, the major component of the fT3SS, is encoded upstream of *flhF* and *flhG*.

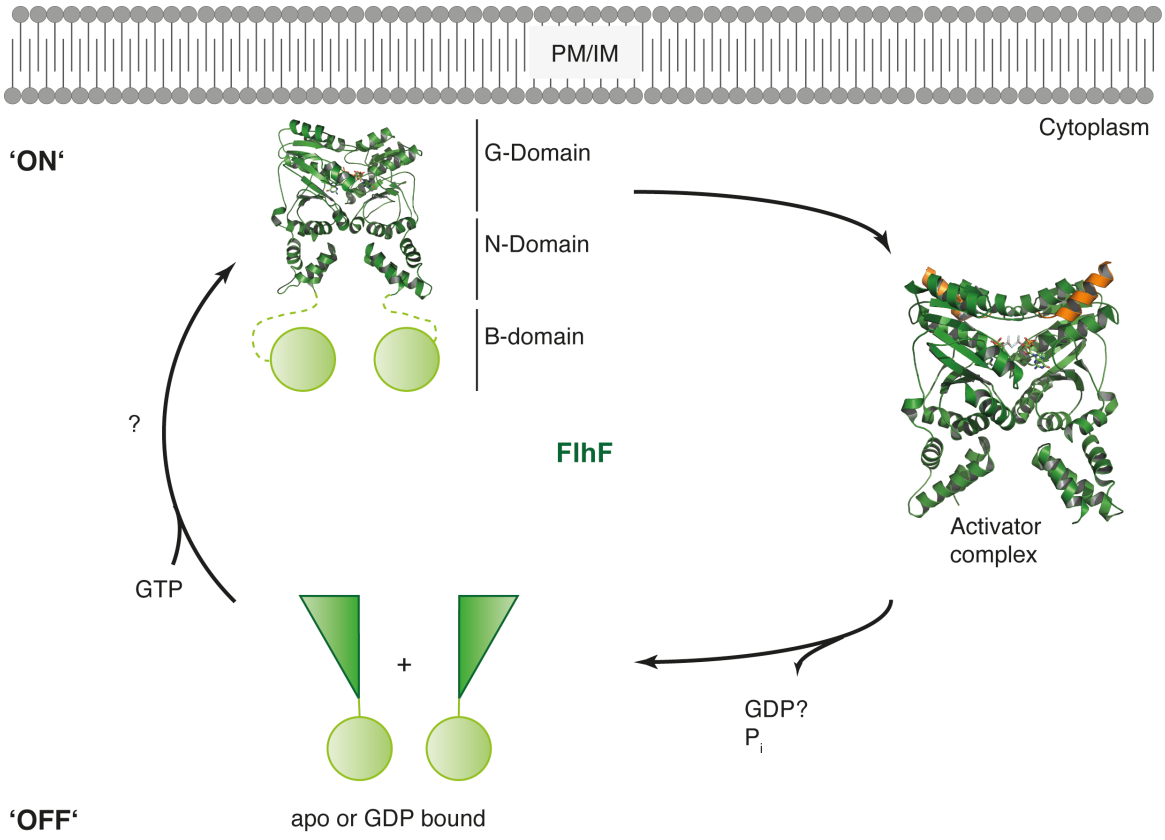

Figure 10. The regulatory circuit of FlhF. FlhF is a molecular switch with two distinct states. In the canonical 'ON' state, FlhF (green) forms a GTP-dependent homodimer (pdb: 2PX0), which localizes to the plasma/inner membrane. With the N-terminus of FlhG (orange), FlhF forms an activator complex (pdb: 3SYN), which triggers GTP hydrolysis of FlhF. Upon hydrolysis the dimer dissociates and FlhF transitions into its monomeric 'OFF' state, where a nucleotide exchange occurs. PM: plasma membrane, IM: inner membrane are abbreviated. Figure was adapted from ref. (16).

FlhG shares key features with SIMIBI class ATPases such as the P-loop (deviant Walker A motif) or the Switch I and II regions. In *B. subtilis*, FlhG directly interacts with the FlhF dimer and is able to stimulate the GTPase of FlhF through an N-terminal helical motif (DQAxxLR; x represents any amino acid). It mimics the SRP-RNA by providing a conserved glutamine residue that reaches into the composite active site and triggers hydrolysis (118). Both proteins form a regulatory circuit where FlhG triggers the transition of the GTP-bound dimeric 'ON' state of FlhF into the monomeric 'OFF' state (**Figure 10**). However, the molecular role(s) of the distinct states of FlhF is still unknown.

1.4.2.3 The role of FlhF and FlhG in monotrichous flagellation

In the monotrichously flagellated *V. alginolyticus* FlhF and FlhG are major determinants for flagella number and position, with FlhF acting as a positive and FlhG as a negative one. Depletion of FlhF results in non-flagellated bacteria whereas knockout of FlhG leads to a hyper-flagellated phenotype. Overexpression of these proteins shows opposing effects (84). In a double deletion of the *flhF* and *flhG* genes, *V. alginolyticus* is severely impaired in motility and completely lacks a flagellum. However, a suppressor mutant in a gene called *sflA* partly restores motility by promoting the production of lateral flagella (126, 127). Furthermore, the polar localization of FlhF in *V. alginolyticus* depends on the presence of FlhG. While in an FlhG depletion strain, FlhF exclusively localizes at a cell pole, wild-type levels of FlhG result in both polar and cytoplasmic localization of FlhF (**Figure 11AB**). Upon overexpression of FlhG, FlhF is mainly distributed in the cytoplasm, indicating that FlhG releases FlhF from the pole (**Figure 11C**) (128). Mutational studies on FlhF revealed that the GTP-binding motif is essential for polar localization of the flagellum (129). In the close relative *V. cholerae*, the causative agent of the human diarrheal disease cholera, deletion of *flhF* and *flhG* resulted in non-flagellated and hyper-flagellated (8-10 flagella) bacteria, respectively. Both mutant strains were non motile on soft agar plates. The N-domain of FlhF is vital for its polar localization and FlhF determines polar localization of flagella by recruiting FliF, the earliest component of flagella assembly to the cell pole (125, 130). Furthermore, it has been demonstrated that FlhF and FlhG act as transcriptional regulators of flagellar gene expression. FlhG represses tran-

scription of early class I genes, whereas FlhF acts downstream activating class III gene expression (131).

Figure 11. Role of FlhF and FlhG in *V. alginolyticus*. In *V. alginolyticus* FlhF acts as a positive regulator of flagella biogenesis, whereas FlhG, its counterpart, is a negative regulator that decreases number of flagella. **(A)** In the wild-type situation the interplay between FlhF (green circles) and FlhG (orange circles) results in one flagellum at a single cell pole. **(B)** When FlhG is not present, FlhF localizes mainly to the cell pole and causes the production of multiple flagella at one pole through positive regulation. **(C)** In the presence of an excess of FlhG, FlhF is constantly released from the cell pole and cannot initiate flagella biogenesis, which results in a non-flagellated phenotype. This figure was inspired by ref. (128).

Similar to *Vibrio* species, deletion of the FlhG homologue FleN in *P. aeruginosa* abolishes motility and leads to hyper-flagellated bacteria with 3-6 flagella (86). However, in *P. aeruginosa* that lacks FlhF, flagella are no longer restricted to the cell pole but emerge from random positions along the cell body. In addition, an *flhF* mutant strain swims with lower velocity and lacks swarming motility (132). Further investigation revealed that FlhF is not only required for flagellar assembly but also plays a crucial role in flagellar rotation. Replacing FlhF in *P. aeruginosa* by a hydrolysis-deficient FlhF variant (FlhF R215G) severely impairs swimming motility as well as the ability to rotate the flagellum (133). The closely related *Pseudomonas putida* exhibits on average two polar flagella per cell. Deletion of FlhF results in a random distribution of a slightly augmented number of flagella (~3.2 per cell). Overexpression increases the number of polar flagella to 12 ± 2 flagella per cell. In both cases motility is abolished or severely affected (134). In the monotrichous plant pathogen *Xanthomonas oryzae* FlhF deviates from its homologues in other bacteria by two transmembrane-like domains, and its deletion strongly affects motility (135). FlhF and FlhG are essential determinants of flagellar location and number in many monotrichously flagellated bacteria. How-

ever, their specific effects slightly vary in different species, indicating subtle differences in the respective mode of action or interaction network.

1.4.2.4 Amphitrichous and lophotrichous flagellation

In the field of lophotrichous and amphitrichous bacteria two pathogens emerged as model organisms to study flagellation and motility as crucial virulence factors. *H. pylori*, a causative agent of gastric ulcers, has 2-6 polar flagella. Deletion of *flhG* (*ylxH*) eliminates flagella and thereby motility. Furthermore, in an *H. pylori flhG* deletion strain, transcription of intermediate and late flagellar genes is impaired (64). In the amphitrichous *C. jejuni*, a common cause of gastroenteritis in humans, deletion of FlhG leads to less motile bacteria, which are hyper-flagellated at least at one cell pole (88). Upon disruption of FlhF *C. jejuni* is non-motile and produces no flagella or just a single flagellum at one pole (136). Notably, in *C. jejuni* FlhG is not only involved in flagellar biogenesis, but also in cell division. Together with flagellar C-ring proteins FlhG prevents polar cell division by an as-of-yet unknown mechanism (88).

1.4.2.5 Peritrichous flagellation

The Gram-positive soil bacterium *B. subtilis* possesses 20-25 lateral flagella arranged in a grid-like pattern that is symmetrically organized around the midcell (71). Fluorescence labelling of the flagellar component FliM showed that basal bodies have a minimal distance of 0.39 ± 0.1 µm. Again, FlhF and FlhG play a key role in the formation of the peritrichous flagellation pattern. When *flhF* was mutated in the context of the FliM-GFP fusion, *B. subtilis* retained wild-type motility as well as the equivalent number of basal bodies. However, the distribution becomes more random and basal bodies tend to cluster at the cell pole. On the other hand, in a Δ*flhG* strain basal bodies appeared to be clumped together and the number seemed to be reduced. As observed for *flhF* deletion neither swimming nor swarming motility is significantly affected. A double knockout of *flhG* and *flhF* resembles the phenotype of a Δ*flhF* strain (71).

1.4.3 Interaction partners of FlhF and FlhG

FlhF as well as FlhG share a high sequence homology and a similar architecture throughout many bacteria with diverse flagellation patterns (**Figure 9**). This indicates that both proteins act according to the same mechanistic principles in all these organisms. However, there are subtle variations of phenotypic behaviour of FlhF and FlhG, such as the aflagellated phenotype in *H. pylori*, upon disruption of *flhG*. While *Vibrio* species that lack FlhF also lack flagella, deletion of *flhF* in *Pseudomonas* leads to an aberrant localization of flagella. FlhF and FlhG seem to transcriptionally regulate different gene classes in these different organisms. All these subtle variations indicate that the key for maintenance of specific flagellation patterns is encoded in the interaction partners of FlhF and FlhG. Assuming this scenario is correct, one would expect species-independent as well as species-specific proteins that interact with FlhG and FlhF.

Besides FlhG, FlhF might interact with the flagellar MS-ring protein FliF as it recruits the earliest flagellar component FliF to the old cell pole in *V. cholerae* (125). FliF is conserved in all flagellated bacteria and may thus represent a species-independent interaction partner. FlhG directly interacts with the c-di-GMP-dependent master regulator of flagellar gene transcription, FleQ, in the polar flagellated *P. aeruginosa* (137). FlhG furthermore decreases the ATPase activity of the AAA+-type ATPase FleQ. This negative effect on the ATPase is also observed with c-di-GMP. In the presence of both FlhG and c-di-GMP, the ATPase activity is massively decreased, indicating a cooperative inhibition (138). FleQ homologues are present in many polarly flagellated γ-proteobacteria (138). Notably, a FleQ homologue is missing in the peritrichously flagellated *B. subtilis* implying that this would be an example for a species-specific interaction partner of FlhG. In *V. cholerae* the polar 'landmark' protein HubP was identified as an interaction partner of FlhF as well as FlhG. HubP and FlhF independently localize to the cell pole, but both proteins are required for correct localization of FlhG (108, 139). As observed for FleQ/FlrA, HubP is missing in *B. subtilis* or *H. pylori* and may again represent a species or maybe a pattern-specific interaction partner FlhG and FlhF. However, the full extent of the interaction network in which FlhF and FlhG are embedded remains elusive and will be further addressed in this PhD thesis.

1.5 Cell division site determination

Most bacteria replicate by binary fission leading to the formation of two equal daughter cells that each receive one chromosome. Correct positioning of the cell division plane and temporal control of fission is essential for bacterial reproduction. Aberrant Z-ring location leads to miniature cells lacking DNA and vital cellular structures. Interestingly, in many rod-shaped bacteria cell division occurs at midcell, indicating that this process is subject to strict spatio-temporal control (140). The assembly of the cytokinetic Z-ring, which is a ring-like structure of the bacterial tubulin homologue FtsZ, initiates cell division (141-143). Extensive research revealed the Min system, whose name is derived from the miniature cell phenotype, to be a major determinant of spatially correct Z-ring assembly, which acts as a negative regulation system. Polymerization of a MinCD complex starting at the pole provides an efficient inhibitor of FtsZ polymerisation, restricting Z-ring formation to midcell. To complement the Min system, many bacteria employ the Noc System, which binds to the membrane and the DNA simultaneously, preventing septum formation through chromosomes (144-148). In contrast to many other bacteria, *C. crescentus* divides asymmetrically into a stalked replication-competent mother cell and smaller, flagellated swarmer cell. Lacking a conventional Min system, the ATPase MipZ acts as an inhibitor of the cytokinetic Z-ring. Through its interaction with ParB involved in chromosome portioning, MipZ localizes to the cell poles when the replicated chromosomes segregate, restricting Z-ring assembly to midcell (149).

1.5.1 The Min system in *E. coli*

The Min system was discovered in *E. coli* through a mutant in the min genes which resulted in the formation of miniature cells without DNA load (minicell phenotype), indicating incorrect cell division (150). As described below, *E. coli* has become the model organism to study cell division and cytokinesis (reviewed in: (112, 113)). Extensive research using genetic and biochemical methods revealed three proteins MinC, MinD and MinE to constitute the core of the *E. coli* Min system that spatio-temporally regulates cell division by excluding Z-ring assembly

from midcell (151, 152). The SIMIBI class ATPase MinD forms ATP-dependent homodimers that are able to interact with phospholipids through a C-terminal amphipathic helix acting as membrane targeting sequence (MTS) (153, 154). The membrane-associated MinD dimer recruits the potent Z-ring inhibitor MinC. This protein prevents FtsZ polymerization through its interaction with FtsZ and therefore inhibits Z-ring formation wherever it is associated with MinD (152, 155).

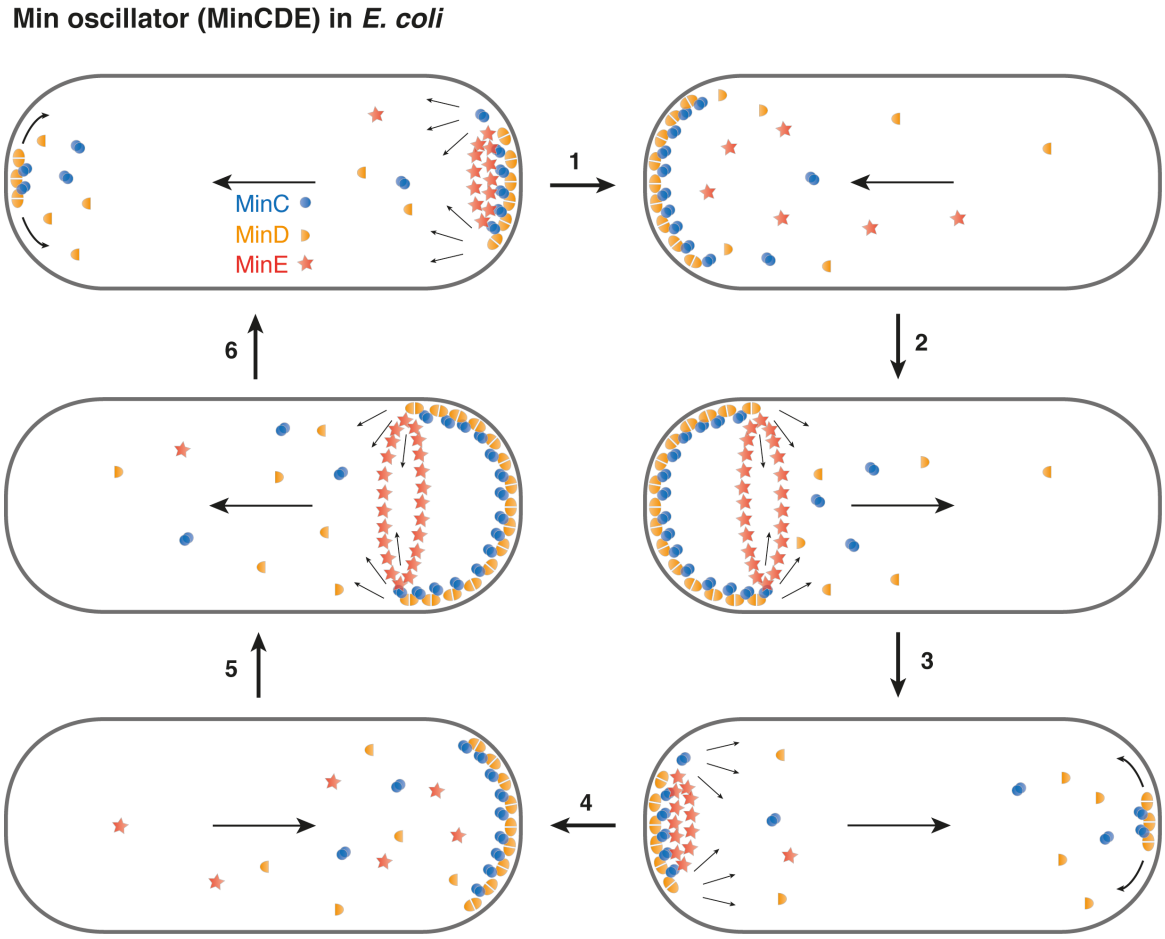

Figure 12. The Min oscillator of *E. coli*. The schematic cycle of the Min oscillation in *E. coli* is initiated with a MinCD complex starting to assemble at one cell pole towards midcell, forming copolymeric structures **(1)**. Subsequently MinE interacts with the MinCD polymer and disassembles the MinCD complex through stimulation of the MinD ATPase **(2)**. MinD and MinC monomers or dimers dissociate from the membrane and diffuse to the opposite cell pole where assembly is reinitiated **(3)** and follows the same features **(4-6)**. This concerted movement leads to a minimum of the cell division inhibitor MinC at midcell. This figure was adapted from ref. (112).

The topological specificity factor MinE also interacts with MinD on an interface that partly overlaps with the MinC binding site. It furthermore stimulates the

ATPase activity of MinD, which leads to disassembly of the MinCD complex (156, 157). The MinCD complex starts to assemble at the cell poles and polymerizes towards midcell, where MinE disintegrates MinCD. This leads to a pole-to-pole oscillation of the MinCD complex and generates a time-averaged MinC concentration with a minimum at midcell where cell division occurs (**Figure 12**) (158). A close relative of *E. coli* that shares the genetic architecture of the Min system is *S. putrefaciens*. *minC*, *minD* and *minE* are clustered on a genomic locus constituting a transcriptional unit.

1.5.2 The Min system in *B. subtilis*

In the spore forming Gram-positive *B. subtilis,* the Min system lacks the ATPase-stimulating MinE as well as the characteristic oscillation behaviour of these proteins described in *E coli*. DivIVA replaces MinE as topological specificity factor in *B. subtilis* and is essential for the polar recruitment of MinD (159). DivIVA does not stimulate the ATPase of MinD and therefore share only low sequence homology with MinE. Recent studies identified an additional protein (MinJ) to be crucial for cell division and to function as an intermediary between MinD and DivIVA (160, 161). The MinCD complex assembles in a stable arrangement from the poles towards midcell, again inhibiting cell division at midcell (**Figure 13**) (159, 162).

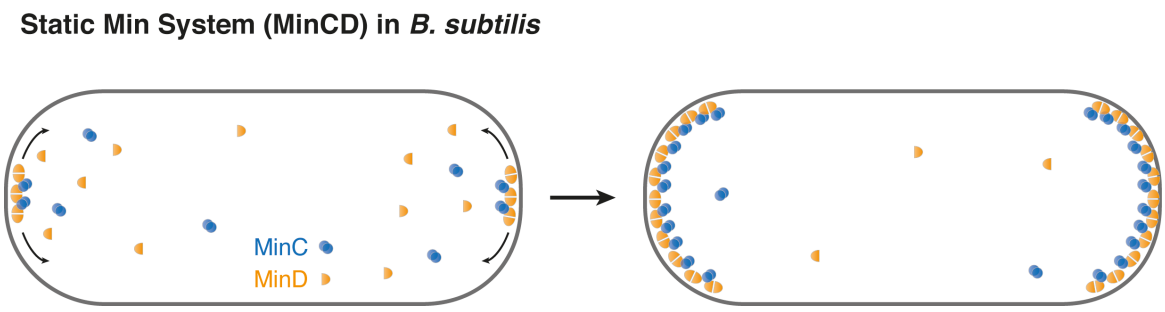

Figure 13. Static Min system in *B. subtilis*. With the lack of MinE, the *B. subtilis* Min system also lacks the characteristic oscillation. However, the MinCD complex also assembles from the cell poles towards midcell. This leads to a static appearance of the Min proteins in *B. subtilis*.

However, to which extent this polymer is intrinsically dynamic through adenosine triphosphate (ATP) hydrolysis and nucleotide exchange processes remains

unclear. Recent studies demonstrated that the ATPase of MinD in *B. subtilis* is not required for membrane association but rather for polar localization and recruitment of MinC (163, 164). Whether and how the ATPase of MinD is stimulated in the absence of MinE is unknown.

1.5.3 Cell division site determination in *C. jejuni*

C. jejuni lacks both a canonical Min system and a MipZ 'landmark' system. Instead, another MinD/ParA-like ATPase, FlhG, is involved in determination of the future cell division plane at midcell. In addition, FlhG is involved in controlling the correct number and location of flagella as observed for many bacteria. However, how FlhG can control both processes, cell division plane determination and flagellation pattern maintenance, remains elusive. Research on flagellar proteins in *C. jejuni* addressing the link between positioning of flagella and the cell division plane revealed the C-ring proteins FliM and FliN to be involved in correct cell division (88).

1.6 Chemotaxis

Survival of bacteria strongly depends on their ability to sense and to respond to environmental changes, avoiding nutrient poor zones and high concentrations of toxic substances. Furthermore, flagellated pathogens rely on chemotaxis to find and invade their hosts. This not only requires motility but also a chemosensory system rendering bacteria capable of sensing the quality and composition of their environment. Information acquired by chemosensors then has to be processed and translated into a plan of action, referred to as chemotaxis (**Figure 14**) (reviewed in: (165, 166)). Bacteria possess a wide spectrum of intra- and extracellular sensors in order to monitor their environment.

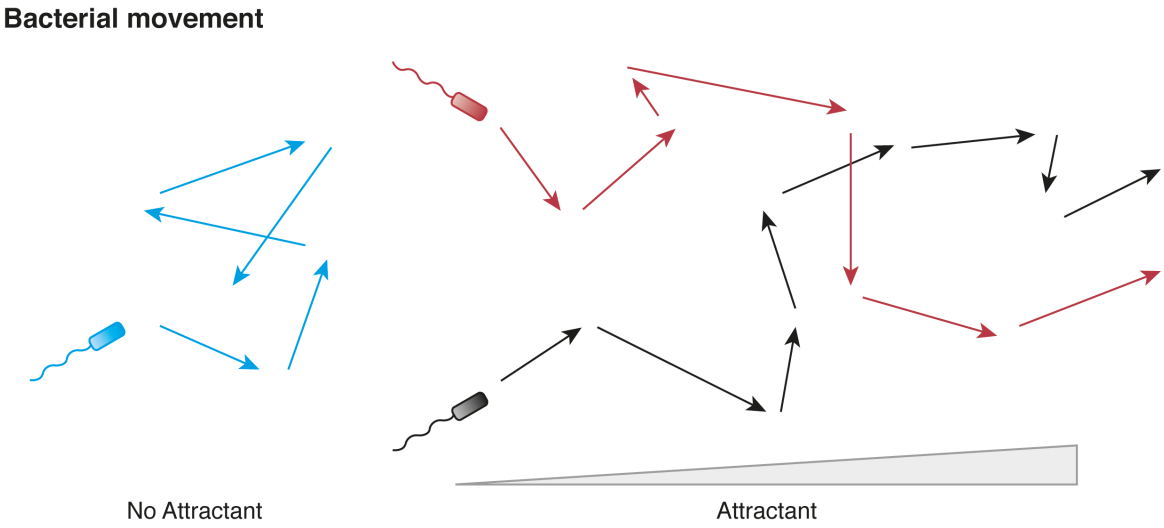

Figure 14. Bacterial movement. Bacteria are able to follow attractants and avoid repellents through a process called chemotaxis. In the absence of either repellent or attractant the movement can be described by the same principles as Brownian motion (*left*). Upon sensing attractants, bacteria are able to move along the gradient towards high attractant concentration (*right*). The arrows represent the trajectory of the bacterial movement.

1.6.1 The chemosensory system

Attractants or repellents are recognized by chemoreceptors: dimeric, trans-membrane proteins with a periplasmic ligand binding domain and a cytoplasmic kinase-signalling domain. Upon ligand binding the signal is propagated through the membrane and leads to the phosphorylation of a chemotaxis response regulator. Chemoreceptors can react to a plethora of attractants (amino acids, sugars or metabolic intermediates) or repellents (transition metals) (167). In many bacteria, thousands of chemoreceptor proteins are clustered in a hexagonal arrangement as ‘trimers of dimers’ in the polar region of the cell as chemoreceptor array (168-171). The receptors form a ternary signalling complex with the histidine protein kinase CheA and a linker protein (CheW). Methylation of the chemoreceptors allows bacteria to compare the current situation with the previous one in a process called adaptation, representing a primitive memory (172). The bacterial sensory system is not restricted to attracting or repelling substances but also includes fa-

vourable growth conditions such as pH or redox properties (energy taxis) or even optimal light intensity for photosynthesis (phototaxis) (173-175).

Notably, a recent study revealed that spatial regulation of chemotaxis arrays in *V. parahaemolyticus* relies on the ParA/MinD-like ATPase ParC. Through its interaction with ParP, ParC is capable of recruiting chemoreceptor arrays to the cell pole. The hydrolysis cycle of the ATPase, with its distinct states, plays a key role for this recruitment; however, the role of the putative ParC dimer and its exact mechanism remains unclear (117).

1.6.2 Characteristics of chemotaxis

In *E. coli* chemotaxis signalling begins with binding of a repellent to a chemoreceptor, inducing a conformational change that is transmitted through the membrane to CheA via the signalling domain of the chemoreceptor and the linker protein CheW, inducing autophosphorylation of CheA (**Figure 15**). Phosphorylated CheA (CheA-P) is able to phosphorylate its cognate response regulators CheY and CheB. CheY-P, in turn, diffuses from the chemosensory cluster to the flagellum, where it binds to the flagellar C-ring components FliM and FliN and switches the rotational state of the flagellum from CCW (default: ‘run’) to CW (‘tumble’) and causes the bacterium to tumble more often (55, 176, 177). CheB-P acts as a methylesterase and mediates the methylation status of the chemoreceptors, hence regulating adaptation. The signalling cascade is terminated by the phosphatases CheZ and CheR that efficiently dephosphorylate CheY-P (178, 179).

In *B. subtilis* the chemotaxis signalling cascade appears inverted compared to *E. coli*. In the default state the flagellum rotates clockwise which causes *B. subtilis* to tumble (‘tumble’). Upon sensing attractants, CheA is autophosphorylated, which leads to an increase in CheY-P that binds to the flagellar C-ring and switches the rotation to counter clockwise, inducing straight swimming (‘run’) (**Figure 15**). Furthermore, the chemotaxis system in *B. subtilis* is more complex and includes additional factors such as the adaptation mediator CheD another linker protein between the chemoreceptor and CheA, CheV (reviewed in: (180-182)).

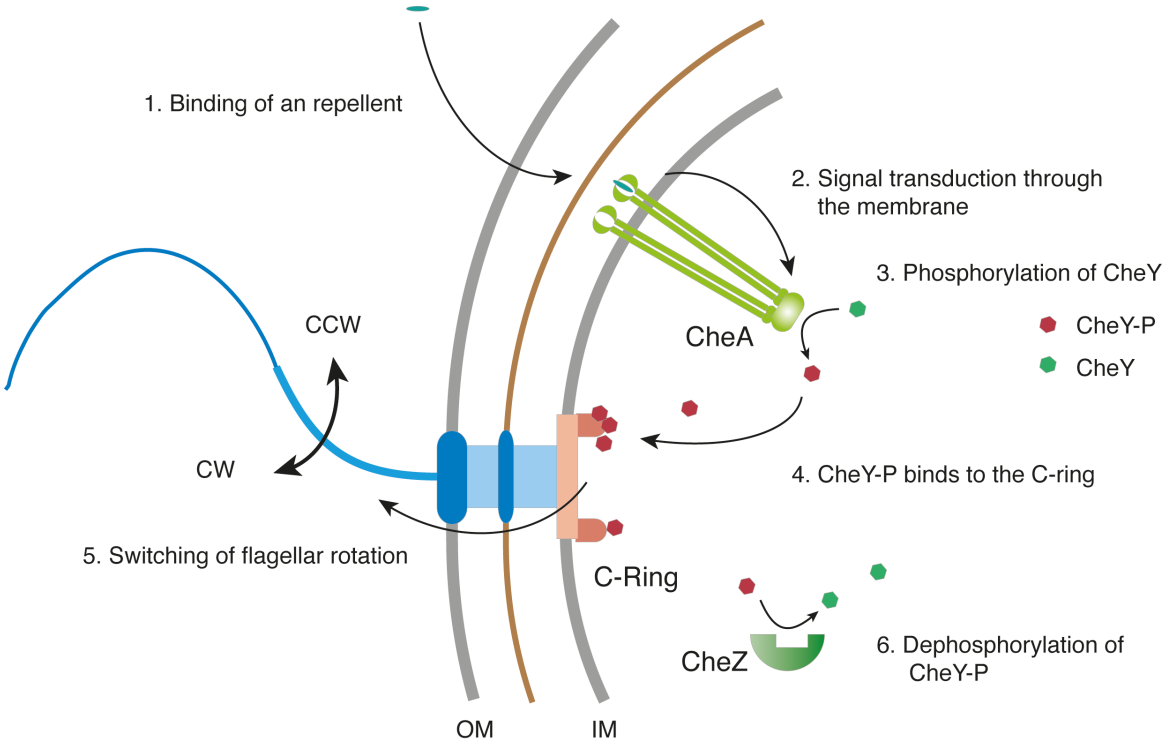

Figure 15. Scheme of chemotaxis. Chemotaxis starts with the perception of environmental cues (*e.g.* attractants) by (chemo)receptors (light green) (1). The signal is transduced through the membrane and translated into a response through phosphorylation of CheA (light green ovals) (2), which in turn phosphorylates CheY (green hexagons) producing CheY-P (3). CheY-P (red hexagons) binds to the flagellar C-ring (red) (4) and causes the flagellum to switch the direction of rotation from clockwise (CW) to counter clockwise (CCW) or *vice versa* (5). The phosphatase CheZ (green) triggers dephosphorylation of CheY-P and therefore resets the system and renders it capable of reacting to further stimuli (6). OM stands for outer membrane, while IM represents the inner membrane.

In *B. subtilis* three proteins are involved in the inactivation of CheY-P. CheC is able to dephosphorylate CheY-P. Formation of a dimeric complex between CheC and CheD enhances the ability of the former to dephosphorylate the CheY-P 5-fold. In addition, the flagellar C-ring component FliY comprises a CheC-like phosphatase domain, harbouring two active sites to inactivate CheY-P (183-187).

R. sphaeroides represents an organism of complex tactic behaviour, comprising a broad range of different external stimuli, such as oxygen, light, some amino acids, specific sugars as well as organic acids (reviewed in: (165, 188)). Two sets of flagellar genes *fla1* and *fla2* in the genome of *R. sphaeroides* encode two independent flagella systems, each of them providing a fully functional flagellum

(189). However, *R. sphaeroides* exclusively expresses *fla1*, resulting in a flagellum with a unidirectional motor (190, 191). Therefore, *R. sphaeroides* navigates by turning the rotation of the flagellum 'ON' (run) and 'OFF' (tumble) instead of switching the direction of flagellar rotation (192).

1.6.3 CheY interacts with the flagellar C-ring

The final response regulator and integrated chemotaxis signal, CheY-P, controls the direction of flagellar rotation. Therefore, CheY-P is sensed by the flagellar C-ring protein FliM through binding to a conserved motif (LSQxEIDALL; 'EIDAL' motif) at the N-terminus of FliM. The crystal structure of CheY in complex with the N-terminal peptide of FliM revealed that the helical N-terminus of FliM binds to a helix-β-strand-helix motif formed by helices α4 and α5 and strand β4 of CheY. Structural analysis revealed the interaction of an amphipathic interface of CheY with the helical 'EIDAL' motif, which also exhibits an amphipathic character (193, 194).

Aim of the work

Despite the plethora of bacterial species, only a handful flagellation patterns are known in nature, which are reproducibly established during each cell division cycle. Moreover, flagellation patterns served as early taxonomic criterion in microbiology, as flagellation is easily observed under the microscope. In many flagellated bacteria, two nucleotide binding proteins FlhF and FlhG play an essential role to establish and maintain different flagellation patterns.

However, the precise mechanism underlying flagellation pattern control still remains elusive. It is unclear how FlhF and FlhG interact with the flagellar system to assign the future flagellar assembly site and restrict flagella to a certain number. While a crystal structure of FlhF was published in 2007 and more recent studies showed a direct interaction between FlhF and FlhG, information about FlhG is currently scarce.

Herein, I set out to analyse the crystal structure of FlhG (195), uncover its specific features and elucidate its interaction network in the Gram-positive peritrichous *B. subtilis* and the Gram-negative monotrichous *S. putrefaciens*. I wanted to understand how the mechanistic features of these two proteins shape the regulatory module that controls the number and location of flagella. Furthermore, I aimed at comparing mechanistic features and interaction partners of FlhF and FlhG in *B. subtilis* and *S. putrefaciens* to get insights into how universal and species-specific features are interconnected to regulate different flagellation patterns.

In order to complement structural and biochemical data I aimed at establishing hydrogen deuterium exchange mass spectrometry in Marburg to conveniently investigate protein-protein interaction interfaces. I therefore cooperated with Dr. Uwe Linne from the Mass Spectrometry Facility of the Chemistry Department of Philipps-Universtiy Marburg.

Results

2.1 FlhG is a MinD-like ATPase

FlhG belongs to the MinD/ParA type superfamily of ATPases (196). As MinD, FlhG exhibits the characteristic features of SIMIBI class ATPases (119). A detailed sequence alignment of MinD and FlhG proteins from different organisms revealed that FlhG and MinD share conserved motifs for ATP hydrolysis (P-loop or deviant Walker A motif, Switch II region), magnesium coordination (Switch I region) as well as ATP binding (ATP binding motifs) (**Figure 16**). This strongly indicates that FlhG is an ATPase like MinD and may exhibit similar mechanistic features, such as ATP-dependent dimerization.

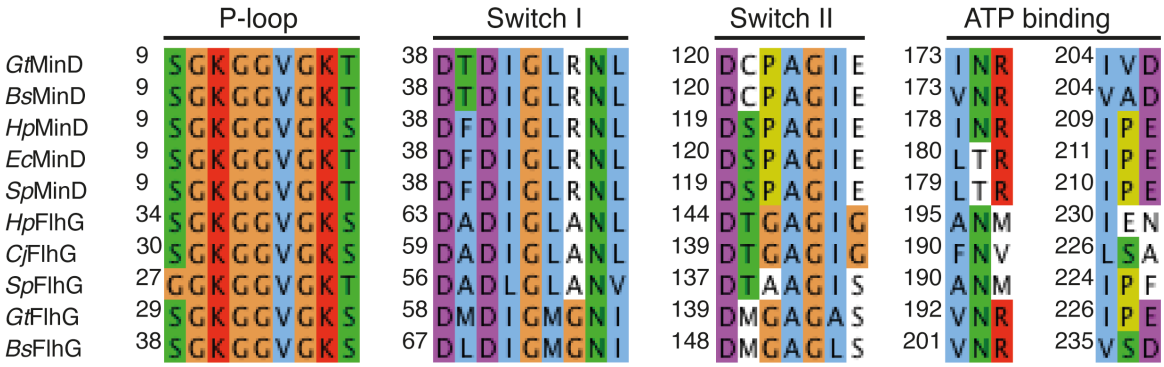

Figure 16. Vital ATPase motifs. A sequence alignment indicates that MinD and FlhG proteins from different organisms share the essential motifs for ATP binding, Mg^{2+} coordination (Switch I) as well as ATP hydrolysis (P-loop and Switch II). Organisms are abbreviated in the following way: *Geobacillus thermodenitrificans* (*Gt*); *B. subtilis* (*Bs*); *H. pylori* (*Hp*); *E. coli* (*Ec*); *S. putrefaciens* (*Sp*) and *C. jejuni* (*Cj*).

2.1.1 Purification of FlhG

The availability of pure and homogeneous protein in sufficient amounts is a pre-requisite for any biochemical or structural analysis. Purification of FlhG of *B. subtilis* however, yielded only low amounts of poorly soluble protein accompanied by heavy precipitation. Changing the hexa-histidine $(His)_6$-tag from N- to C-terminus even decreased the solubility additionally. Different buffer conditions did not improve either the solubility or the yield of the protein. Therefore, the homologue of the moderate thermophile soil bacterium *G. thermodenitrificans* NG 80 was employed for the following biochemical and structural analysis of FlhG (197). Especially in crystallography it is a common technique to exploit the increased stability and potentially increased solubility of orthologous proteins from thermophile organisms to augment purification yields and crystallization success (198, 199). Typical representatives for thermophile organisms in crystallography are *Aquifex aeolicus* or *Thermotoga maritima* (200, 201).

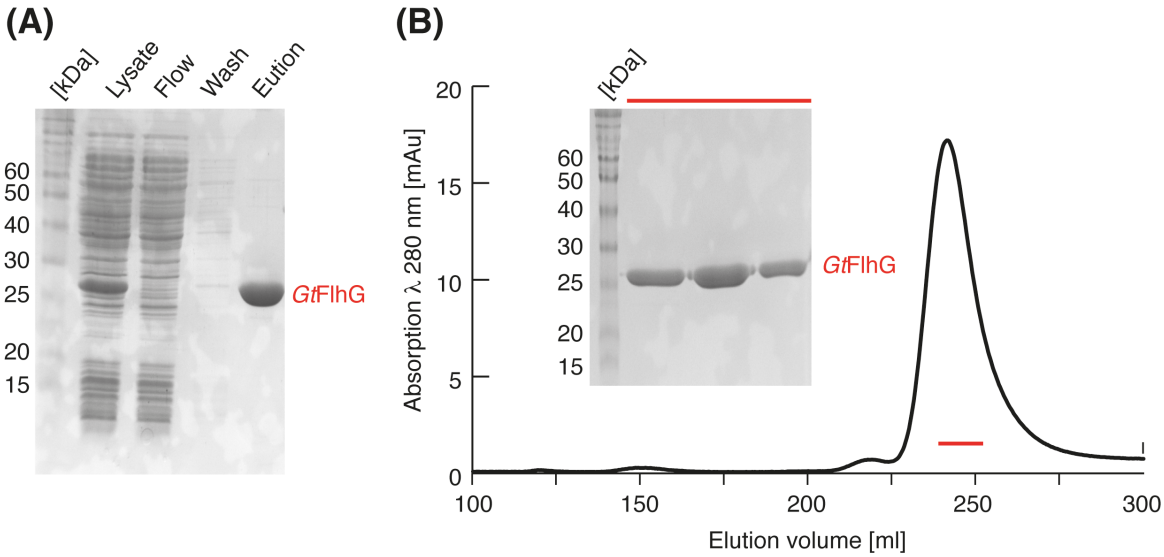

Figure 17. Purification of *Gt*FlhG. (A) displays the Coomassie-stained SDS-PAGE of the Ni-NTA affinity purification of *Gt*FlhG. After elution, pure *Gt*FlhG was obtained in reasonable amounts. **(B)** The size exclusion chromatogram shows a single peak. The inlay represents the corresponding Coomassie-stained SDS-PAGE of the peak fractions (indicated in red), confirming that *Gt*FlhG is the major protein component of the peak fractions.

Therefore, *Gt*FlhG carrying a $(His)_6$-tag at its N-terminus was produced recombinantly in *E. coli* and purified by a two-step protocol including Ni-NTA affinity chromatography and subsequent size exclusion chromatography (SEC) (**Figure 17**). A detailed protocol is provided in the materials and methods section.

Not only was *Gt*FlhG more stable than its mesophilic orthologue from *B. subtilis*, but also exhibited enhanced solubility, although it still precipitated at higher concentrations. Thus, purification yielded sufficient amounts of protein for biochemical assays as well as crystallography. The protein concentration was determined using the absorbance at 280 nm with a nano drop and a predicted extinction coefficient (web.expasy.org/protparam), which was 24 400 $M^{-1}cm^{-}$ for *Gt*FlhG.

2.1.2 ATPase activity of FlhG

To assess whether *Gt*FlhG is indeed an ATPase as indicated by alignments (**Figure 16**), a high performance liquid chromatography (HPLC)-based ATP hydrolysis assay was employed. Purified *Gt*FlhG was therefore incubated with ATP for 1h at 37 °C and subsequently subjected to isocratic (flow rate 0.8 ml/min) reversed-phase HPLC using a C18 column. 2 mM ATP was added to the protein to start the reaction. The nucleotides ATP and adenosine diphosphate (ADP) were monitored on the UV detector at 260 nm and quantified by determining the respective peak areas using ChemStation.

This assay provided evidence that *Gt*FlhG is indeed an ATPase with an activity of 51.2 ± 2.4 $nmol(ATP)*h^{-1}*nmol(enzyme)^{-1}$ under assay conditions. As a control the D60A variant of *Gt*FlhG was generated, which is supposed to be defective in magnesium binding and therefore catalytically silent. Our hydrolysis assays corroborated this assumption, as no catalytic activity of *Gt*FlhG D60A was detectable. Upon addition of lipids from a commercial *E. coli* polar lipid extract (Avanti polar lipids), the ATPase activity of *Gt*FlhG increases by factor of 1.4 to 82.1 ± 3.6 $nmol(ATP)*h^{-1}*nmol(enzyme)^{-1}$ under assay conditions (**Figure 18A**). This shows the importance of lipids for the ATPase activity of FlhG and indicates a possible membrane interaction of FlhG during the ATPase cycle. However, a

hydrolysis activating protein (like MinE for MinD in *E. coli*) was not identified, although several putative candidates were tested (FliM/FliY, DivIVA, GpsB).

(A)

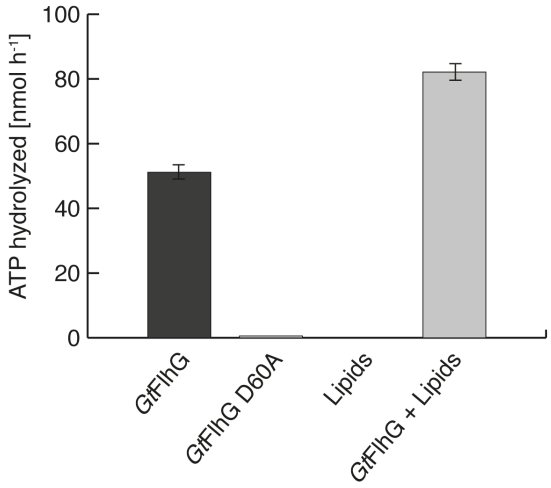

(B)

	ATPase activity [nmol(ATP)*h^{-1}*nmol(enzyme)$^{-1}$]
*Ec*MinD	4.4[a]
*Ec*MinD + *Ec*MinE + lipids	35.5[a]
*Gt*FlhG	51.2 ± 2.4
*Gt*FlhG + lipids	82.1 ± 3.6

Figure 18. ATP hydrolysis of *Gt*FlhG. (A) The results of the HPLC-based hydrolysis assays display the catalytic activity of *Gt*FlhG, the catalytic deficient variant *Gt*FlhG D60A and *Gt*FlhG in the presence of lipids. Lipids alone have no effect on ATP hydrolysis. The experiments were performed in triplicates indicated by the error bars. **(B)** The table summarizes the catalytic activity of *Gt*FlhG and *Ec*MinD under the respective assay conditions. [a] The results for *Ec*MinD are taken from ref (202).

The ATPase activity of MinD from *E. coli* was determined using an assay based on radioactive labelled ATP (203, 204). The assay was also performed at 37 °C for 1 h, however, only 1 mM ATP was supplemented to the reaction. *Ec*MinD displayed a basal ATPase activity of 4.4 nmol(ATP)* h^{-1}*nmol(enzyme)$^{-1}$ under the respective conditions (202). Upon addition of MinE, which triggers ATP hydrolysis in MinD, and the presence of phospholipids the activity increased to 35.5 nmol(ATP)* h^{-1}*nmol(enzyme)$^{-1}$ (**Figure 18B**) (202). These data indicate that the hydrolysis rate of *Gt*FlhG rather corresponds to the hydrolysis rate of an activated *Ec*MinD/MinE complex in the presence of phospholipids than to MinD in its apo state. This remains plausible, even considering that, in the initial assays 1 mM ATP instead of 2 mM was used, and that *Gt*FlhG is derived from a moderate thermophile organism with an optimal performance at elevated temperatures.

2.1.3 Crystallization of FlhG

Purified *Gt*FlhG was concentrated to ~11 mg/ml. Crystallization was performed by the sitting drop method in 96-well plates and initial hits were obtained in the Joint Center for Structural Genomics (JCSG) core suite I B3 (0.1 M HEPES, pH 7.5; 10 % (w/v) Polyethylenglycol (PEG) 8000). The crystal quality was improved using fine and additive screens as well as seeding with small crystal fragments (**Figure 19**) (195).

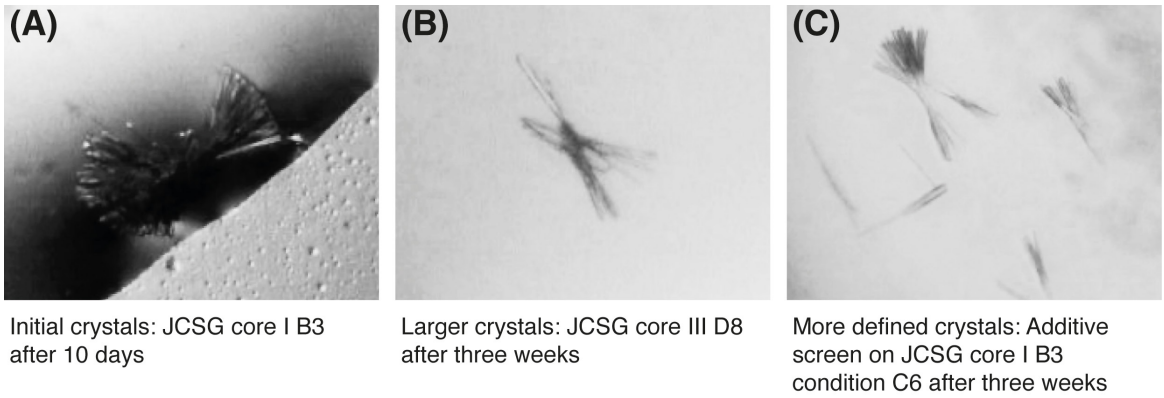

Figure 19. Crystallization of *Gt*FlhG. (A) Initial needles were obtained in JCSG core I B3 (0.1 M HEPES, pH 7.5; 10 % (w/v) PEG 8000) after 10 days of growth. **(B)** After three weeks more defined needles were observed in JCSG core III D8 (0.1 M HEPES, pH 7.0; 5 % (w/v) PEG 6000). **(C)** An additive screen (96 conditions) on JCSG core I B3 also provided more defined needles in condition C6 (0.1 M HEPES, pH 7.5; 10 % (w/v) PEG 8000 + 0.1 M urea). The figure was adapted from ref. (195).

High quality crystals were gained after three weeks and flash frozen in liquid nitrogen after a short incubation in a cryo-protecting solution that consisted of mother-liquor supplemented with 20 % (v/v) glycerol.

2.1.4 Structure determination and refinement of FlhG

Data collection was performed at the European Synchrotron Radiation Facility (ESRF) in Grenoble, France under cryogenic conditions (100 K) at the beamline ID 23-2 to a diffraction limit of 2.8 Å resolution (195). Data were recorded with a DECTRIS PILATUS 6M detector. Data processing was carried out using iMosflm (205) and the CCP4-implemented program SCALA (206). The structure of apo-

FlhG was solved by molecular replacement (MR) with CCP4-integrated PHASER (207) using a monomer of the *Ec*MinD dimer (pdb: 3QL9) as search model at 2.8 Å resolution (**Table S1**). Structures were manually built in COOT (208) and refined using PHENIX refine (209). The structure was refined to an R_{work}/R_{free} of 17.7/22.8. The crystal structure of the *Gt*FlhG monomer was deposited in the protein data bank (pdb) with the entry 4RZ2. Figures were designed with PyMol (www.pymol.org).

2.1.5 Crystal structure of monomeric FlhG

To get insights into the structure and the functional role of FlhG, its crystal structure was determined at 2.8 Å resolution (**Table S1**). The structure was complete except for amino acid residues 1-20 and 265-274 most likely due to flexibility or degradation.

The overall shape of the *Gt*FlhG monomer resembles a half sphere and exhibits the typical MinD fold. The protein core is composed of 7 parallel and one antiparallel β-strands which are surrounded by 10 α-helices (**Figure 20A**). The monomeric structures of *Gt*FlhG and MinD from *E. coli* (pdb: 3QL9) superimpose with a root mean square deviation (r.m.s.d.) of 2.3 $Å^2$ for 160 Cα-atoms revealing a highly conserved protein core with minor deviations in the helical periphery (153).

The main peripheral changes in *Gt*FlhG include an extension of helix α7, and a loop that replaces two helical segments, one between α6 and β7 and the other between β7 and α7 found in MinD (**Figure 20BC**). Structural analysis identified FlhG as a MinD-like ATPase, sharing fold and structural elements for ATP hydrolysis and dimerization.

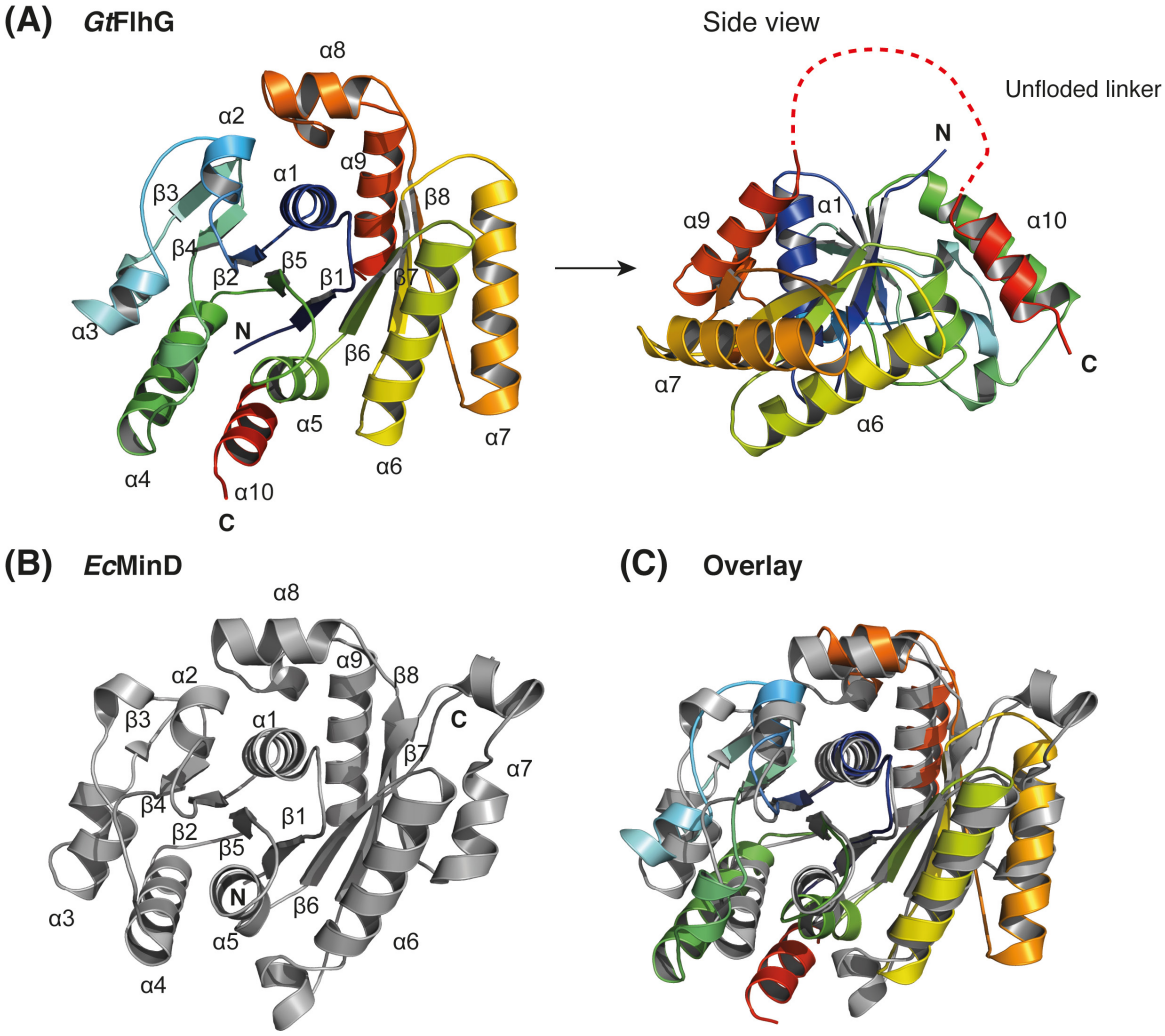

Figure 20. Crystal structure of *Gt*FlhG. (A) shows the cartoon representation of the monomeric crystal structure of *Gt*FlhG (pdb: 4RZ2) coloured in rainbow from the bottom as well as a lateral side. Secondary structure elements as well as N- and C-terminus are indicated. A flexible linker (indicated as dashed line) connects the protein core and α10. **(B)** displays a cartoon representation of a *Ec*MinD monomer in grey (pdb: 3Q9L) and **(C)** represents an overlay of *Gt*FlhG (rainbow) and *Ec*MinD (grey).

2.2 FlhG interacts with the membrane via its MTS

A hallmark feature of MinD is its C-terminal amphipathic helix, which tethers the MinD dimer to the membrane, thereby recruiting MinC to the membrane where it inhibits the polymerisation of FtsZ (151, 210). Moreover, it generates two distinct locally separated states during the ATPase cycle, an ATP-dependent dimer at the membrane and a monomer, which is diffusible in cytoplasm and thus these states

are crucial for the regulation process. Sequence alignments strongly indicate that this C-terminal amphipathic helix is conserved in FlhG from different organisms (**Figure 21A**). Additionally, helical wheel projections of *Ec*MinD and *Gt*FlhG emphasise the amphipathic propensity of the C-terminus of FlhG from *G. thermodenitrificans* (rzlab.ucr.edu) (**Figure 21B**). The C-terminus of *Gt*FlhG seems to possess a strong amphipathic character, compared to *Gt*MinD and *Bs*FlhG.

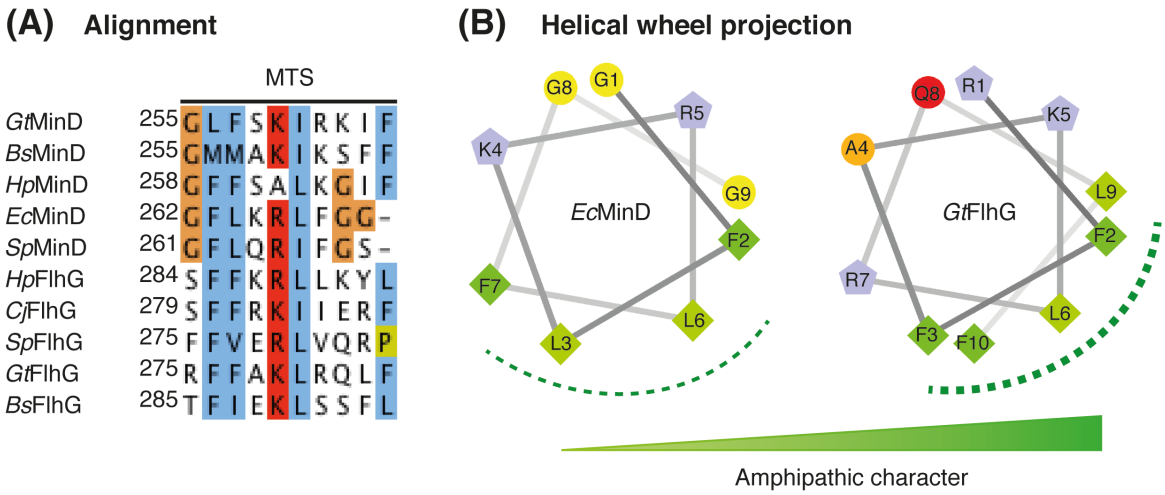

Figure 21. A C-terminal amphipathic helix. (A) Sequence alignment of the C-terminal helix of MinD and FlhG proteins displays conserved residues. Organisms are abbreviated: *G. thermodenitrificans* (*Gt*); *B. subtilis* (*Bs*); *H. pylori* (*Hp*); *E. coli* (*Ec*); *S. putrefaciens* (*Sp*) and *C. jejuni* (*Cj*). **(B)** A helical wheel projection of the C-terminal helix of *Ec*MinD and *Gt*FlhG reveals an amphipathic character (www.rzlab.ucr.edu). The hydrophobic side is depicted as dashed line. The increasing amphipathic character is indicated in shades of green.

2.2.1 Crystal structure of the C-terminal amphipathic helix

The crystal structure of the *Gt*FlhG monomer resolves the C-terminal amphipathic helix, which has never been resolved in any available MinD structure so far.

Helix α10 is nestled into a hydrophobic groove mainly formed by helices α4 and α5 (**Figure 22**). The structure suggests that this C-terminal helix α10 plays an essential role in membrane binding of FlhG, in the same way as observed for MinD (163).

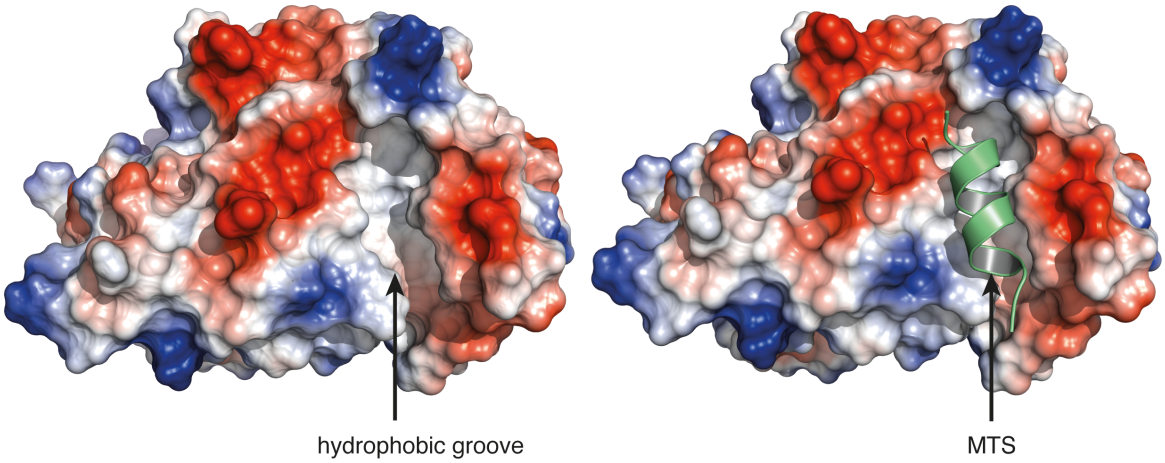

Figure 22. Hydrophobic cleft for MTS binding. The Electrostatic surface (positive charges are indicated in blue, negative charges in red) of *Gt*FlhG (pdb: 4RZ2) shows the hydrophobic cleft (indicated by an arrow, *left*) into which the MTS (lime green) is bound (*right*) in the monomeric crystal structure of *Gt*FlhG.

2.2.2 α10 is an autonomous and transplantable MTS

To investigate whether helix α10 functions as membrane targeting sequence, a fusion protein was generated, which comprises helix α10 adjacent to a green-fluorescent reporter protein (GFP). The *gfp-α10* fusion was expressed in *E. coli* and its subcellular localization was observed using high-resolution fluorescence microscopy (**Figure 23AB**). Indeed, GFP-α10 exclusively localized at the cytoplasmic side of the inner membrane implicating that helix α10 constitutes an autonomous and transplantable MTS. To show that membrane localization results from helix α10 a mutation was introduced which was supposed to abolish membrane association.

As hydrophobic interactions play a vital role for membrane attachment, two highly conserved neighbouring phenylalanine residues (F275 and F276) within helix α10 were replaced by alanine (GFP-α10 F2A). Uniformly fluorescent *E. coli* cells were observed upon production of GFP-α10 F2A displaying that helix α10 attaches GFP to the membrane (**Figure 23AB**). Furthermore, this also shows that phenylalanine 275 and 276 are crucial for the function of the MTS in *Gt*FlhG.

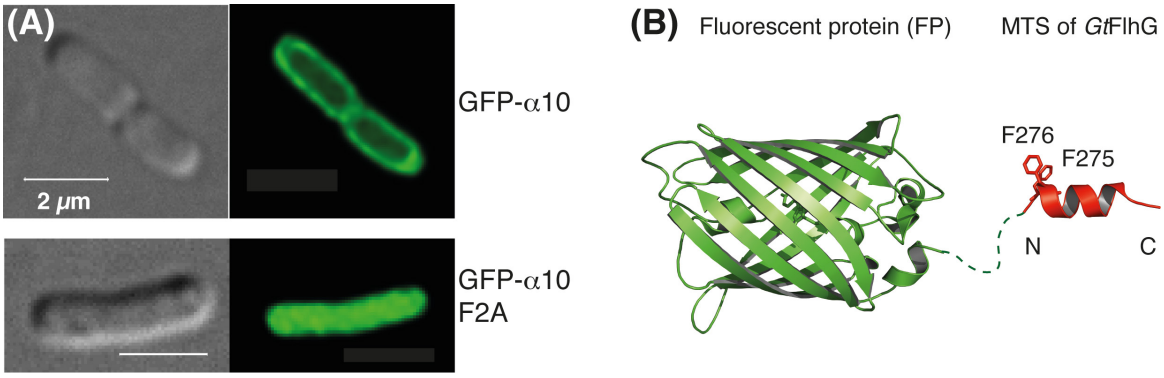

Figure 23. Autonomous MTS of FlhG. (A) Fluorescence microscopy images of *E. coli* expressing *gfp-α10* (*top*) and *gfp-α10 F2A* (*bottom*) show that helix α10 of *Gt*FlhG is an autonomous MTS. The scale bars equal 2 µm as indicated. **(B)** displays a scheme of the GFP-α10 (pdb: 1F0B (FP); pdb: 4RZ2 (*Gt*FlhG MTS)) fusion construct used for this experiment. Amino acid residues F275 and F276 of *Gt*FlhG are shown as sticks and are indicated.

2.2.3 Flotation assays

To further characterize the ability of *Gt*FlhG to associate with membranes, flotation assays with large unilamellar vesicles (LUVs) were performed (195). The vesicles were composed of 70 % of the neutral phospholipid 2-oleoyl-1-palmitoyl-*sn*-glycero-3-phosphoethanolamine (PE) and 30 % of the anionic phospholipid 1-palmitoyl-2-oleoyl-*sn*-glycero-3-phospho-(1'-rac-glycerol)(sodium salt) (PG), which represents the composition of a model membrane (211) and were generated using an extrusion technique. The target protein was incubated with LUVs as well as the respective nucleotide and subsequently overlaid with a gradient of iodixanol. During ultra centrifugation LUVs float from the bottom to the top of the centrifugation tube along the gradient of iodixanol dragging vesicle bound proteins with them (**Figure 24A**). After centrifugation the content of the tubes were separated into three samples (top, middle and bottom) and their protein content was visualized using Coomassie-stained SDS-PAGE (**Figure 24B**). In this case, *Gt*FlhG was incubated with LUVs and additionally either ADP or 5′-adenylylimidodiphosphate (AMPPNP), which is a non-hydrolysable analogue of ATP.

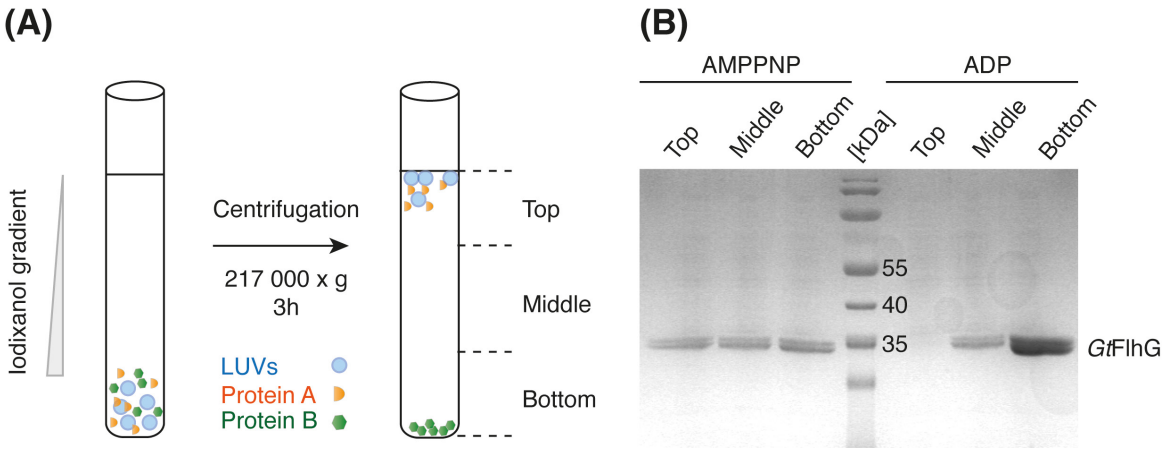

Figure 24. Flotation assays. A scheme of the flotation assays is given in **(A)**. LUVs (blue) float along an iodixanol gradient (indicated in grey) during ultra-centrifugation carrying LUV bound proteins (orange) with them to the top, while unbound proteins (green) remain at the bottom. **(B)** Coomassie-stained SDS-PAGE of the flotation experiment (195). The iodixanol gradient was separated into three fractions.

In the presence of ADP the major portion of *Gt*FlhG remained in the bottom fraction and a minor part was observed in the middle fraction, indicating no or only weak interaction with the vesicles. Upon addition of AMPPNP, *Gt*FlhG was detected in all three fractions in equal amounts (**Figure 24B**). This demonstrates that the interaction of *Gt*FlhG and lipids is ATP-dependent, which is reminiscent to MinD.

2.3 Crystal structure of homodimeric FlhG

Our membrane interaction studies revealed that FlhG and MinD share the same nucleotide dependent membrane binding behaviour. The ability of MinD to associate with lipid membranes depends on the presence of ATP, due to the dimerization of MinD, which is induced upon ATP addition. This led to the assumption that FlhG, as MinD, is able to form homodimers. In order to crystallize the *Gt*FlhG homodimers, a variant of FlhG (D60A) was generated that is deficient in magnesium binding and hence catalytically inactive, as confirmed by our HPLC-based hydrolysis assays (**Figure 18**). The respective mutation in MinD was used to successfully crystallize MinD in its dimeric state (153).

2.3.1 Purification of FlhG D60A

*Gt*FlhG D60A was purified as stated for the wild-type protein and also heavily precipitated as observed for *Gt*FlhG. In short, *Gt*FlhG D60A was purified using a His trap column and subsequently subjected to SEC (**Figure 25**). The UV detection during SEC revealed that *Gt*FlhG D60A was obtained in larger amounts, than *Gt*FlhG, evident through increased peak height and thus peak area. After SEC, *Gt*FlhG D60A was concentrated to 12 mg/ml, where it heavily precipitated. The concentration was determined on the nano drop (ε = 24 400 $M^{-1}cm^{-1}$).

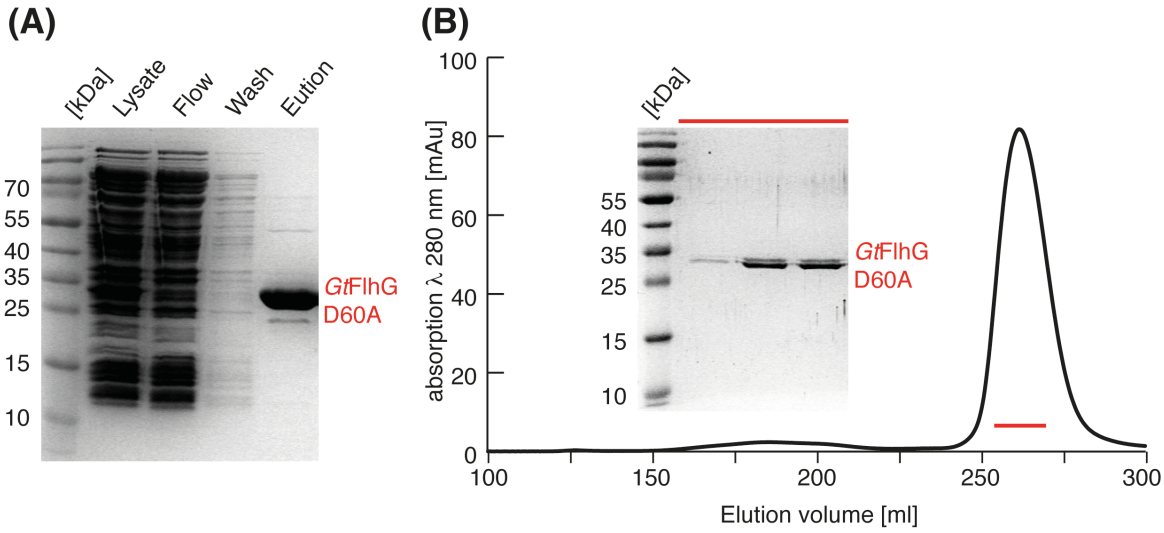

Figure 25. Purification of *Gt*FlhG D60A. (A) displays the Coomassie-stained SDS-PAGE of the Ni-NTA affinity purification of *Gt*FlhG D60A. The elution fraction mainly contains *Gt*FlhG D60A. **(B)** The size exclusion chromatogram shows a single peak. The inlay represents the corresponding Coomassie-stained SDS-PAGE of the peak fractions (indicated in red) confirming that *Gt*FlhG D60A is the major protein component of the peak fractions.

2.3.2 Crystallization of FlhG D60A

Again, crystallization was performed by the sitting drop method in 96-well plates using the JSCG core suite screens in the presence of ATP and adenylyl-imidodiphosphate (AMPPNP). With AMPPNP no crystals were observed even after several weeks. In the presence of ATP however, high quality crystals were

gained after three weeks in JCSG core I in C10 (0.1 M HEPES, pH 7.0; 20 % (w/v) PEG 6000) (**Figure 26**). Crystals were flash frozen in liquid nitrogen after a short incubation in a cryo-protecting solution that consisted of mother-liquor supplemented with 20 % (v/v) glycerol (195).

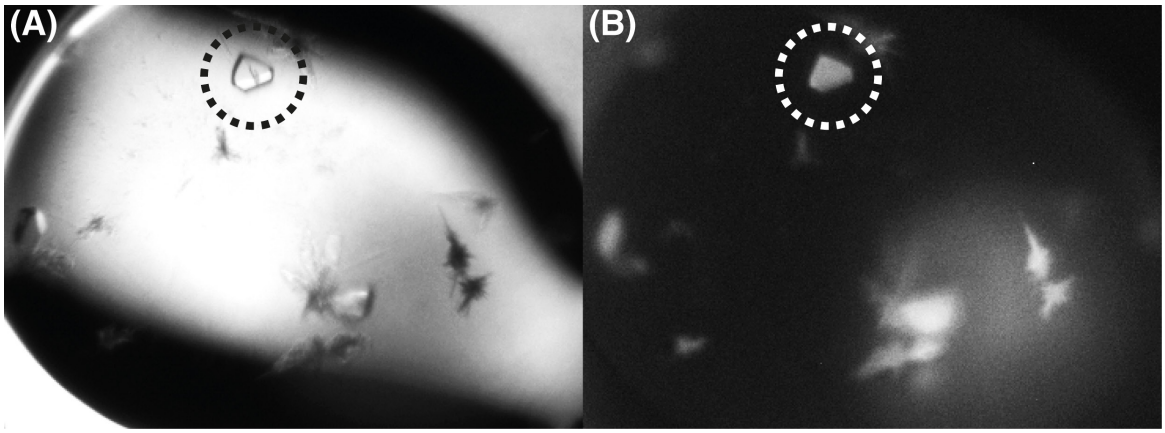

Figure 26. Crystallization of *Gt*FlhG D60A. (A) shows crystals of *Gt*FlhG D60A in the presence of ATP grown after three weeks in JCSG core I, C10 (0.1 M HEPES, pH 7.0; 20 % (w/v) PEG 6000). **(B)** The UV image of the *Gt*FlhG D60A crystals indicates that these crystals are indeed protein crystals. The indicated crystal (dashed lines) diffracted to 1.8 Å. The figure was adapted from ref. (195).

2.3.3 Structure determination of FlhG D60A

Diffraction data of the indicated crystal (**Figure 26**) were collected at the ESRF in Grenoble, France under cryogenic conditions (100 K) at the beamline ID 23-1 to a diffraction limit of 1.8 Å resolution (195). Data were recorded with a DECTRIS PILATUS 6M detector. Diffraction images were processed using iMosflm (205) and the CCP4-implemented program SCALA (206). The structure of dimeric *Gt*FlhG D60A was solved by MR with CCP4-integrated PHASER (207) using monomeric *Gt*FlhG (pdb: 4RZ2) as search model at 1.9 Å resolution (**Table S1**). The structures were manually built in COOT (208) and refined using PHENIX refine (209). The structure was refined to an R_{work}/R_{free} of 22.1/26.0. Two ADPs were identified in the active sites of the *Gt*FlhG D60A dimer. The crystal structure of the *Gt*FlhG D60A dimer was deposited in the pdb with the entry 4RZ3. Figures were designed with PyMol (www.pymol.org).

2.3.4 Overall structure of FlhG D60A

The crystal structure of *Gt*FlhG D60A was obtained at 1.9 Å resolution (**Table S1**) and the structure was complete except for the first 20 amino acids and residues 265-287 due to either flexibility or degradation. The structure revealed an ADP bound *Gt*FlhG dimer, even though ATP was added prior to crystallization. This is presumably a result of the extended time period that was necessary for crystal growth (3-4 weeks). As for the monomer, the FlhG homodimer shows significant structural similarity to that of *Ec*MinD with an r.m.s.d. of 2.8 $Å^2$ over 329 C_α-atoms. Both dimers resemble an ellipse-like shape with similar dimensions of approximately 60 x 45 x 40 Å (**Figure 27**).

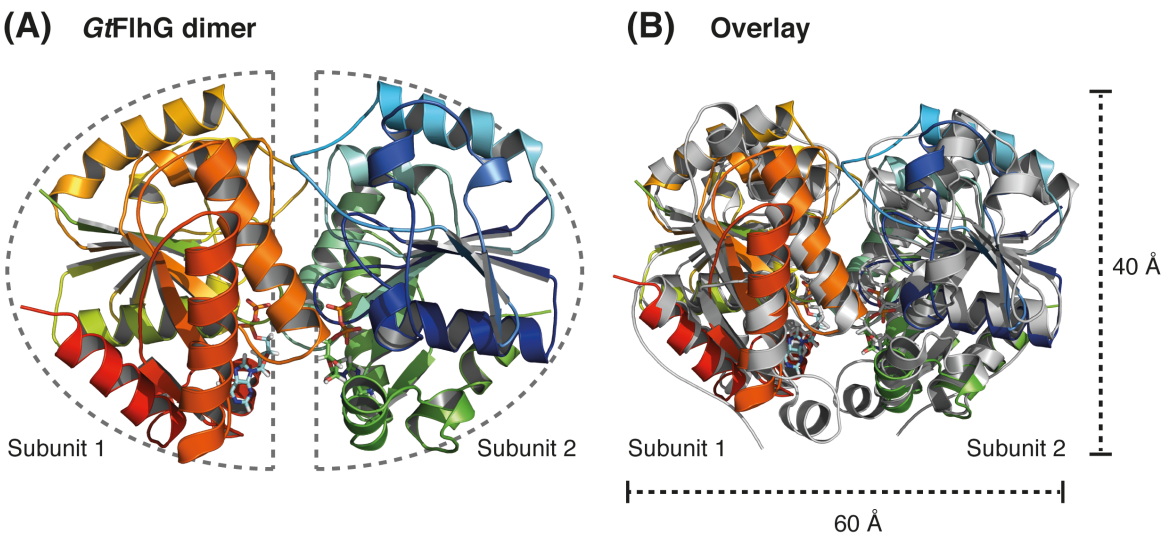

Figure 27. Structure of the *Gt*FlhG dimer. (A) Overview of the crystal structure of *Gt*FlhG D60A dimer (pdb: 4RZ3) presented as cartoon and coloured in rainbow. Grey dashed lines indicate the subunits of the dimer. **(B)** The overlay of the *Gt*FlhG dimer (rainbow) and the dimeric structure of *Ec*MinD (grey; pdb: 3Q9L) shows close structural homology. Dashed bars indicate the size of the dimers.

The subunits are arranged in the same 'face-to-face' orientation with similar P-loop distances of 3.7 and 3.8 Å between the P-loop glycines (*i.e.*, G32 and G12 in *Gt*FlhG and *Ec*MinD, respectively). As observed for MinD, the active site of FlhG is composed of highly conserved key motifs responsible for ATP binding, magnesium coordination or ATP hydrolysis. The prominent P-loop or deviant Walker A

motif of MinD/ParA ATPases (GKxxxGKT/S) is composed of a loop region and an adjacent helical turn (**Figure 28AB**) (212-214). It is involved in binding the phosphate moieties of ATP, by forming several hydrogen bonds between the amide nitrogen of the polypeptide backbone and the β-phosphate (**Figure 28B**). The P-loop contains two highly conserved lysine residues that fulfil vital tasks during the catalytic cycle. The second lysine (K36 in *Gt*FlhG) forms a polar interaction with oxygen of the γ-phosphate being involved in the positive cage, which neutralizes the dense negative charges of the nucleotide. The first one (K31 in *Gt*FlhG) is part of the dimer interface and spans into the active site of the other subunit providing the catalytic lysine for ATP hydrolysis. The P-loop constitutes the most important motif reflected by the fact that a whole family of GTPases and ATPases is named after this motif (P-loop NTPases) (119).

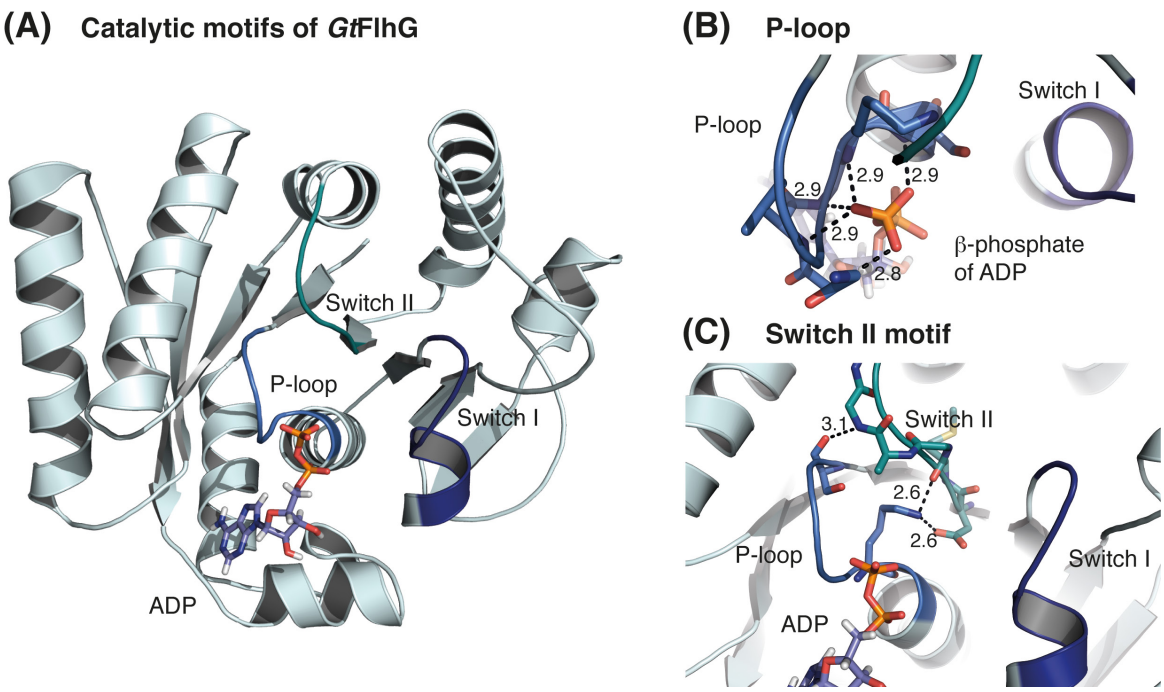

Figure 28. Catalytic motifs of *Gt*FlhG. (A) shows an overview of *Gt*FlhG (pdb: 4RZ3) with ADP bound in the active site. Catalytically important motifs are coloured in blue (P-loop), dark blue (Switch I) and cyan (Switch II). **(B)** The P-loop coordinates the β-phosphate of ADP in a nest of backbone amide moieties. The distances between the phosphate oxygen atoms and the amide nitrogen atoms are depicted in dashed lines. **(C)** The Switch II region indirectly contributes to ATP hydrolysis by stabilizing the P-loop through polar contacts. Hydrogen bonds are indicated with dashed lines and the respective distances are depicted.

The so-called Switch I motif (DIxxxNI) coordinates the magnesium ion, which is essential to compensate the accumulation of negative charges through the phosphate groups of ATP (**Figure 28**). Aspartate 60, which was replaced by Ala in order to obtain the structure of the FlhG dimer, is a key residue of the Switch I motif. Therefore, *Gt*FlhG D60A is supposed to be defective in magnesium binding and hydrolysis, locking the ATPase in an ATP bound dimeric state.

The Switch II motif assists in shaping the active site of the ATPase by forming polar contacts with the P-loop. The Switch II motif is less conserved than the other two and only indirectly involved in the ATP hydrolysis. However, it has an important function in the second row (**Figure 28C**).

The adenine base of the ATP is coordinated through arginine 194, which is able to form π-stacking interactions with the aromatic ring system of the base. Arginine 194 is held in place by glutamate 228 (**Figure 29A**). Nucleotide specificity is provided by a small motif conserved among ATPases. In order to distinguish ATP from other nucleotides like GTP, the ATPase has to read the topology of the distal end of the nucleotide.

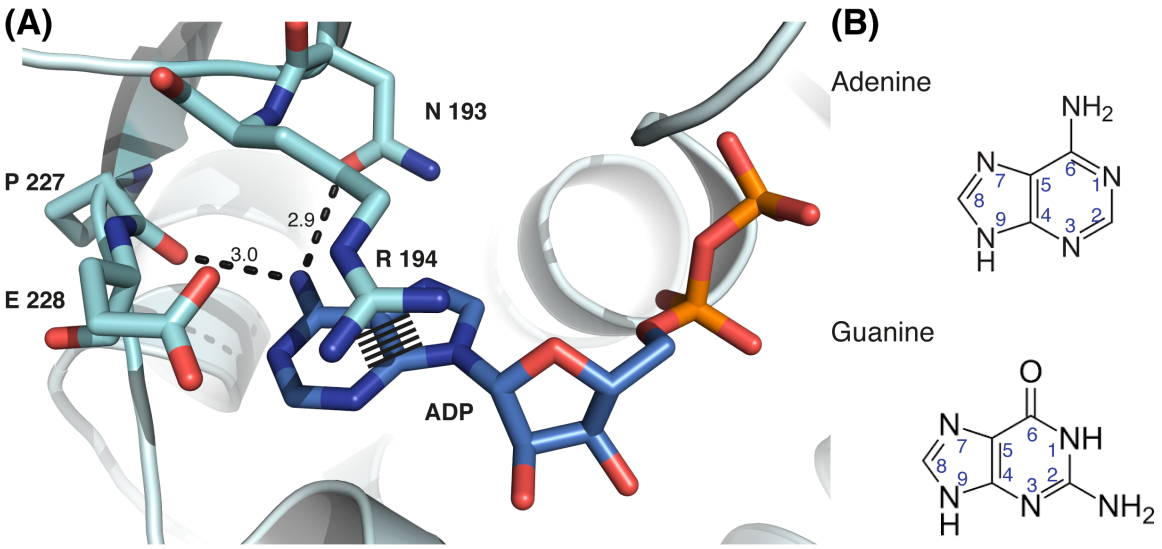

Figure 29. ATP coordination. (A) gives a detailed view of the nucleotide coordination of *Gt*FlhG (pdb: 4RZ3). Crucial residues are indicated. The dashed lines mark the hydrogen bonds to the amino group at position 6 of ADP, which provide the specificity for adenosine nucleotides. **(B)** shows the chemical structures of adenine and guanine, which differ at positions 2 and 6. Numbers indicate the respective positions in the nucleotide.

While adenine possesses an amine group, guanine displays a carbonyl moiety at position 6. Guanine has an additional amino group at position 2, which is absent in adenine (**Figure 29B**). The carbonyl group of the backbone of proline 227 as well as the side chain carbonyl group from asparagine 193 form hydrogen bonds with the amino group at position 6 of the adenine base. Binding of GTP would force two to three carbonyl oxygen atoms in close proximity, which would immediately generate a repulsive interaction (**Figure 29A**).

Structural comparison of the composite active sites of the *Gt*FlhG and *Ec*MinD homodimers shows that all elements required for ATP hydrolysis (P-loop and Switch II motif), magnesium binding (Switch I motif) and nucleotide binding are structurally conserved between FlhG and MinD (**Figure 30**). Furthermore, the nucleotide itself is located at the same position and in a highly similar orientation in both proteins (**Figure 30**). These findings fit ideally to previous results all demonstrating that FlhG and MinD share the same hallmark features such as ATP-dependent homodimerization and membrane association.

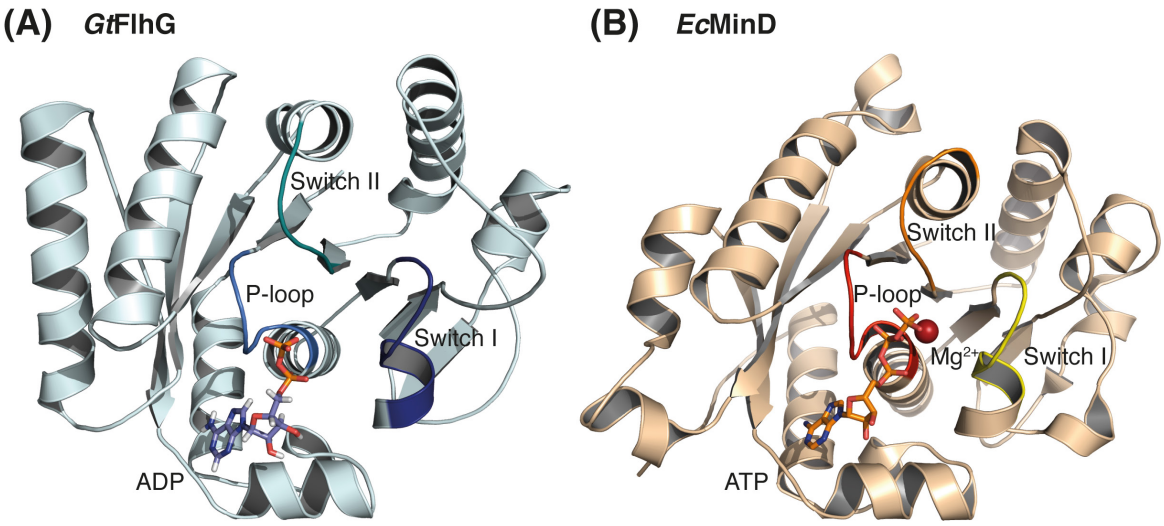

Figure 30. Catalytic motifs in FlhG and MinD. Overview of *Gt*FlhG (pdb: 4RZ3) **(A)** in light cyan and *Ec*MinD (pdb: 3Q9L) **(B)** in orange with ADP and ATP bound in the active site, respectively. Catalytically important motifs of *Gt*FlhG are coloured in blue (P-loop), dark blue (Switch I) and cyan (Switch II). The respective regions of *Ec*MinD are indicated in red (P-loop), yellow (Switch I) and orange (Switch II).

However, an evident difference between *Gt*FlhG and *Ec*MinD is a protrusion in *Gt*FlhG that originates from an extension of helix α7 of about two to three turns

(**Figure 31A**). *Ec*MinD instead possess two short additional helical segments, one before helix α6 (α6a) and one adjacent helix α7 (α7b) (**Figure 31B**). These topological differences may represent modified interaction interfaces, allowing MinD and FlhG to interact with different proteins. Notably, *Ec*MinD exhibit a larger dimer interface (~1000 Å^2) than *Gt*FlhG (~700 Å^2). The short helical segment in front of helix α7 contributes to dimer formation in MinD, which is absent in *Gt*FlhG. On the other hand helix α7 of FlhG is longer forming the C-ring interface.

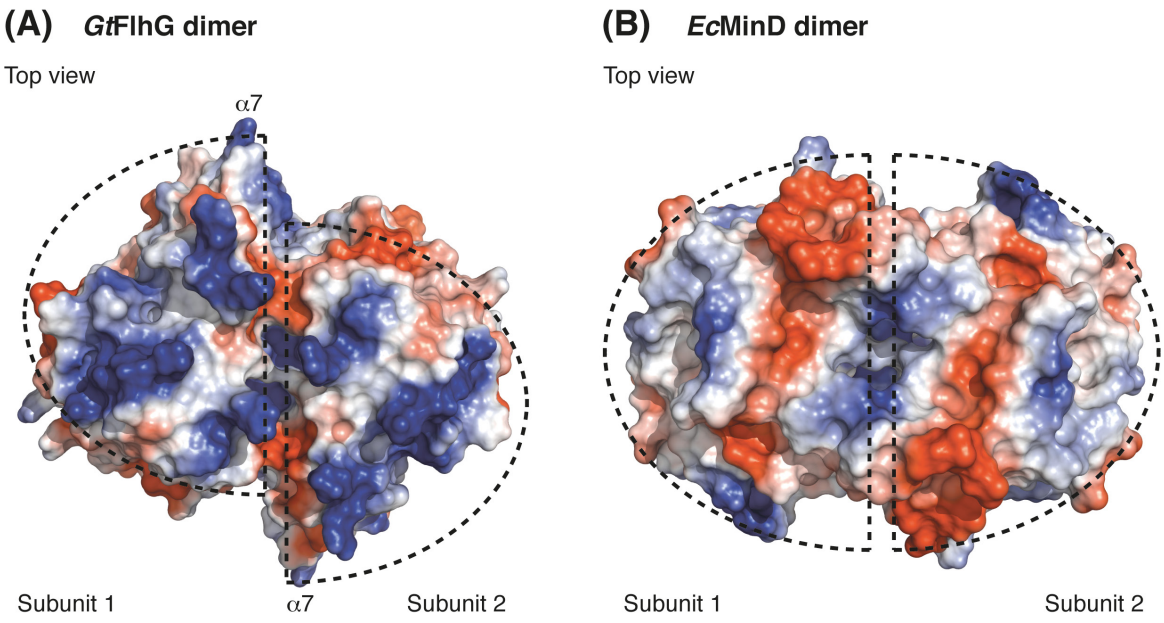

Figure 31. Electrostatic surface of FlhG and MinD. Electrostatic surface representation of *Gt*FlhG (pdb: 4RZ3) **(A)** and *Ec*MinD (pdb: 3Q9L) **(B)** displays differences in surface charge distribution. Furthermore, helix α7 of *Gt*FlhG is indicated and forms a wing-like protrusion at either side of the FlhG Dimer. Surface charges are colour-coded from positive (blue) to neutral (white) to negative (red).

Also the C-terminal tip of helix α1 of *Ec*MinD is involved in dimer formation through polar contacts to helix α1 of the other subunit within the dimer (**Figure 32**). This might indicate that the *Ec*MinD dimer is more stable than the *Gt*FlhG dimer.

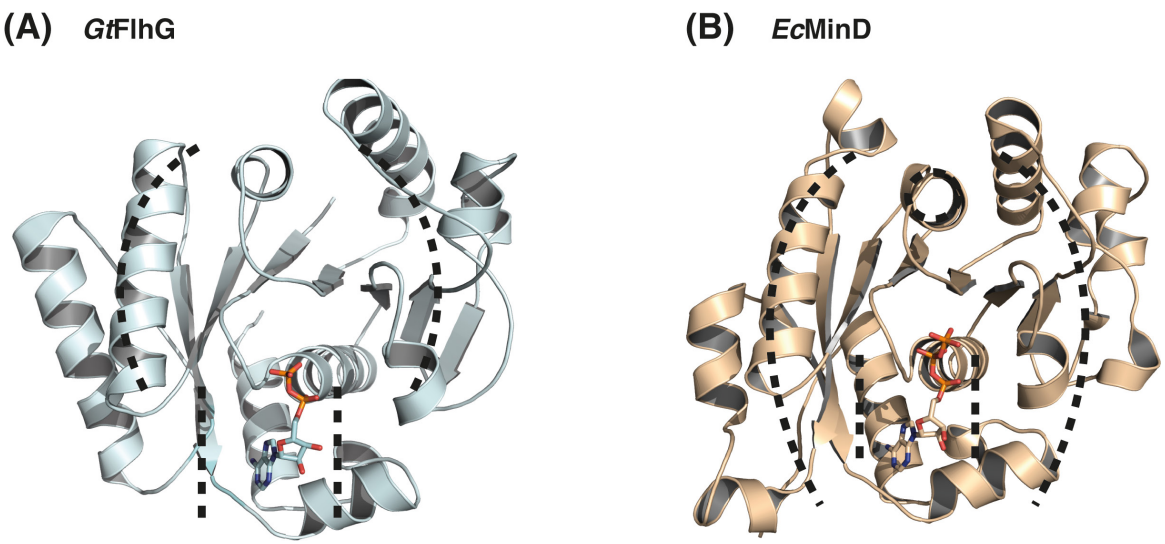

Figure 32. Dimer interfaces of the FlhG and MinD Dimers. Monomers of the *Gt*FlhG dimer (pdb: 4RZ3) **(A)** and the *Ec*MinD dimer (pdb: 3Q9L) **(B)** are shown in light cyan and orange, respectively. The black dashed lines indicate the respective dimer interface.

Taken together, *Gt*FlhG and *Ec*MinD share the same MinD/ParA ATPase fold and all vital motifs for ATPase activity. Subtle topological differences include helix α7 and the neighbouring regions, resulting in a larger dimer interface in *Ec*MinD and wing-like protrusion in the *Gt*FlhG dimer. These topological modifications may hint towards interaction interfaces with different proteins.

2.3.5 Conformational rearrangements upon dimerization

Intriguingly, the MTS, which was present in the structure of the *Gt*FlhG monomer, is absent in the homodimer. Furthermore, *Gt*FlhG features significant structural rearrangements upon changing between the monomeric, MTS bound and the dimeric 'closed' state. Monomeric *Gt*FlhG represents the 'open' state because helices α4 and α5 are orientated parallel to each other forming a hydrophobic groove into which the MTS is nestled. Upon transition into the 'closed' conformation a helical segment is transformed into an extensive loop (dimerization loop), which is part of the dimer interface and thus required for dimer formation. The hydrophobic groove is closed through helix α5, which bends towards the protein core (**Figure 33AB**). As a result the MTS is exposed to the environment

and thus able to attach to lipids (**Figure 33AC**). In this state, the MTS is very flexible and can easily be degraded during the crystallization process and is therefore no longer visible in the crystal structure of the *Gt*FlhG homodimer.

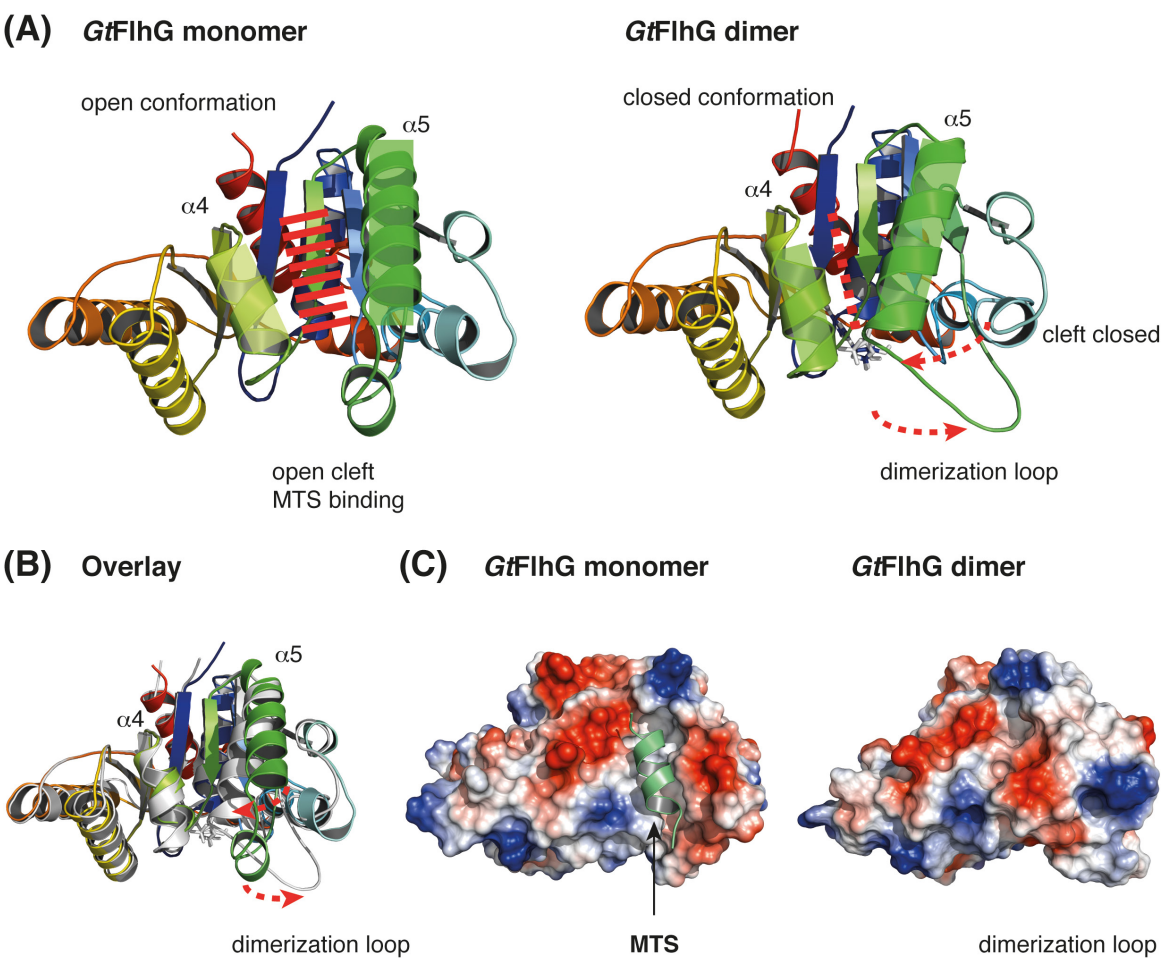

Figure 33. Conformational rearrangements in FlhG. (A) A side-by-side view of the *Gt*FlhG monomeric (pdb: 4RZ2) (*left*) and dimeric (pdb: 4RZ3) (*right*) state coloured in rainbow shows structural rearrangements upon dimer formation. Helices α4 and α5 are indicated. A red dashed line marks the cleft where the MTS binds in the open conformation of *Gt*FlhG. Red dashed arrows mark the major rearrangements. **(B)** displays an overlay of the open monomeric state of FlhG (rainbow) and the closed dimeric state coloured in grey. Red dashed arrows indicated the major rearrangements. **(C)** A Side-by-side view of the electrostatic surface of *Gt*FlhG monomeric (*left*) and dimeric (*right*) state indicates the closure of the MTS cleft in the dimeric state. The green helix represents the MTS in the open state. Surface charges are again colour-coded from positive (blue) to neutral (white) to negative (red).

These findings demonstrate that dimer formation of FlhG seems unlikely to occur as long as the MTS is associated to FlhG because in this state, a part of the di-

mer interface is hidden. Only after exposure of the MTS, the dimer interface is fully revealed and renders FlhG capable of dimer formation. However, whether ATP binding or the presence of lipids trigger the transition from the 'open' to the 'closed' state remains unclear. The fact that *Gt*FlhG is in its monomeric state in solution, which was confirmed by SEC, strongly indicates that the presence of a membrane triggers the conformational transition, which allows dimerization (**Figure 33**). Still, one cannot exclude that dimerization may also require the presence of a membrane and ATP simultaneously. These observations provide the molecular explanation for the interconnection of MTS-mediated membrane association and nucleotide-dependent homodimer formation of *Gt*FlhG.

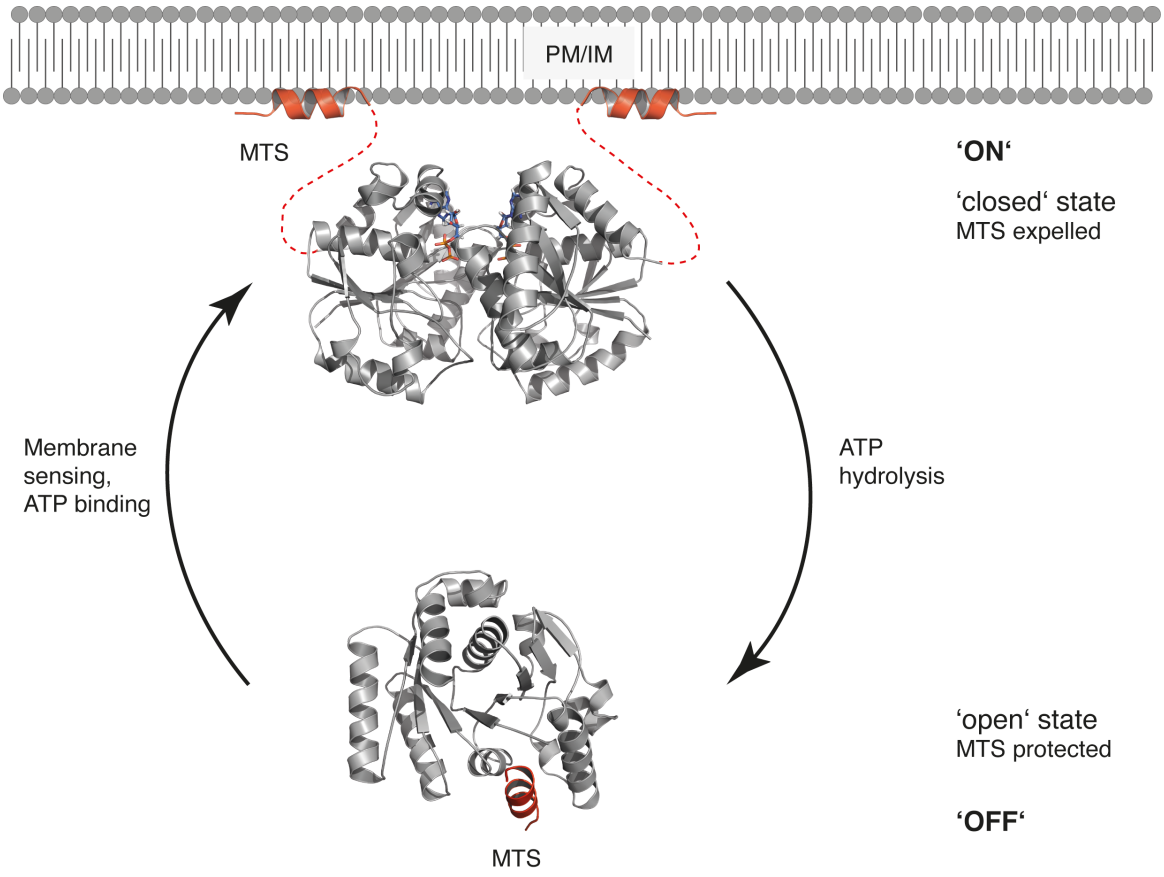

Figure 34. Regulatory circuit of FlhG. The scheme illustrates that FlhG has two distinct state, a dimeric membrane-associated 'ON' state and a cytoplasmic monomeric 'OFF' state and therefore forms a regulatory switch. (MTS: membrane targeting sequence, PM: plasma membrane, IM: inner membrane; pdbs: 4RZ2 and 4RZ3).

Taken together, FlhG is a molecular switch with two spatially separated and mutually exclusive states. In its canonical 'ON' state FlhG is associated to a mem-

brane in its dimeric conformation through its C-terminal MTS. ATP hydrolysis triggers the transition into the canonical 'OFF' state, where monomeric FlhG is freely diffusible in the cytoplasm. In this conformation the MTS is nestled into a hydrophobic cleft of FlhG and thus protected (**Figure 34**).

2.4 The Interaction network of FlhG

Having elucidated fundamental features of FlhG itself, I aimed at investigating how these are implemented in the complex regulatory process of flagellation pattern maintenance. It is therefore necessary to identify interaction partners of FlhG. A summary of the current literature in the introduction section showed that the interaction network of FlhG is poorly understood and essential pieces are still missing. Besides FlhF, no interaction partner of FlhG was identified in *B. subtilis* so far (118). Therefore, an affinity pull down assay with FlhG and an appropriate tag was used as bait against whole cell lysate of *B. subtilis*.

2.4.1 Interaction of FlhG with FliM and FliY

An N-terminal glutathione-S-transferase (GST) fusion of *Bs*FlhG was generated. Immobilized GST-*Bs*FlhG was incubated with freshly prepared cell lysate from *B. subtilis* and the protein content was visualized by Coomassie-stained SDS-PAGE after elution of GST-*Bs*FlhG. Electrospray ionization (ESI) mass spectrometry identified the flagellar C-ring proteins FliM and FliY as putative interaction partners of FlhG (**Figure 35A**) (data of G. Bange and N. Kümmerer).

This interaction was confirmed repeating the pull down experiment with purified proteins from *B. subtilis* (**Figure 35A**) and to be consistent with the structure, also with GST-FlhG, FliM and FliY derived form the thermophile *G. thermodenitrificans* (GST-*Gt*FlhG, *Gt*FliM and *Gt*FliY; **Figure 35B**). Due to their improved solubility and stability further biochemical analysis was performed with proteins from the *G. thermodenitrificans* and labelled respectively.

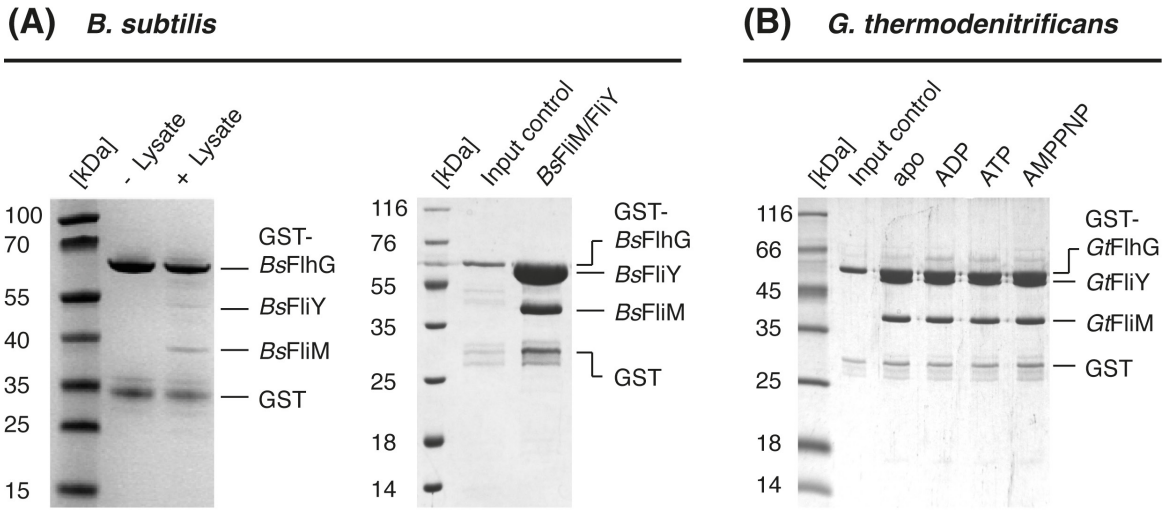

Figure 35. Interaction of FlhG with FliM and FliY. (A) shows the Coomassie-stained SDS-PAGEs of pull down assays with GST-*Bs*FlhG incubated with freshly prepared *B. subtilis* lysate (left). These pull down assays were repeated using a purified *Bs*FliM/FliY complex (*right*). **(B)** shows the Coomassie-stained SDS-PAGE of pull down assays with GST-*Gt*FlhG and a complex of the C-ring proteins *Gt*FliM and *Gt*FliY derived from the moderate thermophile *G. thermodenitrificans* without nucleotides as well as in the presence of ADP, ATP or AMPPNP.

As a final proof for a stable interaction of these three proteins, a ternary complex was reconstituted on SEC.

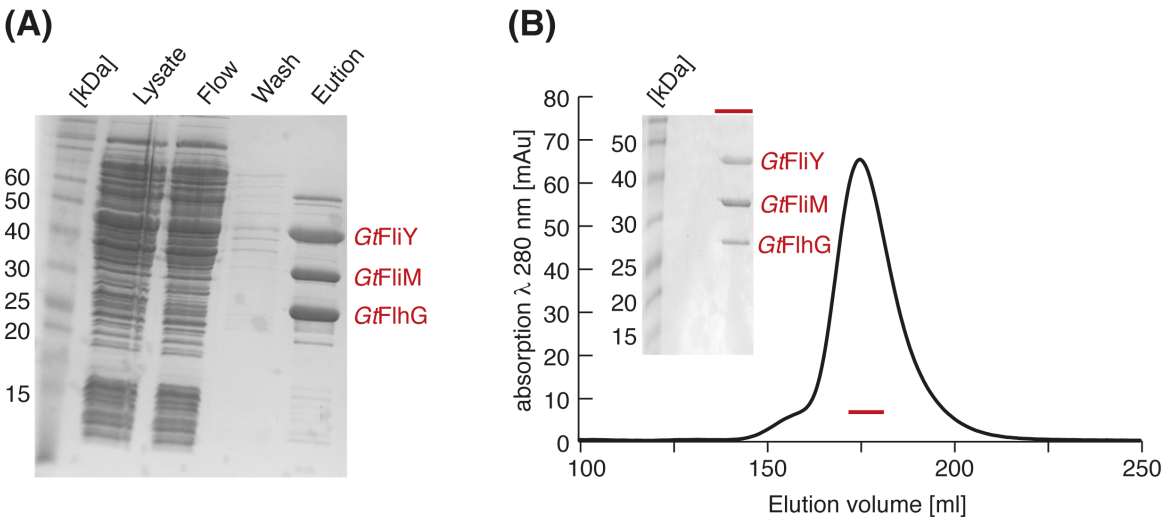

Figure 36. Purification of a ternary complex of *Gt*FliM/FliY/FlhG. (A) displays the Coomassie-stained SDS-PAGE of the Ni-NTA affinity purification of the ternary complex *Gt*FliM/FliY/FlhG. **(B)** shows the respective size exclusion chromatogram shows a single peak. The inlay represents the corresponding Coomassie-stained SDS-PAGE of the peak fractions (indicated in red).

The purification was performed using $(His)_6$-tagged *Gt*FlhG and *Gt*FliM, while *Gt*FliY remained untagged. In this combination contaminating, excrescent FliY is washed away during affinity purification. After Ni-NTA affinity chromatography all three proteins *Gt*FlhG, *Gt*FliM and *Gt*FliY were detected in a 1:1:1 ratio. Subsequent SEC resulted in a single peak (**Figure 36**). The elution volume corresponds to a globular particle of around 2.5 MDa, indicating that *Gt*FlhG, *Gt*FliM and *Gt*FliY form macromolecular complexes *in vitro*.

To characterize the interaction of *Gt*FlhG with the flagellar C-ring, pull down experiments were also performed in the presence of different nucleotides (ADP, ATP and AMPPNP). However, none of the nucleotides had any influence on the interaction, demonstrating that FlhG binds to the flagellar C-ring in a nucleotide independent manner (**Figure 35B**). To dissect whether *Gt*FlhG binds to *Gt*FliM or *Gt*FliY or both, interaction assays were attempted with the single proteins. *Gt*FlhG and *Gt*FliY directly interact with each other and form a stable dimeric complex. *Gt*FliM on the other hand was hardly produced in *E. coli* and purification failed due to insolubility. Co-production of *Gt*FliM with *Gt*FlhG also flailed to result a dimeric complex, because *Gt*FliM was not produced. However, the co-production of *Gt*FliM with *Gt*FliY led to a stable dimeric complex of *Gt*FliM and *Gt*FliY, which was easy to purify. These findings indicate that only *Gt*FliY directly interacts with *Gt*FlhG and not *Gt*FliM. However, a *Gt*FliM/FliY complex binds to *Gt*FlhG via *Gt*FliY.

Considering the close homology between FlhG and MinD, I also aimed at investigating whether FlhG is capable of replacing MinD as the core of the Min system to correctly localize the future cell division plane. As the interaction between MinD and MinC is the key to position a potent Z-ring inhibitor, FlhG is supposed to interact with MinC in order to replace MinD as the central ATPase of the Min system. Interaction studies using GST-tagged *Gt*FlhG on GST beads and purified *Gt*MinC were performed and analysed on Coomassie-stained SDS-PAGE. No interaction of *Gt*FlhG and *Gt*MinC was observed, while the interaction with a *Gt*FliM/FliY complex served as a positive control (**Figure 37**).

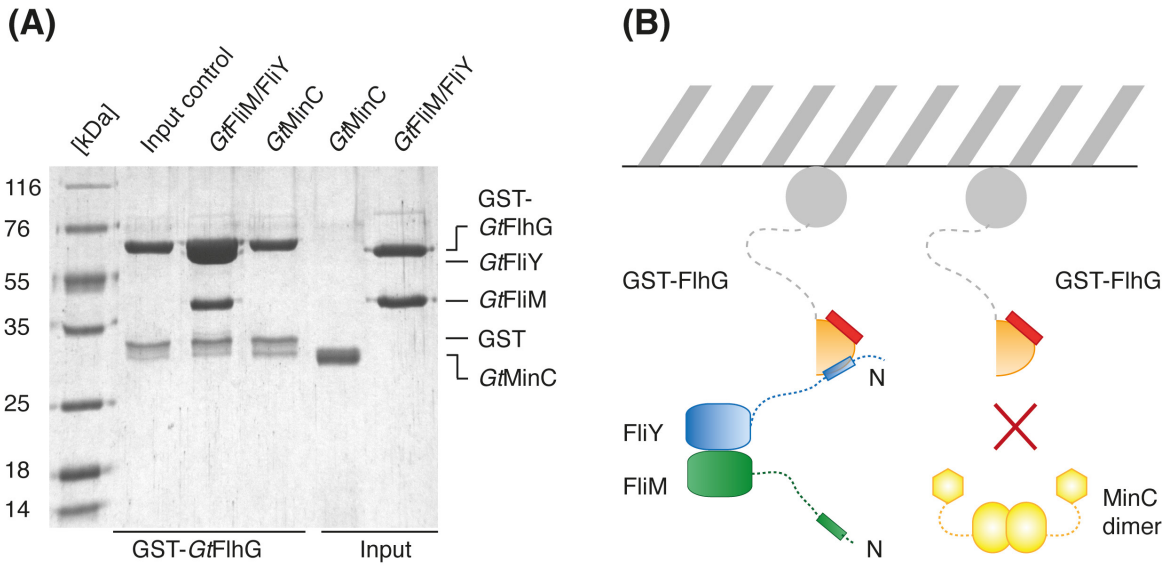

Figure 37. FlhG does not interact with MinC. (A) Coomassie-stained SDS-PAGE of interaction assays using GST-*Gt*FlhG, a complex of the C-ring proteins *Gt*FliM and *Gt*FliY as well as *Gt*MinC. The input control of GST-*Gt*FlhG is displayed in the first lane, whereas lanes four and five represent controls for *Gt*FliM/FliY and *Gt*MinC, respectively. **(B)** represents a scheme of the corresponding pull down experiment displayed in **(A)**. The upper part shows the immobilized GST-tag of FlhG in grey. The lower part shows the proteins used in the assay.

Given the fact that *Gt*FlhG and *Gt*MinC are not able to interact with each other, the possibility that FlhG may replace MinD in cell division site determination seems very unlikely. A final proof will consist in the replacement of MinD by FlhG in *B. subtilis*. Alternatively it can be tested whether FlhG is able to rescue the cell division defect of a *B. subtilis minD* deletion strain.

2.4.2 Mapping of protein-protein interfaces by $^{1}H/^{2}H$ exchange mass spectrometry (HDX)

To gain further insights into the binding mode of FlhG and FliY, the interface was assessed using hydrogen deuterium exchange mass spectrometry (HDX), a technique that allows a convenient mapping of protein-protein binding interfaces. This method was implemented in Marburg in the scope of this PhD work in collaboration with Dr. Uwe Linne from the mass spectrometry facility of the Chemistry Department (Philipps University, Marburg). A detailed description of

the principle of HDX as well as the setup including illustrations is provided in the special methods section of the results (see 2.11. Methods section: $^{1}H/^{2}H$ exchange mass spectrometry). A brief explanation of the experiment and the outcome is provided in the following. The protein of interested is incubated in deuterated buffer leading to an exchange of amide protons to deuterium. The exchange reaction is quenched by decreasing the pH to 2.5 and the temperature to 0 °C. After injection into HPLC the protein is on-line digested on a pepsin column and peptic peptides are separated and subsequently analysed by ESI mass spectrometry. The degree of deuterium incorporation relates to the flexibility and exposure to solvent of the respective region of the protein (**Figure 65**). Assuming that a binding motif gets more rigid when bound in a protein-protein complex, the decrease of deuterium incorporation in specific regions of a protein upon complex formation (shielding), indicates the putative interface.

2.4.3 The binding interface of FliM/FliY on FlhG

To investigate the binding interfaces in the ternary *Gt*FlhG/FliM/FliY complex, *Gt*FlhG, *Gt*FliY and the complexes *Gt*FliY/FliM, *Gt*FlhG/FliY and *Gt*FlhG/FliY/FliM were prepared. After dilution in deuterated buffer, amide proton exchange was allowed for 30 and 60 s prior to quenching and the deuterium incorporation of the peptic peptides was determined.

In a first step the deuterium incorporation into *Gt*FlhG was analysed to elucidate the interface on *Gt*FlhG. Three regions were identified, which show a significant decrease of deuterium incorporation when *Gt*FlhG is either bound to *Gt*FliY or part of the *Gt*FlhG/FliY/FliM complex. However, no difference in deuterium incorporation was observed between the dimeric *Gt*FlhG/FliY and the ternary *Gt*FlhG/FliY/FliM complex again implicating that *Gt*FlhG only directly interacts with *Gt*FliY, not with *Gt*FliM.

Two of the three regions are located in close proximity with region R1 covering helix α6 and the adjacent β-strand β7 and region R2 containing two thirds of helix α7. The third region R3, which only responds weakly to complex formation, comprises the amino acids from helix α8 to helix α9 (**Figure 38**). The strongest decrease in deuterium incorporation (>30 %) was observed in region R2, which

comprises the C-terminal half of the exposed helix α7. The neighbouring helix α6 also exhibited decreased deuterium uptake upon complex formation, although to a lesser extent (5-10 %). This might be either due to conformational effects from helix α7 or helix α6 takes also part in *Gt*FliY binding. A third region at a lateral side of *Gt*FlhG responded very weakly to complex formation (< 5 %), which is more likely due to secondary effects than direct binding. Hence, helix α7 was the best candidate for the interface.

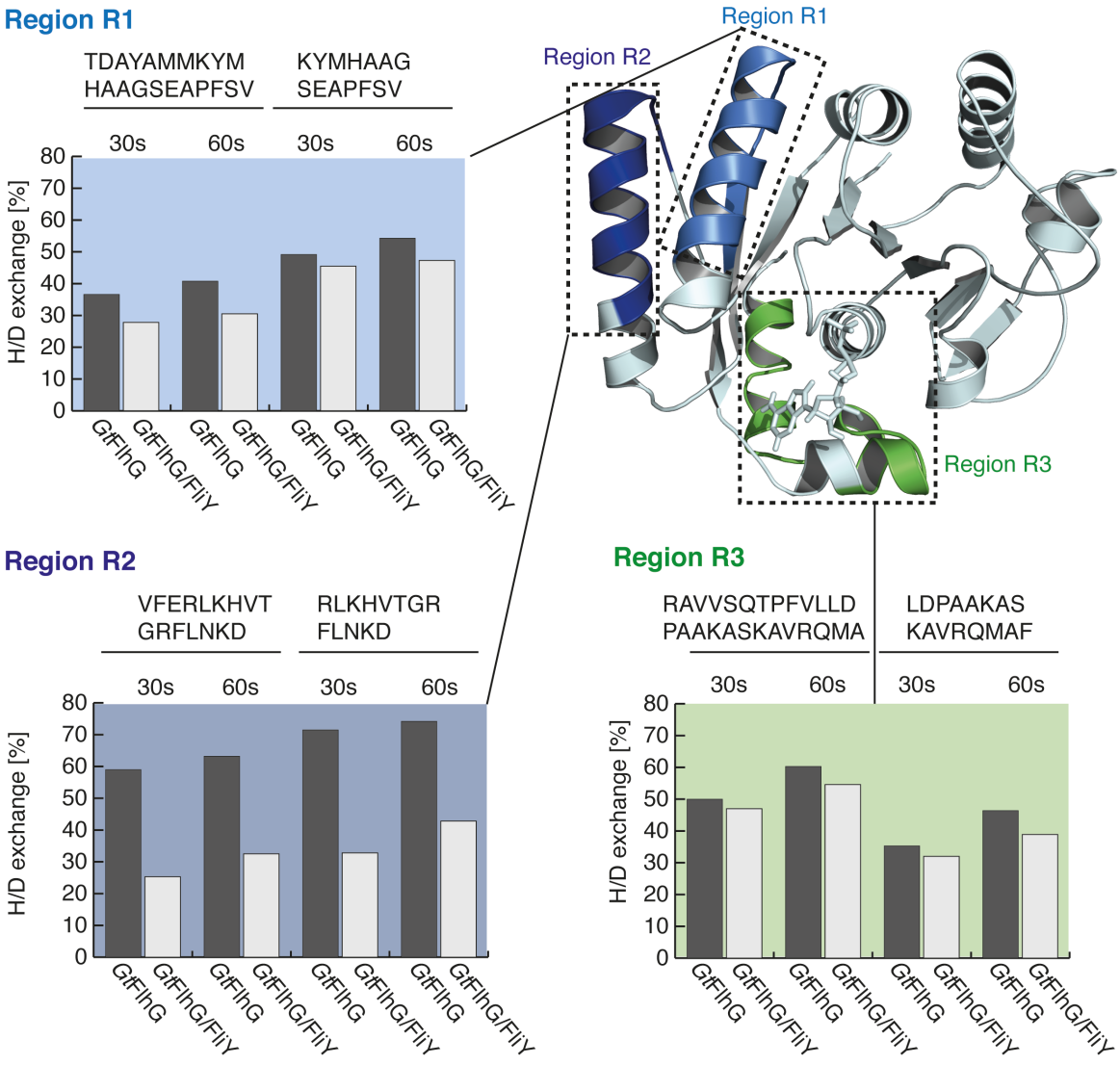

Figure 38. HDX Measurements reveal the FlhG/FliY Interface. HDX measurements revealed three regions (R1, R2 and R3) of *Gt*FlhG that exhibited a decrease of deuterium uptake in the complex with *Gt*FliY. Deuterium uptake of two representative peptides of R1 to R3 is shown for *Gt*FlhG and the *Gt*FlhG/FliY complex after 30 s and 60 s in incubation in deuterated buffer. The respective regions are indicated in the structure of *Gt*FlhG (pdb: 4RZ3) (*top, right*) and are coloured-coded accordingly.

To confirm our HDX findings, surface exposed residues within the region R2 were varied and the ability to bind *Gt*FliY was assessed in Ni-NTA pull down assays from cell lysate. In a first step six variations were made in helix α7 (R199E, Y202D, R207E, H210L, R214E, F215S), where the strongest protection occurred (**Figure 39C**). The interaction studies revealed that a single variation of either residue arginine 207 or phenylalanine 215 is sufficient to abolish the interaction of *Gt*FlhG and *Gt*FliY (**Figure 39A**).

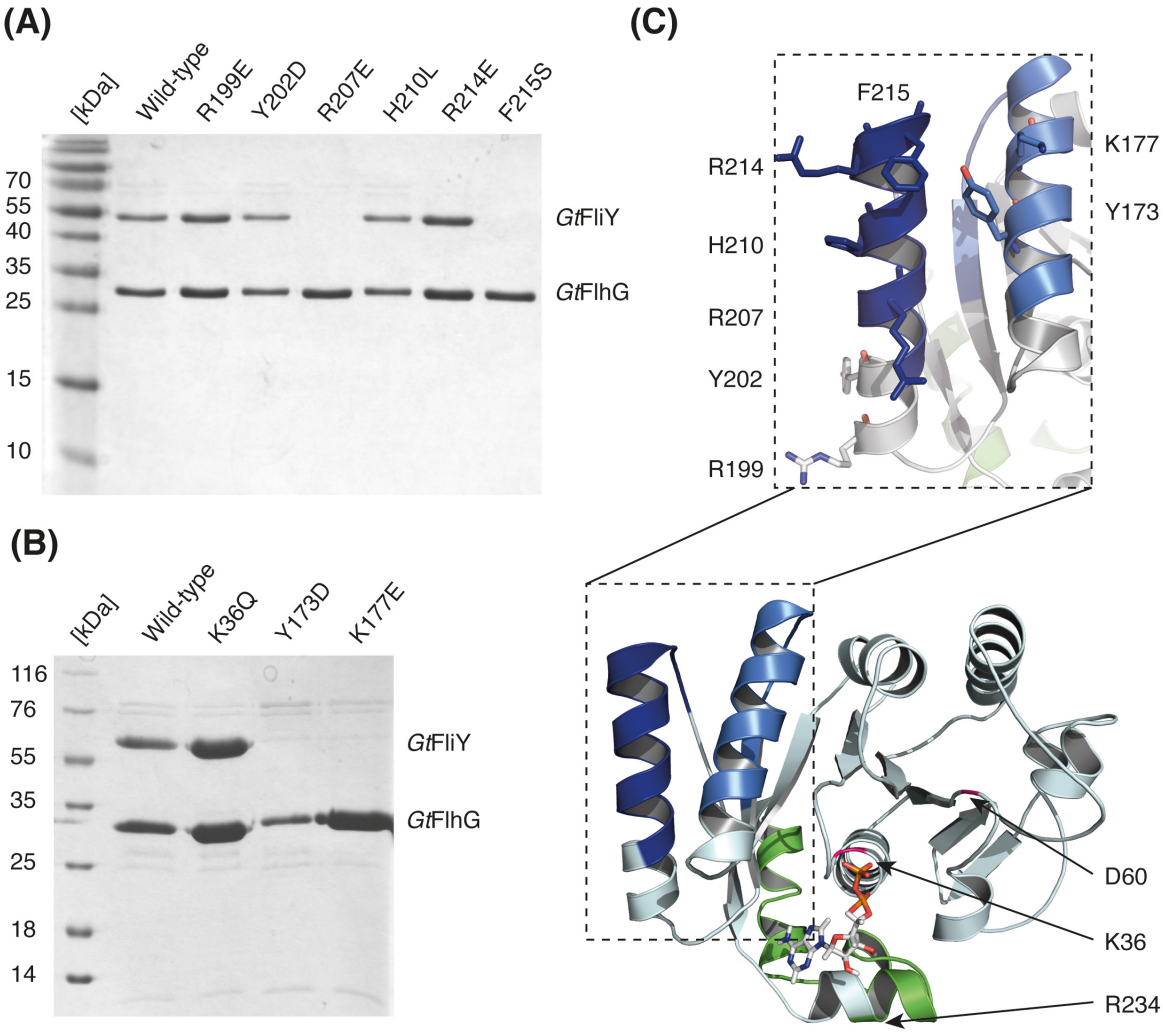

Figure 39. Variants of FlhG (1). (A) shows the Coomassie-stained SDS-PAGE of Ni-NTA affinity pull down experiments using *Gt*FlhG with an N-terminal $(His)_6$ tag and the indicated variants, all located in region R2 (see **Figure 38**) as well as untagged *Gt*FliY. Variants shown in **(B)** are either located in region R1 (Y173D and K177E) or in the P-loop (K36Q), which presumably abolishes catalytic activity. **(C)** shows the structure of *Gt*FlhG (pdb: 4RZ3) coloured as indicated before (see **Figure 38**). The arrows mark the position of the varied residues. The inlay shows helices α6 and α7 with the varied residues indicated as sticks.

Based on these results, more variations were introduced into region R1 (Y173D and K177E), which identified another two residues that are crucial for the interaction (**Figure 39B**). As a control the hydrolysis deficient *Gt*FlhG variants K36Q and D60A were also tested towards their ability to bind *Gt*FliY. No difference in the binding compared to wild-type *Gt*FlhG was observed, which again confirms that the binding is independent of nucleotides (**Figure 39B** and **Figure 40A**).

In another control experiment the distant but surface exposed arginine 234 was replaced by glycine, which again had no effect on the interaction of *Gt*FlhG and *Gt*FliY (**Figure 40A**). In order to proof the importance of the interface, the pull down assays were repeated now testing whether the *Gt*FlhG variants are able to bind a complex of *Gt*FliM and *Gt*FliY. Ni-NTA affinity interaction assays against untagged *Gt*FliM/FliY corroborated previous findings and emphasized the essential role of tyrosine 173, lysine 177, arginine 207 and phenylalanine 215 for C-ring binding (**Figure 40B**).

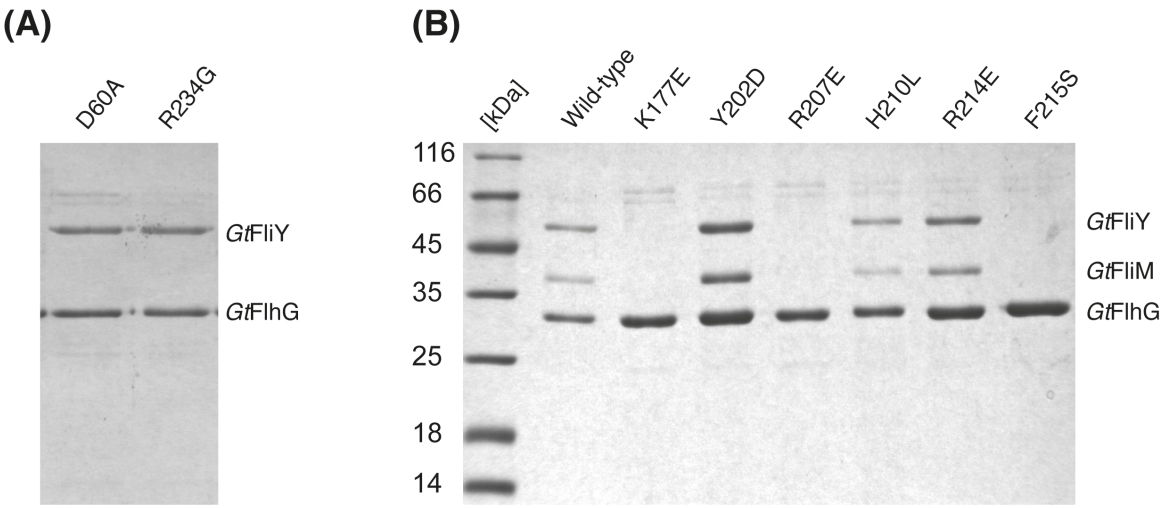

Figure 40. Variants of FlhG (2). (A) shows the Coomassie-stained SDS-PAGE of Ni-NTA affinity pull down experiments using the indicated *Gt*FlhG variants with an N-terminal $(His)_6$ tag as well as untagged *Gt*FliY. *Gt*FlhG D60A is defective in Mg^{2+} coordination and lacks catalytic activity. *Gt*FlhG R234G is a variant in a surface exposed arginine in close proximity to R3. **(B)** Ni-NTA affinity experiments were repeated using an untagged *Gt*FliM/FliY complex instead of *Gt*FliY. *Gt*FlhG variants are located in region R1 (Y173D and K177E) or R2 (Y202D, R207E, H210L, R214E and F215S).

All four residues, Y173 and K177 on helix α6 and R207 and F215 on helix α7 are located on neighbouring helices and point away from the protein core and towards each other, forming a composite interaction site for *Gt*FliY (**Figure 41**).

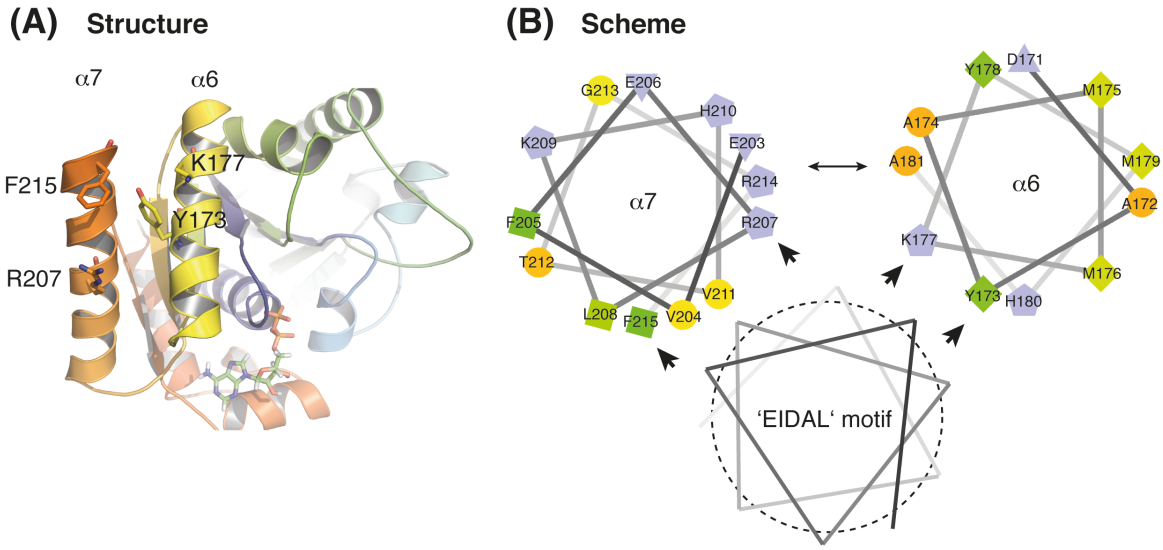

Figure 41. Scheme of the FlhG, FliY binding interface. (A) The cartoon representation of *Gt*FlhG (pdb: 4RZ3; rainbow) displays the FliY binding interface. Essential residues are shown as sticks and labelled accordingly. Important secondary structure elements are indicated. **(B)** shows a scheme of the respective interaction interface depicting helices α6 and α7 as helical wheel projections. The N-terminal 'EIDAL' motif of FliY is indicated as grey helix. The black arrows mark the amino acid residues that are essential for the interface.

2.4.4 The binding interface of FlhG on FliY

Analysis of the deuterium incorporation not only delivered the interface on *Gt*FlhG, but also provided hints for the counterpart on *Gt*FliY. Since the very N-terminus of *Gt*FliY displayed a decrease in deuterium content in the *Gt*FlhG/FliY complex (**Figure 42B**). This region contained a conserved motif (LSQxEIDALLN; 'EIDAL' motif) that is also present at the N-terminus of *Gt*FliM. Notably, *Gt*FliM and *Gt*FliY show very similar domain architecture, with an N-terminus that comprises the 'EIDAL' motif, a globular middle domain with identical fold and a C-terminal FliN homology domain, which serves for oligomerisation (**Figure 42A**) (54).

This raises the question why *Gt*FliY is able to bind *Gt*FlhG and apparently not *Gt*FliM, although both proteins share a conserved N-terminus. To investigate the

binding mode of FlhG and the C-ring components, *Gt*FliM and *Gt*FliY variants were generated, which lack the conserved N-terminus, specifically the first 25 and the first 27 amino acid residues, respectively (FliM-ΔN and FliY-ΔN). Combining full length *Gt*FliM, *Gt*FliY and the N-terminally truncated versions resulted in four *Gt*FliM/FliY complexes that i) have both 'EIDAL' motifs, ii) lack the 'EIDAL' motif of FliM, iii) lack the EIDAL motif of FliY, or iv) lack both N-termini.

In vitro pull down assays with $(His)_6$-tagged FlhG revealed that only the 'EIDAL' motif of *Gt*FliY is necessary and sufficient to bind *Gt*FlhG (**Figure 42C**). These findings also indicate that subtle variations within the 'EIDAL' motifs of *Gt*FliM and *Gt*FliY mark specificity for the ability to bind *Gt*FlhG or not.

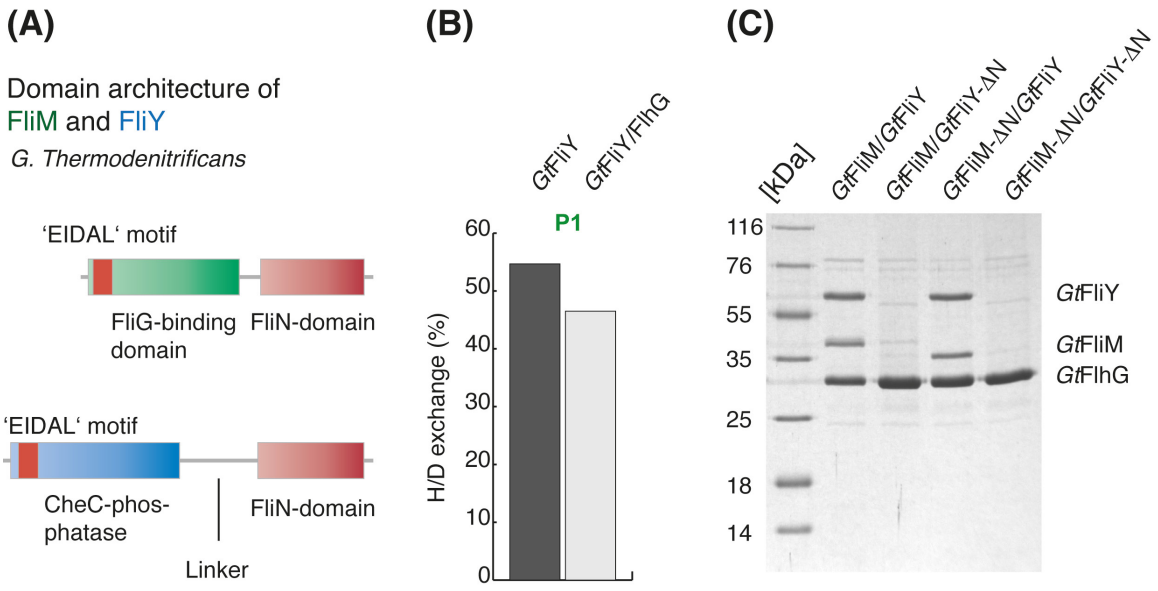

Figure 42. FlhG interacts with the N-terminus of FliY. (A) shows the domain architecture of the C-ring proteins FliM and FliY of *G. thermodenitrificans*. Domains are colour-coded and labelled. **(B)** displays the deuterium uptake of the N-terminus of *Gt*FliY (12-28) alone and in complex with *Gt*FlhG after 30 s incubation in deuterated buffer. P1: DALLRGMDDSDHVPALH. **(C)** shows a Coomassie-stained SDS-PAGE of pull down assays using *Gt*FlhG with an N-terminal $(His)_6$ tag and *Gt*FliY, *Gt*FliM as well as the respective N-terminal deletion variants (*Gt*FliM-ΔN and *Gt*FliY-ΔN) without tag.

2.4.5 The binding of FlhG and CheY to FliM/FliY

The 'EIDAL' motif of FliM plays an essential role in chemotaxis signalling (176, 193, 194). The phosphorylated response regulator of the chemotaxis signal cascade CheY-P binds to the 'EIDAL' motif of FliM to control the rotatory direction of the flagellum upon external stimuli, switching it from CW to CCW or *vice versa*. To investigate whether FlhG and CheY-P can compete for the 'EIDAL' motifs in the FliM/FliY complex or whether each protein binds to its own 'EIDAL' motif, competitive interaction assays were performed. 1 nmol of the GST-*Gt*FlhG fusion protein was immobilized and incubated with a purified *Gt*FliM/FliY complex to result the ternary GST-*Gt*FlhG/FliM/FliY complex. This complex was further incubated with increasing amounts of purified *Bs*CheY (from 0.2 nmol to 40 nmol) to see whether a quaternary complex is formed upon addition of *Bs*CheY or whether *Bs*CheY is able to detach *Gt*FliM/FliY from GST-*Gt*FlhG, which implicates a competitive binding situation.

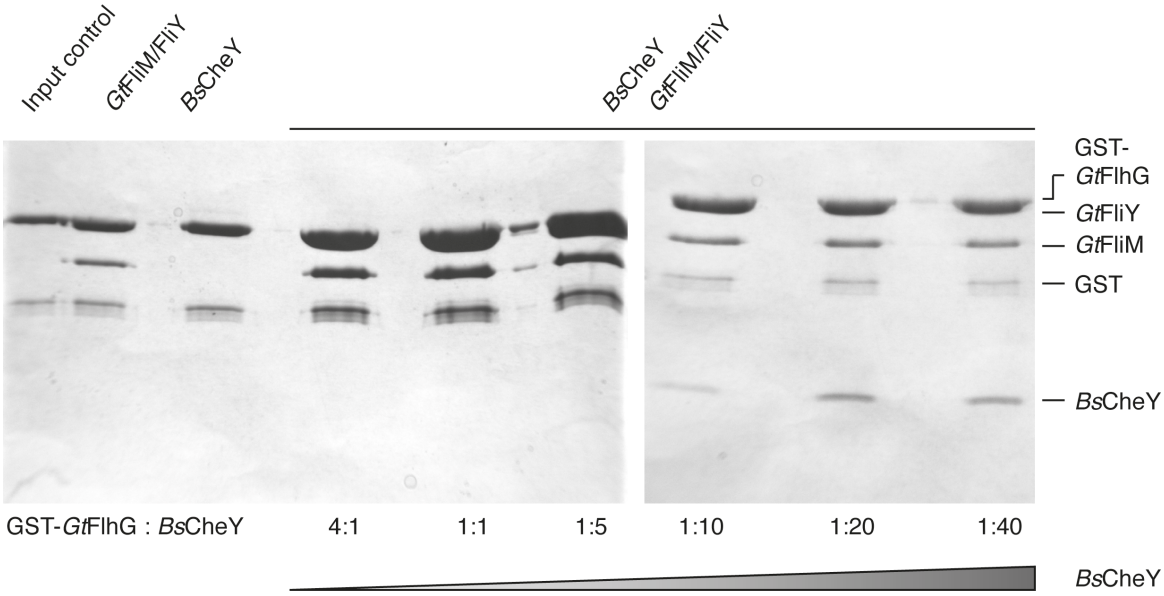

Figure 43. Interaction of FlhG and CheY with FliM/FliY. Competitive pull down assays were carried out, forming a ternary complex of GST-*Gt*FlhG and purified *Gt*FliM/FliY, which was subsequently incubated with increasing amounts of *Bs*CheY. The Coomassie-stained SDS-PAGE of the interaction assay reveals the formation of a quaternary complex at high *Bs*CheY concentration. The ratio of GST-*Gt*FlhG to *Bs*CheY is indicated at the bottom and the respective controls are provided in the first three lanes.

CheY derived from *B. subtilis* was used for these interaction experiments in combination with FlhG, FliM and FliY from *G. thermodenitrificans*. This seems justified considering the fact that CheY from *B. subtilis* and *G. thermodenitrificans* share 48 % identity and 80 % conserved residues including the relevant interaction interface with FliM. The pull down experiment displayed the formation of a quaternary complex (**Figure 43**).

However, binding of *Bs*CheY to the ternary complex is only observed upon addition of a large excess of *Bs*CheY. This indicates a low binding affinity of *Bs*CheY to *Gt*FliM/FliY, which may be caused by the use of a protein from a different organism, in this case *B. subtilis.* These findings open up two possible scenarios. Both *Bs*CheY and *Gt*FlhG can simultaneously bind to the C-ring complex *Gt*FliM/FliY or the binding affinity of *Bs*CheY to *Gt*FliM/FliY is not high enough to release *Gt*FliM/FliY from GST-*Gt*FlhG. To distinguish between both possible interaction modes, the binding assays were repeated using GST-*Bs*CheY (1 nmol) as anchor for *Gt*FliM/FliY and *Gt*FlhG as releasing factor.

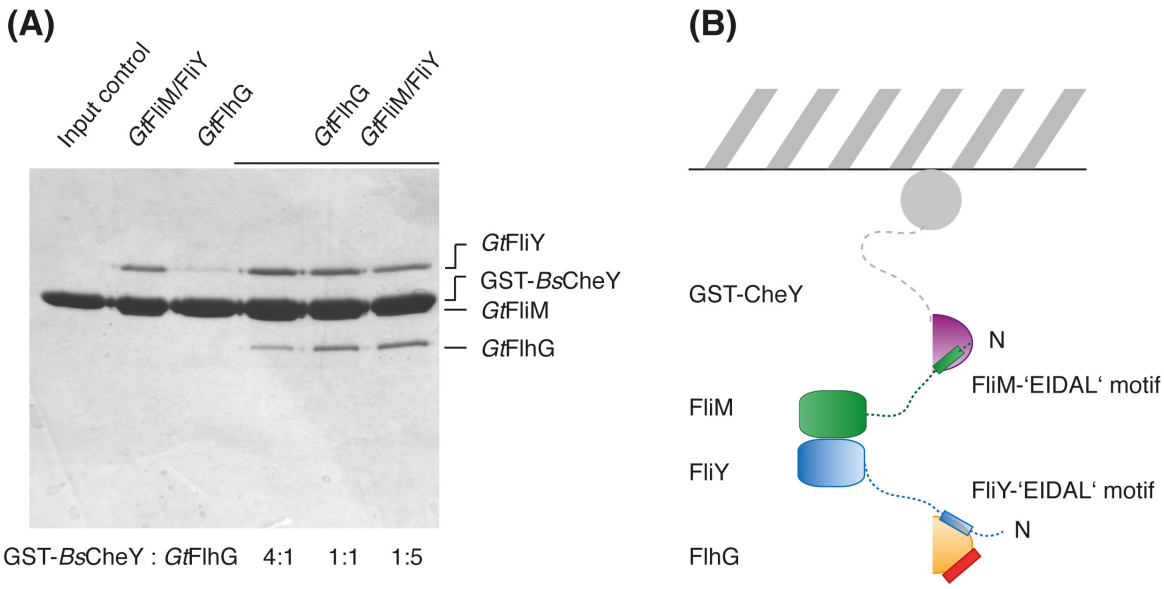

Figure 44. Interaction of FlhG and CheY with FliM/FliY 02. (A) shows a Coomassie-stained SDS-PAGE of competitive interaction experiments performed using a ternary complex of GST-*Bs*CheY and *Gt*FliM/FliY, which was subsequently incubated with increasing amounts of *Gt*FlhG. The ratio of GST-*Bs*CheY to *Gt*FlhG is indicated at the bottom and the respective controls are provided in the first three lanes. **(B)** displays the scheme of a quaternary complex composed of GST-*Bs*CheY/*Gt*FliM/FliY/FlhG. The upper part shows the immobilized GST-tag in grey and the lower part shows the proteins used in the assay.

Again, a GST-*Bs*CheY/*Gt*FliM/FliY complex was incubated with increasing amounts of *Gt*FlhG (from 0.25 nmol to 5 nmol) displaying the formation of a quaternary complex of all four proteins. Without *Gt*FliM/FliY, *Gt*FlhG does not interact with *Bs*CheY. But as soon as the C-ring complex is present *Gt*FlhG attaches to the ternary complex GST-*Bs*CheY/*Gt*FliM/FliY even at very low amounts, indicating a high affinity of *Gt*FlhG towards *Gt*FliM/FliY (**Figure 44**). These experiments exclude the possibility of a competitive binding situation.

As two 'EIDAL' motifs are present at the *B. subtilis*/*G. thermodenitrificans* C-ring complex it can be argued that FlhG binds to the 'EIDAL' motif of FliY, while CheY interacts with the 'EIDAL' motif of FliM (**Figure 44**). This raises the question concerning the specificity of the highly conserved 'EIDAL' motif. Are there additional binding sites that may facilitate the discrimination between FlhG and CheY? Further investigations will be necessary to answer these questions in detail.

2.4.6 Macromolecular shape of the FlhG/FliM/FliY complex

SEC revealed that the ternary complex *Gt*FlhG/FliM/FliY forms large particles with an estimated size of around 2.5 MDa. Electron microscopy was employed to determine the shape and to get insights into the morphology of this complex. By imaging a dimeric complex of *Gt*FliM and *Gt*FliY as well as the ternary *Gt*FlhG/FliM/FliY complex, I aimed at elucidating the impact of FlhG on the flagellar C-ring complex *Gt*FliM/FliY. As the ternary complex *Gt*FlhG/FliM/FliY, dimeric *Gt*FliM/FliY was easy to purify using the well-established protocol including an initial Ni-NTA affinity purification followed by SEC.

For the purification the C-terminal $(His)_6$-tagged version of *Gt*FliM was employed, while the *Gt*FliY carried no tag. After the Ni-NTA affinity column *Gt*FliM and *Gt*FliY were eluted in a stoichiometric ratio of 1:1. SEC displayed a single peak, containing both proteins (**Figure 45**). According to size standard measurements the particle size of the eluted *Gt*FliM/FliY complex was approximately 2 MDa. Complexes of similar size were also observed for the ternary complex *Gt*FlhG/FliM/FliY (**Figure 45**).

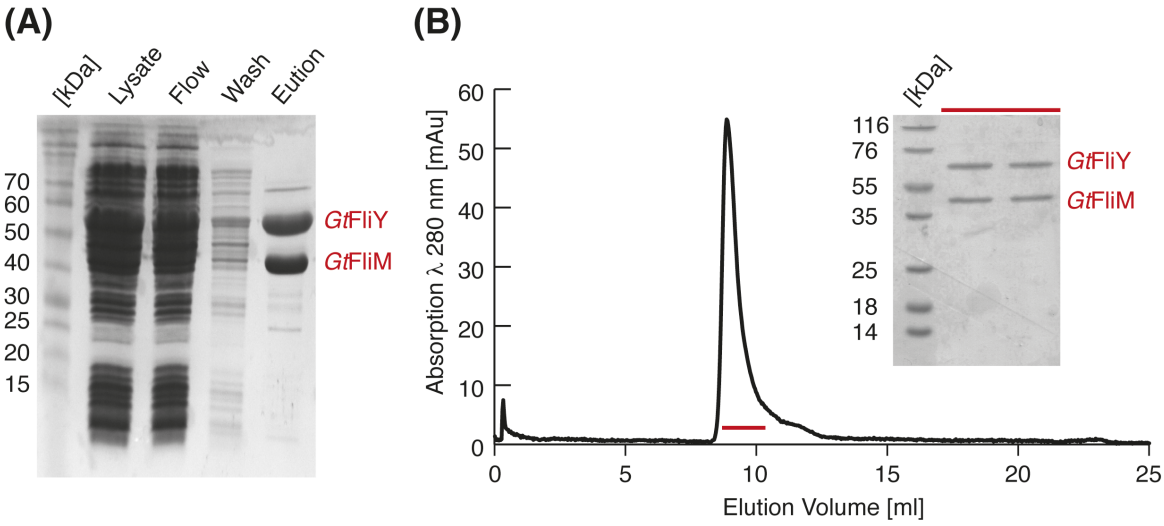

Figure 45. Purification of a *Gt*FliM/FliY complex. (A) displays the Coomassie-stained SDS-PAGE of the Ni-NTA affinity purification of the dimeric complex *Gt*FliM/FliY. **(B)** The respective size exclusion chromatogram shows a single peak. The inlay represents the corresponding Coomassie-stained SDS-PAGE of the peak fractions (indicated in red).

Electron microscopy was performed in collaboration with Dr. Andreas Klingl and Dr. Katrin Bolte in the laboratory of Prof. Dr. Uwe Maier (Philipps University, Marburg). The electron microscopy samples of the complexes *Gt*FliM/FliY and *Gt*FlhG/FliM/FliY were taken after SEC and imaged using negative stain electron microscopy. The samples were prepared on copper grids and stained using uranyl acetate.

*Gt*FliM/FliY resulted in large globular particles. A class of ring-like particles appearing in different orientations on the grid with different sizes and diameters was observed (**Figure 46**). The size of the particles was in range of 16 to 39 nm in diameter, with an average of 25.1 ± 4.6 nm over 150 particles.

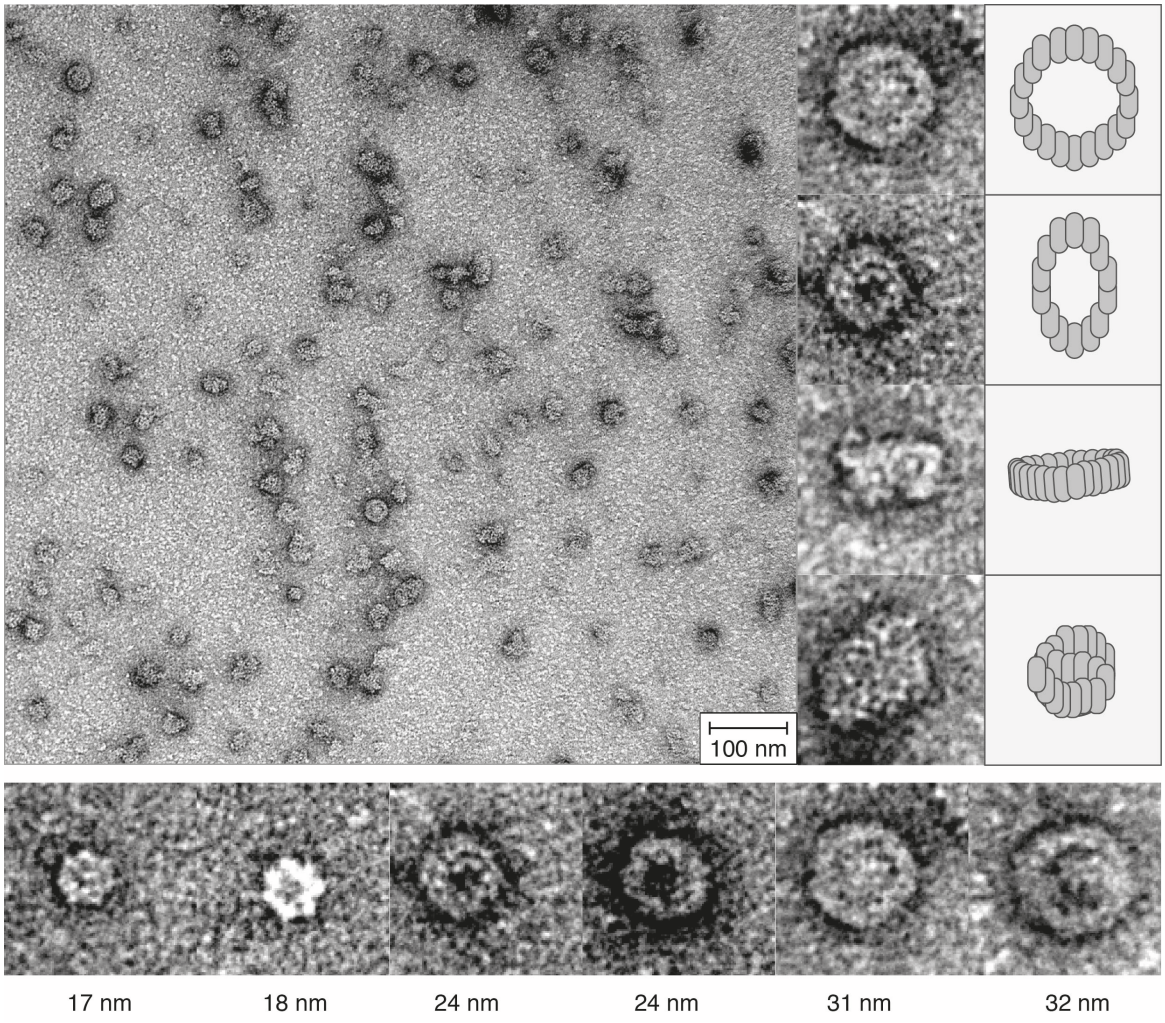

Figure 46. Electron micrographs of *Gt*FliM/FliY. A negative stain electron micrograph shows an overview of *Gt*FliM/FliY particles. Ring-shaped particles in different orientations are depicted and combined with a schematic drawing (*right*). Ring-shaped particles exhibiting different diameters are display at the bottom to indicate the size distribution.

Electron micrographs of the ternary complex *Gt*FlhG/FliM/FliY displayed similar particles in shape and size. Again, a class of ring-shaped particles was visible, that were slightly larger in size after particle analysis. The diameter of these particles was 30.8 ± 5.7 nm on average (n=150), with a distribution ranging from 18 to 43 nm (**Figure 47**). As indicated on SEC the ternary complex forms larger aggregates, which may be simply due to the presence of an additional protein in the complex. It also might indicate that FlhG influences the size of the FliM/FliY complexes, which seem to form spontaneously. The electron micrographs demonstrate that a complex comprising FliM and FliY, autonomously adopt a ring-like shape similar to the native C-ring. Upon addition of FlhG the particles

increase in size and diameter, indicating that the presence of FlhG fosters larger aggregates. However, electron microscopic studies on purified basal bodies revealed a diameter between 42 and 47.4 ± 2.4 nm of the C-ring of the sodium driven flagellum of *S. enterica* (215-217). This indicates that the C-ring complexes obtained after purification of the *Gt*FliM/FliY complex seem to be significantly smaller in diameter than the native C-ring in the flagellum. As these reports investigated the sodium driven flagellum of *S. enterica*, the results are not directly comparable to the proton driven flagella of *B. subtilis*.

Therefore, the size of the C-ring of the peritrichous flagella of *B. subtilis* still remains elusive.

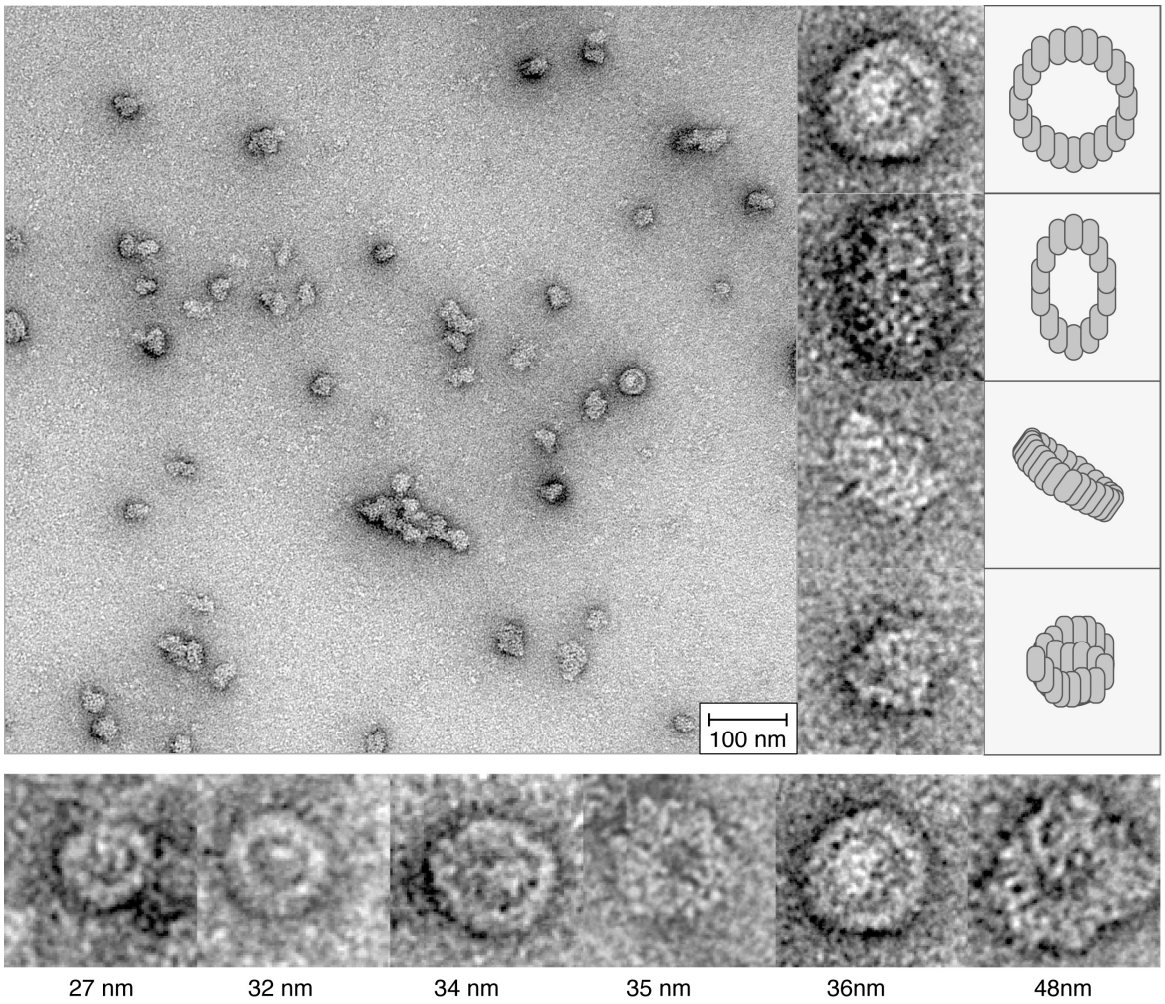

Figure 47. Electron micrographs of *Gt*FliM/FliY/FlhG. A negative stain electron micrograph shows an overview of *Gt*FliM/FliY/FlhG particles. Ring-shaped particles in different orientations are depicted and combined with a schematic drawing (*right*). Ring-shaped particles exhibiting different diameters are display at the bottom to indicate the size distribution.

Triplicate measurements of these complexes revealed that the shape of the particles were reproducible. However, the diameter of the ring-like structures displayed a strong variation, rendering the quantification of the rings and the differentiation between the dimeric and the ternary complex difficult. It seems that the size of the particles depended on the concentration step of the sample between nickel affinity chromatography and SEC. The higher the samples were concentrated after affinity purification the smaller the diameter of the rings appeared afterwards on electron microscopy.

Our results demonstrate that C-ring particles composed of FliM and FliY autonomously adopt a circular shape and form large C-ring particles or pre-C-ring particles. In the presence of FlhG these particles retain their circular shape but appear slightly larger in size. However, our experiments also showed that more factors influence the size of the C-ring particles such as the concentration of the sample and the conditions during purification.

2.4.7 The interaction of FlhG with FliG

The flagellar C-ring is composed of three components FliY, FliM and also FliG, which was neglected in our experiments so far. In the mature flagellum, FliG interacts with the integral membrane protein FliF and is therefore located in close proximity to the plasma membrane (**Figure 48**). Our *in vitro* interaction studies showed that FlhG interacts with the C-ring complex FliM/FliY. However, as FlhG is not integral part of the flagellum at some point FlhG has to be released from the C-ring before flagella biogenesis is completed.

To investigate a putative interaction between FliG and FlhG, a GST fusion of *Gt*FliG was generated and GST-*Gt*FliG was incubated with *Gt*FlhG, nucleotides and lipids, derived from an *E. coli* lipid extract. In the absence of nucleotides and lipids *Gt*FlhG binds weakly to GST-*Gt*FliG. However, in the presence of ATP and lipids a strong interaction between *Gt*FlhG and GST-*Gt*FliG was observed (**Figure 48**).

This indicates that *Gt*FlhG not only interacts with the flagellar C-ring protein *Gt*FliY but also with *Gt*FliG. Whether FlhG has any influence on the switching of

the motor remains unclear. However, its partner FlhF has an influence on the rotation of the flagellum in *P. aeruginosa*. Besides mislocalization, flagella in a *P. aeruginosa* FlhF deletion strain are unable rotate (133).

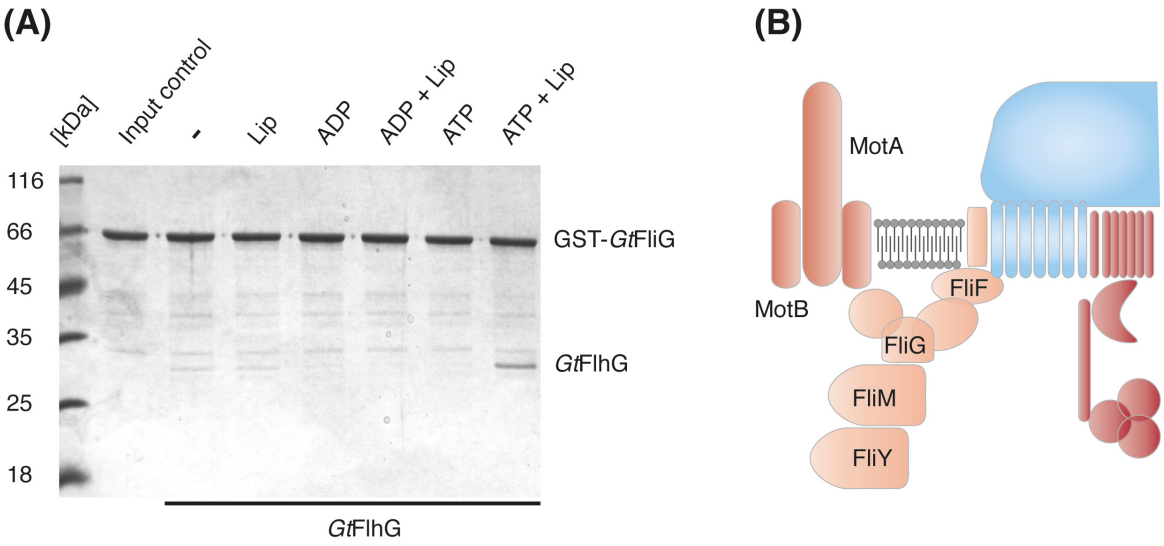

Figure 48. Interaction of FlhG and FliG. (A) shows the Coomassie-stained SDS-PAGE of pull down assays incubating GST-*Gt*FliG and *Gt*FlhG in the absence and presence of lipids (Lip), ADP or ATP and indicated combinations. **(B)** displays a detailed scheme of the C-ring composition and architecture (light red) at the flagellar basal body. Motor components are coloured in red, the type III secretion system in dark red and further components are illustrated in blue.

FliG is located close to the plasma membrane through its interaction with the integral membrane protein FliF. In the presence of ATP and lipids FlhG is also positioned at the plasma membrane due to dimer formation and exposure of the MTS. In this scenario a possible interaction between FliG and FlhG occurs at the flagellar basal body involving the FlhG dimer, although a functional role for this interaction remains elusive.

2.4.8 GpsB as putative interaction partner of FlhG

In *B. subtilis* GpsB (also YpsB) was identified as a DivIVA paralogue and component of the cell division machinery (reviewed in: (218, 219)). It associates with the divisome at a late stage (220). The rather small protein (98 amino acids) interacts with the cell division protein EzrA in *B. subtilis* and *Streptococcus pneumonia*

(221, 222). In *B. subtilis* GpsB also interacts with the catalytic domain of the Ser/Thr kinase PrkC, which on the other hand is able to phosphorylate threonine 75 of GpsB (221, 223). Phosphorylated GpsB in turn regulates the PrkC kinase, inhibiting phosphorylation of PrkC substrates (221). Previous work indicated that GpsB might also be connected to flagellar assembly or flagellation pattern control (personal communication G. Bange) and was therefore considered as putative interaction partner of FlhG. In a first step, the coding region for GpsB was amplified and transferred into a pGAT3 expression vector, which generated a N-terminal GST fusion protein of GpsB (GST-*Bs*GpsB). Due to 62 % identity and 94 % conservation of GpsB from *B. subtilis* and *G. thermodenitrificans* the following binding experiments were performed with GST-*Bs*GpsB and *Gt*FlhG. In the binding studies, purified GST-*Bs*GpsB was immobilized on GST-beads and incubated with purified *Gt*FlhG in the absence and presence of ATP (**Figure 49A**). These pull down assays revealed a weak interaction between GST-*Bs*GpsB and *Gt*FlhG in the presence of ATP. In a next step, the influence of different nucleotides on the interaction was investigated. The results show that without nucleotides the signal of *Gt*FlhG was barely visible, while in the presence of ADP, ATP and the non-hydrolysable analogue AMPPNP, the signal for *Gt*FlhG increased. The strongest interaction was observed in the presence of ATP (**Figure 49B**).

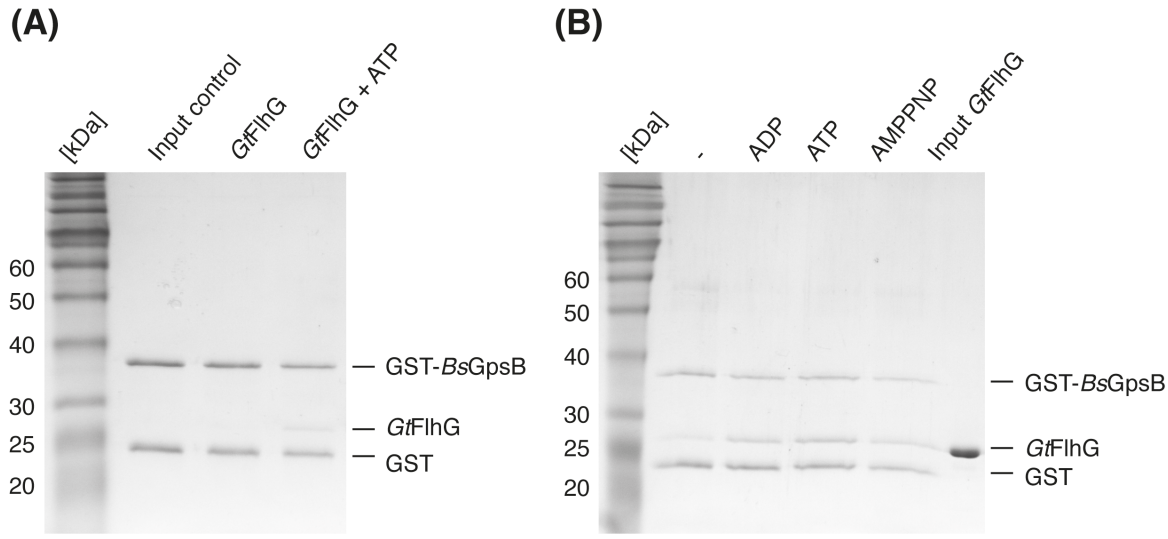

Figure 49. Interaction of FlhG and GpsB. (A) shows a Coomassie-stained SDS-PAGE of pull down experiments using GST-*Bs*GpsB and *Gt*FlhG with and without ATP. **(B)** In addition to **(A)**, interaction experiments were repeated in the presence of ADP and AMPPNP.

Time resolved interaction assays, varying the incubation time of GST-*Bs*GpsB on beads and *Gt*FlhG, were additionally performed. *Gt*FlhG and ATP were pre-incubated in a ratio of 1:400 (*Gt*FlhG:ATP) for 20 min at 0 °C prior to the assay. Subsequently, *Gt*FlhG/ATP was added to GST-*Bs*GpsB and incubated for different time periods ranging from 1 to 120 min. Analysis by Coomassie-stained SDS-PAGE, displayed a decrease in affinity of *Gt*FlhG to GST-*Bs*GpsB over time (**Figure 50A**). This may indicate that *Gt*FlhG binds to *Bs*GpsB in its ATP bound state. Upon hydrolysis, the complex falls apart releasing FlhG. A subsequent exchange of the nucleotide in FlhG renders FlhG-ATP competent to again bind GpsB again. With increasing incubation time more ATP is consumed which leads to a decreased binding of FlhG-ATP to GpsB. However, our HPLC-based hydrolysis assays showed no stimulation of the ATPase activity of *Gt*FlhG upon addition of GST-*Bs*GpsB (**Figure 50B**).

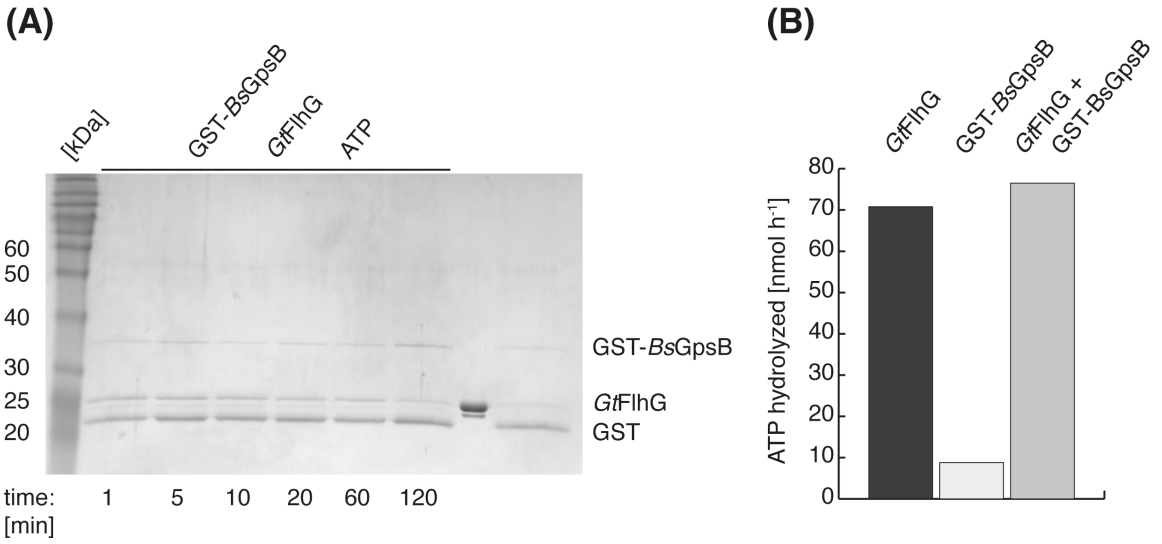

Figure 50. Interaction of FlhG and GpsB in the presence of ATP. (A) shows a Coomassie-stained SDS-PAGE of time-resolved pull down assays using GST-*Bs*GpsB, *Gt*FlhG and 0.25 mM ATP. Incubation times are stated at the bottom. **(B)** displays preliminary hydrolysis assays of *Gt*FlhG, GST-*Bs*GpsB and a mixture of both proteins. Experiments were not performed in triplicates and thus lack the error bars.

This may exclude the possibility that GpsB is the activator of the FlhG ATPase. However, GST-*Bs*GpsB seemed to have a weak ATPase activity itself, which may be caused by autophosphorylation of GpsB, which opens up the possibility that GpsB might interact with FlhG in its phosphorylated state. This also explains

why the affinity is increased upon addition of ATP. However, it does not explain why the affinity decreases over time. Taken together, the experiments show a nucleotide-dependent interaction between FlhG and GpsB. This may point towards an interaction of GpsB with an ATP-bound FlhG dimer.

To investigate the interaction interface on GpsB, it was further subdivided into three smaller fragments and cloned into a pGAT3 GST-fusion vector (**Figure 51A**). The first construct only comprises the N-terminus of GpsB (amino acids 1-24), in the second one the C-terminus is excluded (amino acids 1-70) and the third one consists of amino acids 21-98. Interaction assays employing GST-*Bs*GpsB 1-24 and *Gt*FlhG were inconclusive, because both proteins were indistinguishable on a Coomassie-stained SDS-PAGE. GST pull down assays were repeated using GST-*Bs*GpsB 21-98 and *Gt*FlhG. In the presence of ATP a weak interaction between GST-*Bs*GpsB 21-98 and *Gt*FlhG was visible, as observed for full length GST-*Bs*GpsB, indicating that the N-terminus is negligible for the interaction (**Figure 51B**).

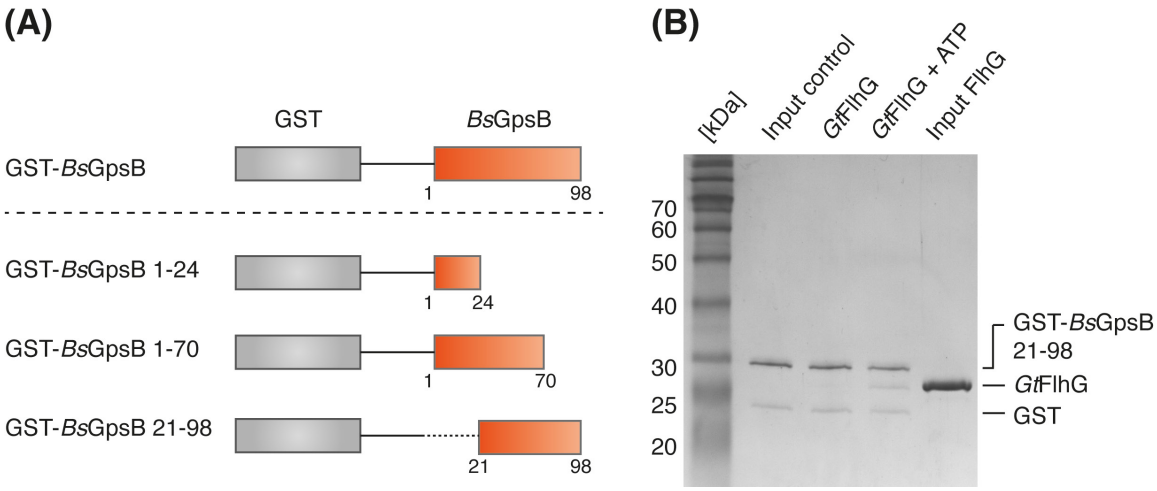

Figure 51. Truncated variants of GpsB. (A) shows a scheme of the GST-*Bs*GpsB truncation constructs which were generated to further investigate the interaction of FlhG and GpsB. **(B)** shows the Coomassie-stained SDS-PAGE of interaction assays employing GST-*Bs*GpsB 21-98 and *Gt*FlhG in the absence or presence of ATP. The first and the last lane provide input controls.

Previous experiments showed that ATP is necessary for FlhG homodimer formation, which is closely connected to membrane association. Repeating the presented interaction assays in the presence of lipid vesicles may provide further insights into the interaction of FlhG and GpsB.

2.5 Localization of FlhG in *B. subtilis*

To get further insights into the physiological role of the ATPase, FlhG was visualized in *B. subtilis* using a fluorescent protein (FP). A fusion protein consisting of FlhG and a yellow FP (YFP) was integrated into the original genomic locus in *B. subtilis* PY79 through a pSG1164 vector. This work was performed in close collaboration with Dr. Felix Dempwolff of the group of Prof. Dr. Peter Graumann (Philipps University, Marburg). *B. subtilis* was grown to late log phase and immobilized on soft agar pads for microscopy.

2.5.1 FlhG is highly dynamic in *B. subtilis*

In *B. subtilis* FlhG displays a highly dynamic behaviour, forming mainly foci at the membrane with a short half-life. In fact, a closer look revealed two subpopulations of *Bs*FlhG foci. The major fraction (76.6 %) is highly mobile and changes location in the millisecond range. The second minor fraction (23.4 %) resides at a specific location with an average resting time of around 29.0 ± 22.6 s (n=61) (**Figure 52**). This observation corroborates the structural and biochemical analysis predicting a dynamic behaviour between a membrane bound and a cytoplasmic state. Fluorescence microscopy indicates that *Bs*FlhG forms larger aggregates at membrane. The number of proteins per aggregate as well as the size of the aggregates is either not accessible or below the resolution limit of the technique and can therefore not be determined. How the formation of oligomeric structures contributes to number of flagella or positioning remains elusive.

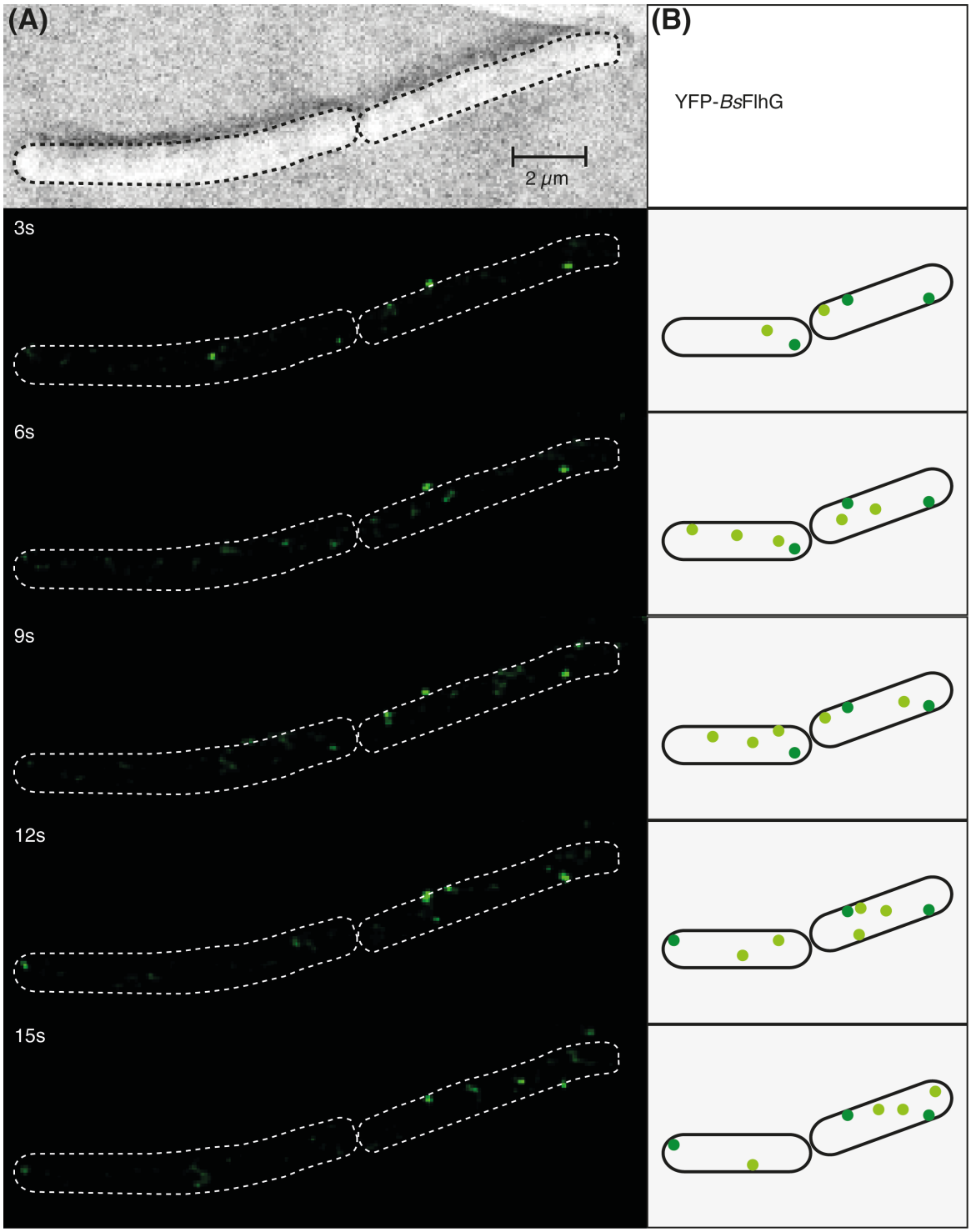

Figure 52. Localization of FlhG in *B. subtilis*. (A) depicts a time-course of images of fluorescently labelled FlhG in *B. subtilis* showing the cellular behaviour of FlhG. Dashed lines indicated the outline of *B. subtilis* cells and a bright-field image is included on top. The scale bar equals 2 µm. **(B)** shows a cartoon illustrating the FlhG foci. Static foci are coloured in dark green, movable foci are shown in light green.

2.5.2 FlhG co-localizes with FliM

In order to connect the dynamic behaviour of FlhG with the localization of flagella, a fluorescent marker for flagellar basal bodies was introduced into *B. subtilis*. A fusion protein of *Bs*FliM with an adjacent cyan-coloured FP (CFP) was integrated into *B. subtilis* PY79 at an ectopic site in the genome as an additional copy to the native FliM. Based on this strain YFP-FlhG was integrated into its original locus generating a double fluorescently labelled *B. subtilis* strain. Fluorescence microscopy displayed FliM-CFP mainly engaged in static foci located at the membrane, reflecting the distribution of the basal bodies (**Figure 53**). As the employed strain carried two FliM copies, the native one and the fluorescently labelled FliM at the *amyE* site, fewer foci than the reported 20-25 basal bodies were counted (71).

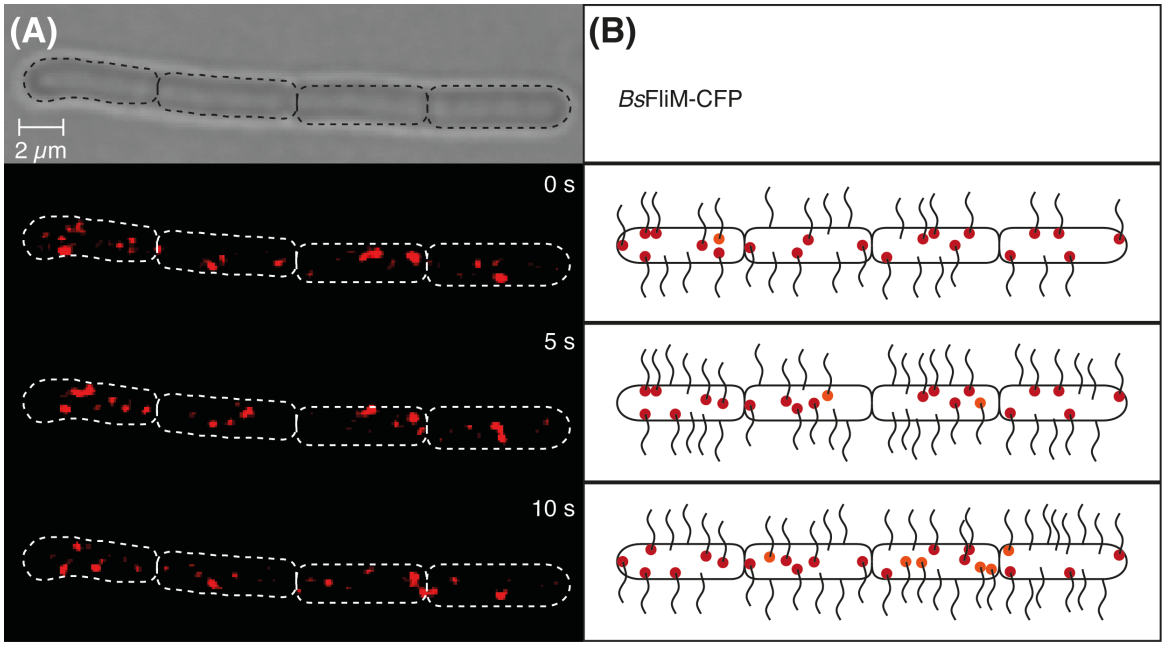

Figure 53. Localization of FliM in *B. subtilis*. (A) shows a series of images of *B. subtilis* with fluorescently labelled FliM. A bright-field image is provided at the top. Dashed lines indicate the outline of single *B. subtilis* cells. The scale bar equals 2 μm. **(B)** shows a cartoon illustrating the distribution of basal bodies in the cell. Foci are coloured-coded according to their behaviour, static (dark red) and movable (light red). The number of flagella exceeds the number of basal bodies due to the presence of the native *fliM* gene in addition to an ectopic *fliM-cfp*.

YFP-FlhG in contrast was still highly mobile again appearing in dynamic foci at the membrane. This also proofed to be a convenient indicator for the functionality of YFP-FlhG. Previous studies demonstrated that upon deletion of FlhG, basal

bodies tend to clump together forming larger aggregates. As basal bodies appeared normal in size and distribution considering the lower number due to the two FliM copies, the YFP-FlhG fusion protein is functional and executes its job in flagellation pattern maintenance. Fluorescence microscopy also revealed that a subpopulation of the static FlhG foci co-localizes with a fraction of basal bodies with an average residing time of 33.0 ± 20.1 s (n=31). This shows that FlhG is not an integral part of the basal body (**Figure 54**). However, it associates with the flagellar C-ring at a specific stage.

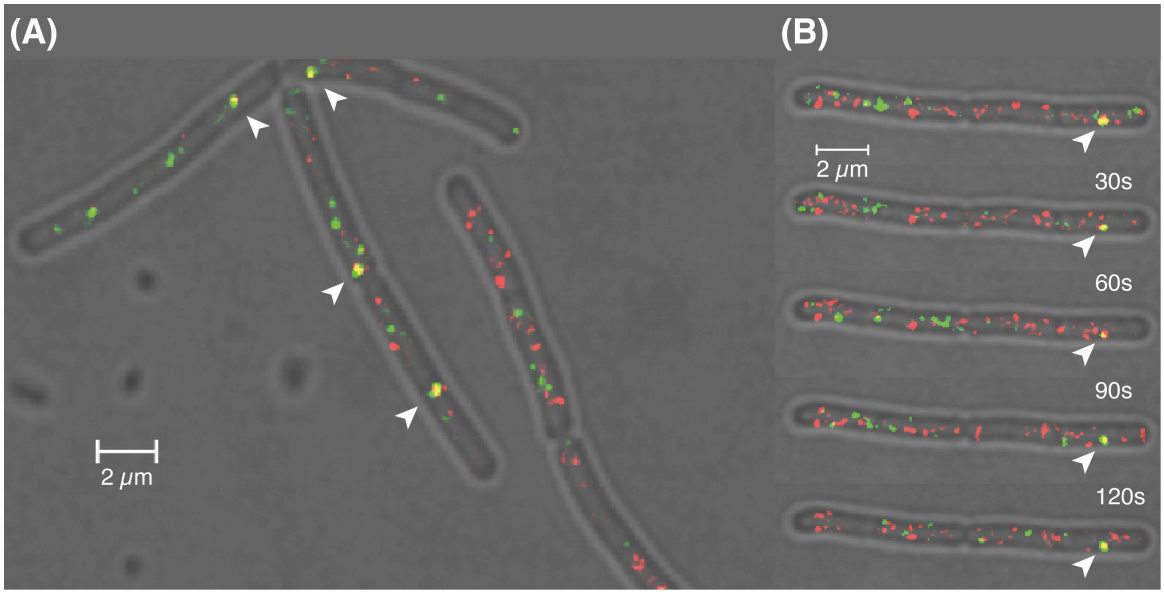

Figure 54. Co-localization of FliM and FlhG. (A) provides an overview picture of several *B. subtilis* cells, while **(B)** shows a time course of images. YFP-FlhG is shown in green, whereas FliM-CFP is coloured in red. White arrows indicate co-localization of both proteins. All scale bars equal 2 µm.

As FlhG co-localizes only with a fraction of basal bodies, FlhG is probably required during a specific phase, presumably of basal body biogenesis, due to the fact that flagella are inherited and not disassembled. This led to the working hypothesis that FlhG may bind to a FliM/FliY complex in the cytoplasm and delivers the C-ring building blocks to a nascent basal body. Prof. D. B. Kearns (Indiana University Bloomington, USA) kindly provided the plasmid for a strain expressing fluorescently labelled FliM.

2.6 FlhG delivers FliM and FliY to nascent flagellar C-rings

Fluorescence microscopy revealed that FlhG temporarily co-localize with FliM, and as such with flagellar basal bodies. This led to the idea that FlhG may be involved in the flagellar assembly itself. In this scenario FlhG would definitely play a role in C-ring assembly, as it is able to interact with a FliM/FliY complex in a nucleotide independent manner and additionally with FliG depending on the presence of ATP and lipids.

2.6.1 FlhG renders FliM/FliY capable of binding FliG

To further assess flagellar C-ring assembly and the influence of FlhG *in vitro*, GST-*Gt*FliG served as anchor point to build up the C-ring (**Figure 55**). For the reconstitution of the flagellar C-ring, GST-*Gt*FliG was attached to GST-beads and subsequently incubated with a *Gt*FliM/FliY complex in the presence and absence of *Gt*FlhG. In the absence of FlhG the *Gt*FliM/FliY did not interact with GST-*Gt*FliG.

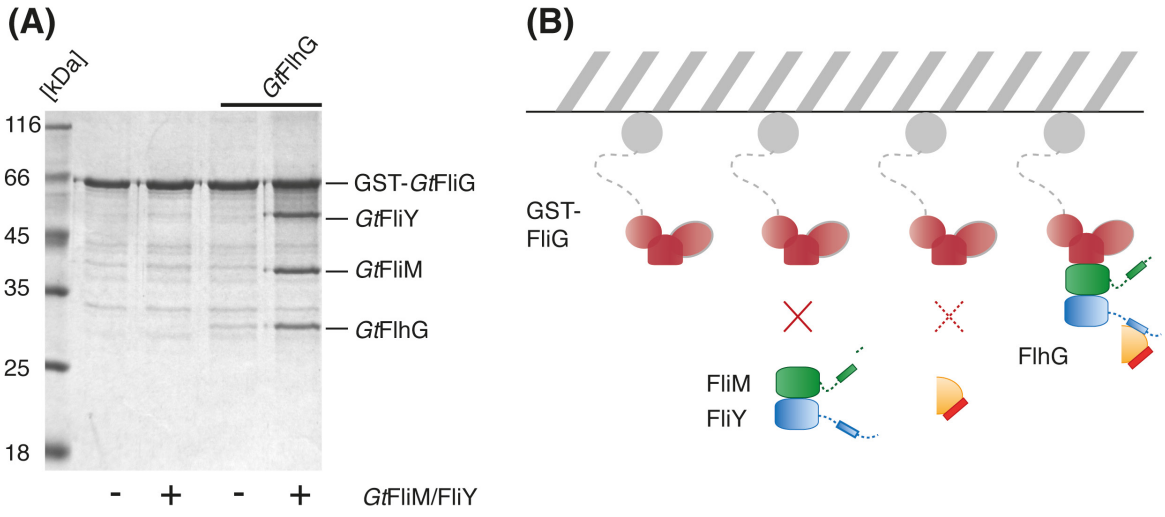

Figure 55. FlhG-assisted interaction of FliG and FliM/FliY. (A) shows the Coomassie-stained SDS-PAGE of interaction studies employing GST-*Gt*FliG (lane 1, input control) incubated with *Gt*FliM/FliY (lane 2), *Gt*FlhG (lane 3) and *Gt*FliM/FliY as well as *Gt*FlhG (lane 4). **(B)** displays a scheme illustrating the pull down experiment. The upper part shows the immobilized GST-tag in grey, the lower part indicates the proteins used in the assay.

In the absence of the *Gt*FliM/FliY complex a very weak interaction between *Gt*FlhG and GST-*Gt*FliG is detectable, as it was also observed previously. However, upon addition of *Gt*FlhG a quaternary complex of GST-*Gt*FliG/FliM/FliY/FlhG is formed with a stoichiometric ratio of approximately *Gt*FlhG:*Gt*FliM:*Gt*FliY of 1:1:1 (**Figure 55**). This indicates that FlhG is required for correct assembly of the C-ring under *in vitro* conditions.

2.6.2 FlhG assists in the assembly of FliM/FliY to FliG depending on ATP and lipids

To see whether the assembly only requires the binding of FlhG to the FliM/FliY complex or whether membrane association and the ATPase activity is required for this process, the C-ring assembly pull down assays were repeated in the presence of nucleotides and phospholipids. In the absence of *Gt*FlhG, a complex of *Gt*FliM/FliY did not interact with GST-*Gt*FliG. Also, the interaction of *Gt*FlhG with GST-*Gt*FliG in absence of *Gt*FliM and *Gt*FliY is barely visible. The formation of the quaternary complex of the flagellar C-ring and *Gt*FlhG is observed when all four proteins are present. The further addition of ADP, ATP or ATP and lipids did not change the situation. However, in the presence of ADP and lipids the signal for *Gt*FlhG, *Gt*FliM and *Gt*FliY increased to a stoichiometric ratio exceeding 1 compared to GST-*Gt*FliG, indicating the assembly of oligomeric C-ring complexes at the GST-*Gt*FliG (**Figure 56**).

Why this is observed in the presence of ADP and lipids but not upon ATP and lipid addition appears enigmatic at first, but a closer look at the assay conditions, showed that they were carried out in phosphate buffered saline (PBS) at 0 °C. The low temperature and the absence of magnesium in the buffer led to the conclusion that under these conditions the ATPase of *Gt*FlhG is barely active and therefore did not exhibit the expected behaviour. On the other hand the combination of ADP and lipid may mimic the post hydrolysis state and may therefore trigger the assembly of the C-ring components under these conditions. To confirm this hypothesis, interaction assays were performed under modified conditions. Instead of PBS buffer the assays were carried out in SEC buffer, containing 20 mM $MgCl_2$ and at 37 °C to be closer to physiological temperatures.

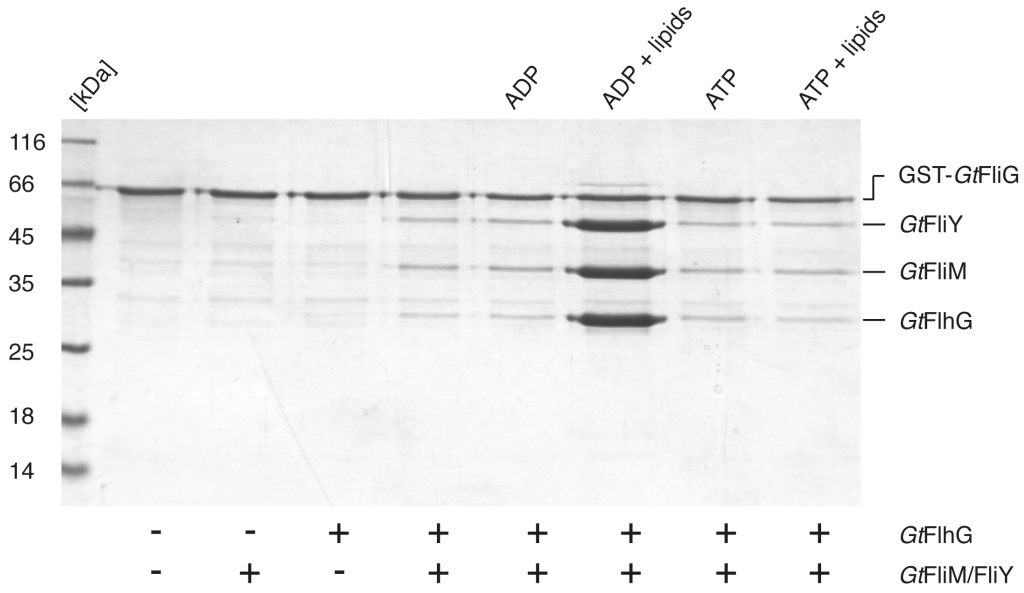

Figure 56. **Influences on the interaction of FliG, FliM, FliY and FlhG.** The Coomassie-stained SDS-PAGE shows pull down assays investigating the influence of the presence of nucleotides or lipids or the combination on the ability of *Gt*FliM/FliY/FlhG to interact with *Gt*FliG. Proteins were used in the same constitution as stated in the interaction assay before.

Furthermore, ATP and lipids were supplemented to this experiment. Under these conditions, an interaction between GST-*Gt*FliG and the *Gt*FliM/FliY complex was observed after 5 min of incubation resulting in a stoichiometric ratio of approximately 1:1:1. As described before *Gt*FlhG interacts with GST-*Gt*FliG in the presence of ATP and lipids also displaying a stoichiometric ratio of approximately 1:1 after 5 min incubation (**Figure 57**). Pull down assays including all four components were incubated for different periods of time (<1, 1, 5, 10, 30 and 60 min) to be able to monitor the gradual assembly of C-ring components at GST-*Gt*FliG, which would be expected according to the hypothesis from the last experiment. Upon very short incubation of *Gt*FlhG and *Gt*FliM/FliY with GST-*Gt*FliG a quaternary complex with a stoichiometry of 1:1:1:1 was observed. After only 5 min the stoichiometric ratio of *Gt*FlhG, *Gt*FliM and *Gt*FliY exceeded 1 compared to GST-*Gt*FliG. After 10 min of incubation the Pull down assays displayed a similar stoichiometry as observed before for ADP and lipids at low temperature and the absence of Mg^{2+}, again indicating the assembly of oligomeric C-ring building blocks at GST-*Gt*FliG (**Figure 57**). These results match the expectation based on the previous experiment.

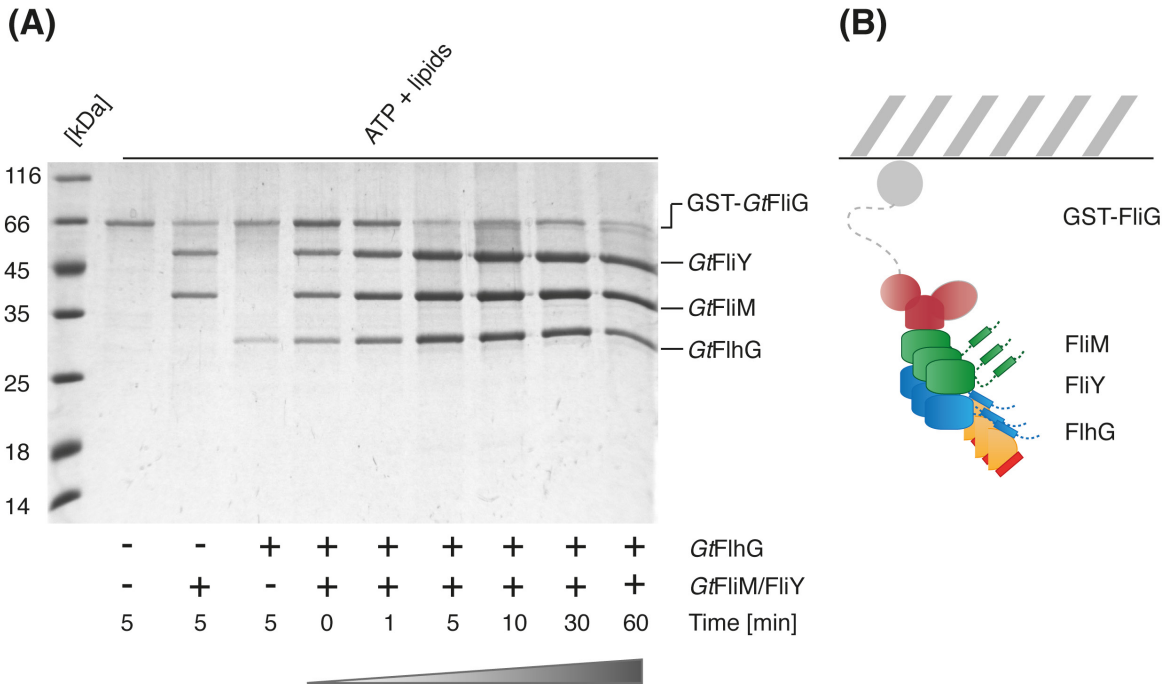

Figure 57. Assembly of oligomeric C-ring structures. (A) shows the results of time-resolved pull down experiments, which were performed using GST-*Gt*FliG, *Gt*FliM/FliY as well as *Gt*FlhG incubated with ATP and lipids. The Coomassie-stained SDS-PAGE shows the control pull downs in lane 1-3 and different incubation times ranging from a couple of seconds (0 min) to 60 min. The grey bar indicated increasing incubation time. **(B)** displays a scheme of the assembly of oligomeric *Gt*FliM/FliY/FlhG complexes at GST-*Gt*FliG. The upper part shows the immobilized GST-tag in grey, the lower part indicates the proteins used in the assay.

Since under special conditions an ADP bound state may mimic the situation observed for the presence of ATP and lipids under more physiological conditions, these results implicate that the energy generated by the ATP hydrolysis does not play a vital role in this process. The ATPase is probably rather a molecular switch that uses ATP to generate two distinct states, which are important to coordinate certain events. ATP hydrolysis therefore solely constitutes the transition between both states.

2.7 FlhG in *S. putrefaciens*

The Gram-negative marine bacterium *S. putrefaciens* CN-32 is the ideal organism to complement the study on the MinD/ParA ATPase FlhG performed in *B. subtilis*. Not only is *S. putrefaciens* Gram-negative and possesses a different

monotrichous flagellation pattern, but it exhibits two different flagella systems. The gene cluster of the primary flagella system encodes the *S. putrefaciens* orthologue of FlhG and produces a single polar flagellum. The additional secondary system is encoded in a second, independent gene cluster, producing one or two lateral flagella, which are responsive neither to regulation through FlhG nor to chemotaxis. Besides the possibility to study pattern maintenance in monotrichous flagellation, it provides a second independent system as the perfect negative control for further investigations. This project was carried out in close collaboration with Prof. Dr. Kai Thormann (Justus Liebig University, Gießen). Cell biology, genetics and *in vivo* manipulations were performed by Florian Rossmann in the Thormann lab and will be briefly summarized. I complemented the *in vivo* study with biochemistry and *in vitro* interaction studies in *S. putrefaciens*.

2.7.1 FlhG in a monotrichous Gram-negative bacterium

In *S. putrefaciens,* FlhG is encoded on the polar flagellar gene cluster adjacent downstream to *flhF*. A detailed sequence alignment displayed that *Sp*FlhG retained all essential motifs for the hallmark features such as ATPase activity, dimerization and membrane association (**Figure 16** and **Figure 21A**). Deletion of *flhG* in *S. putrefaciens* CN-32 results in a hyper-flagellated phenotype at the cell pole as observed for *Vibrio species* with 6-12 flagella per cell accompanied by severely reduced motility. However, localization and number of lateral flagella are unaffected by the *flhG* deletion (103). Again, HPLC-based hydrolysis assays confirmed that FlhG is an ATPase. Replacement of *Sp*FlhG by a hydrolysis deficient variant (*i.e.* FlhG K29A) leads to hyper-flagellation at the cell pole and severe motility defects, demonstrating that in *S. putrefaciens* the ATPase activity plays a crucial role to restrict the number of polar flagella. In *S. putrefaciens* FlhG exhibits a C-terminal amphipathic helix that presumably is responsible for membrane association. Introduction of a double phenylalanine mutant in *S. putrefaciens* (*i.e.* F275A and F276A), that in *G. thermodenitrificans* silenced the membrane association ability of the MTS, showed the same phenotype as the *flhG* deletion strain, indicating that not only the disruption of the ATPase activity but also the

impairment of the membrane association ability is detrimental to the monotrichous flagellation pattern (103).

2.7.2 FlhG interacts with the flagellar C-ring

Having confirmed the main features of FlhG in *S. putrefaciens*, new questions arose. Does FlhG also interact with the flagellar C-ring components in a monotrichously flagellated bacterium? Can FlhG bind to both the polar and the lateral C-ring in *S. putrefaciens*? Does FlhG interact with the flagellar C-ring in a similar way as observed in *B. subtilis/G. thermodenitrificans*?

The first step to address this task consisted of interaction studies with the C-ring proteins *Sp*FliM$_1$ and *Sp*FliN$_1$ of the polar system and *Sp*FliM$_2$ and *Sp*FliN$_2$ of the lateral system. Pull down assays, testing all four possible C-ring combinations (*Sp*FliM$_1$/FliN$_1$, *Sp*FliM$_1$/FliN$_2$, *Sp*FliM$_2$/FliN$_1$ and *Sp*FliM$_2$/FliN$_2$), demonstrated that FliM and FliN are system-specific and only interact with their cognate C-ring partners. No interaction was observed between proteins from different flagellar systems (**Figure 58**). For these Ni-NTA interaction assays FliM carried a C-terminal (His)$_6$-tag, while FliN was not tagged. Further interaction studies were performed using an N-terminal GST fusion variant of *Sp*FlhG (GST-*Sp*FlhG) carrying additionally a (His)$_6$-tag, (His)$_6$-tagged versions of FliM$_{1/2}$ and untagged FliN$_{1/2}$.

Ni-NTA affinity pull down assays revealed the presence of all produced proteins, although GST-*Sp*FlhG is visible in large excess. GST affinity interaction studies revealed that only the polar C-ring complex *Sp*FliM$_1$/FliN$_1$ is able to bind the GST-*Sp*FlhG (**Figure 58B**). These findings were confirmed by Ni-NTA affinity pull down assays with (His)$_6$-tagged *Sp*FlhG where both C-ring complexes *Sp*FliM$_1$/*Sp*FliN$_1$ *Sp*FliM$_2$/*Sp*FliN$_2$ carried no affinity tag (**Figure 58C**). These experiments revealed that *Sp*FlhG exclusively interact with the polar C-ring complex *Sp*FliM$_1$/*Sp*FliN$_1$, giving a molecular explanation why FlhG only affects the polar pattern.

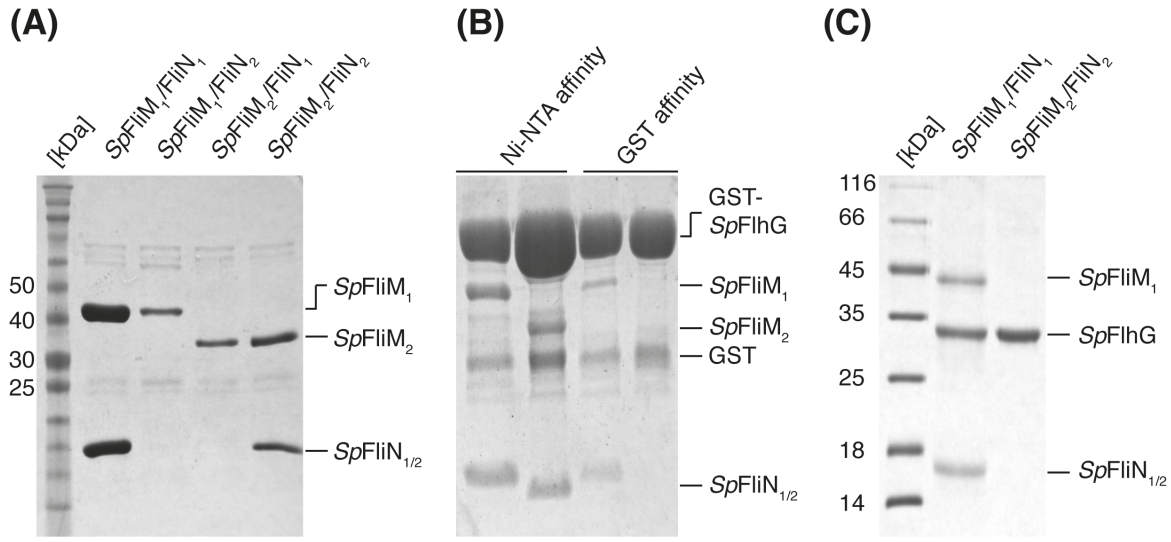

Figure 58. Interaction FlhG, FliM and FliN in *S. putrefaciens*. (A) shows the Coomassie-stained SDS-PAGE of Ni-NTA affinity pull down assays employing *Sp*FliM$_1$ and *Sp*FliM$_2$ carrying a (His)$_6$-tag as well as FliN$_1$ and FliN$_2$ without tag. **(B)** The Coomassie-stained SDS-PAGE shows Ni-NTA affinity and GST affinity pull down experiments of the GST-*Sp*FlhG with *Sp*FliM$_1$/FliN$_1$ and GST-*Sp*FlhG with *Sp*FliM$_2$/FliN$_2$. The experiments were carried out as described in the text. The Ni-NTA affinity (lanes 1 and 2) experiments served as the positive control to monitor the presence of all components. **(C)** shows the Coomassie-stained SDS-PAGE of interaction studies employing (His)$_6$-tagged *Sp*FlhG and untagged C-ring complexes *Sp*FliM$_1$/FliN$_1$ and *Sp*FliM$_2$/FliN$_2$.

2.7.3 The N-terminus of FliM$_1$ mediates FlhG interaction

A closer look at the domain architecture of the different C-ring components in *S. putrefaciens* revealed that the polar FliM$_1$ displays features of the canonical FliM including a N-terminal 'EIDAL' motif, a globular middle domain containing FliG binding motifs and a C-terminal FliN homology domain. However, the lateral FliM$_2$ lacks the 'EIDAL' motif at its N-terminus and the middle domain of FliM$_2$ does not share the characteristic motifs required for the interaction with FliG. Only the C-terminal FliN-domain seems conserved. Both FliN$_1$ and FliN$_2$ only consist of a short FliN-domain (**Figure 59A**). This led to the assumption that *Sp*FlhG interacts with the N-terminal 'EIDAL' motif of *Sp*FliM$_1$ in *S. putrefaciens*, as observed for the 'EIDAL' motif of FliY in *B. subtilis*. Again the first 27 amino acids of FliM$_1$ were deleted generating *Sp*FliM$_1$-ΔN.

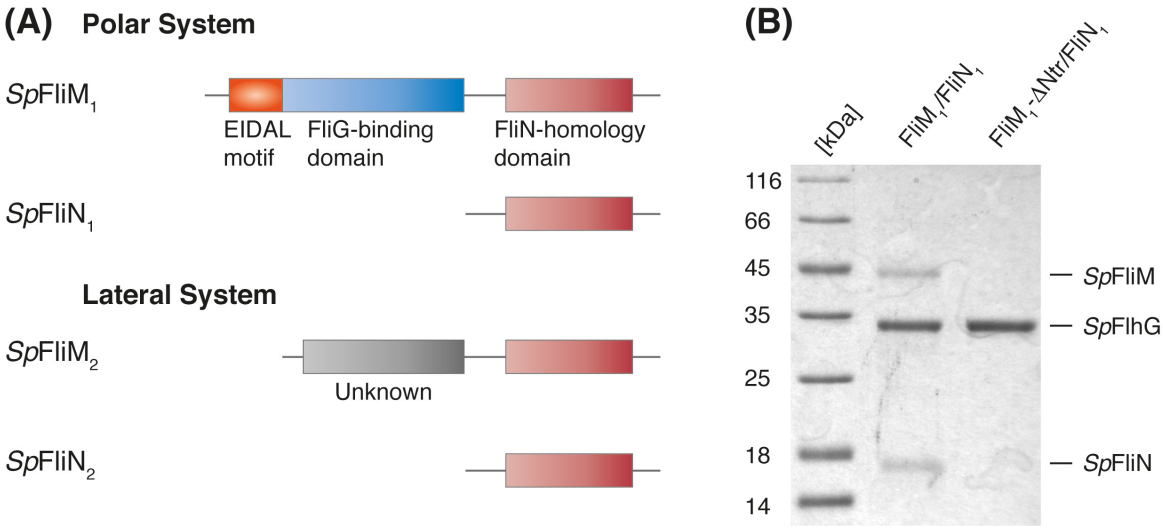

Figure 59. Two flagella systems. (A) shows the domain architecture of the C-ring components FliM and FliN of the polar (*Sp*FliM$_1$ and *Sp*FliN$_1$) and lateral flagella system (*Sp*FliM$_2$ and *Sp*FliN$_2$) of *S. putrefaciens*. **(B)** shows the Coomassie-stained SDS-PAGE of pull down assays using *Sp*FlhG carrying a (His)$_6$-tag and untagged C-ring proteins.

Interaction assays revealed that a polar C-ring complex lacking the N-terminus of FliM$_1$ was not able to interact with *Sp*FlhG (**Figure 59B**). The N-terminal EIDAL motif of FliM$_1$ mediates thus the interaction of FlhG with the C-ring complex *Sp*FliM$_1$/*Sp*FliN$_1$.

2.8 Compatibility of FlhG and the C-ring components of *G. thermodenitrificans* and *S. putrefaciens*

In both, *B. subtilis* and *S. putrefaciens*, FlhG is a ParA/MinD ATPase, which is supposed to form dimers and attaches to the membrane through a C-terminal membrane targeting sequence. Furthermore, it interacts with a conserved 'EIDAL' motif present in the C-ring complex FliM/FliY in *G. thermodenitrificans* and FliM$_1$/FliN$_1$ in *S. putrefaciens*. As a synthetic approach I wanted to know whether FlhG would be able to recognize C-ring components from the other organism *in vitro*. Some of the experiments were performed by Sabrina Henche in the scope of a 6 weeks practical course under my supervision.

2.8.1 Compatibility of the FlhG and C-ring components *in vitro*

GST affinity pulldown assays were performed, using GST-*Gt*FlhG and GST-*Sp*FlhG as bait and the C-ring complex FliM/FliY from *G. thermodenitrificans* as prey. The interaction between GST-*Gt*FlhG and *Gt*FliM/*Gt*FliY was confirmed and served as a positive control (**Figure 60**). However, GST-*Sp*FlhG also interacts with *Gt*FliM/*Gt*FliY almost equally strong as GST-*Gt*FlhG (**Figure 60**). This indicated that FlhG might be exchangeable between different species.

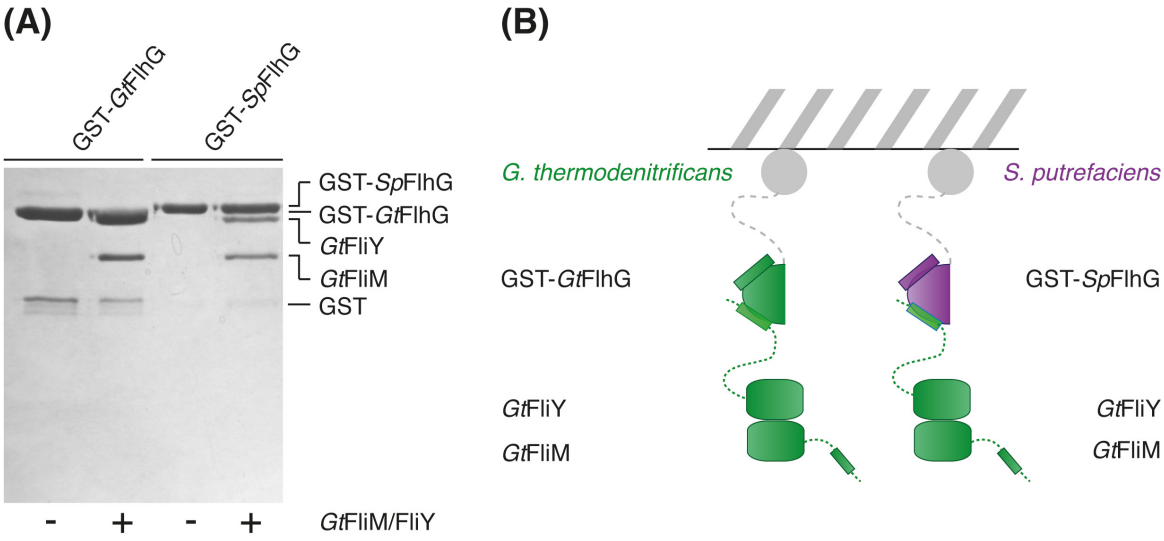

Figure 60. Compatibility of a C-ring complex. (A) shows the Coomassie-stained SDS-PAGE of interaction studies employing GST-*Gt*FlhG and GST-*Sp*FlhG as well as a purified *Gt*FliM/FliY complex. **(B)** shows a scheme of the interaction assays described in **(A)**. The upper part shows the immobilized GST-tag in grey, the lower part indicates the proteins used in the assay. Green represents proteins derived from *G. thermodenitrificans*, while proteins of *S. putrefaciens* are depicted in purple.

Based on these initial results, the interaction studies were modified and extended now including GST-*Gt*FlhG and GST-*Sp*FlhG as bait and all combinations of the C-ring proteins *Gt*FliM, *Gt*FliY, *Gt*FliM$_1$ and *Gt*FliN$_1$ as prey (**Figure 61A**). Pull down assays were performed as described without the presence of nucleotides or lipids. The native ternary complexes GST-*Gt*FlhG/FliM/FliY and GST-*Sp*FlhG/FliM$_1$/FliN$_1$ served as positive controls and this interaction was clearly visible on the Coomassie-stained SDS-PAGE (**Figure 61B**). Besides *Gt*FliM/FliY, GST-*Gt*FlhG seems to interact with the *S. putrefaciens* C-ring complex *Sp*FliM$_1$/FliN$_1$ and weakly with *Gt*FliM/*Sp*FliN$_1$. Upon incubation of GST-*Gt*FlhG

with *Sp*FliM$_1$ and *Gt*FliY, GST-*Gt*FlhG interacts with *Gt*FliY. However, the signal for *Sp*FliM$_1$ was missing indicating that *Sp*FliM$_1$ and *Gt*FliY do not interact with each other. On the other hand GST-*Sp*FlhG strongly binds to *Sp*FliM$_1$/FliN$_1$ as well as the C-ring complex FliM/FliY from *G. thermodenitrificans*. The interaction of GST-*Sp*FlhG with the complex *Gt*FliM/*Sp*FliN$_1$ was barely visible.

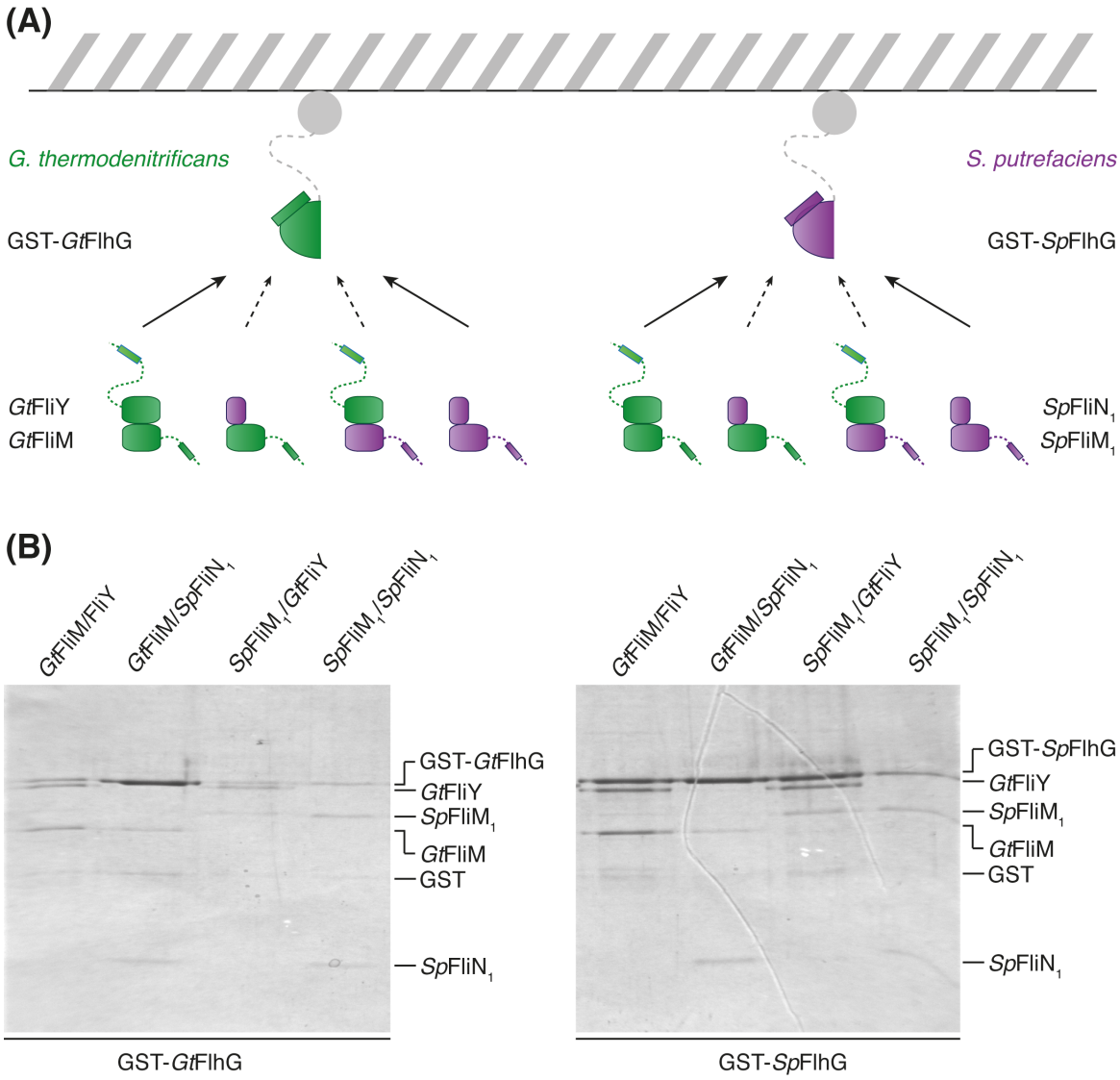

Figure 61. Compatibility of flagellar components from different organisms. (A) displays a scheme of the interaction assays shown in (B). Components are colour-coded according to the respective species, *G. thermodenitrificans* in green and *S. putrefaciens* in purple. **(B)** shows the respective Coomassie-stained SDS-PAGE of interaction assays employing GST-*Gt*FlhG and GST-*Sp*FlhG and the respective combinations of C-ring complexes shown in (A).

Incubation of GST-*Sp*FlhG with *Sp*FliM$_1$ and *Gt*FliY results in a strong *Gt*FliY signal and a much weaker signal for *Sp*FliM$_1$, again pointing to a incomplete or impaired complex formation between *Sp*FliM$_1$ and *Gt*FliY (**Figure 61B**). These interaction studies demonstrated that FlhGs from both species strongly bind to their cognate C-ring complexes as well as to the C-ring complexes of the other species. FlhG seems thus interchangeable concerning C-ring interaction between *G. thermodenitrificans/B. subtilis* and *S. putrefaciens* at least under *in vitro* assay conditions. However, Chimeric C-ring complexes seem either not to form at all or be defective in FlhG interaction. As FlhG seemed to be compatible in both species, we aimed at generating an *S. putrefaciens* strain carrying *Bs*FlhG or *Gt*FlhG instead of its native *Sp*FlhG. This was done in laboratory of Prof. Dr. Kai Thormann. However, it turned out to be much more difficult to exchange components of the flagellation pattern control system *in vivo* (personal communication K. Thormann).

2.9 FlrA in *S. putrefaciens*

FleQ/FlrA is the c-di-GMP dependent master regulator of flagellar gene expression in many polarly flagellated γ-proteobacteria. It activates the transcription of early flagellar genes initiating the transcription cascade that results in the biosynthesis of a flagellum. C-di-GMP is a ubiquitous second messenger affecting the transition between a motile free swimming lifestyle and the formation of adhesive biofilms, modulating transcription, translation, enzyme activity as well as protein-protein interaction (reviewed in: (224-229)). Recent studies demonstrated that FleQ and FlhG directly interact with each other in the monotrichous *P. aeruginosa*. A sequence alignment of *Pa*FleQ and *Sp*FlrA the master regulator of flagellar gene transcription in *S. putrefaciens* show a conserved domain architecture and high sequence homology, indicating a similar mode of action in both organisms. I therefore started to investigate FlrA in *S. putrefaciens*. These experiments were performed by Sabrina Henche in the scope of a master project under my supervision.

2.9.1 FlhG interacts with FlrA in *S. putrefaciens*

To confirm the interaction of *Sp*FlrA and *Sp*FlhG an N-terminal GST fusion construct of FlrA was generated (GST-*Sp*FlrA). *In vitro* interaction studies revealed that FlhG indeed interacts with FlrA in *S. putrefaciens*. While, without nucleotides only a weak interaction is observed, the interaction affinity increases upon addition of ADP or ATP. This effect was not obtained by addition of AMPPNP (**Figure 62**).

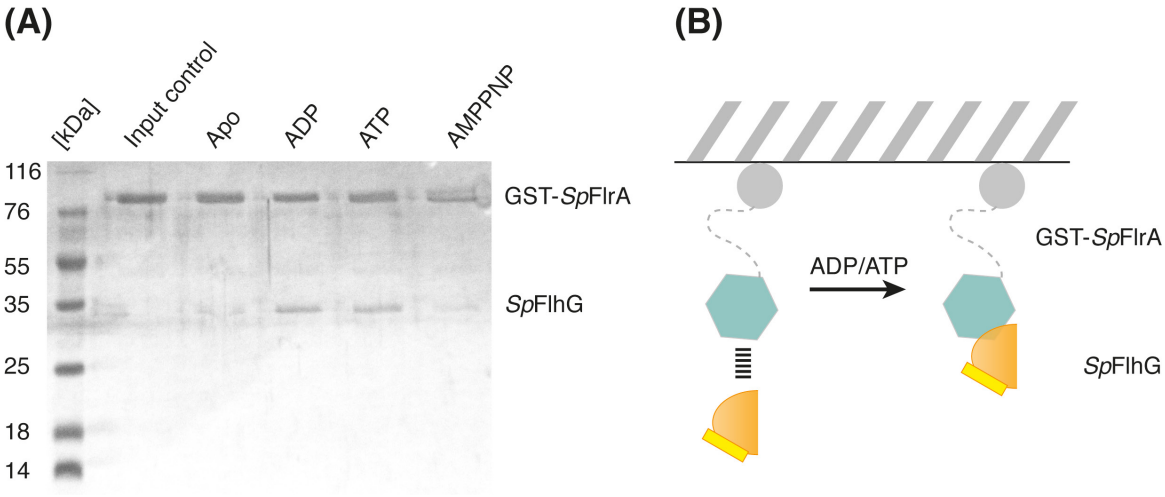

Figure 62. Interaction of FlhG and FlrA in *S. putrefaciens*. (A) shows the Coomassie-stained SDS-PAGE of GST affinity interaction assays using GST-*Sp*FlrA and purified *Sp*FlhG in the absence or presence of the indicated nucleotides. **(B)** provides a scheme of the pull down assays shown in (A). The upper part shows the immobilized GST-tag of *Sp*FlrA in grey, the lower part indicates the proteins used in the assay.

According to our *in vitro* binding assays, FlhG and FlrA interact in a nucleotide dependent manner. However, as both proteins comprise an ATPase, it is not clear whether the nucleotide load of FlhG or FlrA or maybe of both is the crucial factor for the interaction. To further assess this task FlrA was subdivided according to its domain architecture (**Figure 63B**). One construct includes the N-terminal FleQ domain (*Sp*FlrA-FleQ), another one the C-terminal DNA binding domain with the characteristic helix turn helix motif (*Sp*FlrA-DNA). The third sub-construct of FlrA contains the AAA+ ATPase domain, constituting the middle part of FlrA. In pull down assays GST-*Sp*FlhG was now used as a bait, whereas the domains of FlrA carrying a $(His)_6$-tag were the prey. Due to insolubility of the ATPase do-

main, the interaction studies were performed with the N- and C-terminus of FlrA. While the DNA binding domain of FlrA clearly interacts with FlhG, no interaction was observed with the N-terminal FleQ domain (**Figure 63AC**). Again, the interaction was strongly enhanced by addition of ADP as observed for full length FlrA. These experiments indicate that the nucleotide load of the FlhG ATPase strongly influences the interaction of FlhG and FlrA. This might implicate that FlrA interacts with the FlhG homodimers.

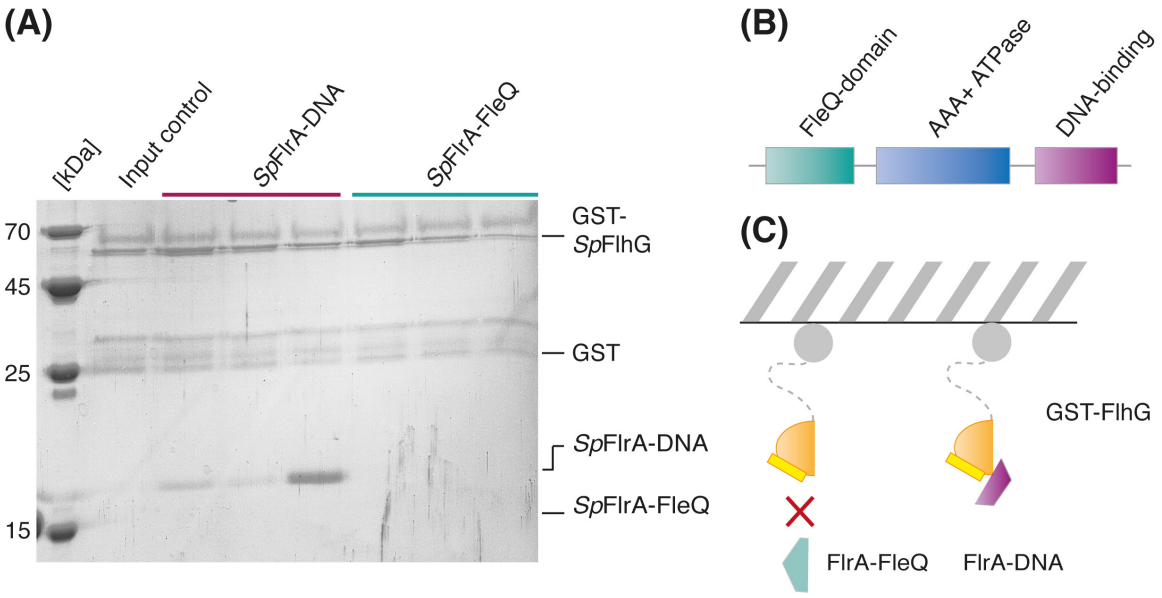

Figure 63. Interaction of FlhG and FlrA in *S. putrefaciens*. **(A)** shows the Coomassie-stained SDS-PAGE of GST affinity pull down assays using GST-*Sp*FlhG and the N-terminal FleQ domain of *Sp*FlrA (*Sp*FlrA-FleQ) as well as the C-terminal DNA-binding domain of *Sp*FlrA (*Sp*FlrA-DNA). The addition of nucleotides is indicated. **(B)** displays the scheme of the domain architecture of FlrA in *S. putrefaciens*. **(C)** provides a scheme of the pull down assays shown in **(A)**. The upper part shows the immobilized GST-tag of *Sp*FlhG in grey, the lower part indicates the proteins used in the assay.

Initial experiments confirmed the connection of FlhG and the master regulator of flagellar gene expression FlrA in *S. putrefaciens*. The interaction seems to be mediated through the DNA-binding domain of FlrA, which raises the question whether FlhG competes with DNA in binding to FlrA. Whether FlhG may release FlrA from the promotor regions of flagellar genes and thereby inhibit flagellar gene expression needs to be further addressed. How FlhG may influence the ATPase of FlrA as reported previously also remains elusive.

2.10 HubP in *S. putrefaciens*

In *P. aeruginosa* HubP is reported as a polar 'landmark' protein, which recruits a plethora of proteins including several MinD/ParA ATPases to the cell pole, thereby directly interacting with FlhF and FlhG. HubP is composed of a periplasmic LysM domain, an adjacent transmembrane helix and an extensive disordered cytoplasmic domain, which is supposed to function as an interaction platform for many polar proteins.

The HubP orthologue (*Sp*HubP) of *S. putrefaciens* shares the same domain architecture and is assumed to exhibit similar cellular functions. The cytoplasmic domain of *Sp*HubP contains acidic repetitive motifs of around 30 amino acids in length with small variations (EIAAELDxELxxxxxxxDDIDALLA(D/E)FD). In collaboration with the Thormann group (Justus Liebig University, Gießen), we aimed at further elucidating interaction partners of *Sp*HubP. Susanne Brenzinger therefore generated a fusion protein of the cytoplasmic domain (amino acids 102-580) of HubP adjacent to a GST tag (GST-HubP$_{102-580}$). A GST- and (His)$_6$-tagged cytoplasmic domain of HubP was produced in *E. coli* BL21 (DE3) under Isopropyl β-D-1-thiogalactopyranoside (IPTG) induction and purified using a two-step protocol, consisting of GST-trap affinity chromatography and subsequent SEC.

Pull down assays with freshly prepared cell lysate of a *hubP* deletion strain of *S. putrefaciens* CN32 were performed and visualized on Coomassie-stained SDS-PAGE after elution. Signals corresponding to putative interaction partners were analysed by mass spectrometry (**Figure 64**). GST-HubP$_{102-580}$ which was not incubated with lysate from *S. putrefaciens*, served as input control. To exclude unspecific interactions with the GST tag, purified GST was used as second control for this assay.

Protein signals that appeared in neither control were assumed as specific interaction partners. Mass spectrometry analysis revealed two prominent groups of interaction partners. The first group is related to the chemotaxis system including (ArcA, an uncharacterized methyltransferase (Sputcn32_1759), a putative signal transduction protein and an uncharacterized histidine kinase), the second group comprises the ribosomal proteins of the large subunit L1 to L3 (**Table S2**).

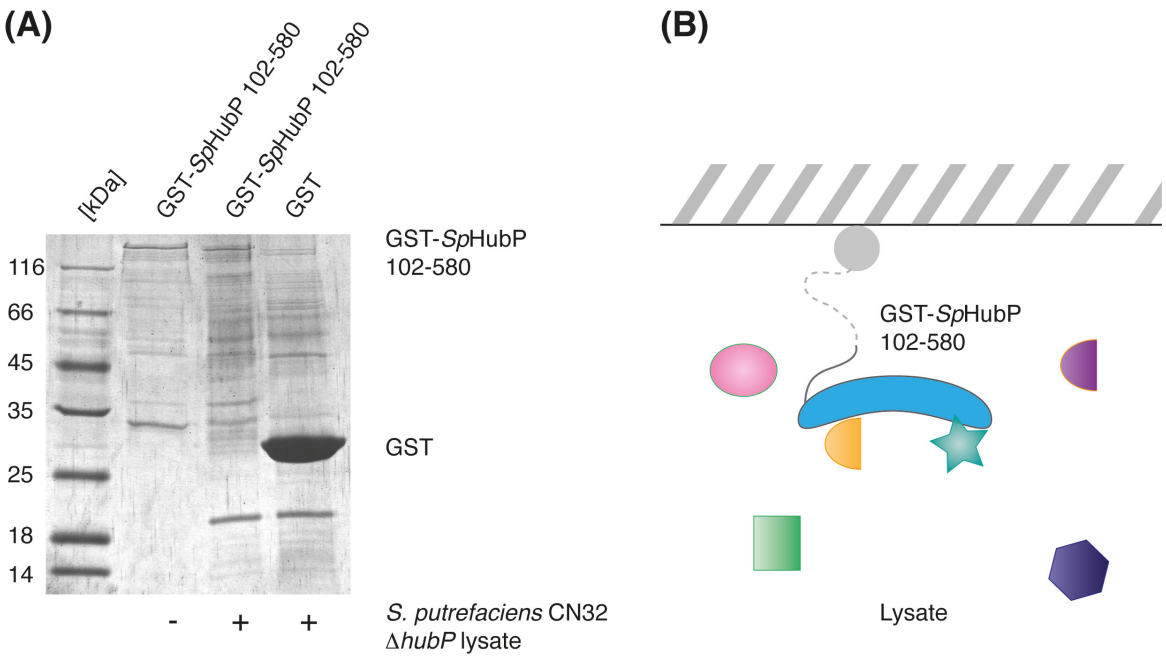

Figure 64. HubP interaction network. (A) shows the Coomassie-stained SDS-PAGE of GST affinity interaction assay using a GST fusion of the cytoplasmic domain of HubP (GST-*Sp*HubP 102-580) and freshly prepared lysate of a S. putrefaciens Δ*hubP* strain. **(B)** illustrates the pull down assay of **(A)**. The upper part shows the immobilized GST-tag of HubP in grey and HubP in blue. The lower part represents the plethora of possible interaction partners in the lysate of the *S. putrefaciens* CN32 Δ*hubP*.

The first group of proteins corroborate to the previously reported function of HubP as polar 'landmark' protein that especially orchestrates chemotaxis proteins (139). However, the ParA/MinD ATPases (ParA, ParC, MinD and FlhG) and FlhF were not identified in the pull down experiments, although the interaction is reported in literature. This may indicate a very weak or transient interaction of these nucleotide-binding proteins with HubP emphasizing the dynamic of the system (139). The full extent of the task spectrum of HubP remains elusive and may go beyond simple scaffolding functions.

2.11 Method section: $^{1}H/^{2}H$ exchange mass spectrometry

HDX has emerged as a powerful tool to study protein dynamics and protein-protein interfaces, complementing canonical methods of structural biology, such as X-ray crystallography and nuclear magnetic resonance (NMR) (reviewed in: (230-

234)). Traditionally hydrogen/deuterium exchange was investigated employing NMR analysis (reviewed in: (235)). First studies using amide proton exchange in combination with mass spectrometry date back to the 1990s (236). HDX allows the assessment of the flexibility and dynamic behaviour of proteins by measuring the incorporation of deuterium into the backbone of amino acids. In the scope of this work this method was implemented in Marburg in cooperation with Dr. Uwe Linne (head of the mass spectrometry facility of the Chemistry Department, Philipps University, Marburg).

2.11.1 Functional principle of HDX

HDX employs the effect that hydrogen and deuterium as isotopes may freely replace each other in molecules without changing their chemical properties. Upon incubation of a molecule in deuterated solvent hydrogen is replaced by deuterium depending on the nature of the chemical bond and the respective pK_a value. The exchange rate of the amide hydrogen of the protein backbone proofed to be in a suitable kinetic window, being fast enough to get high exchange rates after short incubation in deuterium rich buffer, but also being slow enough under specific conditions leaving enough time to digest the protein, separate the peptides by HPLC and analyse the deuterium content by ESI mass spectrometry (**Figure 65**). Hydrogen atoms directly bound to carbon show much slower exchange rates, whereas hydrogen atoms within the polar, acidic or basic side chains of amino acids exchange and re-exchange too fast to be detected. The exchange rate of the hydrogen atoms also depends on their solvent accessibility within a molecule. Amide bonds of the protein backbone involved in the formation of secondary structure elements (*i.e.* α-helices and β-strands) exchange much slower than amide hydrogens bound in surface exposed loop regions. The incorporation of deuterium into a protein therefore correlates to its flexibility and its propensity to form secondary structure elements. This allows estimating the flexibility and also the secondary structure elements of proteins.

The protein of interest is diluted into a deuterium containing buffer and incubated for a specific time, which may range from 20 s to several hours, allowing the exchange of hydrogen to deuterium. The exchange reaction is subsequently

quenched by lowering the pH to 2.5 and decreasing the temperature to 0 °C. A pepsin digest of the protein, which can be performed on the HPLC through a pepsin column, provides peptic peptides still labelled with deuterium. These peptides are separated and analysed by mass spectrometry, resulting in peptides with increased mass and a specific signal shape. The deuterium incorporation is calculated as the mass difference of the centroids of the deuterated version of a peptide and its non-deuterated counterpart (**Figure 65**).

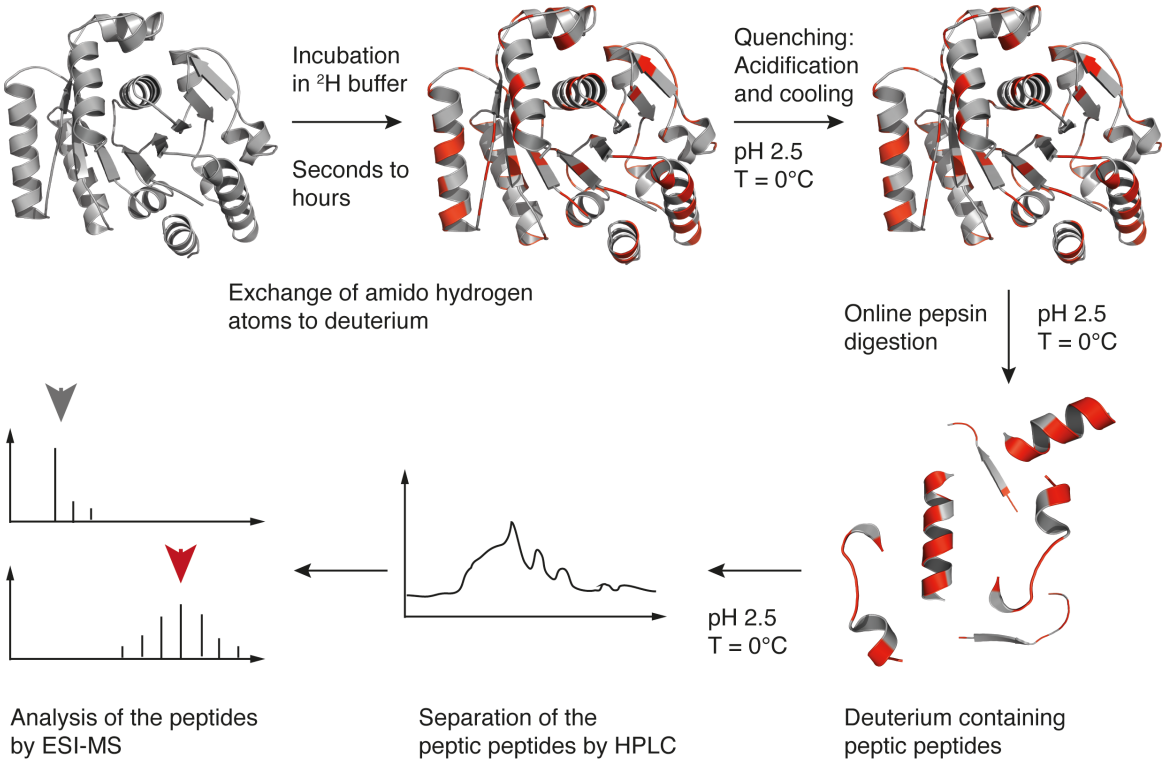

Figure 65. Principle of 1H/2H exchange mass spectrometry. The scheme displays the essential steps of HDX measurements. Deuterium incorporation is visualized in red. The deuterium incorporation is calculated as the centroid mass difference of the non-deuterated peptide (grey arrow) and its deuterated counterpart (red arrow). Pdb code of the shown structure: 4RZ2.

2.11.2 HDX in life sciences

In the life sciences HDX emerged as an ideal complementation to classic structural biology, aiming at elucidating the structure at highest possible resolution. HDX allows assessing protein dynamic in solution without the need of crystals and without size limitations that are faced using NMR. It offers the possibility to

identify flexible regions in proteins that may prevent crystallization, which strongly improves the process of construct optimization (**Figure 66A**).

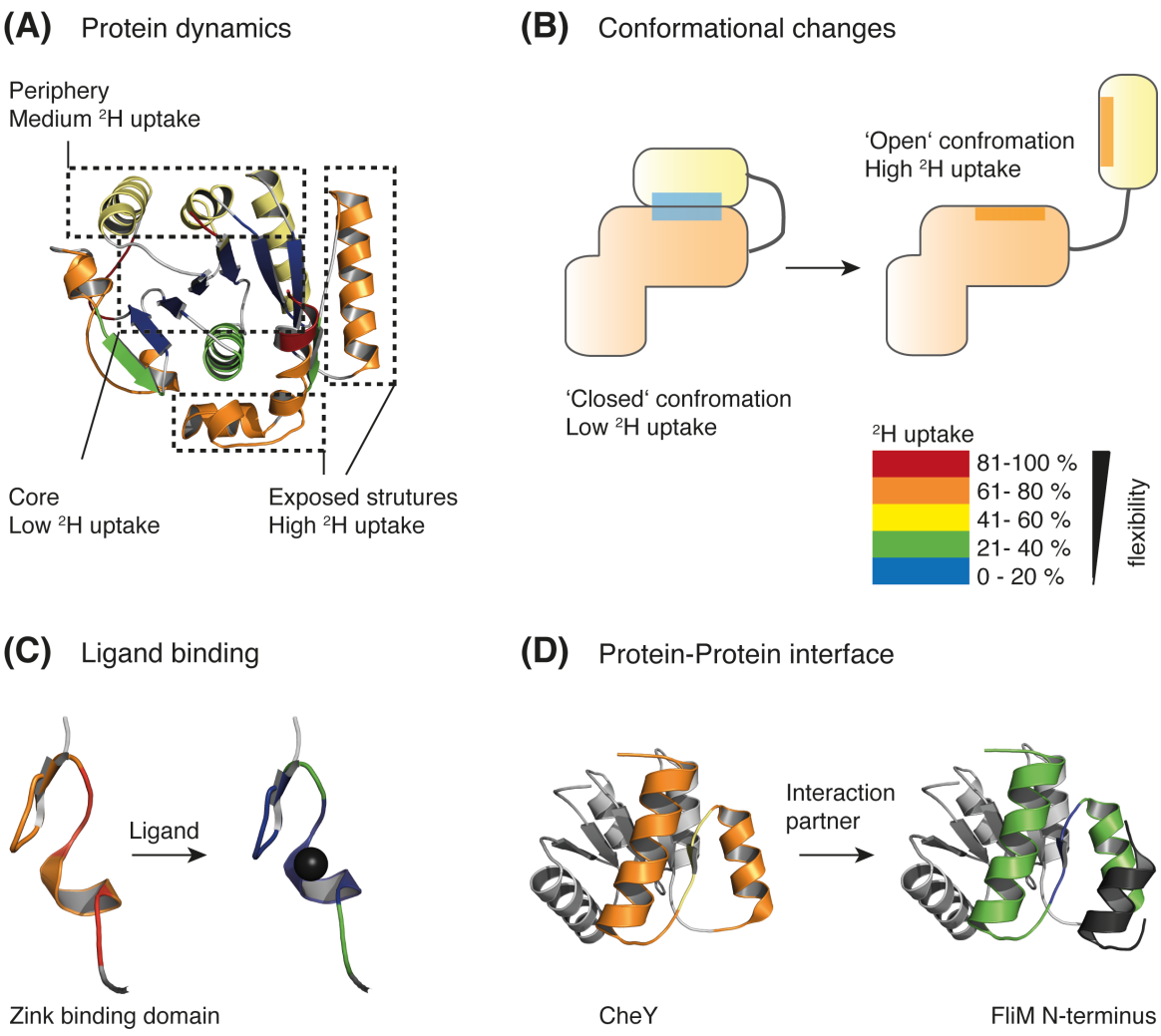

Figure 66. Application of HDX. HDX is suitable to determine general protein dynamics and flexibility. The higher the deuterium uptake the more flexible and solvent accessible is the respective region of the protein. **(A)** depicts the example of a protein structure to demonstrate the regional differences in deuterium uptake. **(B)**, **(C)** and **(D)** all show examples for the application of HDX. **(B)** shows how conformational rearrangements can be visualized when the two states differ in deuterium incorporation. **(C)** shows the binding of a small ligand to a protein. The binding site exhibits strong shielding in deuterium uptake upon ligand binding. **(D)** Similar to (C) protein-protein interfaces can be calculated from the decrease in deuterium incorporation of the single protein and the complex with its interaction partner. Pdb codes of the shown structures: 4RZ3 (A); 3E2U (C); 2B1J (D).

HDX may assist in locating the rearrangement and reveal the participating structural elements. This method is also a popular tool to study protein folding

and unfolding processes (**Figure 66B**). In addition, it also allows the mapping of protein-protein interaction interfaces by measuring the flexibility of a protein bound in a complex compared to the single protein. Regions that gain rigidity upon complex formation are very likely to participate in the interaction interface. With the same technique a binding site of a ligand can be easily determined (**Figure 66CD**). Even the arrangement of proteins within large structures such as viral capsids can be addressed (237, 238). Proteins that undergo large conformational changes can be challenging to address with classic structural biology. For HDX measurements a concentrated protein solution is diluted into deuterated buffer and incubated for a specific time that may range from several seconds to several hours to allow deuterium uptake. Upon acidification using a quench buffer (pH 2.2) and decreasing the temperature to 0 °C the exchange reaction is slowed down to a degree, which allows to digest the protein with pepsin, separate the peptides on an HPLC system and analyse the peptic peptides by ESI mass spectrometry. A very convenient way of treating the protein is an on-line digestion on a pepsin column implemented into the HPLC system (**Figure 67**).

2.11.3 Setup and implementation of HDX in Marburg

In collaboration with Dr. Uwe Linne, I constructed and established the method of amide proton exchange in Marburg including the packing of the trap column, the pepsin column and the HPLC setup as well as the control of all components using ChemStation (version).

2.11.3.1 Preparation of the pepsin column

The pepsin column for the inline digestion of labelled proteins was prepared by immobilizing pepsin onto POROS® AL 20 µm resin. Amino groups of lysine residues of pepsin (Roche) form a Schiff base with accessible aldehyde moieties of the resin. Thus, pepsin is covalently attached to the resin and can be used in HPLC.

In a first step 160 mg pepsin was dissolved in 50 mM sodium citrate (pH 4.4). Subsequently, 0.5 g POROS® AL, 20 µm was added and 5 times inverted, which leads to the formation of the Schiff base between the resin and pepsin. Afterwards, two dry crumbs (3 mm diameter) of sodium cyanoborohydride (Sigma Aldirch), which is hygroscopic, were added. Adding 100 µl of 2 M sodium sulphate every 3 min over a time period of 2 h, 4 ml in total results in salting out of the pepsin on the resin surface increasing the local concentration and the immobilization efficiency. The mixture was incubated over night at 4 °C and inverted from time to time. After addition of 160 µl of 2 M TRIS (pH 7.6) buffer the mixture was again incubated at 4 °C for 2-4 h and inverted now and then. Finally, the mixture was washed 7 times with 0.1 % formic acid and subsequent centrifugation at 700 rpm, for 3 min at 4 °C. The ready prepared pepsin resin is stored in 0.1 % formic acid and 0.05 % sodium azide at 4 °C. The protocol was kindly provided by Marta Boysen from the group of Prof. Dr. M. Mayer (ZMBH, Heidelberg).

The column was packed according to the manufacturer's instruction using the guard column kit (Postnova analytics GmbH).

2.11.3.2 Preparation of the trap column

POROS® R1, 10 µm Self Pack® Media (Applied Bioysytems) was employed as resin for the trap column. Dr. Uwe Linne packed the column according to the manufacturer's instruction using the guard column kit (Postnova analytics GmbH).

2.11.3.3 Implementation of the HPLC setup

HDX measurements require a system including two HPLC pumps. The first one provides an isocratic flow, which transports the sample from the sample loop at the injection valve via the pepsin column where proteins are degraded to peptides to the trap column, which binds the peptic peptides. At this point the second valve switches to allow the elution of the peptides from the trap column using a gradient of acetonitrile and water (**Figure 67**). Subsequently the peptides are separated on the separation column and directly injected to the mass spectrometer by ESI.

Accordingly the setup was constructed using an injection valve with a sample loop and a connection to the isocratic HPLC pump. The pepsin column bridges the injection valve and the 6-port valve, where the trap column is located and to which the second HPLC pump is connected. Upon switching of the second valve peptides are eluted from the trap column, separated on the C18 column, which is located on the bridge to the mass spectrometer and subsequently analysed at the orbitrap Velos pro (Thermo Scientific) (**Figure 67**). The whole setup was controlled using the ChemStation (Agilent).

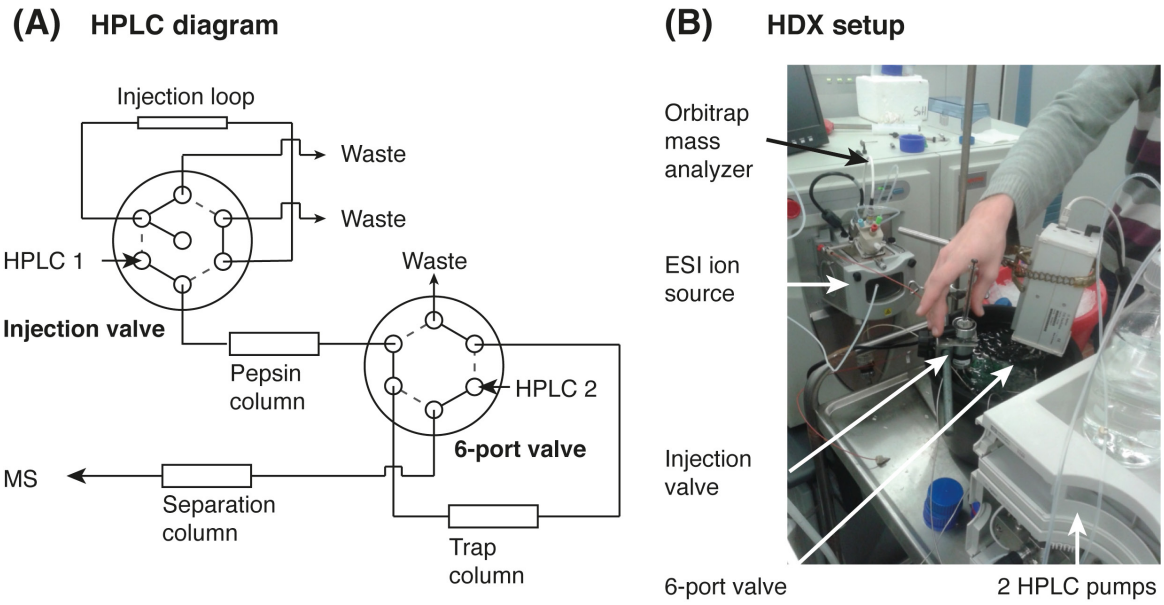

Figure 67. The HDX setup. (A) shows a scheme of the HPLC setup, including two pumps (HPLC 1 and HPLC 2), two valves (an injection valve and a 6-port valve) and three columns (a pepsin column, a trap column and a separation column). **(B)** displays a picture of the actual setup. White arrows indicate essential parts in the picture. Dr. Uwe Linne kindly provided the photograph.

2.11.3.4 Data analysis

A list of possible peptides from the protein of interest plays a key role for data analysis, as pepsin degrades proteins unspecifically rendering the prediction of peptides almost impossible. Prior to amide proton exchange each protein is subjected to an MS/MS run, to identify as many peptides as possible. The peptide list was generated using the Mascot server (Matrix Science). The resulting list was modified in Excel (Microsoft) to fit the requirements for HDX workbench.

Having the peptide list with the respective retention time for each peptide, data analysis was performed using HDX workbench, which was developed in the laboratory of Patrick Griffin at the scripps research institute (Florida, USA) particularly for HDX using an orbitrap as mass analyser (239). The program searched each mass spectrometry file (.raw files) for the respective peptides and assigned the centroid of the signal. The natural occurrence of certain isotopes especially ^{13}C leads to a specific shape of the mass peaks of larger molecules such as peptides. For smaller peptides the monoisotopic peak displays the highest intensity followed by smaller peaks with a mass difference of one atomic unit (au). For larger peptides with (< 10 amino acids) the influence of ^{13}C leads to a change in peak intensities.

The intensity of the first and, for even larger peptides, the second isotope peak exceeds the monoisotopic peak, leading to a specific overall peak shape. Since the incorporation of deuterium is based on statistical events, the overall peak shape is transformed into a Gaussian-like shape. The centroid of a mass peak constitutes the centroid of the distribution over all isotopic peaks for a specific molecule (**Figure 65**).

Based on the mass difference of the signal centroids of the native peptide and the deuterium labelled peptide the deuterium uptake were calculated. The calculation implemented the length of the peptide as well as its charge state.

The capacity of peptides to incorporate deuterium was estimated according to the length (each amino acid can take up one deuterium) except the first two amino acids of a peptide as well as proline, which lacks the amide proton. These values were considered as complete labelling and hence 100 % exchange.

Possible deuterium uptake:

Possible uptake of deuterons = (length of the peptide) – 2 (the first 2 amino acids) – number of proline residues

2.12 Application of HDX in other projects

After the implementation and the successful application of HDX in the FlhG project, I contributed to two other projects providing HDX measurements. One of the

projects is related to flagellar assembly and describes the path of flagellin subunits from its production to the flagellar type III secretion export gate. The second project is about two second messenger alarmones ppGpp and pppGpp, especially their production through the small alarmone synthetase 1 (SAS1) of *B. subtilis*. Surprisingly, SAS1 is exclusively allosterically regulated by pppGpp, not by ppGpp.

2.12.1 Interaction of the Flagellin/FliS complex with FliW

During the assembly of the flagellar filament, around 20 000 copies of flagellin (*hag* gene) have to be produced, guided to the fT3SS, exported to the filament cap and assembled into the filament (17). This highly ordered mass production of protein not only requires an efficient production line, but also involves quality control procedures and feedback regulation at different steps within the production line. Damaged or misfolded flagellin subunits have to be removed from the process prior to export, since they would otherwise get stuck within the filament tube and block further filament assembly. On the other hand, in order to avoid the formation of futile polymers within the cell, polymerization of flagellin has to be inhibited until a flagellin subunit has reached its assembly destination at the tip of the filament. To guarantee a smooth preparation of flagellin assembly, several interaction partners or chaperones not only regulate the transcription and translation of the *hag* message but also confirm proper folding and protect flagellin subunits. For example, FliS interacts with the C-terminus of flagellin, which is crucial for polymerisation, forming a 1:1 complex and therefore preventing intracellular flagellin from polymerisation (240-242). In addition, FliS enhances the interaction of flagellin with FlhA, which forms the export gateway, promoting flagellin secretion (24, 243). In *S. enterica* FliS additionally interacts with the anti-sigma factor FlgM, also binding in a 1:1 ratio at overlapping binding sites to flagellin and influences flagellar gene expression (244). Recently, FliW and orthologues were identified as novel flagellar assembly factors in *B. subtilis*, *C. jejuni* and *Treponema pallidum* (245). FliW interacts with a complex of flagellin and FliS as well as with CsrA, an RNA binding protein that regulates the transcription of the *hag* message. CsrA blocks the Shine-Dalgarno (SD) sequence of flagellin pre-

venting *hag* transcription. Upon secretion of flagellin FliW is released from the ternary complex and now is able to bind CsrA, which is release from the SD sequence. This event lifts the transcription inhibition of the *hag* message, providing a feedback regulation of flagellin production depending on the export (246).

The importance of the flagellin regulation is reflected in the universal domain architecture of flagellin in different bacteria (19). Flagellin exhibits a highly conserved N- and C-terminus combined with an insertion of variable length in different species. The conserved N- and C-terminal helix (also D0-N and D0-C domains) form the core of the flagellar filament interacting with neighbouring D0 domains. Surrounding the core, the D1 domains build another ring structure to stabilize the helical filament.

As the D0 domain, the D1 domain is composed of an N-terminal part (D1-N), which lays adjacent downstream the D0-N domain and a C-terminal part D1-C in front of the D0-C domain. The region in between varies between species and may comprise D2 and D3 domains, which can be glycosylated (**Figure 68**).

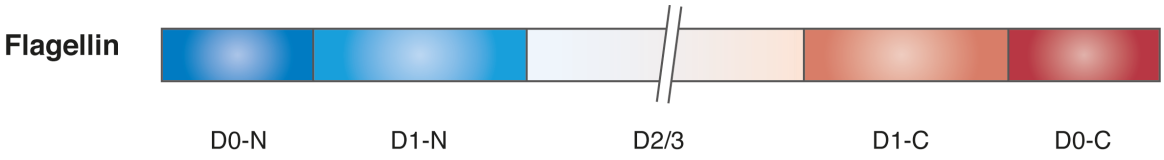

Figure 68. Domain architecture of Flagellin. While the D0 and D1 domain are highly conserved and form the helical core of the filament, D2/3 domains are variable in size and exposed on the surface of the filament modifying its chemical properties.

In the flagellar filament the D0 and D1 domain are in a coiled coil conformation suitable to form a super helix with many more flagellin building up the flagellar filament. In the cytoplasm flagellin forms a complex with its cognate chaperone FliS. The D0-C domain warps around the four-helix bundle of FliS shielding the C-terminus (**Figure 69**).

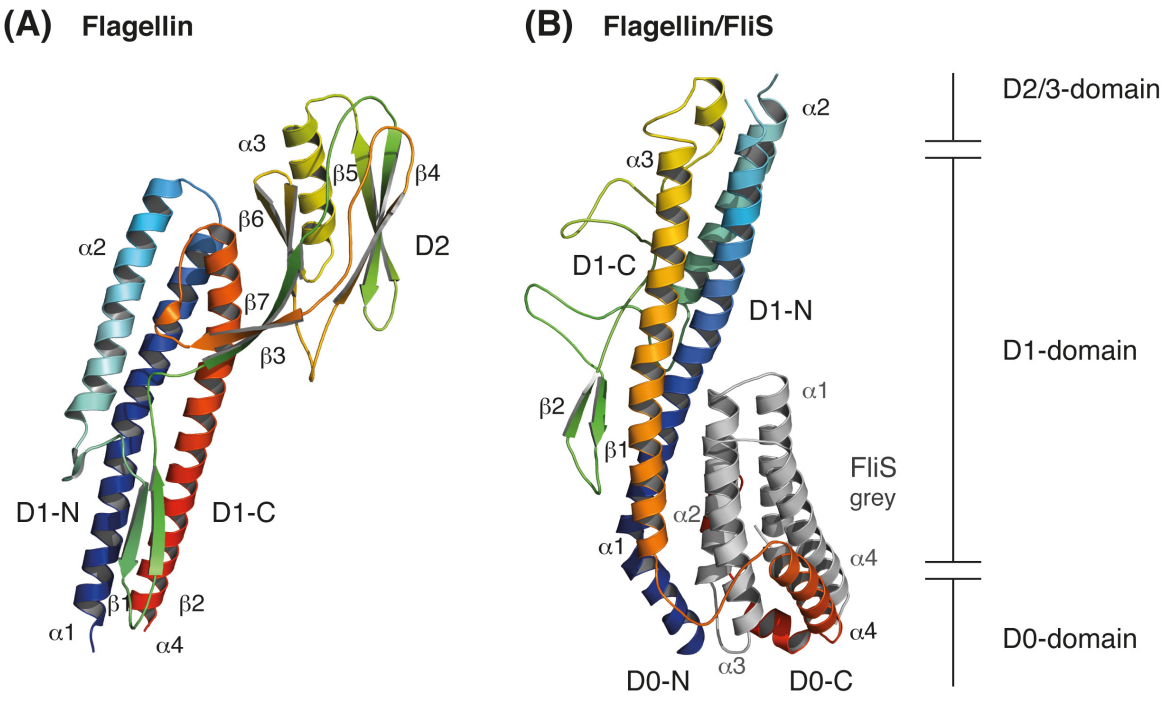

Figure 69. Crystal structure of Flagellin and a Flagellin/FliS complex. (A) shows the crystal structure of flagellin of *P. aeruginosa* (pdb: 4NX9) coloured in rainbow. The crystal structure of a flagellin/FliS complex of *B. subtilis* (unpublished structure, G. Bange) is shown in **(B)**. Flagellin is coloured in rainbow and FliS in grey. Domains as well as secondary structure elements are indicated.

FliW binds to a flagellin FliS complex. However, the exact binding mode remains elusive. A recent study stated that the flagellin-FliW interface is located in the C-terminal part of the D1 domain. Especially asparagine 255 seems to play a crucial role for FliW binding (246). To get further insights into the binding mode of flagellin/FliS and FliW, HDX was applied to determine the protein-protein interface of the flagellin/FliS/FliW complex of *B. subtilis*. The flagellin/FliS complex, FliW and a ternary complex consisting of flagellin/FliS/FliW were labelled with deuterium, digested and the peptic peptides analysed by mass spectrometry. HDX measurements indicated dramatic changes in flagellin upon formation of the ternary complex with FliW. The D0-C domain of flagellin displayed a massive increase (> 40 %) in deuterium uptake in the presence of FliW (**Figure 70**). Also the corresponding regions in FliS, especially helix α3 (> 10 %) and part of helix α4 (~5 %) became more accessible to deuterium upon addition of FliW. This indicates that the tight conformation of the flagellin/FliS complex gained flexibility with

FliW. The significant difference in the increase of deuterium uptake between flagellin (~40 %) and FliS (~10 %) might either be due to an interaction of FliS and FliW involving the very same region in FliS or a partial unfolding of the flagellin C-terminus. The second scenario would be in line with a recent publication reporting, that flagellin is exported in an partial unfolded state (247). Two regions in the flagellin D1-N and D1-C domain located in close proximity exhibit a decrease in deuterium incorporation in the presence of FliW and may give a hint for the flagellin FliW interface (**Figure 70**). In agreement with the literature, the reported asparagine 255 is located within the responding region in the D1-C domain.

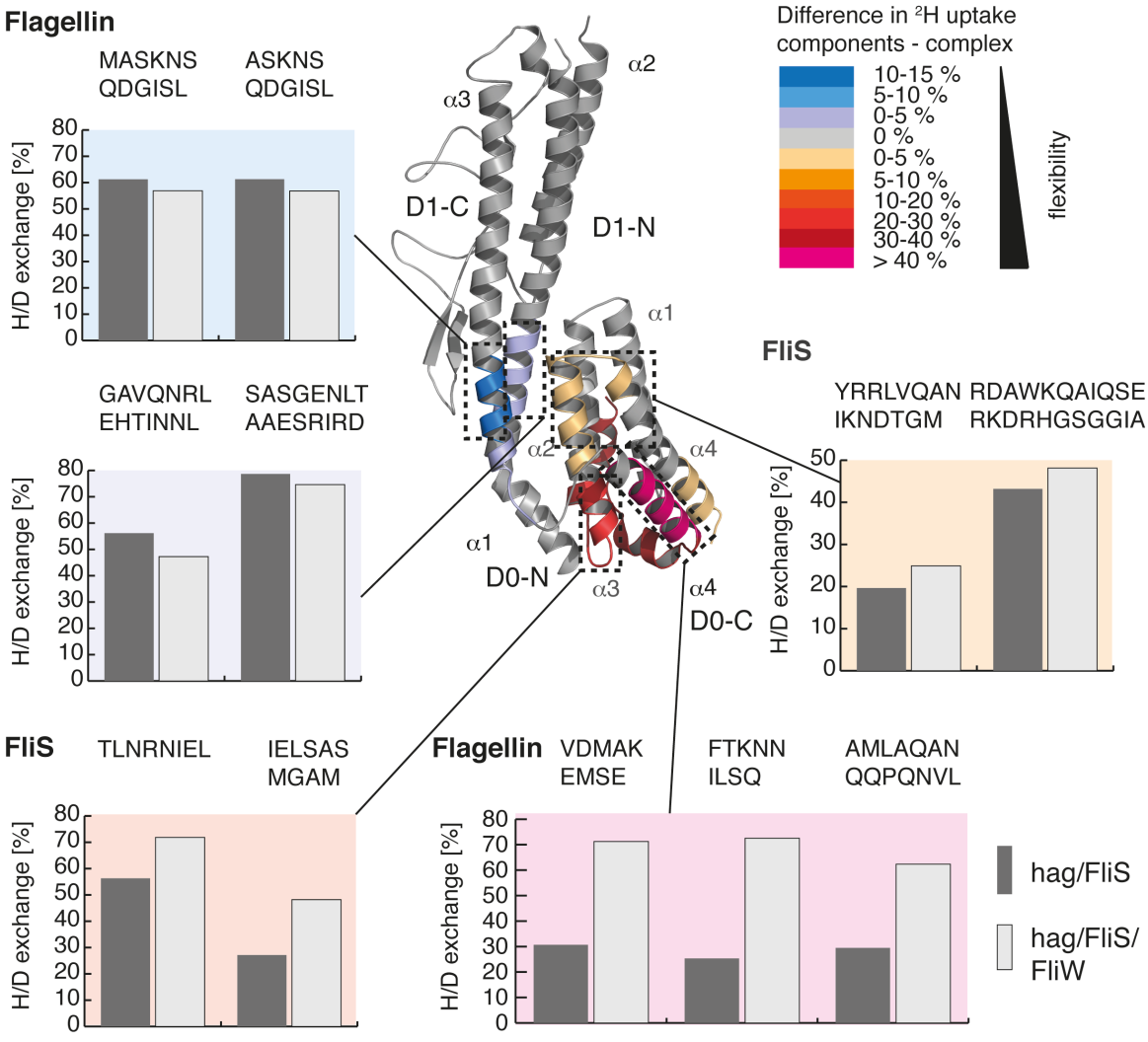

Figure 70. HDX of Flagellin/FliS. Changes in the deuterium incorporation of the flagellin/FliS complex upon formation of a ternary complex with FliW are coloured on the crystal structure (unpublished structure, G. Bange) according to the colour-code on the right. The coloured panels display the deuterium incorporation of representative peptides of the coloured regions of the flagellin/FliS complex (dark grey) and the ternary complex (light grey).

Data analysis of FliW also identified two regions where deuterium uptake is decreased in the presence of the flagellin/FliS complex. In a helical turn between β-strand β6 and helix α1 deuterium incorporation dropped 10-15 %, while another helical turn in close proximity between β7 and β8 displayed an uptake decrease of 5-10 % (**Figure 71**).

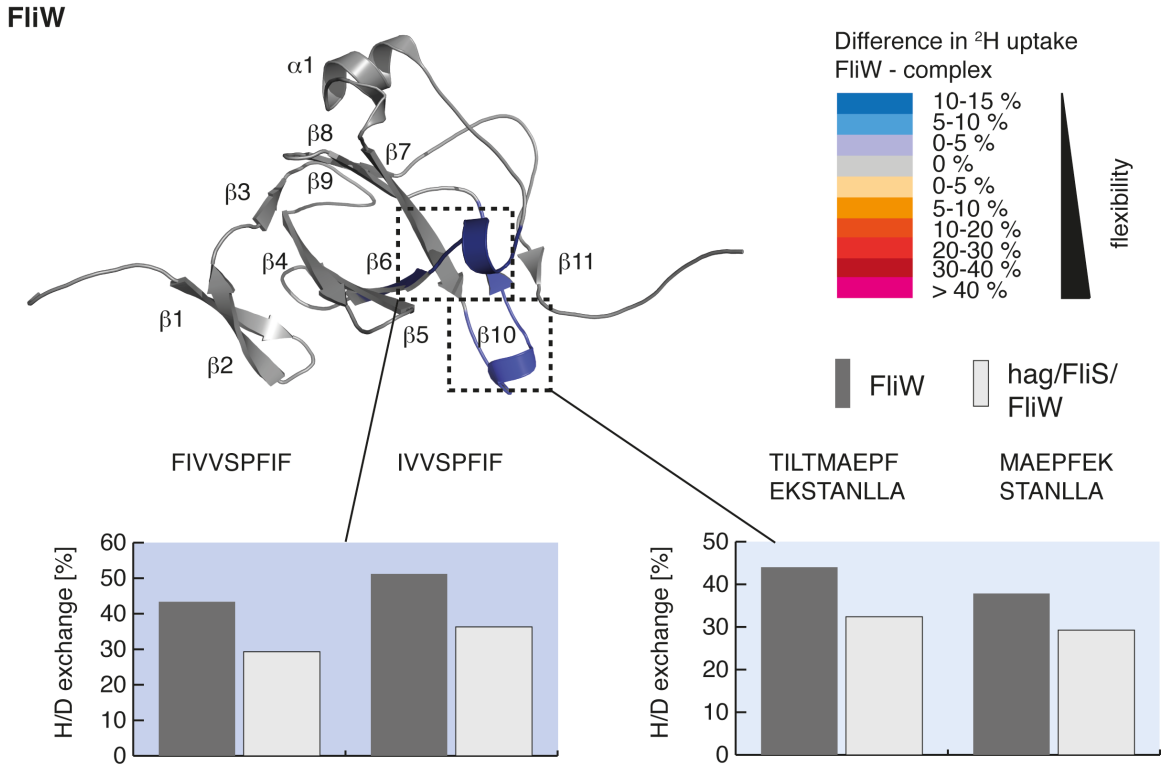

Figure 71. HDX of FliW. Changes in deuterium uptake of FliW upon formation of a ternary complex with flagellin/FliS are coloured in the crystal structure (pdb: 2AJ7) according to the colour-code on the right. The coloured panels display the deuterium incorporation of representative peptides of the coloured regions of FliW (dark grey) and the ternary complex (light grey).

These two regions in FliW may match the regions in the D1 domain of flagellin, which responded to FliW addition and may form the protein-protein interface. HDX measurements provided two putative interaction sites between flagellin and FliW. The results are in agreement with current literature. However, further mutational studies will be necessary to proof the HDX results and to pinpoint the crucial amino acid residues.

2.12.2 Elucidating the mechanism of the small alarmone synthetase 1 (SAS1)

Stringent response, which is mediated by two alarmones ppGpp and pppGpp, is a bacterial stress response program activated upon nutritional starvation or many other forms of stress (reviewed in: (248-251)). RelA is a key player for stringent response and associated to ribosomes, where it is capable of sensing ribosomes that are blocked by unloaded tRNAs (252). RelA comprises an N-terminal alarmone hydrolase domain as well as an adjacent alarmone synthetase domain and in the C-terminal part regulatory domains and the ribosome interaction site (**Figure 72**). Ribosome associated RelA is able to hydrolyse alarmones, while the synthetase is silent. Upon amino acid starvation, RelA is released from the ribosome and produces the alarmones ppGpp and pppGpp as stress response signal, while the hydrolase domain is inactive (253-255). These alarmones are able to globally reprogram bacterial growth, cell cycle and metabolism by regulating many vital cellular processes to ensure bacterial survival under stress conditions (248). ppGpp and pppGpp have been considered as acting collectively as second messengers, however recent studies indicate that the two alarmones have different effects on cellular processes, such as growth rate or transcription (256).

In *B. subtilis* and *S. aureus* two other proteins SAS1 (also: RelP) and SAS2 (also: RelQ) were recently identified that share the alarmone synthetase domain with RelA (257-260).

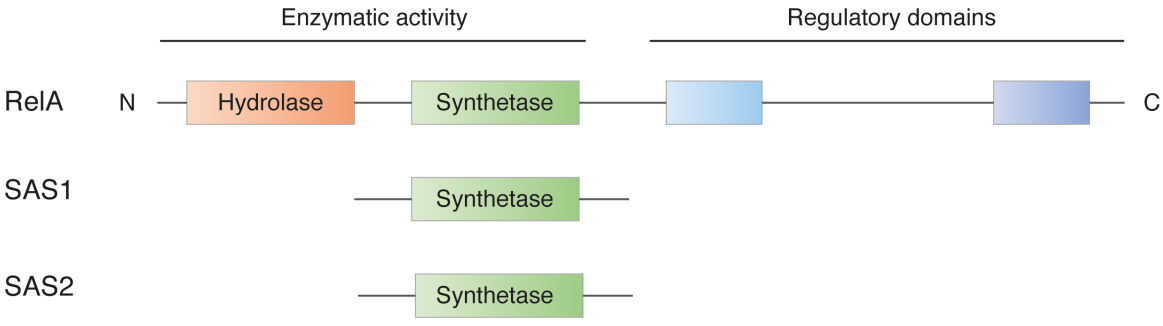

Figure 72. Domain architecture of RelA, SAS1 and SAS2. All three proteins, RelA, SAS1 and SAS2 share the conserved synthetase domain (green). RelA responsible for stringent response possesses an additional N-terminal hydrolase domain (red) and a C-terminal part involved in ribosome association (blue).

In contrast to RelA these two small alarmone synthetases only consist of the synthetase domain (**Figure 72**).

Wieland Steinchen purified, crystallized and obtained a structure of SAS1 from *B. subtilis* in different nucleotide loaded states. SAS1 produces both alarmones ppGpp from ATP and GDP and pppGpp from ATP and GTP (personal communication Wieland Steinchen). SAS1 forms an oval shaped tetramer with a prominent cleft in the middle (**Figure 73**).

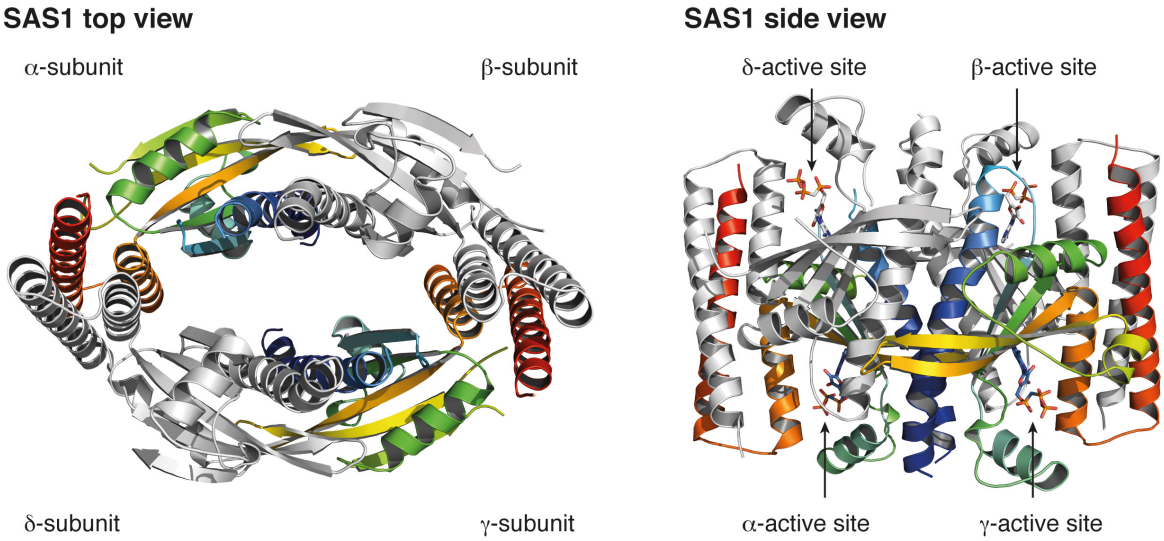

Figure 73. Crystal structure of SAS1. Cartoon representation of the crystal structure of SAS1 of *B. subtilis* (pdb: 5DEE) shows an oval-shaped tetramer coloured in rainbow and grey from top view (left) and side view (right). Arrows indicate the four active sites of the subunits.

The SAS1 monomer exhibits three characteristic helices, α1, α4 and α5, which in combination with the two long β-strands β3 and β4 provide the interfaces for tetramer formation. The active site is located in the middle, where the non-hydrolysable AMPCPP is bound by two highly conserved motifs (GR(V/P)KxxxS and DIA(G/A)LR) (**Figure 74**). The crystal structure of the RelA hydrolase and synthetase domain (pdb: 1VJ7) display a GDP associated to the active site of the synthetase domain. An overlay of the synthetase domain of RelA and SAS1 showed that essential regions for alarmone production are structurally almost identical. However, as RelA acts as monomer, it lacks the prominent interface regions of SAS1.

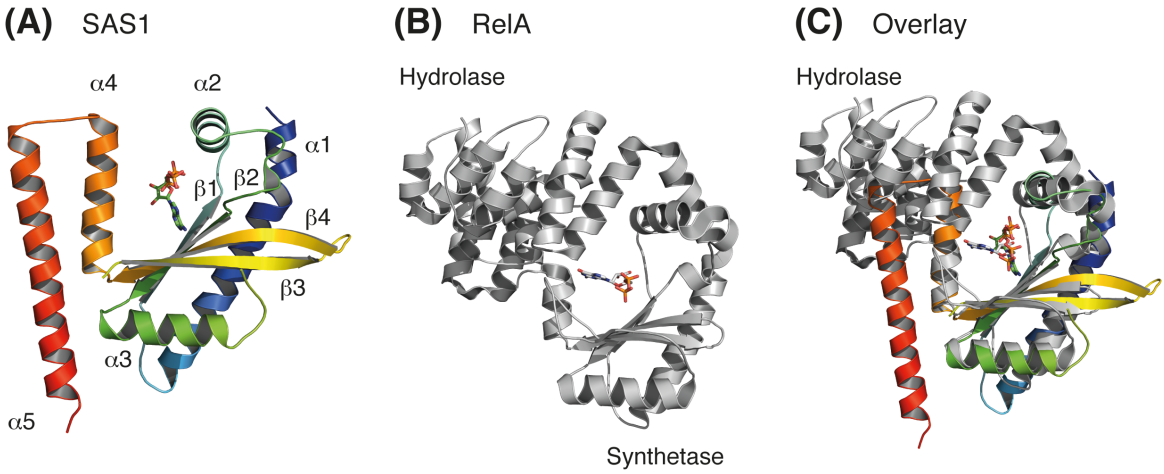

Figure 74. Hydrolase domain of SAS1 and RelA. (A) shows the crystal structure of a SAS1 (pdb: 5DEE) monomer in rainbow with AMPCPP bound in the active site. **(B)** displays the N-terminal part of RelA of *Streptococcus equisimilis* (pdb: 1VJ7) including the synthetase and the hydrolase domain in grey with GDP bound in the active site of the hydrolase domain. **(C)** shows a superimposition of both structures (SAS1 in rainbow, RelA in grey) reveals that they share the synthetase domain.

The overlay of the synthetase domains of RelA and SAS1 not only proofs the structural homology, it also provides an idea of the respective positions of both substrates required for alarmone synthesis in the active site of these synthetases. Based on this structural information about the position of ATP and GDP in the active site, a mechanistic model of alarmone formation by SAS1 can be deduced.

2.12.2.1 Sequential substrate binding

To assess whether ATP or GDP/GTP is the first to bind into the active site, HDX measurements were performed with SAS1 in the presence of different nucleotides. SAS1 was incubated with GDP, GTP or AMPCPP as a non-hydrolysable analogue of ATP for this reaction. These samples were subsequently diluted in deuterium containing buffer and after quenching and pepsin digestion, the deuterium uptake of the peptic peptides was analysed and compared to apo SAS1. While SAS1 incubated with GDP or GTP displayed almost identical deuterium uptake as apo SAS1, incubation of SAS1 with AMPCPP revealed a significant decrease in deuterium incorporation and hence protection in the regions that are responsible for ATP binding (**Figure 75**). This indicates that ATP is the first sub-

strate to enter the active site of SAS1. If this is true, a further decrease of deuterium uptake in catalytically important regions is expected upon incubation of SAS1 with AMPCPP and GDP or GTP. In these cases both substrates may bind to the active site, however AMPCPP inhibits the reaction to the respective product. Therefore, SAS1-AMPCPP-GTP and SAS1-AMPCPP-GDP were subjected to amide proton exchange and analysed after pepsin digest. An additional decrease of deuterium uptake was observed for both samples in regions essential for catalysis and GDP or GTP binding (**Figure 75**).

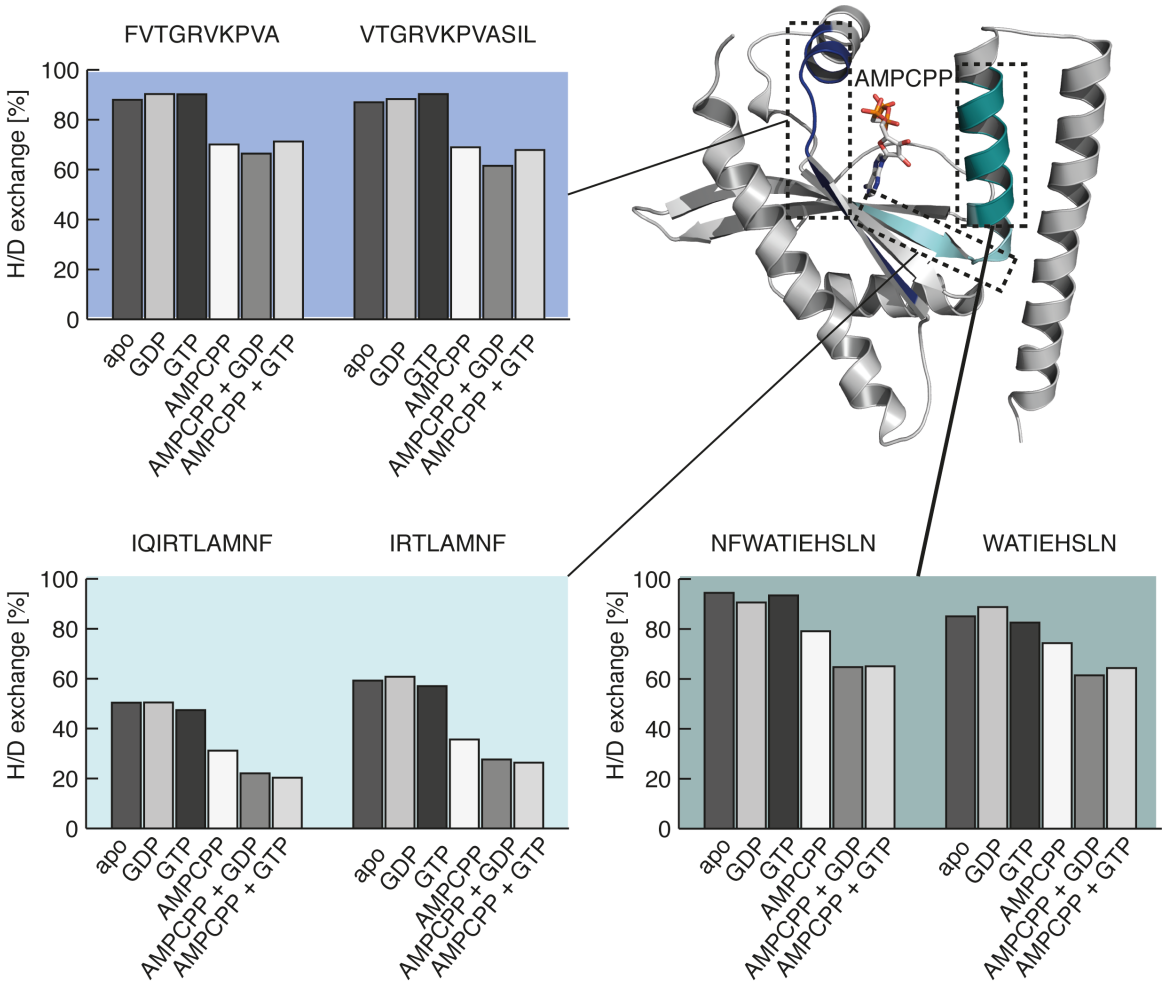

Figure 75. HDX of SAS1. Changes in deuterium uptake of SAS1 upon binding of nucleotides are coloured in the crystal structure (pdb: 5DEE). The coloured panels display the deuterium incorporation of representative peptides of the coloured regions of SAS1 and the respective nucleotide combinations.

These findings corroborate to the hypothesis of a sequential ordered substrate binding mechanism in which ATP is the first substrate that enters the active site.

Catalysis occurs upon binding of the second substrate, which may either be GDP or GTP (**Figure 76**).

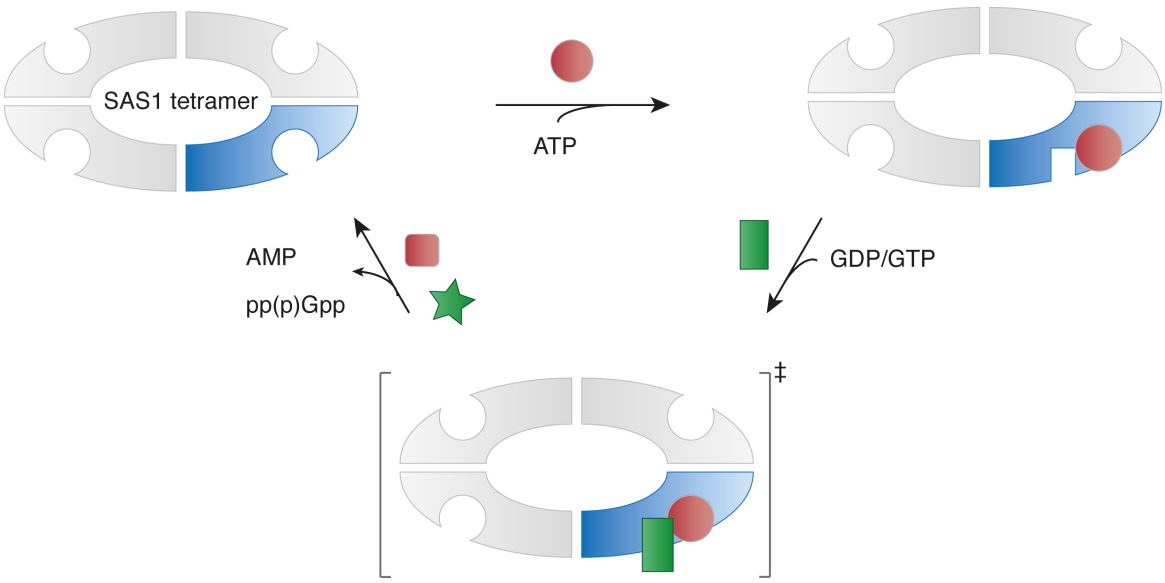

Figure 76. Sequential binding of the substrates ATP and GTP/GDP. The scheme depicts the catalytic cycle of SAS1, with ATP binding as the first step and subsequent association of GDP/GTP. The transition state is indicated by the double dagger. After the release of the products pp(p)Gpp and AMP, apo SAS1 may undergo another cycle. The catalytic cycle is exemplified by one SAS1 monomer (blue). Adenosine nucleotides are coloured in red, guanosine nucleotides in green.

2.12.2.2 Catalytic mechanism

SAS1 catalyses the formation of (p)ppGpp by transferring a pyrophosphate from ATP onto the 3' hydroxyl group of GDP or GTP releasing adenosine monophosphate (AMP) as a by-product. The reaction implicates the cleavage of a phosphoric anhydride bond while simultaneously forming a phosphoric ester. According to the sequential binding, ATP is the first molecule to invade the active site and gets tightly locked in an unusual tense U-shaped conformation by 4 highly conserved motifs (GRV/PKxxxS; DIAGLR; RDYI; EIQIRT). The adenine base is tightly sandwiched between two conserved arginine residues arginine 46 and arginine 77. The phosphate groups are bent towards the adenine base forcing the ribose sugar into an unfavourable almost planar conformation. Arginine 46 conducts this unusual scene, being not only part of the tight cage of adenine but also

forming polar contacts to the oxygen of the ribose ring as well as to the α-phosphate group (**Figure 77A**). This unusual tense conformation resulted in an activation of ATP, which renders it vulnerable for the subsequent pyrophosphate transfer. The β- and γ-phosphate are held in place by coordination to a magnesium ion, which is attached to SAS1 through aspartate 72 and indirectly bound to glutamate 139 mediated through a water molecule. Water molecules occupy the two remaining coordination sites of Mg^{2+}. A positive pocket consisting of lysine 48, arginine 56 and arginine 59 neutralizes the negative charges from the γ-phosphate. The second step consists in the entrance of GDP into the active site (**Figure 77A**). Guanine is bound to Arginine 105 through π-stacking and probably by residues of a flexible region forming an extensive loop (**Figure 77B**).

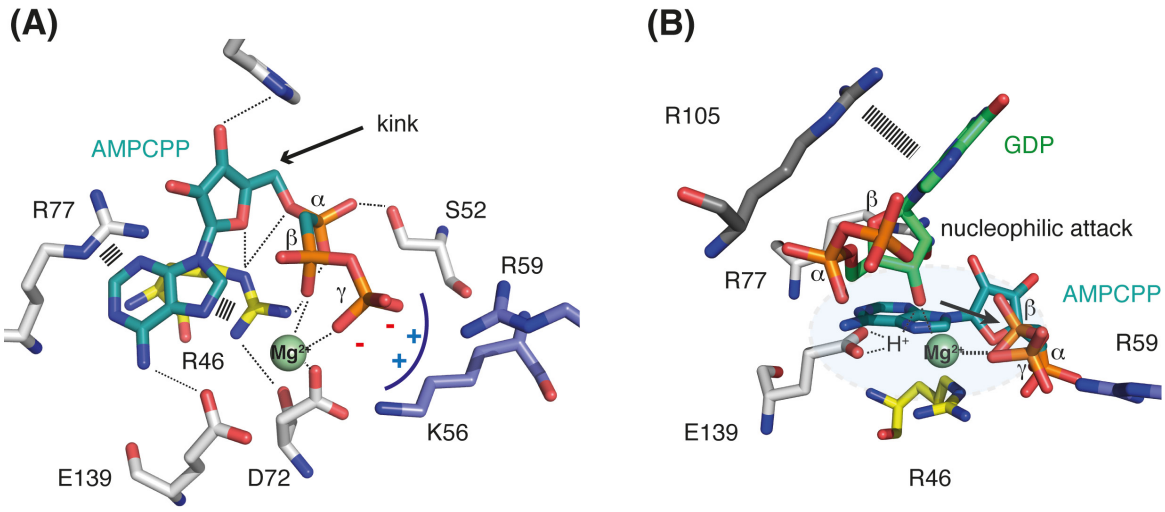

Figure 77. ATP coordination and nucleophilic attack. (A) shows how AMPCPP (deep teal) is coordinated in an unusual kinked conformation in the active site of SAS1 (5DEE). A black arrow indicates the kink of AMPCPP and dashed lines indicate interactions. **(B)** displays a superimposition of the active sites of AMPCPP (deep teal) bound SAS1 and GDP (green) bound RelA (dark grey; pdb: 1VJ7). The attacking 3'-OH group of the ribose of GDP in the centre of the image and the arrow indicates the direction of nucleophilic attack towards the β-phosphate of AMPCPP. The proton of the 3'-OH moiety is indicated.

Crucial for the reaction is the activation of the 3'-hydroxyl group of GDP (GTP) for the nucleophilic attack. The close proximity to magnesium strongly indicates that the hydroxyl group is deprotonated by coordination to the metal ion. Glutamate 139 serves as proton-relays to capture the resulting proton (**Figure 77B** and

Figure 78). The activated hydroxyl group of the GDP ribose attacks the positively polarized phosphor of the β-phosphate group performing a second order nucleophilic substitution (S_N2) (**Figure 78**). After anhydride bond cleavage the AMP conformation can immediately be relaxed by turning the α-phosphate towards the exit, indicating a possible mechanism for AMP release.

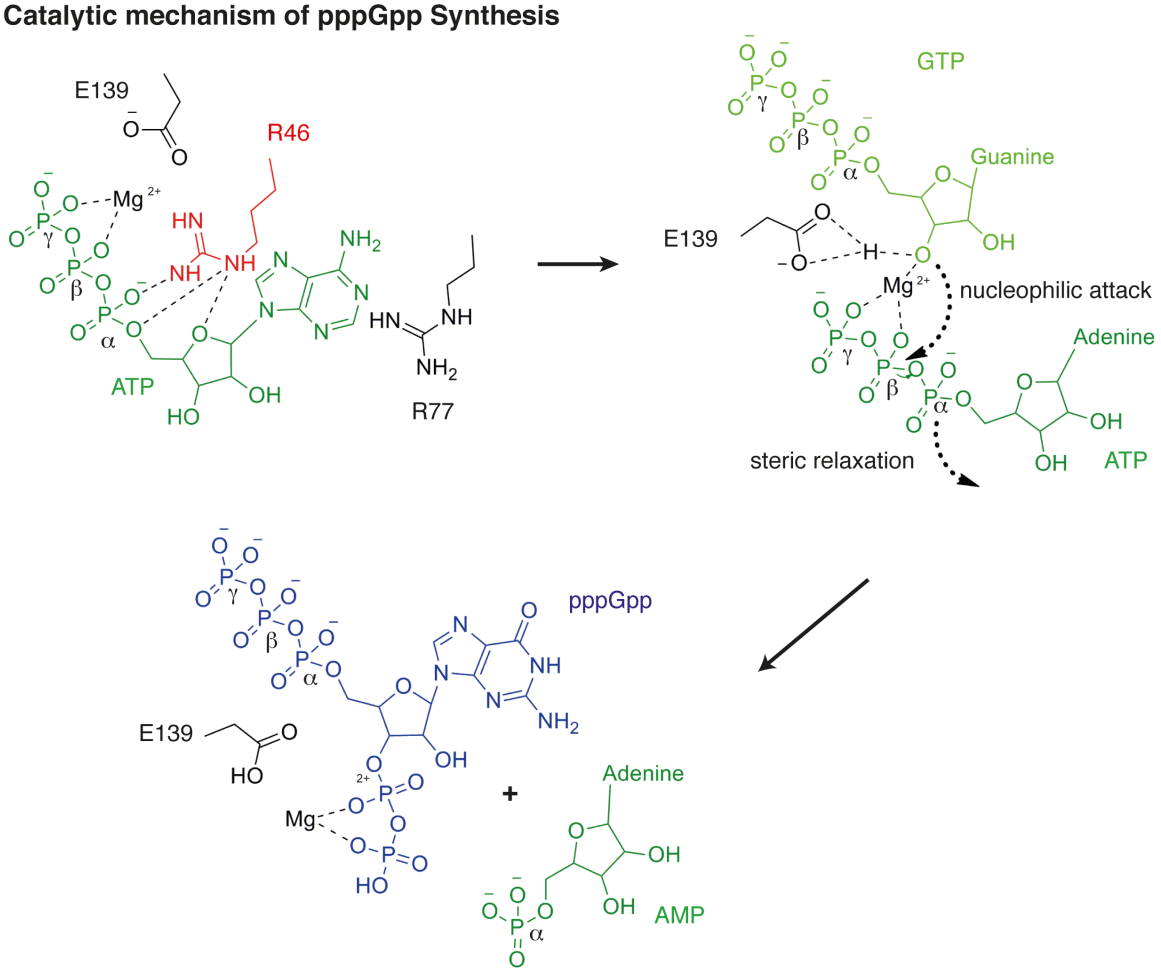

Figure 78. Catalytic mechanism of alarmone synthesis. The scheme illustrates the catalytic mechanism of alarmone synthesis using the example of pppGpp production. The substrates ATP, GTP and the side product AMP are shown in green, light green and green, respectively. The alarmone pppGpp is displayed in blue.

2.12.2.3 Binding site of additional pppGpp

The crystal structure of the product state of SAS1 revealed that 6 pppGpp molecules bind to a SAS1 tetramer. Four are located in the active site of each subunit

and two are observed in the in the central cleft of the oval shaped tetramer (**Figure 79B**).

To proof that only pppGpp but not ppGpp binds to the central cleft of the SAS1 tetramer, SAS1 was incubated with ATP and GDP as well as ATP and GTP allowing the formation of the respective alarmones. After dilution into deuterium buffer, quenching and pepsin digestion, the deuterium uptake of the resulting peptides was analysed by mass spectrometry.

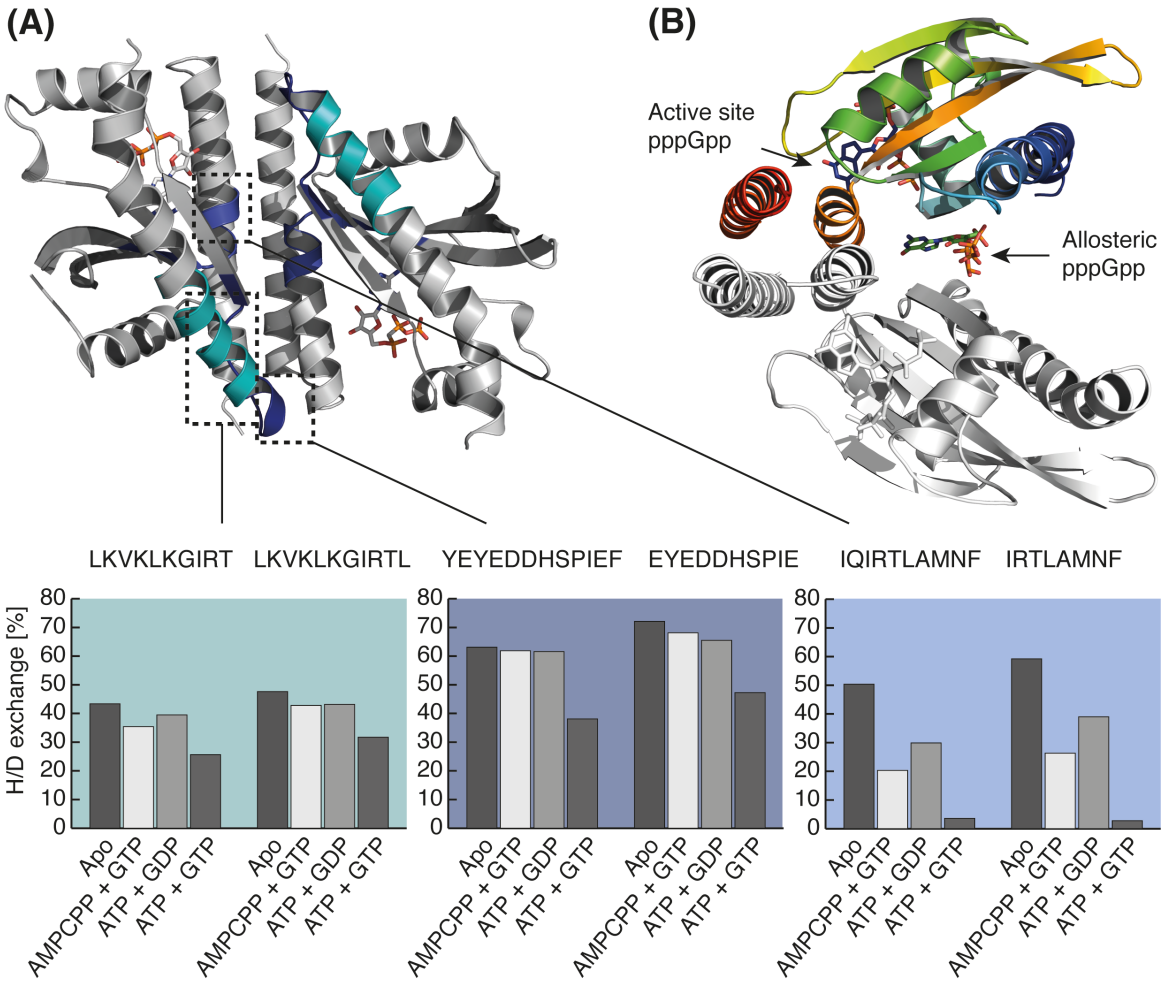

Figure 79. Allosteric regulation of SAS1 through pppGpp. (A) shows changes in deuterium uptake of SAS1 upon binding of the stated nucleotides that are coloured in the crystal structure of SAS1 (5DED). The panels display the deuterium incorporation of representative peptides of the coloured regions of SAS1 as well as the respective nucleotide combinations. **(B)** The cartoon representation of two subunits (rainbow and white) of the SAS1 tetramer (5DED) with two pppGpps bound in the active sites and one pppGpp bound in central cleft.

In the presence of ATP and GDP protection only occurs in regions of SAS1 involved in substrate binding and catalysis. However, with ATP and GTP additional peptides displayed a protection of deuterium incorporation (**Figure 79A**). These peptides are part of the central cleft and correspond to the binding site of the additional pppGpps observed in the crystal structure (**Figure 79AB**). These findings led to the conclusion that SAS1 can distinguish between the alarmones ppGpp and pppGpp.

Discussion

3.1 FlhG forms a molecular switch

FlhG is a molecular switch with two distinct and spatially separated states. It can either be located in the cytoplasm as a monomer, which represents the 'OFF' state according to the canonical ATPase/GTPase switch paradigm, or FlhG forms ATP-dependent, spatially restricted homodimers at the plasma membrane using a C-terminal MTS, which is considered the 'ON' state (**Figure 34**). The transition from 'OFF' to 'ON' state depends on the presence of ATP and the possibility to associate with the plasma membrane. Kinetically, this process depends on the dissociation rate of ADP and the binding affinity of ATP, which triggers the nucleotide exchange. In many small GTPases, a GTP exchange factor (GEF) facilitates the nucleotide exchange (reviewed in: (261)). However, no additional protein involved in exchanging ADP to ATP has been identified for FlhG or other dimeric ATPases so far.

The switch from the 'ON' to the 'OFF' state is achieved by ATP hydrolysis. The basal hydrolysis rate of *Gt*FlhG of 0.85 min^{-1} seems high compared to the basal ATPase activity of MinD (turnover: 0.07 min^{-1}) and rather corresponds to the turnover rate of the activated MinD/MinE complex in the presence of lipids (0.58 min^{-1}). The difference to MinD probably arises due to the fact that *Gt*FlhG is derived from a thermophile bacterium and hence the protein is more robust and optimized for higher temperatures. The typical basal turnover of a small GTPase is 0.3 min^{-1} on average, but it may vary between the different families ranging from 0.003 to 3 min^{-1} (262-264). In the presence of a GTPase activating protein (GAP) hydrolysis is enhanced 10 fold to 10 000 fold and drives the GTPase back to its 'OFF' state, exceeding the hydrolysis rates of FlhG and MinD (265, 266). This may implicate for FlhG that it is slowly cycling between 'ON' and 'OFF' state and therefore might act as a pulse generator during flagellar biogenesis.

3.1.1 FlhG and FlhF

FlhG does not constitute an isolated molecular switch, but is embedded into a regulatory network. Considering the molecular switch scheme of FlhF described in the introduction (**Figure 10**), it became evident that FlhF and FlhG constitute a regulatory device with two connected switches that control number and location of Flagella (**Figure 80**). Accordingly, such a module can acquire four instead of two states ('ON'/'ON', 'ON'/'OFF', 'OFF'/'ON', 'OFF'/'OFF') and therefore control a more complex system. Although many states have been structurally characterized, only little is known about the dynamics of this system.

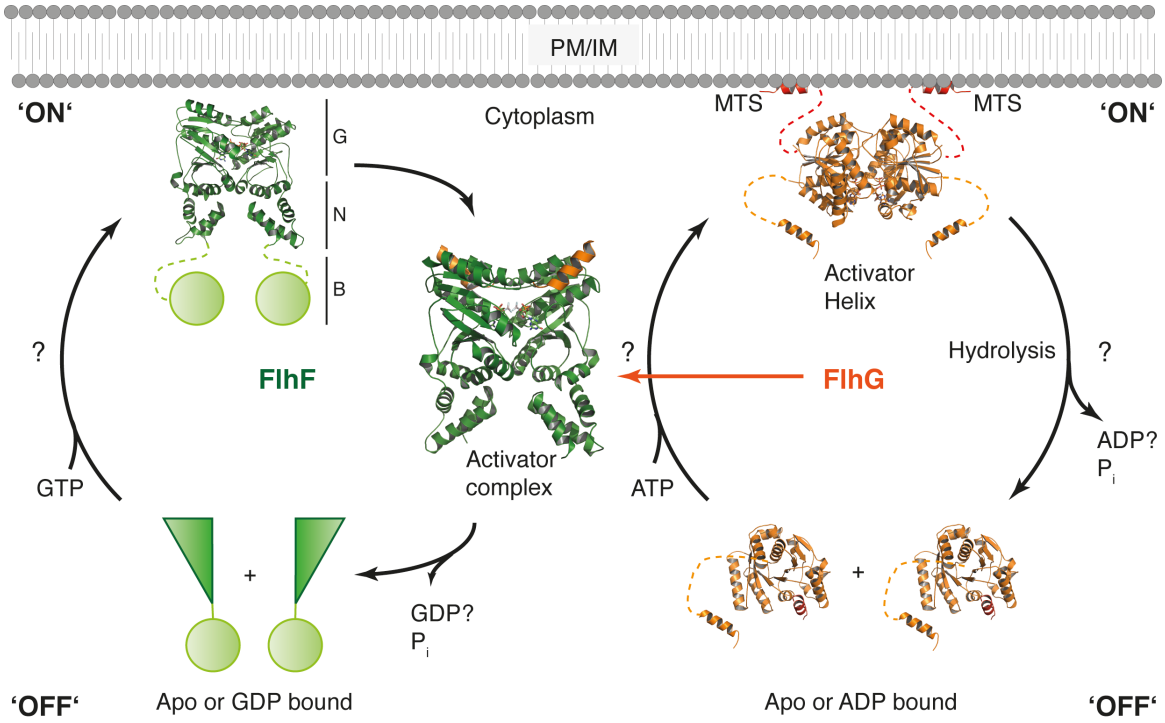

Figure 80. A regulatory module with two interconnected switches. The regulatory circuits of FlhF (*left*) and FlhG (*right*) are shown side-by-side. Both circuits are connected by the stimulation of the FlhF GTPase through the N-terminus of FlhG in the activator complex (pdb: 3SYN). FlhF is shown in green (pdb: 2PX0) and FlhG is shown in orange (pdbs: 4RZ2, 4RZ3). Question marks indicate that an additional factor might be missing or that these processes are not completely understood. (MTS: membrane targeting sequence, PM: plasma membrane, IM: inner membrane). This figure was adapted from ref. (16).

GTP hydrolysis of FlhF is triggered by the activator helix of FlhG through a hetero-tetrameric activator complex involving an FlhF dimer and two FlhG subunits. However, whether activation requires an FlhG dimer and therefore may take place at the plasma membrane remains unclear. Localization of FlhF at the membrane and the fact that FlhG promotes the cytoplasmic localization of FlhF leads to a scenario, in which dimeric FlhG induces hydrolysis of an FlhF dimer at the membrane (128). Further factors that may influence the nucleotide exchange rate of FlhF or FlhG as well as an activator of the ATP hydrolysis of FlhG have not been identified so far. This interconnected switch allows the control of complex regulatory processes. Furthermore, the possibility that FlhF and FlhG may possess state-specific interaction partners, adds another level of complexity to this biological regulatory device.

3.2 Molecular evolution of a MinD-like ATPase

It is a common motif in nature that existing modules, devices or architectures are slightly modified in the course of evolution and used for more than one purpose. Prominent examples are two-component kinase systems, which are involved in signalling processes and found in almost all organisms (reviewed in: (267-269)). Another example is the β-propeller fold of various proteins with different functions ranging from peptidases to ribosomal chaperones (270, 271) (reviewed in: (272, 273)). The close homology of MinD and FlhG provides an evident example of how regulatory modules can be adapted and diversified to adopt different tasks. Along these lines, the bacterial MinD-like ATPases are involved in the spatial regulation of macromolecular complexes such as ParA controlling chromosome segregation and ParC the regulation of chemotaxis arrays, Soj being involved in chromosome segregation, transcriptional regulation and sporulation (115-117, 274-276).

3.2.1 Of FlhG and MinD

The high degree of homology between MinD and FlhG renders it very likely that FlhG emerged as gene duplication from MinD or *vice versa*. In the scope of evo-

lution, proteins were modified and diversified. FlhG acquired an additional N-terminal domain, harbouring the activator motif (DQAxxLR) to stimulate the FlhF GTPase. Furthermore, the epitope for cargo binding was modified so that MinD is able to recruit the cell division inhibitor MinC.

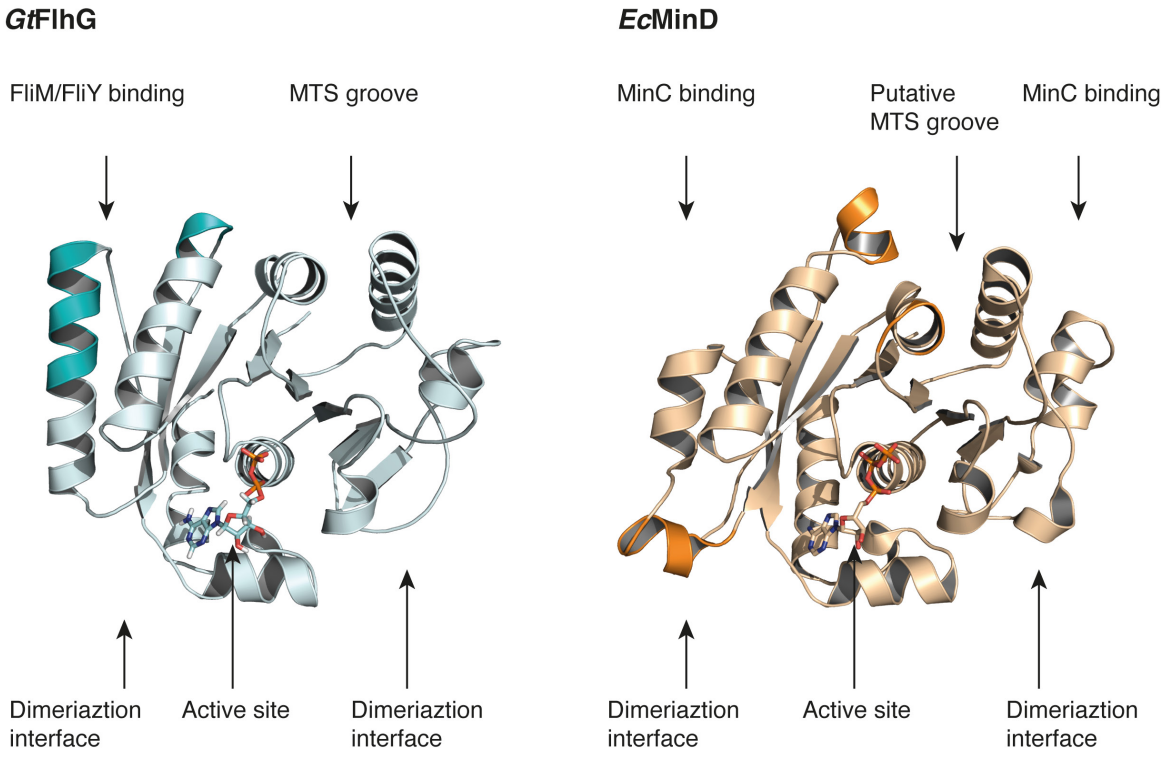

Figure 81. Side-by-side view of FlhG and MinD. The side-by-side view of FlhG (pdb: 4RZ3) (light teal) and MinD (pdb: 3Q9L) (light orange) emphasizes the similarities of both MinD/ParA ATPases. Vital parts of the proteins are depicted and structural differences are indicated through colours in FlhG (deep teal) and MinD (orange). This figure was adapted according to ref. (103).

The topology of the respective region on FlhG changed in a way that FlhG is not able to bind MinC but acquired affinity for the N-terminal 'EIDAL' motif of the flagellar C-ring components FliM/FliY (**Figure 81**). The dimerization interface was slightly modified through an additional helix.

3.2.2 The link between cell division and flagellar assembly

Topological differences between MinD and FlhG and the corresponding ability of MinD to bind MinC and FlhG to interact with FliY indicate that both systems devi-

ated to function independently from each other. However, deletion of *flhG* in *B. subtilis* not only leads to mislocalization and clumping of flagellar basal bodies, but also produces a mini-cell phenotype similar to a *minD* deletion, although to a lesser extent. Therefore, a functional connection between both seemed to have remained. Since FlhG is not able to bind MinC, a shared interaction partner might provide this connection. No further interaction partners of MinD are known in *B. subtilis*. As part of the divisome, GpsB might serve as a connection between both systems and may thus coordinate the presence of MinD and FlhG at the division site, where both proteins occur. Still, experimental proof of a physical interaction between MinD and GpsB is missing so far. It also remains elusive how such an interaction leads to a minicell phenotype in the absence of FlhG.

3.3 FlhG as putative flagella C-ring assembly factor

Not only have I uncovered the nature of the FlhG circuit, but also characterized novel interaction partners of FlhG, providing hints concerning the biological role of FlhG. *In vitro* interaction assays indicate a role of FlhG in flagellar C-ring assembly, demonstrating that a FliM/FliN(Y) complex requires FlhG to smoothly assemble with FliG as well as the temporal co-localization of FliM and FlhG. Combining our *in vitro* and *in vivo* data with literature reports, two possible scenarios for the involvement of FlhG in C-ring assembly become evident. In the first scenario FlhG adopts the role of a flagellar C-ring assembly factor, whereas in the second scenario FlhG acts as negative flagellar regulator preventing a FliM/FliN(Y) complex from assembly into mature C-ring structures.

3.3.1 A model of C-ring assembly

My *in vitro* interaction assays with purified FlhG and purified C-ring components point towards a model where FlhG represents an assembly factor for the biogenesis of flagellar C-rings. Accordingly, FlhG interacts with FliM and FliN(Y) in the cytoplasm in a nucleotide independent fashion, forming a ternary targeting complex, which is delivered to the nascent basal body by the ability of FlhG to interact with membrane lipids as well as FliG. FliG is anchored to the basal body via FliF,

which initiates flagallar assembly (125). I was able to demonstrate that FlhG not only interacts with the FliM/FliN(Y) complex but also renders the C-ring complex potent to interact with FliG. In the absence of FlhG, the FliM/FliN(Y) complex shows a reduced affinity for FliG, while severe flagella assembly defects were observed on phenotypic level (71). Sensing membrane lipids, FlhG undergoes a conformational rearrangement switching from the 'open' to the 'closed' state. This drives the ATP dependent dimerization of FlhG, which may orchestrate another C-ring complex in close proximity to the nascent flagellum (**Figure 82**).

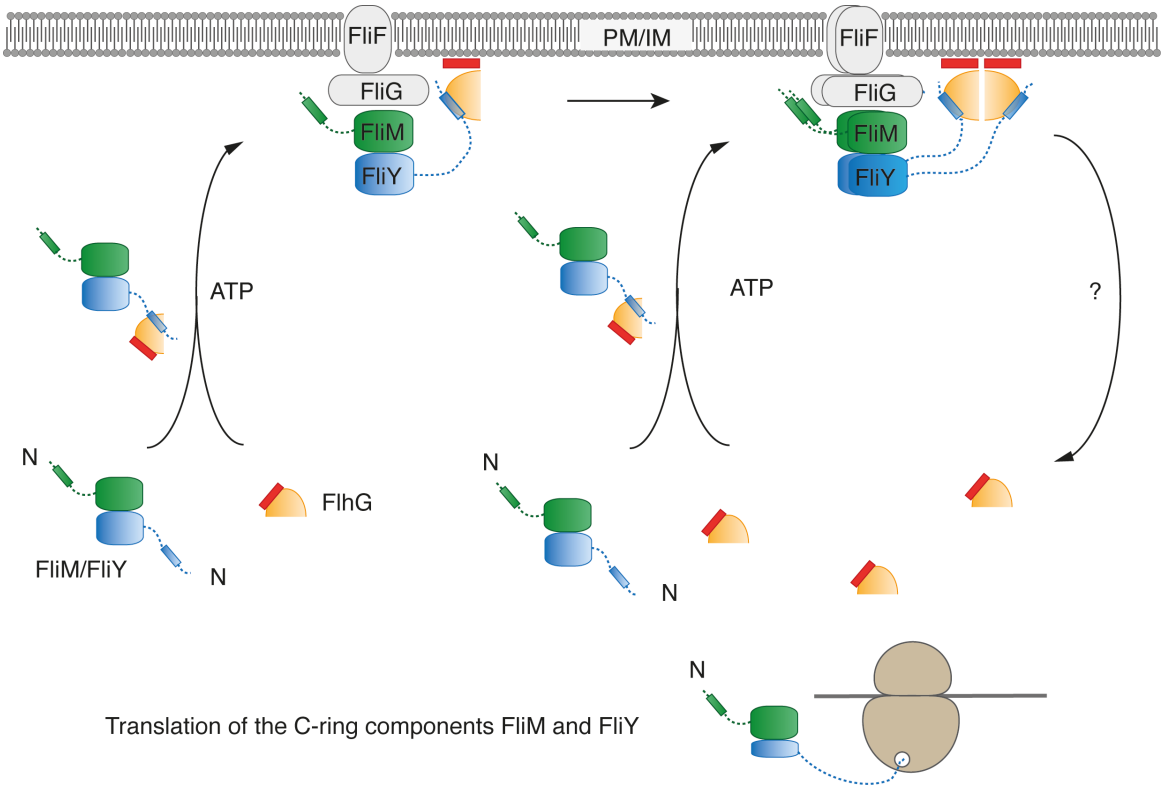

Figure 82. FlhG-assisted C-ring assembly. In this scenario FlhG assists in C-ring assembly by binding to the C-ring complex FliM/FliY in the cytoplasm, recruiting the flagellar components to the nascent flagellum. At the nascent basal body FlhG coordinates the assembly of FliM/FliY to FliG in an ATP dependent manner to result a complete C-ring. How FlhG is released from the basal bodies remains elusive and is thus indicated with a question mark. This figure was inspired by ref. (103).

Accordingly, FlhG might gradually allocate C-ring building blocks in correct positional arrangement for the assembly. Stimulated hydrolysis, which is enhanced by the presence of lipids as well as FliG may facilitate and accelerate the correct assembly of the C-ring architecture in an ATP dependent fashion.

Enhanced ATP hydrolysis of FlhG also drives the disintegration of the FlhG dimer and the transition from the ‘closed’ into the ‘open’ state, resulting in detachment from the membrane. Monomeric FlhG is subsequently mobile in the cytoplasm and again free to encounter another FliM/FliY complex.

A major issue with the model of FlhG-assisted C-ring assembly lies in the fact that deletion of *flhG* in *B. subtilis* has an influence on the flagellation pattern, but does not impair swimming or swarming motility (71). However, a severe motility defect would be expected upon incorrect assembly of a vital structure as the flagellar C-ring. Fluorescently labelled basal bodies in an *flhG* deletion strain of *B. subtilis,* appear aggregated and randomly distributed throughout the entire cell body. The morphology of these clumped C-ring aggregates was beyond the resolution limit of the microscopy technique. It was concluded that these aggregates represent tufts of intact flagella, as the motility was not impaired (71). How *B. subtilis* is motile with these tufts or why disruption of the pattern does not affect motility as observed for monotrichously flagellated bacteria was not explained.

In contrast to *in vivo* studies in monotrichously flagellated bacteria, where FlhG acts as negative regulator of number of flagella, this model promotes a positive role of FlhG for flagella biogenesis. Our data in *S. putrefaciens* confirmed studies in *V. alginolyticus* and *P. aeruginosa* that deletion *flhG* resulted in a hyper-flagellated phenotype (85, 86, 128). Upon overproduction of FlhG, *V. alginolyticus* failed to assemble flagella (84). In the monotrichously flagellated organisms *P. aeruginosa* and *S. putrefaciens* FlhG interacts with the master regulator of flagellar gene expression FleQ/FlrA, which is not present in the genome *B. subtilis* (137, 138). Accordingly, the deletion of *flhG* in *B. subtilis* seemed not to result in an increased number of basal bodies (71). This leads to the conclusion that the regulation of the number of flagella in monotrichously flagellated bacteria may occur on transcriptional level, where FlhG prevents production of flagellar genes via FleQ/FlrA. This does not interfere with a putative role of FlhG in the assembly of the flagellar C-ring. Furthermore, I was able to demonstrate that FlhG in *S. putrefaciens* is able to interact with the flagellar C-ring through the conserved ‘EIDAL’ motif as seen in *B. subtilis*.

Moreover, *in vivo* localization of FlhG displays that it only temporarily resides at the flagellum, while the release of FlhG from flagellar C-ring complexes was not

observed *in vitro*. This led to the conclusion that an additional, so far unidentified factor must be responsible for the release of FlhG from the fully assembled C-ring. First trials with proteins that are located in close proximity to the C-ring in the flagellum were unsuccessful. This might indicate that a certain substructure or protein of the basal body has to be completely assembled, before FlhG can be released from the C-ring as part of a quality control mechanism for flagellar biogenesis.

3.3.2 FlhG blocks C-ring assembly

Based on its role as a negative regulator of the number of flagella, FlhG might also prevent FliM/FliN(Y) from the assembly into the nascent C-ring, by forming a stable ternary complex with FlhG. In this scenario the ternary complex FlhG/FliM/FliN(Y) is not able to assemble with FliG *in vivo* (**Figure 83**).

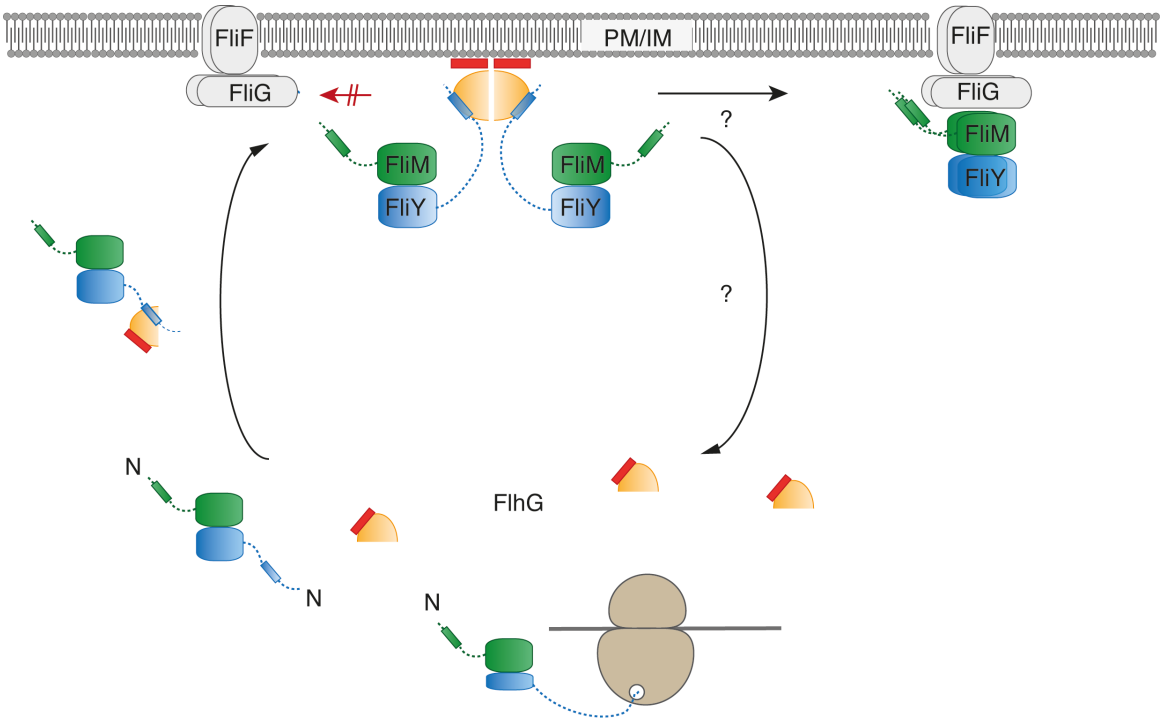

Figure 83. FlhG inhibits C-ring assembly. In this scenario FlhG may inhibit the assembly of FliM/FliY complexes to FliG through formation of a ternary complex, depicted by a red arrow. This scenario might immediately explain the negative regulatory role of FlhG on flagella number, observed in *Pseudomonas species*, *Vibrio species* and *Shewanella species.* In this scenario additional factors would be required to release the inhibition as well as FlhG from the membrane, indicated by question marks. This figure was inspired by ref. (103).

FlhG may allocate FliM/FliN(Y) complexes at the flagella assembly site, but inhibits C-ring assembly as long as FlhG interacts with FliM/FliN(Y). This requires an additional factor, which releases FlhG from FliM/FliY to complete C-ring assembly.

3.4 Flagella assembly and chemotaxis

Bacterial motility and chemotaxis are necessarily linked processes resulting in the directed movement of bacteria towards favourable conditions. The interaction of the final chemotactic response regulator CheY-P with the flagellar C-ring protein FliM provides the interface between both processes adjusting cellular movement to environmental conditions. Upon binding of CheY-P to FliM, the flagellum can switch its direction of rotation from CW to CCW or *vice versa*. This determines the ratio of 'run' and 'tumble' movements. Phosphatases subsequently clear the CheY-P signal through dephosphorylation of CheY-P to CheY, rendering it susceptible for further external stimuli (**Figure 15**).

3.4.1 Significance of the 'EIDAL' motif at the flagellar C-ring

The interaction of CheY-P and FliM is mediated by the conserved N-terminal 'EIDAL' motif of FliM. Structural analysis revealed an amphipathic interface of CheY with the helical 'EIDAL' motif (193, 194). In *B. subtilis* one side of the helical motif binds via polar interaction, while the other side attaches to CheY through a hydrophobic patch. Gln8, Asp12 and Asn16 from the conserved 'EIDAL' motif (LS**Q**xEI**D**ALL**N**) form the polar face, while Ile 11, Leu14 and Leu 15 (LSQxE**I**DA**LL**N) are involved in hydrophobic interactions.

In *B. subtilis*, the flagellar C-ring possesses two EIDAL motifs, one at both C-ring proteins FliM and FliY. While CheY-P interacts with the 'EIDAL' motif of FliM, I was able to demonstrate that the 'EIDAL' motif of FliY binds to the ATPase FlhG (55, 176, 277). This implicates that the EIDAL motifs have to be able to discriminate between these proteins, even though sequence alignments of the N-termini of FliM and FliY are highly homologous (**Figure 84**).

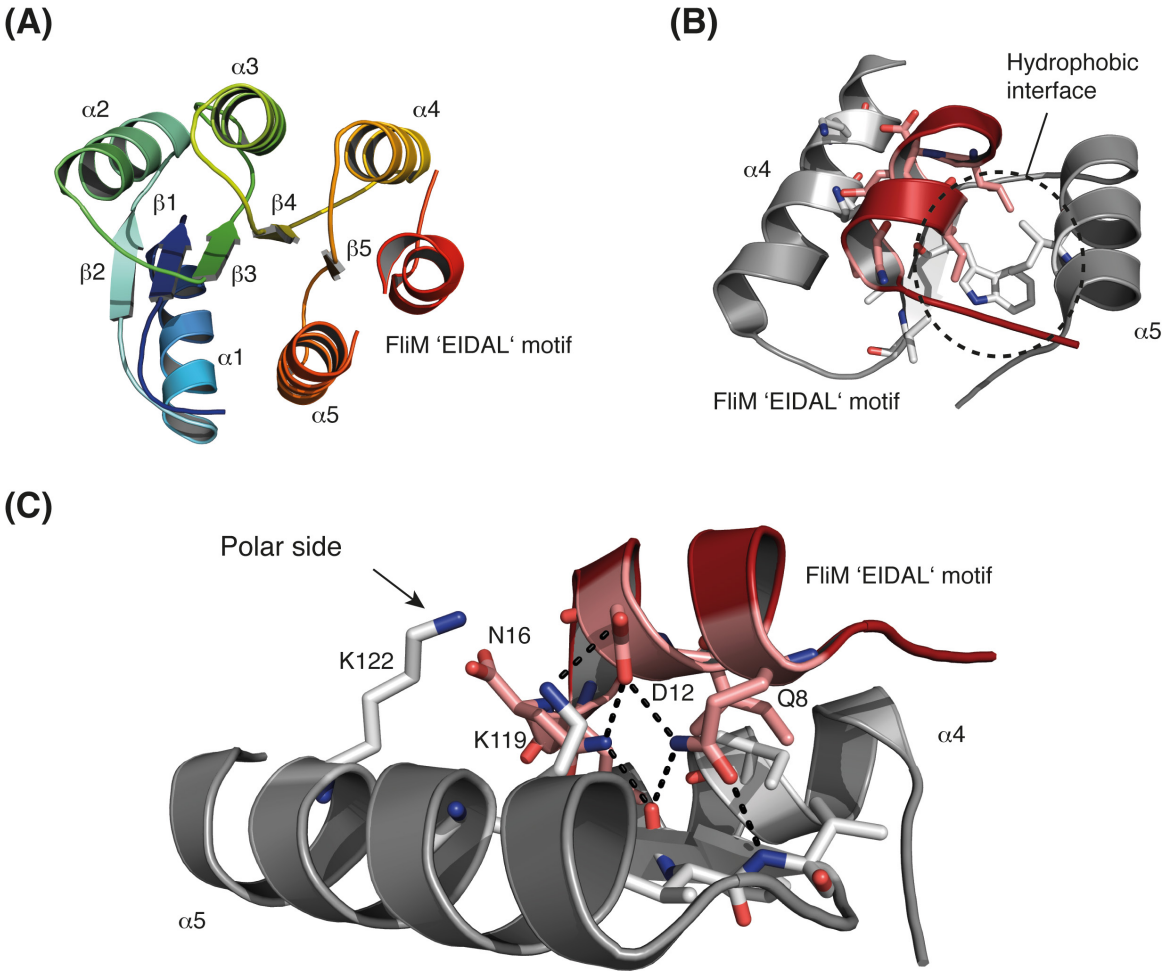

Figure 84. Interaction of CheY with FliM 'EIDAL'. (A) displays the cartoon representation of CheY in complex with the N-terminus of FliM of *B. subtilis* (pdb: 2B1J) coloured in rainbow. Secondary structure elements are depicted and the N-terminus of FliM (red) is indicated. **(B)** illustrates the hydrophobic side of the interaction interface of CheY (grey) and FliM-'EIDAL' (red) highlighted by a dashed circle. Important residues are marked as sticks. The polar side of the interface of CheY and FliM coloured as in **(B)** is shown in **(C)**. Polar contacts are indicated with dashed lines and essential residues are indicated.

In the Gram-negative bacterium *S. putrefaciens*, the C-ring of the polar flagellum comprises FliM and FliN and therefore only one 'EIDAL' motif at the N-terminus of $FliM_1$. In the lateral system, $FliM_2$ lacks the conserved 'EIDAL' motif completely. Our studies showed that FlhG interacts with the 'EIDAL' motif of the polar $FliM_1$, raising the question about the CheY-P interface. Previous studies demonstrated that only the polar system responds to chemotaxis, indicating that again the 'EIDAL' motif, which is absent in the lateral system, provides the binding site for

CheY-P. Assuming that both proteins share the same interaction interface at the flagellar C-ring, a competitive situation is expected in *S. putrefaciens*.

The specificity for FlhG or CheY in *B. subtilis* or the promiscuity to interact with both FlhG and CheY, which might occur in *S. putrefaciens*, can either be encoded in subtle differences of the 'EIDAL' motifs themselves or may be provided by their respective protein environment. An alignment of the first 30 amino acids of *Bs*FliM, *Bs*FliY, *Gt*FliM, *Gt*FliY and *Sp*FliM$_1$ shows that the 'EIDAL' motifs indeed exhibit subtle differences on amino acid level (**Figure 85**). All 'EIDAL' motifs that are supposed to bind FlhG (*i.e.* 'EIDAL's from *Bs*FliY, *Gt*FliY, *Sp*FliM$_1$) share a conserved aspartate within the 'EIDAL' motif and a conserved glycine residue after the 'EIDAL' motif (residues marked with an arrow). 'EIDAL' motifs that are supposed to exclusively bind CheY on the other hand, share a conserved SxGEM motif in close proximity after the 'EIDAL' motif (**Figure 85**).

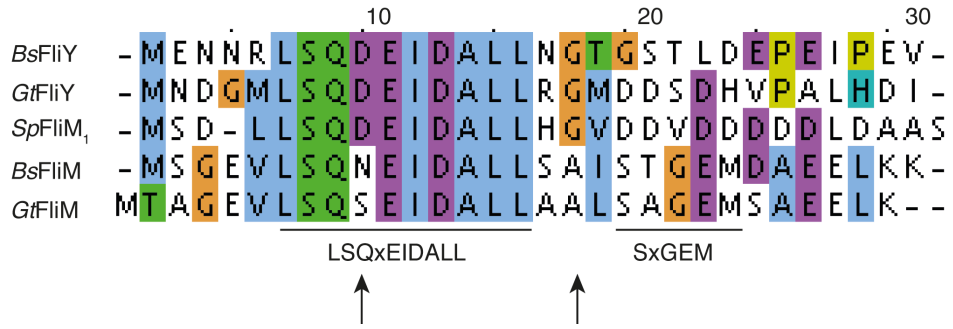

Figure 85. Alignment of 'EIDAL' motifs. The alignment includes the 30 N-terminal residues of *Bs*FliY, *Gt*FliY, *Sp*FliM$_1$, *Bs*FliM and *Gt*FliM. The arrows mark two residues putatively vital for discrimination between FlhG and CheY. Organisms are abbreviated: *G. thermodenitrificans* (*Gt*); *B. subtilis* (*Bs*); *S. putrefaciens* (*Sp*).

Whether these slight variations are sufficient to differentiate between FlhG and CheY or allow the binding of both, needs further experimental proof. The observed variations and similarities may also result from phylogenetic issues, as the alignment only comprises 5 motifs, of which 4 are taken from Firmicutes.

Whether FliM$_1$ in *S. putrefaciens* is indeed capable of binding CheY as well as FlhG also needs further experimental investigations. However, if this holds true, a scenario is possible where FlhG has a higher affinity to the 'EIDAL' motif than CheY-P, preventing CheY-P from binding to the flagellar C-ring during flagellar biogenesis. And therefore inhibit chemotaxis signalling while the flagellum is

under construction. This scenario again involves an additional factor, which releases FlhG from the C-ring upon completion of basal body or C-ring assembly.

3.4.2 CheC phosphatase domain of FliY

The third C-ring component in *B. subtilis*, FliY, displays an unusual domain architecture compared to its orthologues FliN. In addition to the FliN-homology domain at the C-terminus, it comprises an N-terminal 'EIDAL' motif and a globular middle domain. This globular domain represents a CheC-like phosphatase with two active sites that is able to dephosphorylate the chemotactic response regulator CheY-P (183, 184). In *B. subtilis* FliY together with CheC and CheD are responsible to restore CheY-P levels after external stimuli (187).

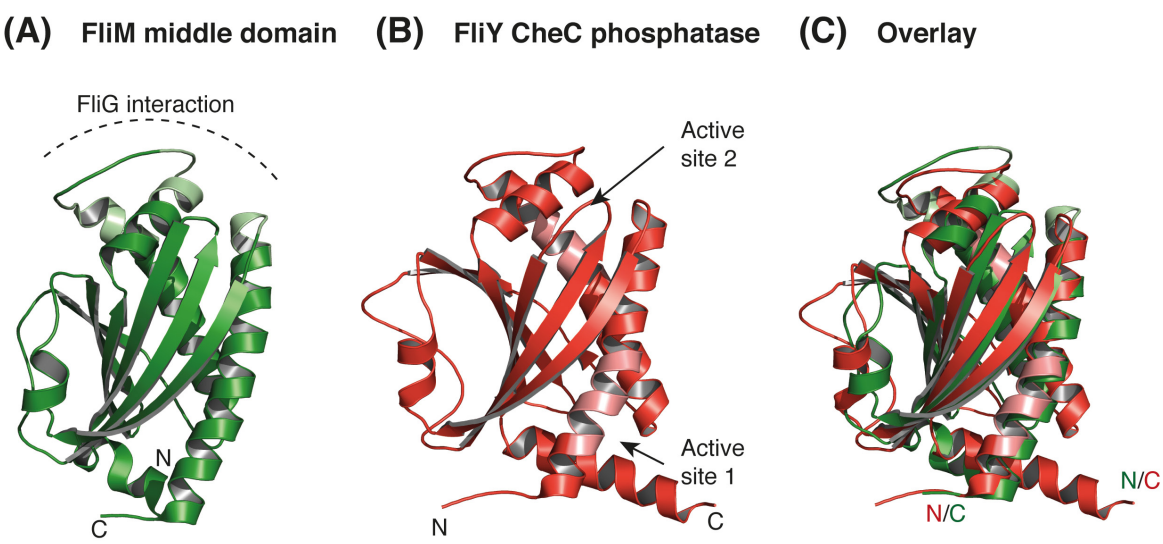

Figure 86. The FliM and FliY middle domains. (A) shows the cartoon representation of the middle domain of FliM of *H. pylori* (pdb: 4FQ0) displayed in green. A dashed line marks the interaction interface with FliG. **(B)** shows the cartoon of the crystal structure of the CheC-like phosphatase domain of FliY of *T. maritima* (pdb: 4HYN) in red. Active sites are indicated in light red and marked by arrows. **(C)** An overlay of both structures reveals the close structural homology of both domains.

A structural comparison of the middle domain of FliM, which is responsible to bind FliG and the CheC phosphatase of FliY display a high structural homology. Both domains share the same fold with two long helices nestled to an arch composed of six antiparallel β-strands, surrounded by three short helices (**Figure 86**). In

FliM the C-terminal tip of helix α2, the N-terminal tip of helix α3 and a loop region in between form the platform for the interaction with the middle domain of FliG (278). The active sites of the phosphatase of FliY are located in the N-terminal segment of both long helices (**Figure 86B**). Although, the structures also revealed that the FliM-FliG interface region on FliM is structurally conserved in FliY, it is not able to interact with the FliG middle and C-terminal domain, as it was observed for FliM (**Figure 87AB**) (279). On sequence level one motif of the interface is conserved in FliY (DxhhGGxG), while a second one exhibits opposite charges (RxxxxIE in FliM, ExxxxIK in FliY) (**Figure 87C**).

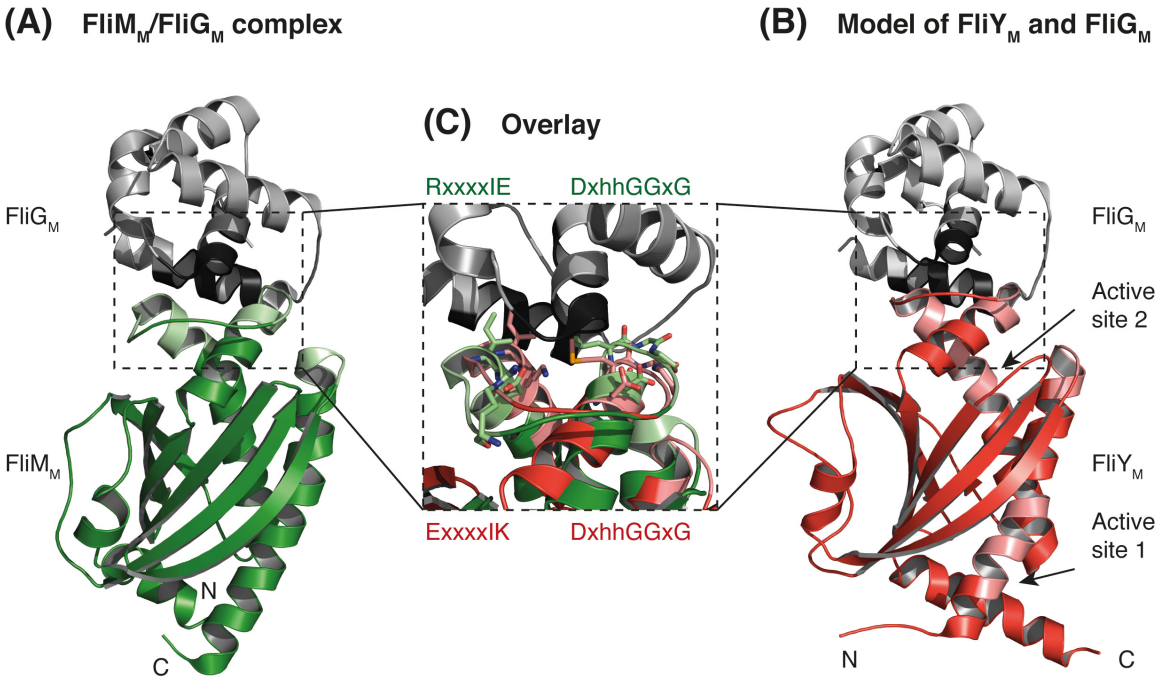

Figure 87. The FliM/FliG interaction interface. (A) displays a cartoon representation of a complex of the middle domain of FliM (FliM$_M$, green) and the middle domain of FliG (FliG$_M$, grey; pdb: 4FQ0). The interaction interface is coloured in light green (FliM$_M$) and black (FliG$_M$). **(B)** indicates a model of a putative complex of the FliY CheC phosphatase domain (FliY$_M$, red; pdb: 4HYN) and the FliG middle domain (grey). **(C)** The inlay provides a detailed image of the interaction interface with superimposed FliM$_M$ and FliY$_M$ structures. Vital residues are shown as sticks and important motifs are depicted in the one letter code in the respective colour.

The presence of a CheC phosphatase, which inactivates phosphorylated CheY at the flagellar C-ring, where it fulfils its task of switching the rotation of the flagellum, is an unusual feature among bacteria. However, compared to *E. coli*,

B. subtilis possesses an inverse chemotaxis system meaning in its default state *B. subtilis* tumbles, while *E. coli* swims smoothly. Niche-specific conditions might render a fast regeneration of elevated CheY-P levels more important for *B. subtilis* than *E. coli*.

3.5 Differential regulation of flagellation patterns

One aim of this doctoral thesis was to investigate how the conserved regulatory device consisting of FlhF and FlhG can regulate monotrichous flagellation in *S. putrefaciens*, peritrichous flagellation in *B. subtilis* as well as other flagellation patterns in different bacteria. Our experimental approach revealed that FlhG exhibits the same key features and acts according to the same principles in *S. putrefaciens* and *B. subtilis*. Therefore, the discrimination is not encoded in FlhG itself. Whether FlhF is capable of directing flagella to the cell pole in polarly flagellated bacteria and positioning flagella at a lateral site in peritrichously flagellated bacteria is not clear. The fact that both proteins exhibit species-specific interaction partners in different organisms provides a second possible scenario that allows the discrimination between different patterns in versatile organisms. Corroborating literature reports, our data demonstrate that FlhG interacts with universally conserved proteins such as components of the flagellar C-ring as well as proteins, which are specific for a certain bacterial family or for several species. In the following, these proteins will be called species-specific interaction partners. A combination of universal and species-specific interaction partners provides an ideal basis to regulate different flagellation patterns in versatile organisms based on the same principles.

3.5.1 Species-independent interaction partners of FlhF and FlhG

The interaction between FlhF and FlhG and the stimulation of the FlhF GTPase through the N-terminal activator motif of FlhG is central to the interconnection between both regulatory circuits and therefore constitutes a universal feature of this module. This interaction is only characterized in *B. subtilis* so far (118). As highly conserved building blocks of the flagellar basal body FliF and FliG might

represent candidates for species-independent interaction partners for FlhF and FlhG, respectively. Our data demonstrates that FlhG interacts with FliG in the presence of ATP and lipids in *G. thermodenitrificans*. Due to the high conservation of FliG in different bacterial species, it can be assumed that FliG is general member of the FlhG interaction network. However, further experimental data are required to confirm this interaction in different organisms. The interaction of FlhG and FliG seems to play a role during C-ring assembly, although the exact mechanism is unclear. FlhF is required to direct FliF to the cell pole in *P. aeruginosa*, whether this is achieved through physical interaction of FlhF and FliF or indirectly remains elusive (125).

3.5.2 Diversity of C-ring components

The flagellar C-ring is an essential part of the flagellar basal body harbouring the switch complex and is thus present in all flagellated bacteria. However, its architecture differs between bacterial species. While FliG and FliM are highly conserved, the third component FliN(Y) differs in size and domain composition. All FliN(Y) proteins share a highly conserved C-terminal dimerization domain of approximately 12 kDa (FliN-homology domain). In *Vibrio*, *Shewanella* and *Pseudomonas species*, which are mainly monotrichously flagellated, FliN only consists of this domain. In *H. pylori* and *C. jejuni*, FliN comprises an additional 20 kDa domain located N-terminally to the FliN domain. The actual function of this domain has not been elucidated so far. In *B. subtilis* and *G. thermodenitrificans* FilY is composed of a CheC-phosphatase domain followed by a predicted unstructured linker region of 40-80 amino acids and the conserved FliN domain at its C-terminus. In contrast to all other FliN(Y) homologues, it also contains an ‘EIDAL’ motif at the very N-terminus (**Figure 88**). Although FlhG interacts with the flagellar C-ring in *S. putrefaciens* and *B. subtilis*, it interacts with different C-ring components in these two species. These differences in the architecture of the C-ring and the variation of the FlhG binding sites was neglected so far and may play a vital role in the maintenance of different flagellation patterns.

3.5.3 Species-specific interaction partners of FlhF and FlhG

Besides FliG, FliM and FliY, FlhG interacts with proteins, which are limited to certain bacterial species or families. In the mainly monotrichously flagellated *Vibrio*, *Shewanella* and *Pseudomonas species* FlhG interacts with the master regulator of flagellar gene transcription FleQ/FlrA, which might restrict flagella number to one in these bacteria. Bacteria with more than one flagellum lack a FleQ/FlrA homologue protein (**Figure 88**). Thus, flagellar gene transcription relies on different regulatory mechanisms.

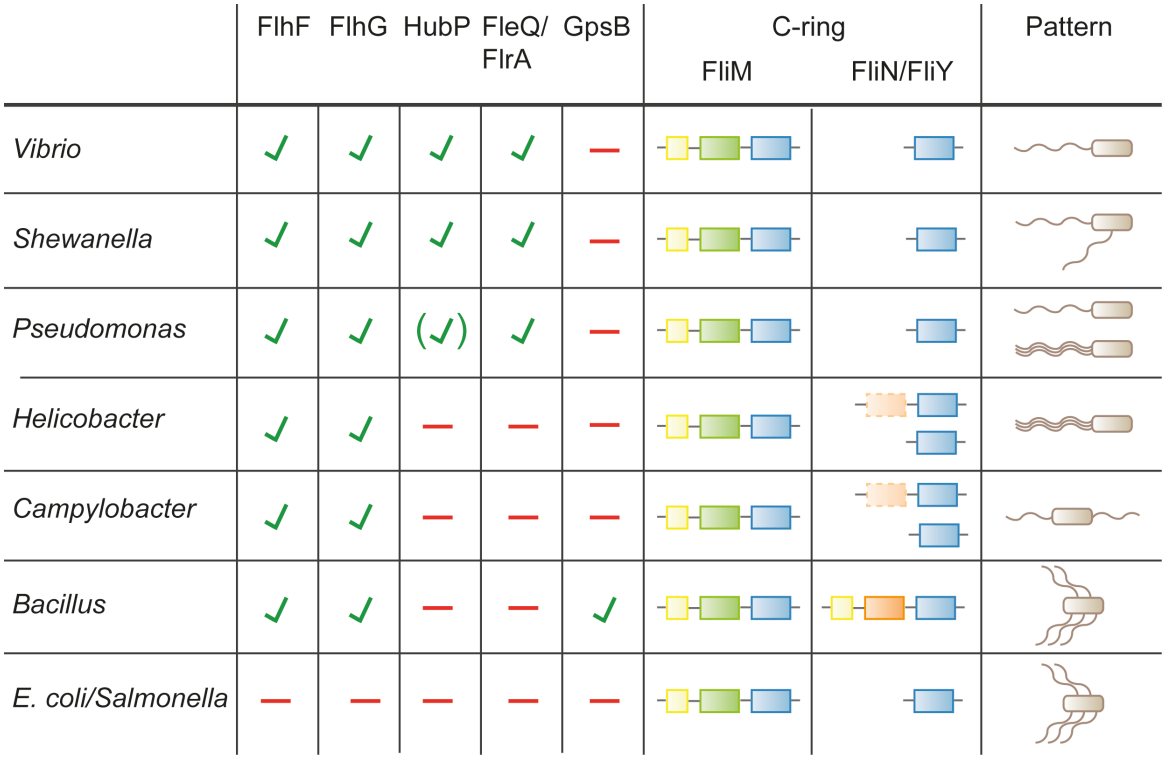

Figure 88. Interaction partners of FlhF and FlhG. The occurrence of interaction partners of FlhF and FlhG in different bacterial families possessing FlhF as well as FlhG is summarized with the C-ring composition and the flagellation pattern of the respective bacteria. This figure was adapted from ref. (16).

FleQ/FlrA, the polar 'landmark' protein HubP is only present in the genome of *Vibrio*, *Shewanella* and maybe *Pseudomonas species* and is known to interact with FlhF as well as FlhG (**Figure 88**). It is involved in the polar recruitment of FlhG and might therefore play a role for the positioning of a flagellum at the cell pole. Since a HubP homologue is missing in the genome of the peritrichous

B. subtilis, but also in the lophotrichous *H. pylori* and the amphitrichous *C. jejuni*, the polar location of the flagella are determined differently in both ε-proteobacteria. The fact that FlhF finds its polar location independently of HubP indicates that the polar 'landmark' protein is not necessary for the initial placement of the flagellum. The plethora of interaction partners of HubP implicates an essential role in different cellular processes such as chromosome partitioning, chemotaxis and flagellation patterns control. Though, the actual mechanism remains unclear. GpsB a member of the late divisome on the other hand is exclusively found in *B. subtilis* and closely related species (*e.g. G. thermodenitrificans*) and interacts with FlhG in an ATP-dependent manner. Functional implications of this interaction are still to be deduced and experimentally assessed. All these examples, summarized in **Figure 88**, provide an idea of how a conserved molecular switch may control different flagellation patterns depending on the respective interaction network. At this point we begin to understand the complex regulatory mechanisms underlying the determination of number and location of flagella in many bacteria.

Although *E. coli* exhibits peritrichous flagellation as *B. subtilis*, it relies on a different system for regulating number and location of flagella. *E. coli* lacks FlhF and FlhG as well as many interaction partners of these proteins and can therefore be considered as an exception concerning flagellation pattern regulation.

3.5.4 The interaction network of FlhF and FlhG

To further understand the regulatory network around FlhG and FlhF, it is not sufficient to identify interaction partners, it is also essential to characterize at which state and where these interacting proteins influence FlhG and FlhF.

Since purified FlhG is in its monomeric state, the *in vitro* pull down assays point towards an interaction of the FliM/FliN(Y) with monomeric FlhG in *B. subtilis* as well as *S. putrefaciens*. In addition, the flagellar C-ring complex FliM/FliN(Y) interacts with FlhG in a nucleotide independent fashion. *In vivo* co-localization of FlhG and FliM is observed at the membrane, implicating that FliM may interact with the dimeric membrane-associated FlhG. All this data suggest that FlhG is able to bind the C-ring complex FliM/FliY in its monomeric as well as in its dimeric

state, which is also supported by the crystal structures, showing that the interaction interface, helices α6 and α7, is available in both conformations (**Figure 89**). The interaction with the third C-ring component FliG strongly depends on the presence of ATP and lipids, that mimic a membrane. I therefore conclude that FlhG interacts with FliG as a membrane-associated homodimer. This interaction might take place at the nascent flagellar basal body where FliG binds to the integral membrane protein FliF (**Figure 89**).

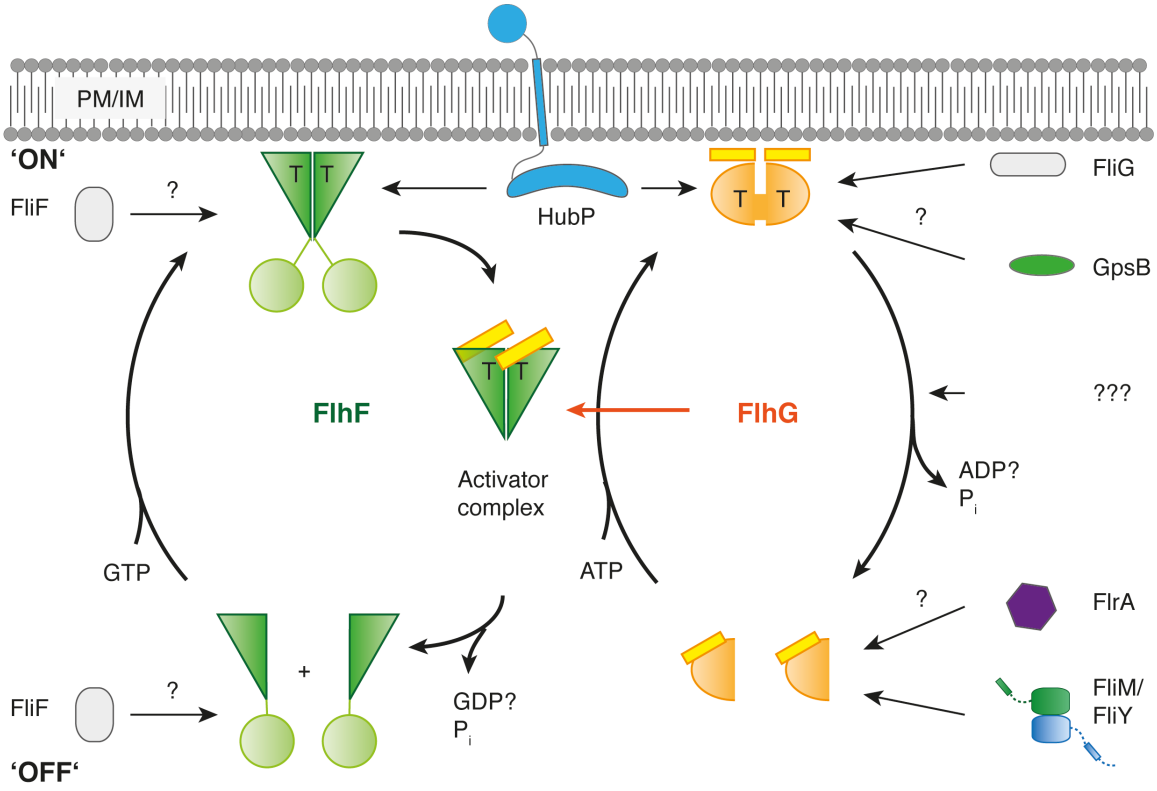

Figure 89. The interaction network of FlhF and FlhG. The scheme illustrates the regulatory circuit of FlhF and FlhG, displaying interaction partners of both proteins and at which stage these proteins presumably interact with FlhF or FlhG (PM: plasma membrane and IM: inner membrane).

The limited data on the interaction with GpsB points towards an interaction in close proximity to the membrane, as the binding is exclusively observed in the presence of ATP (**Figure 89**). As part of the divisome GpsB is located at the membrane corroborating this hypothesis. However, further characterization of the interaction is still needed.

Since FlhG interacts with the DNA binding domain of FlrA in *S. putrefaciens*, it may prevent FlrA from binding to the promotor region of flagellar genes thus in-

hibiting gene transcription. I infer that in monotrichously flagellated bacteria, FlhG allows the assembly of one flagellum, coordinates the biogenesis of the basal body in concert with FlhF and binds the master regulator FleQ/FlrA after completion of the basal body preventing the assembly of a second flagellum. FlhG may thus interact with FleQ/FlrA after release from the membrane in its monomeric state in the cytoplasm. In *V. cholerae* the integral membrane protein HubP serves as a polar landmark and directly interacts with FlhG and FlhF at the cell pole (**Figure 89**) (139). This scenario would indicate that it interacts with an FlhF and FlhG dimer, although direct evidence is missing. Further studies are also required to elucidate the mode of interaction of FlhG or FlhF and HubP. The recruitment of the first component of the flagellar basal body FliF through FlhF might indicate an interaction between these two proteins. However, a putative interaction between FlhF and FliF is not biochemically characterized in literature. Since FliF is an integral membrane protein, an indirect recruiting mechanism seems more probable than direct interaction. As FlhF belongs to the family of SRP-GTPases, it might be involved in co-translational targeting and insertion of FliF into the membrane at the correct location at the cell pole.

Although parts of the network have now been elucidated, there are still puzzle pieces missing to obtain a complete picture. Especially, further insights into the cellular role of FlhF will be crucial to understand the regulatory mechanisms underlying flagellation pattern control. In this context the so far uncharacterized B-domain of FlhF seems to be the key to elucidate the biological function of FlhF. In summary, in monotrichous bacteria FlhG is mainly involved in regulating the number of flagella, whereas FlhF seems to determine the position of flagellar assembly. Presumably, further factors that contribute to the complex regulatory network that determines number and location of the flagella biogenesis have to be identified.

3.5.5. Current working hypothesis

Consolidating literature as well as our data, I infer a working hypothesis in which FlhF initiates flagellar biogenesis by directing the first component of the basal body to the future flagellar assembly site. Whether this targeting step is realised

through the association of FlhF with a special ‘landmark’ protein (e.g. HubP) or through interaction with specific lipids, enriched at the correct location is still enigmatic. The fact that polar localization of FlhF occurs independently of HubP in *V. cholerae* may point towards the second scenario (**Figure 90A**).

During basal body biogenesis, FlhG assists in the assembly of the flagellar C-ring by recruiting and facilitating the correct assembly of the FliM/FliN(Y) complex to FliG, which is supposed to complete the flagellar basal body (**Figure 90B**). Whether the assembly itself or a polar ‘landmark’ protein directs FlhG to its correct location remains unclear. Accumulation of FlhG in close proximity to the membrane leads to ATP-dependent dimerization of FlhG and presumably to an interaction with FliG. After the assembly of the basal body FlhF and FlhG reside at the nascent flagellum, where the FlhG dimer may trigger the GTP hydrolysis of FlhF. Subsequently, the FlhF dimer falls apart and FlhF is released from the membrane, entering its inactive cytoplasmic ‘OFF’ state (**Figure 90C**). How FlhG is released from the membrane remains elusive. However, *in vivo* localization demonstrates that it only temporarily resides at the basal body. The presence of special lipids might either be sufficient to trigger release or an additional factor will be required to stimulate ATP hydrolysis of FlhG. The requirement of a complete basal body or a substructure for the release of FlhG would represent a convenient control mechanism of the flagellar basal body, prior to the secretion of late flagellar substrates. After assembly of the first basal body, FlhG may inhibit the transcription of flagellar genes to restrict the number of flagella to one through its interaction with the flagellar master regulator FleQ/FlrA in monotrichously flagellated bacteria (**Figure 90D**). How the number of flagella is determined in other bacteria is still not clear. Notably in *H. pylori* deletion of *flhG* leads to aflagellated bacteria, indicating an opposite effect of FlhG on the number of flagella and a different mechanism of counting (64).

Our current working model emphasises that the full extent of the complex regulatory network that underlies flagellation pattern maintenance is still unknown. Although I was able to provide new insight into the molecular mechanism of FlhG and to identify novel interaction partners and putative candidates, crucial puzzle pieces are still missing

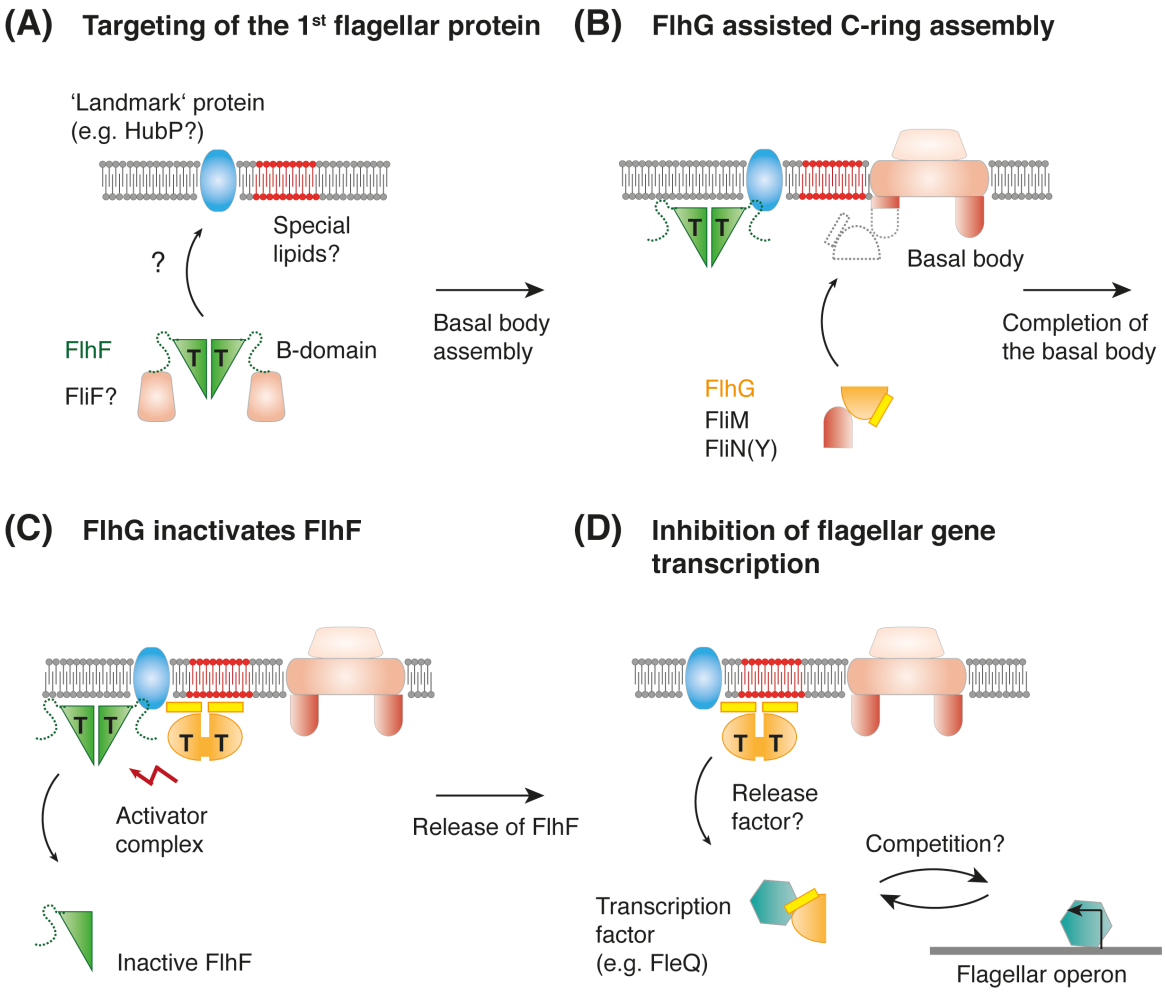

Figure 90. Current working hypothesis. (A) shows how FlhF is involved in targeting the first component of the flagellum to the future assembly site. How this is achieved remains unclear. 'Landmark' proteins such as HubP as well as a special lipid composition might play a role for this process. After initiation of basal body assembly, FlhG assists in assembling the flagellar C-ring, which is one of the last components of the basal body **(B)**. **(C)** shows how after completion of the basal body assembly FlhG is able to inactivate FlhF by stimulating GTP hydrolysis. The FlhF dimer falls apart and dissociates from the membrane. How FlhG is released from the basal body remains enigmatic. A special release factor or certain lipids might be of importance for FlhG release. In its monomeric, cytoplasmic state FlhG might interact with the master regulator of flagellar gene transcription FlrA in monotrichously flagellated bacteria to restrict the number of flagella to one **(D)**. This figure was adapted from ref. (16).

The challenges I faced by reconstituting C-ring assembly *in vitro*, displayed that there might be more than a couple of proteins to flagellar regulation. It seems likely that it also requires the presence of special lipids, secondary metabolites or other cellular components.

Future perspective

4.1 Hallmarks of flagellation pattern maintenance

In this work I provided evidence that the regulatory circuit of FlhG is conserved and operates according to the same mechanistic features in many flagellated bacteria through a comparative study using the peritrichous Gram-positive *B. subtilis* and the monotrichous Gram-negative *S. putrefaciens* as model organisms. FlhG seemed to be involved in the biosynthesis of the basal body presumably coordinating the assembly of the C-ring. Since C-ring assembly is a late step of basal body biogenesis, it does neither explain how the number nor the location of flagella is determined. Referring to the discussion, we are just beginning to understand the mechanisms of flagellar organisation and important puzzle pieces are still missing. Especially, enlightening three major processes, detailed in the following, might become crucial to elucidate the mechanisms of the regulatory network underlying flagellation pattern control.

4.1.1 Determination of the flagellar assembly site

To get insights into how the location of a future flagellum is determined, it is necessary to know how the first component of a flagellum is targeted to its correct position. A recent study reports that FlhF is directly involved in recruiting the first component of the basal body, the membrane protein FliF (125). The actual mechanism how FlhF directs FliF to the flagellar assembly site is still enigmatic. Since FlhF is the third member of the SRP-GTPase family and forms homodimers, it might represent a kind of ‘pseudo’ SRP system, which recruits ribosomes translating the message of early flagellar components to the future flagellar assembly site. The so far poorly characterized B-domain of FlhF is presumably crucial for this process. However, how FlhF finds the site of flagellar biogenesis re-

mains to be assessed in detail. Although FlhF interacts with the polar 'landmark' protein HubP in *V. cholerae*, it localizes at the cell pole independently of the presence of HubP, implicating that HubP is not the landmark for the future flagellum. Whether another polar 'landmark' protein is responsible for polar localization of FlhF in *V. cholerae* or whether FlhF associates to membrane domains that are enriched with a certain lipid species is subject of future research. Elucidating the molecular mechanisms underlying the localization of FlhF and targeting of early flagellar components to the future flagellar assembly site may greatly contribute to understand formation of the flagellation patterns.

4.1.2 How do bacteria count the correct number of flagella?

After each cell division process, bacteria do not only precisely position new flagella but also reproducibly establish a certain number of these locomotion organelles. It is still unknown how bacteria count the correct number of flagella that has to be assembled. In monotrichous *Vibrio*, *Pseudomonas* and *Shewanella species* FlhG may restrict the number of flagella to one, through its interaction with the master regulator of gene expression FleQ/FlrA. After the assembly of the first flagellum, FlhG simply inhibits the transcription of further early flagellar genes. How this is achieved in bacteria that possess more than one flagellum, remains unclear. Since no FleQ/FlrA homologue is encoded in the genome of these bacteria, determination of the correct number has to rely on a different mechanism. The assembly of more than one flagellum represents a more complex task and might therefore require more sophisticated regulatory devices including feedback loops. The role of FlhG in these transcriptional regulation networks may differ between peritrichous, lophotrichous and amphitrichous bacteria and has to be assessed for each flagellation pattern.

Also, it is not clear how bacteria reinitiate flagellar biosynthesis after cell division, if FlhG blocks the transcription after the assembly of the first flagellum, which would result in at least one aflagellated cell. This strongly indicates that vital cellular processes such as cell division, chromosome partitioning, chemotaxis and the production of the flagellum are intimately linked and may influence each other.

4.1.3 Linking vital cellular processes through MinD/ParA ATPases

MinD/ParA ATPases are central to many spatial orchestration processes in the bacterial cell, for example chromosome segregation through ParA, cell division site determination through MinD, arrangement of chemotaxis arrays through ParC and maintenance of flagellation patterns through FlhG (111-117). To ensure survival and proliferation of a bacterial cell, all these systems have to be orchestrated to guarantee that the chromosomes are segregated prior to cell division or that chemoreceptors are clustered in the neighbourhood of flagella. How these individual systems communicate with each other is still not known. It also remains enigmatic to which degree these systems influence each other. Does the location of flagella influence the positioning of chemotaxis arrays? Or *vice versa*?

In the monotrichous *V. cholerae* the polar 'landmark' protein HubP, which interacts with several MinD/ParA ATPases, may represent a central node for coordinating these vital MinD/ParA ATPase dependent processes. The binding of a certain interaction partner may alter the binding affinities for other interaction partners or even inhibit the binding of certain proteins, thereby orchestrating the spatial distribution of MinD/ParA ATPases. Other bacteria that lack HubP may have developed a different strategy through linking individual systems instead of providing a central hub. In the peritrichous *B. subtilis* GpsB as interaction partner of FlhG and part of the divisome might couple cell division and the flagellar biogenesis. To unravel the complex interconnection of the individual MinD/ParA systems and their mechanistic details, remains a project for future experimental assessment.

Materials and methods

5.1 Materials

5.1.1 Chemicals, enzymes and combustibles

Chemicals were purchased from Sigma Aldrich, Roth and AppliChem in highest purity available. Chemicals were used as received without further purification except stated. Lipids, used for the preparation of LUVs for the usage in flotation assays were purchased from Avanti polar lipids.

Combustible laboratory equipment (1.5/2.0 ml reaction tubes, 15/50 ml Falcon tubes, pipette tips as well as syringes) was supplied by Sarstedt and Braun. Other equipment (pipettes, heating block, vortexers and power supplies) was purchased from Neolab. Electronic pipettes were purchased from eppendorf.

5.1.1.1 Enzymes and cloning equipment

Restriction enzymes and further reagents (dNTPs, BSA solution, reaction buffers) for molecular cloning and genetic manipulations were supplied by New England Biolabs, Biozym Scientific GmbH and Fermentas. Plasmid preparation and gel extraction of amplified or plasmid DNA were performed using kits from Qiagen (QIAprep spin Miniprep kit and QIAquick Gel Extraction Kit, respectively) according to the manual provided by the manufacturer. As size standard for agarose gels, Quick-Load® Purple 2-log DNA ladder (0.1 -10.0 kb) and Gene Ruler^{TM} (1 kb) was employed, which was provided by New England Biolabs and Thermo Scientific, respectively. Protein variants were generated using the QuickChange II site-directed mutagenesis kit ordered from Agilent Technologies. MWG-Biotech AG sequenced all plasmids and PCR products.

5.1.1.2 Protein biochemistry

Purified proteins were concentrated using Amicon Ultra-15 centrifugal filter units (10 k, 30 k and 50 k size exclusion) purchased from Merck Millipore. PageRuler™ prestained protein ladder 10-180 kDa, PageRuler™ unstained broad range protein ladder and Pierce unstained protein MW marker from Life technologies as well as Protein Marker EXtended PS13 (5-245 kDa) supplied by GeneOn, were used as size standards for SDS-PAGEs. Ni-NTA agarose and glutathione sepharose 4B were purchased from Qiagen and GE Healthcare, respectively. Spin columns and other equipment for pull down experiments were supplied by MoBiTec.

5.1.1.3 Crystallization

Crystallization experiments were performed in SWISSCI MRC 2-well and MRC 3-well crystallization plates with 96 conditions on each plate. The JCSG core suite providing 386 crystallization conditions served as initial screen. Individual fine screens and additive screens were prepared in SWISSCI MRC 2-well and MRC 3-well plates. Crystals were looped and flash frozen with equipment (CrystalWand Magentic, Mounted CryoLoops and CrystalCap HT™ Vial) ordered from Hampton Research.

5.1.1.4 Data collection at the ESRF

Diffraction data of crystals was collected at the ESRF in Grenoble, France at the beamlines ID 23-1 and 23-2.

5.1.2 Plasmids

Various plasmids were used in the scope of this work for different purposes. Firstly, pET24d (Kanamycin resistance) and pET16b (Ampicillin resistance) served as vectors for protein production of $(His)_6$-tagged proteins, which also allowed co-production of different proteins due to different resistance markers. N-

terminal GST-fusion proteins were generated using pGAT3 (Ampicillin resistance). Genomic integrations in to *B. subtilis* were performed with pSG1164 (280).

5.1.3 *E. coli* strains

Large-scale protein production for crystallography and biochemical assays was carried out in phage resistant, chemically competent *E. coli* BL21 (DE3) (Life technologies). For plasmid amplification chemically competent *E. coli* DH5α (Life technologies) were employed.

5.1.4 Buffers and growth media

5.1.4.1 Media

E. coli was cultured in LB broth (20 g/l) ordered as a premix from Roth. LB broth was sterilized before usage.

5.1.4.2 List of buffers

PBS buffer was used in pull down assays where stated.

PBS buffer, pH 7.4
137 mM NaCl
2.7 mM KCl
10 mM Na_2HPO_4
1.8 mM KH_2PO_4

E. coli cells were resuspended in lysis buffer before cell lysis and subsequent Ni-NTA purification.

Lysis buffer
20 mM HEPES, pH 8.0
250 mM NaCl
20 mM KCl
20 mM $MgCl_2$
40 mM imidazole

$(His)_6$-tagged proteins were eluted from the Ni-NTA column using the Ni-NTA elution buffer

Ni-NTA elution buffer
20 mM HEPES, pH 8.0
250 mM NaCl
20 mM KCl
20 mM $MgCl_2$
500 mM imidazole

This buffer was used for SEC.

SEC buffer
20 mM HEPES, pH 7.5
200 mM NaCl
20 mM KCl
20 mM $MgCl_2$

GST-tagged proteins were eluted from glutathione sepharose or from a GST-trap column employing GSH elution buffer.

GSH elution buffer
50 mM TRIS, pH 7.9
20 mM glutathione

Quench buffer was employed to stop the $^{1}H/^{2}H$ exchange reaction during HDX measurements.

Quench buffer (HDX)
400 mM KH_2PO_4/H_3PO_4, pH 2.2

LUVs for flotation assays were prepared in flotation assay buffer.

Flotation assay buffer
100 mM Phosphate, pH 7.5
750 mM NaCl
10 mM $MgCl_2$
1.2 M Sucrose

5.1.4 Laboratory equipment

Equipment	Supplier
FPLC systems	
Äkta pruifier	GE Healthcare
Äkta prime	GE Healthcare
Centrifuges	
Sorvall LYNX 6000	Thermo Scientific
A27-8 x 50 Fixed Angle Rotor	Thermo Scientific
Fiberlite™ F9-6 x 1000 LEX Fixed Angle Rotor	Thermo Scientific
Optima MAX-XP Tabletop Ultracentrifuge	Beckmann Coulter
MLS-50 swing out rotor	Beckmann Coulter
Heraeus Meagfuge 40R	Thermo Scientific
Heraeus Fresco 21 Centrifuge	Thermo Scientific
Heraeus Pico 21 Centrifuge	Thermo Scientific
Columns	
HiLoad 26/600 Superdex S200 pg	GE Healthcare
HiLoad 26/600 Superdex S75 pg	GE Healthcare
Superdex S200 10/300 GL	GE Healthcare
HisTrap FF 1 ml and 5 ml	GE Healthcare
GSTrap FF 1 ml	GE Healthcare
EC 250/4.6 Nucleodur HTec 3 µm	Machery/Nagel
HDX equipment	
Orbitrap Velos Pro	Thermo Scientific
HPLC pump 1260 Infinity	Agilent Technologies
HPLC pump 1100 Series	Agilent Technologies
Pepsin column	self-made
Trap column	self-made
EC50/2 NUCLEOSHELL®, C18, 2.7µm	Machery/Nagel
Manual TL injection valve	Agilent Technologies
2/6 SwiValve	Agilent Technologies
Microscopes	
Leica SP 8	Leica
100X HCX PL APO STED Objective (NA 1.4)	Leica
Olympus SZ-ST	Olympus
SZM-2	Optika Microscopes
Incubators	
WiseCube	Wisd laboratory instruments

Incucell	MMM Medcenter Einrichtungen GmbH
SDS-PAGE equipment	Biorad
Agarose Gel equipment	Cleaver Scientific
T 100^{TM} Thermo Cycler	Biorad
M-110L Microfluidizer	Microfluidics
GEL iX20 Imager	Intas
Gryphon LCP	ARI-Art Robbins Instruments
Peristaltic pump	Gilson
NanoDrop Lite	Thermo Scientific

5.2 Methods

5.2.1 Molecular cloning

Genes encoding for the proteins used in this study were amplified from genomic DNA of *B. subtilis* PY79, *G. thermodenitrificans* NG80-2 as well as *S. putrefaciens* CN-32 by polymerase chain reaction (PCR) using Q5 High-Fidelity DNA polymerase according to the manufacturers manual. Primers were designed according to the following gene annotations: *B. subtilis* PY79: (U712_08620 (*flhG*); U712_08570 (*fliM*); U712_08575 (*fliY*); U712_08580 (*cheY*); U712_10735 (*gpsB*); *G. thermodenitrificans* NG80-2: (GTNG_1094 (*flhG*); GTNG_1083 (*fliM*); GTNG_1084 (*fliY*); GTNG_1073 (*fliG*); GTNG_2544 (*minC*); *S. putrefaciens* CN32: (Sputcn32_2560 (*flhG*); Sputcn32_2569 ($fliM_1$); Sputcn32_2568 ($fliN_1$); Sputcn32_3479 ($fliM_2$); Sputcn32_3480 ($fliN_2$); Sputcn32_2580 (*flrA*) Sputcn32_2442 (*hubP*)). A $(His)_6$ tag was encoded in either the *forward* or *reverse* primer. A list of primers used in this work is provided in the appendix (**Table S3**).

Protein variants were generated using the QuickChange II site-directed mutagenesis kit (Agilent Technologies). The *flhG-yfp* fusion was made by cloning the last 500 coding bp of *flhG* (*ylxH* gene) into the plasmid pSG1164 (280). A list of plasmids used in the scope of this work is provided in the appendix (**Table S4**).

5.2.1.1 Plasmid preparation

Plasmid preparation was performed using the QIAprep spin Miniprep kit (Qiagen) according to the manufacturer's manual (www.qiagen.com). Briefly, *E. coli* DH5α were grown over night in the presence of the respective resistance marker and the cells were harvested by centrifugation (3500 x *g*/4000 rpm, 10 min, 4 °C). The cells were subsequently lysed under alkaline conditions. Precipitated cell debris was removed by centrifugation (17 900 x *g*/13 000 rpm, 10 min, 4 °C) after neutralization of the mixture. The supernatant was applied to the respective spin columns, washed with buffer PE and eluted in 50 µl water by centrifugation (17 900 x *g*/13 000 rpm, 2 min, 4 °C). All plasmids were stored at -20 °C.

5.2.1.2 Gel extraction

Amplified DNA was extracted from agarose gels using the QIAquick Gel Extraction kit (Qiagen) according to the manufacturer's manual (www.qiagen.com). Breifly, the desired piece of gel was cut from the agarose gel and dissolved in buffer QG. The solution was applied to the respective spin columns, washed with buffer PE and eluted in 30 µl water by centrifugation (17 900 x *g*/13 000 rpm, 2 min, 4 °C). DNA fragments and linearized vectors were stored at -20 °C.

5.2.2 Strains and growth conditions

All strains constructed in this study are summarized in the appendix (**Table S5**). In *B. subtilis*, an *flhG-yfp* fusion is expressed from the original genetic locus with a xylose inducible promotor controlling the downstream genes. For co-localization studies, a strain expressing *fliM-cfp* from the ectopic *amyE* locus (the plasmid was a kind gift of Daniel B. Kearns) was transformed with chromosomal DNA of the *flhG-yfp* strain. Functionality of *fliM-cfp* fusion has been demonstrated previously (71). The functionality of FlhG was verified intrinsically by co-expression with *fliM-cfp*, because defective FlhG immediately would have led to aberrant FliM foci, which were not observed (71). *E. coli* strains DH5α and BL21 (DE3) as well as *B. subtilis* PY79 were routinely grown in LB medium at 37 °C and 30 °C.

When required, media were supplemented with 100 µg ml^{-1} ampicillin, 50 µg ml^{-1} kanamycin, and/or 10 % (w/v) sucrose.

5.2.3 Protein production and purification

For gene expression, *E. coli* BL21 (DE3) were grown in LB broth in the presence of the respective resistance marker (kanamycin (50 µg/ml) or ampicillin (100 µg/ml)). Large-scale protein production was routinely performed under auto-induction conditions, by adding D(+)-lactose-monohydrate (1.75 % (w/v)) to the medium and by incubating the culture at 30 °C for ~16 h under constant shaking (150 rpm). For induction with IPTG, cells were grown to an optical density (OD_{600}) of approximately 0.8 prior to addition of 1 mM IPTG, except stated for the individual experiment. The cells were incubated 2-3 h after induction at 37 °C under constant shaking (150 rpm). The cells were harvested by centrifugation (3500 x *g*/4000 rpm, 20 min, 4 °C), suspended in lysis buffer and subsequently lysed using the M-110L Microfluidizer.

After centrifugation (63 000 x *g*/23 000 rpm, 20 min, 4 °C) the clarified lysate was applied onto a 1 ml HisTrap FF column equilibrated with 10 column volumes (CV) of lysis buffer. After washing with 50 ml lysis buffer, proteins were eluted using 15 ml Ni-NTA elution buffer. Protein-containing elution fractions were concentrated using Amicon Ultra-15 centrifugal filter units and subsequently applied to SEC, equilibrated with SEC buffer. Fractions were analysed using SDS-PAGE. Protein-containing fractions were pooled and concentrated up to a concentration fitting the experimental requirements. The concentration was determined by spectrophotometer. FliM and FliY were co-expressed and co-purified via a hexa-histidine tag at the C-terminus of FliM. A trimeric complex containing FliM, FliY and FlhG was co-purified using two histidine tags at the C-terminus of FliM and the N-terminus of FlhG.

5.2.3.1 SDS-PAGE

Sodium dodecyl sulphate polyacrylamide gel electrophoresis (SDS-PAGE) was carried out with self-prepared 12.5 % and 15 % polyacrylamide gels. The gels

were casted using the Mini-PROTEAN 3 Multi-Casting Chamber (Biorad) and stored at 4°C. Electrophoresis was performed in a Mini-PROTEAN® Tetra Cell with 240-260 V for 30-40 min. Further equipment for SDS-PAGE was supplied by Biorad and Neolab (power supply). After electrophoresis, the gels were stained with Coomassie Brilliant Blue R-250. A mixture of H_2O (60 % (v/v)), ethanol (30 % (v/v)) and acetic acid (10 % (v/v)) served as destaining solution.

5.2.4 Protein crystallization

All crystallization experiments were carried out by the sitting-drop method at room temperature using the JCSG core suite. The reservoir volume was 50 µl and the drop volume was 1 µl, with a 1:1 mixture of protein and crystallization solution. Crystals of apo-*Gt*FlhG were obtained from an 11.0 mg/ml solution after ~ 3 weeks in 0.1 M HEPES pH 7.5, 10 % (w/v) PEG 8000, 0.1 M urea. Crystals of *Gt*FlhG D60A were obtained from a 12.0 mg/ml solution after ~ 3 weeks in a buffer containing 0.1 M HEPES pH 7.0, 20 % (w/v) PEG 6000. Prior to crystallization, *Gt*FlhG D60A was incubated with 4.4 mM ATP for 1 h on ice.

5.2.5 Data collection, structure determination and analysis

Prior to data collection, crystals were flash-frozen in liquid nitrogen after a short incubation in a cryo-protecting solution that consisted of mother-liquor supplemented with 20 % (v/v) glycerol. Data collection was performed at the ESRF in Grenoble, France under cryogenic conditions beamlines: ID23-2 (*Gt*FlhG) and ID 23-1 (dimeric state of *Gt*FlhG D60A). Data were recorded with a DECTRIS PILATUS 6M detector and processed using iMosflm (205) as well as the CCP4-implemented program SCALA (206). The structures were solved by MR with CCP4-integrated PHASER (207), built in COOT (208) and refined using PHENIX refine (209). Figures containing crystal structures or superimpositions of crystal structures were designed with PyMol (www.pymol.org).

5.2.6 Implementation of hydrogen deuterium exchange mass spectrometry (HDX)

The column equipment (guard columns, frits, precolumn filters) was purchased from Postnova analytics GmbH. POROS® R1, 10 µm Self Pack® Media (Applied Biosystems) served as resin for the trap column. Pepsin was immobilized on POROS® AL, 20 µm Self Pack® Media (Applied Biosystems) using the amino group of lysine residues, which form a Schiff base with free aldehyde moieties of the resin. Roche and Sigma Aldrich supplied pepsin and sodium cyanoborohydride, respectively.

5.2.6.1 preparation of the pepsin column

In a first step, 160 mg pepsin (Roche) was dissolved in 50mM sodium citrate (pH 4.4). Subsequently, 0.5 g POROS® AL, 20 µm was added and 5 times inverted, which leads to the formation of the Schiff base between resin and pepsin. Afterwards, two dry crumbs (3 mm diameter) of sodium cyanoborohydride (Sigma Aldrich), were added. Adding 100 µl of 2 M sodium sulphate every 3 min over a time period of 2 h (4 ml in total) results in salting out of pepsin on the resin surface increasing the local concentration and the immobilization efficiency. The mixture was incubated over night at 4 °C and inverted from time to time. The next after addition of 160 µl of 2 M TRIS (pH 7.6) buffer the mixture was again incubated at 4 °C for 2-4 h and inverted now and then. Finally the mixture was washed 7 times with 0.1 % formic acid and subsequent centrifugation at 50 x g/ 700 rpm, for 3 min at 4 °C. The ready prepared pepsin resin is stored in 0.1 % formic acid and 0.05 % sodium azide at 4 °C. The column was prepared according to the manufacturer's instructions using the guard column kit (Postnova analytics GmbH).

5.2.7 HDX measurements

Hydrogen deuterium exchange experiments were performed as described earlier (211, 281, 282). 200 pmol purified and concentrated *Gt*FlhG, *Gt*FliY as well as

the complexes *Gt*FlhG/FliY, *Gt*FliM/FliY and *Gt*FliM/FliY/FlhG (50 µM) were diluted 10-fold into D_2O-containing SEC buffer and incubated at 37 °C to allow $^1H/^2H$ exchange (50 µl in total). The reaction was subsequently quenched after a certain incubation time (30 or 60 s) by decreasing the temperature to 0 °C and adding 1 equivalent (50 µl) of chilled Quench buffer. The samples were immediately injected onto HPLC. Peptic peptides from the on-line digest were directly analysed by mass spectrometry and the deuterium content was calculated using HDX workbench (239). Relative deuterium incorporation was calculated based on the centroids of the molecular ion isotope distribution extracted from the software. For adjustment, the 0 % control was treated with H_2O buffer. Complete exchange was defined as 95 % of to the possible incorporation and applied to all samples, due to dilution and re-exchange during the HPLC run.

HDX measurements of flagellin/FliS, FliW and flagellin/FliS/FliW were performed by Florian Altegoer according to the described protocol under my supervision. Wieland Steinchen performed HDX measurements of *Bs*SAS1 in different nucleotide loaded states according to the described protocol under my supervision.

5.2.8 Glutathione-S-transferase (GST) binding assays

GST Pull down assays were performed in either PBS buffer at 4 °C or in SEC buffer at room temperature. 0.7 or 1 nmol of purified GST-protein was immobilized on 15 µl Glutathione Sepharose 4B in small filter columns by incubation on a wheel for 15 min. 2 equivalents (1.4 or 2 nmol) of putative binding partners and 2.5 mM of appropriate nucleotides were added and incubated for 10 min at the respective temperature on the wheel, except if stated differently in the experiment. After centrifugation (3500 x *g*/4000 rpm, 1 min, 4 °C), the column was washed 3 times with PBS buffer. Proteins were eluted with 40 µl of GSH elution buffer and analysed by Coomassie-stained SDS-PAGE.

5.2.9 Ni-NTA affinity binding assays

FlhG variants were investigated for their ability to bind FliM/FliY by Ni-NTA affinity Pull down assays from expression cultures. 100 ml expression culture of hexa-histidine tagged FlhG variants and untagged FliM/FliY coexpression were mixed, harvested and lysed as stated (see: 5.2.3 Protein production and purification). 300 µl of Ni-NTA agarose (Qiagen) was added to the clarified lysate and incubated for 15 min on ice. After centrifugation (3500 x *g*/4000 rpm, 15 min, 4 °C) the lysate was discarded and the loaded Ni-NTA agarose was washed 3 times with 500 µl lysis buffer and subsequently centrifuged (3500 x *g*/4000 rpm, 5 min, 4 °C). Proteins were eluted with 300 µl Ni-NTA elution buffer and analysed by Coomassie-stained SDS-PAGE.

5.2.10 Fluorescence microscopy

B. subtilis cells were cultivated in LB broth at 37° C to exponential growth phase (OD_{600} 0.5) and immobilized on coverslips by S750 medium containing agarose pads (1 % w/v). To prepare agarose-pads for fluorescence microscopy, PBS was solidified by adding 1 % (w/v) agarose. *B. subtilis* strains were plated onto LB-agar plates containing 0.5 % xylose and the respective antibiotics. Fluorescence microscopy was performed on a fully automated Leica SP 8 laser scanning microscope equipped with a 100X HCX PL APO STED Objective (NA 1.4), an argon ion laser source and Leica HyD detectors. The images were analysed using the Huygens (Scientific Volume Imaging) and LAS AF (Leica) software.

5.2.11 Hydrolysis assays

ATP hydrolysis was investigated using an HPLC-based assay. FlhG and its D60A variant were diluted to 20 µM (1 nmol) and supplemented with 2 mM ATP (100 nmol) and 25 µl of *E. coli* lipid vesicles. Hydrolysis assays were performed in SEC buffer at 37 °C with an incubation time of 1 h. Subsequent flash freezing in liquid nitrogen stopped the hydrolysis reaction. HPLC measurements were performed with an Agilent 1100 Series HPLC system and a C18 column (Macherey-Nagel). The samples were injected onto HPLC and run for 30 min with a buffer

containing 50 mM KH_2PO_4, 50 mM K_2HPO_4, 10 mM tetrapentylammonium bromide (TPAB) and 15 % (v/v) acetonitrile at 0.8 ml/min flow rate. ADP and ATP were detected by UV light at 260.8 nm and quantified (by peak area) using ChemStation (version: B.04.03; Agilent technologies).

5.2.12 Flotation assays

5.2.12.1 Preparation of large unilamellar vesicles (LUVs)

2-oleoyl-1-palmitoyl-*sn*-glycero-3-phosphoethanolamine (PE) and (1-palmitoyl-2-oleoyl-*sn*-glycero-3-phospho-(1'-rac-glycerol) (sodium salt) (PG) were supplied by Avanti Polar Lipids. Lipids were mixed in a ratio of 70 % PE and 30 % PG and the chloroform was evaporated under reduced pressure for 30 min. LUVs were prepared in flotation assay buffer by extrusion technique (283). After 10 freeze-thaw cycles, lipids were passed 21 times through a 100 nm pore polycarbonate filter (Nucleopore) in a two syringe extruder (Avanti Polar Lipids), resulting large unilamellar vesicles (LUVs).

5.2.12.2 Gradient ultra-centrifugation

SEC purified proteins were mixed with 50 µl of LUV solution and incubated for 20 min. Flotation gradient centrifugation was performed as described previously (284). OptiPrep™ Density Gradient Medium containing 60 % iodixanol was purchased from Sigma Aldrich. Samples were mixed with 360 µl assay buffer containing 50 % iodixanol, overlaid with 1.16 ml of assay buffer with 30 % iodixanol and finally overlaid by 450 µl assay buffer. After ultra-centrifugation for 3 h at 217 000 x *g*/ 45 000 rpm in a swing-out rotor (MLS 50, Beckmann Coulter), the gradient was collected in three fractions (600 µl top, 800 µl middle, 600 µl bottom) and analysed by SDS-PAGE after TCA precipitation. Briefly, the separated fractions were treated with 100 µl trichloroacetic acid (TCA) and incubated overnight at -20 °C. After centrifugation for 20 min with 16 200 x *g*/13 000 rpm at 4 °C, the pellets were washed with chilled acetone (500 µl) twice. Prior to SDS-PAGE analysis, the remaining acetone was evaporated (2 min at 95 °C).

Bibliography

1. Berg HC & Anderson RA (1973) Bacteria swim by rotating their flagellar filaments. *Nature* 245(5425):380-382.

2. Nishihara T & Freese E (1975) Motility of *Bacillus subtilis* during growth and sporulation. *J Bacteriol* 123(1):366-371.

3. Kearns DB & Losick R (2003) Swarming motility in undomesticated *Bacillus subtilis*. *Mol Microbiol* 49(3):581-590.

4. Kearns DB (2010) A field guide to bacterial swarming motility. *Nat Rev Microbiol* 8(9):634-644.

5. McCarter LL (2004) Dual flagellar systems enable motility under different circumstances. *J Mol Microbiol Biotechnol* 7(1-2):18-29.

6. Charon NW*, et al.* (2012) The unique paradigm of *spirochete* motility and chemotaxis. *Annu Rev Microbiol* 66:349-370.

7. Burrows LL (2012) *Pseudomonas aeruginosa* twitching motility: type IV pili in action. *Annu Rev Microbiol* 66:493-520.

8. Mattick JS (2002) Type IV pili and twitching motility. *Annu Rev Microbiol* 56:289-314.

9. Pelicic V (2008) Type IV pili: e pluribus unum? *Mol Microbiol* 68(4):827-837.

10. Burrows LL (2005) Weapons of mass retraction. *Mol Microbiol* 57(4):878-888.

11. Nan B & Zusman DR (2011) Uncovering the mystery of gliding motility in the myxobacteria. *Annu Rev Genet* 45:21-39.

12. Miyata M (2010) Unique centipede mechanism of *Mycoplasma* gliding. *Annu Rev Microbiol* 64:519-537.

13. Kaiser D & Crosby C (1983) Cell movement and its coordination in swarms of *Myxococcus xanthus*. *Cell Motility* 3(3):227-245.

14. Jarrell KF & Albers SV (2012) The archaellum: an old motility structure with a new name. *Trends Microbiol* 20(7):307-312.

15. Shahapure R, Driessen RP, Haurat MF, Albers SV, & Dame RT (2014) The archaellum: a rotating type IV pilus. *Mol Microbiol* 91(4):716-723.

16. Schuhmacher JS, Thormann KM, & Bange G (2015) How bacteria maintain location and number of flagella? *FEMS Microbiol Rev*.

17. Chevance FF & Hughes KT (2008) Coordinating assembly of a bacterial macromolecular machine. *Nat Rev Microbiol* 6(6):455-465.

18. Erhardt M, Namba K, & Hughes KT (2010) Bacterial nanomachines: the flagellum and type III injectisome. *Cold Spring Harb Perspect Biol* 2(11):a000299.

19. Altegoer F, Schuhmacher J, Pausch P, & Bange G (2014) From molecular evolution to biobricks and synthetic modules: a lesson by the bacterial flagellum. *Biotechnol Genet Eng Rev* 30:49-64.

20. Apel D & Surette MG (2008) Bringing order to a complex molecular machine: the assembly of the bacterial flagella. *Biochim Biophys Acta* 1778(9):1851-1858.

21. Doetsch RN & Sjoblad RD (1980) Flagellar structure and function in eubacteria. *Annu Rev Microbiol* 34:69-108.

22. Neidhardt FC*, et al.* (1987) *Escherichia coli and Salmonella typhimurium. Cellular and molecular biology. Volumes I and II* (American Society for Microbiology).

23. Li N, Kojima S, & Homma M (2011) Sodium-driven motor of the polar flagellum in marine bacteria *Vibrio*. *Genes Cells* 16(10):985-999.

24. Bange G*, et al.* (2010) FlhA provides the adaptor for coordinated delivery of late flagella building blocks to the type III secretion system. *Proc Natl Acad Sci USA* 107(25):11295-11300.

25. Minamino T, Imada K, & Namba K (2008) Mechanisms of type III protein export for bacterial flagellar assembly. *Mol Biosyst* 4(11):1105-1115.

26. Suzuki H, Yonekura K, & Namba K (2004) Structure of the rotor of the bacterial flagellar motor revealed by electron cryomicroscopy and single-particle image analysis. *J Mol Biol* 337(1):105-113.

27. Francis NR, Irikura VM, Yamaguchi S, DeRosier DJ, & Macnab RM (1992) Localization of the *Salmonella typhimurium* flagellar switch protein FliG to the cytoplasmic M-ring face of the basal body. *Proc Natl Acad Sci U S A* 89(14):6304-6308.

28. Sourjik V & Armitage JP (2010) Spatial organization in bacterial chemotaxis. *EMBO J* 29(16):2724-2733.

29. Sourjik V & Wingreen NS (2012) Responding to chemical gradients: bacterial chemotaxis. *Curr Opin Cell Biol* 24(2):262-268.

30. Lee LK, Ginsburg MA, Crovace C, Donohoe M, & Stock D (2010) Structure of the torque ring of the flagellar motor and the molecular basis for rotational switching. *Nature* 466(7309):996-1000.

31. Sircar R*, et al.* (2015) Assembly states of FliM and FliG within the flagellar switch complex. *J Mol Biol* 427(4):867-886.

32. Yonekura K, Maki-Yonekura S, & Homma M (2011) Structure of the flagellar motor protein complex PomAB: implications for the torque-generating conformation. *J Bacteriol* 193(15):3863-3870.

33. Bubendorfer S*, et al.* (2012) Specificity of motor components in the dual flagellar system of *Shewanella putrefaciens* CN-32. *Mol Microbiol* 83(2):335-350.

34. Minamino T, Imada K, & Namba K (2008) Molecular motors of the bacterial flagella. *Curr Opin Struct Biol* 18(6):693-701.

35. Zhou J, Lloyd SA, & Blair DF (1998) Electrostatic interactions between rotor and stator in the bacterial flagellar motor. *Proc Natl Acad Sci U S A* 95(11):6436-6441.

36. Yonekura K, Maki-Yonekura S, & Namba K (2003) Complete atomic model of the bacterial flagellar filament by electron cryomicroscopy. *Nature* 424(6949):643-650.

37. Vonderviszt F*, et al.* (1998) Mechanism of self-association and filament capping by flagellar HAP2. *J Mol Biol* 284(5):1399-1416.

38. Maki S, Vonderviszt F, Furukawa Y, Imada K, & Namba K (1998) Plugging interactions of HAP2 pentamer into the distal end of flagellar filament revealed by electron microscopy. *J Mol Biol* 277(4):771-777.

39. Hess JF, Oosawa K, Kaplan N, & Simon MI (1988) Phosphorylation of three proteins in the signaling pathway of bacterial chemotaxis. *Cell* 53(1):79-87.

40. Kihara M, Miller GU, & Macnab RM (2000) Deletion analysis of the flagellar switch protein FliG of *Salmonella*. *J Bacteriol* 182(11):3022-3028.

41. Marykwas DL, Schmidt SA, & Berg HC (1996) Interacting components of the flagellar motor of *Escherichia coli* revealed by the two-hybrid system in yeast. *J Mol Biol* 256(3):564-576.

42. Francis NR, Sosinsky GE, Thomas D, & DeRosier DJ (1994) Isolation, characterization and structure of bacterial flagellar motors containing the switch complex. *J Mol Biol* 235(4):1261-1270.

43. Tang H, Braun TF, & Blair DF (1996) Motility protein complexes in the bacterial flagellar motor. *J Mol Biol* 261(2):209-221.

44. Grünenfelder B, Gehrig S, & Jenal U (2003) Role of the cytoplasmic C terminus of the FliF motor protein in flagellar assembly and rotation. *J Bacteriol* 185(5):1624-1633.

45. Brown PN, Terrazas M, Paul K, & Blair DF (2007) Mutational analysis of the flagellar protein FliG: sites of interaction with FliM and implications for organization of the switch complex. *J Bacteriol* 189(2):305-312.

46. Passmore SE, Meas R, & Marykwas DL (2008) Analysis of the FliM/FliG motor protein interaction by two-hybrid mutation suppression analysis. *Microbiology* 154(Pt 3):714-724.

47. Brown PN, Hill CP, & Blair DF (2002) Crystal structure of the middle and C-terminal domains of the flagellar rotor protein FliG. *EMBO J* 21(13):3225-3234.

48. Lloyd SA & Blair DF (1997) Charged residues of the rotor protein FliG essential for torque generation in the flagellar motor of *Escherichia coli*. *J Mol Biol* 266(4):733-744.

49. Thomas DR, Francis NR, Xu C, & DeRosier DJ (2006) The three-dimensional structure of the flagellar rotor from a clockwise-locked mutant of *Salmonella enterica* serovar Typhimurium. *J Bacteriol* 188(20):7039-7048.

50. Lam KH*, et al.* (2012) Multiple conformations of the FliG C-terminal domain provide insight into flagellar motor switching. *Structure* 20(2):315-325.

51. Park SY, Lowder B, Bilwes AM, Blair DF, & Crane BR (2006) Structure of FliM provides insight into assembly of the switch complex in the bacterial flagella motor. *Proc Natl Acad Sci U S A* 103(32):11886-11891.

52. Paul K & Blair DF (2006) Organization of FliN subunits in the flagellar motor of *Escherichia coli*. *J Bacteriol* 188(7):2502-2511.

53. Paul K, Harmon JG, & Blair DF (2006) Mutational analysis of the flagellar rotor protein FliN: identification of surfaces important for flagellar assembly and switching. *J Bacteriol* 188(14):5240-5248.

54. Brown PN, Mathews MA, Joss LA, Hill CP, & Blair DF (2005) Crystal structure of the flagellar rotor protein FliN from *Thermotoga maritima*. *J Bacteriol* 187(8):2890-2902.

55. Sarkar MK, Paul K, & Blair D (2010) Chemotaxis signaling protein CheY binds to the rotor protein FliN to control the direction of flagellar rotation in *Escherichia coli*. *Proc Natl Acad Sci USA* 107(20):9370-9375.

56. Paul K, Gonzalez-Bonet G, Bilwes AM, Crane BR, & Blair D (2011) Architecture of the flagellar rotor. *EMBO J* 30(14):2962-2971.

57. Minamino T*, et al.* (2009) Roles of the extreme N-terminal region of FliH for efficient localization of the FliH-FliI complex to the bacterial flagellar type III export apparatus. *Mol Microbiol* 74(6):1471-1483.

58. González-Pedrajo B, Minamino T, Kihara M, & Namba K (2006) Interactions between C ring proteins and export apparatus components: a possible mechanism for facilitating type III protein export. *Mol Microbiol* 60(4):984-998.

59. McMurry JL, Murphy JW, & González-Pedrajo B (2006) The FliN-FliH interaction mediates localization of flagellar export ATPase FliI to the C ring complex. *Biochemistry* 45(39):11790-11798.

60. Minamino T & MacNab RM (2000) FliH, a soluble component of the type III flagellar export apparatus of *Salmonella*, forms a complex with FliI and inhibits its ATPase activity. *Mol Microbiol* 37(6):1494-1503.

61. Minamino T, González-Pedrajo B, Oosawa K, Namba K, & Macnab RM (2002) Structural properties of FliH, an ATPase regulatory component of the *Salmonella* type III flagellar export apparatus. *J Mol Biol* 322(2):281-290.

62. Minamino T, González-Pedrajo B, Kihara M, Namba K, & Macnab RM (2003) The ATPase FliI can interact with the type III flagellar protein export apparatus in the absence of its regulator, FliH. *J Bacteriol* 185(13):3983-3988.

63. Notti RQ, Bhattacharya S, Lilic M, & Stebbins CE (2015) A common assembly module in injectisome and flagellar type III secretion sorting platforms. *Nat Commun* 6:7125.

64. van Amsterdam K & van der Ende A (2004) *Helicobacter pylori* HP1034 (*ylxH*) is required for motility. *Helicobacter* 9(5):387-395.

65. Dasgupta N*, et al.* (2003) A four-tiered transcriptional regulatory circuit controls flagellar biogenesis in *Pseudomonas aeruginosa*. *Mol Microbiol* 50(3):809-824.

66. Syed KA*, et al.* (2009) The *Vibrio cholerae* flagellar regulatory hierarchy controls expression of virulence factors. *J Bacteriol* 191(21):6555-6570.

67. Wilhelms M, Molero R, Shaw JG, Tomas JM, & Merino S (2011) Transcriptional hierarchy of *Aeromonas hydrophila* polar-flagellum genes. *J Bacteriol* 193(19):5179-5190.

68. Kearns DB & Losick R (2005) Cell population heterogeneity during growth of *Bacillus subtilis*. *Genes Dev* 19(24):3083-3094.

69. Helmann JD, Marquez LM, & Chamberlin MJ (1988) Cloning, sequencing, and disruption of the *Bacillus subtilis* σ^{28} gene. *J Bacteriol* 170(4):1568-1574.

70. Marquez LM*, et al.* (1990) Studies of σ^{D}-dependent functions in *Bacillus subtilis*. *J Bacteriol* 172(6):3435-3443.

71. Guttenplan SB, Shaw S, & Kearns DB (2013) The cell biology of peritrichous flagella in *Bacillus subtilis*. *Mol Microbiol* 87(1):211-229.

72. Senesi S*, et al.* (2004) Surface-associated flagellum formation and swarming differentiation in *Bacillus subtilis* are controlled by the *ifm* locus. *J Bacteriol* 186(4):1158-1164.

73. Albertini AM, Caramori T, Crabb WD, Scoffone F, & Galizzi A (1991) The *flaA* locus of *Bacillus subtilis* is part of a large operon coding for flagellar structures, motility functions, and an ATPase-like polypeptide. *J Bacteriol* 173(11):3573-3579.

74. Marquez-Magana LM & Chamberlin MJ (1994) Characterization of the *sigD* transcription unit of *Bacillus subtilis*. *J Bacteriol* 176(8):2427-2434.

75. Werhane H*, et al.* (2004) The last gene of the *fla/che* operon in *Bacillus subtilis*, *ylxL*, is required for maximal s^D function. *J Bacteriol* 186(12):4025-4029.

76. Chai Y, Norman T, Kolter R, & Losick R (2010) An epigenetic switch governing daughter cell separation in *Bacillus subtilis*. *Genes Dev* 24(8):754-765.

77. Cozy LM*, et al.* (2012) SlrA/SinR/SlrR inhibits motility gene expression upstream of a hypersensitive and hysteretic switch at the level of s^D in *Bacillus subtilis*. *Mol Microbiol* 83(6):1210-1228.

78. Newman JA, Rodrigues C, & Lewis RJ (2013) Molecular basis of the activity of SinR protein, the master regulator of biofilm formation in *Bacillus subtilis*. *J Biol Chem* 288(15):10766-10778.

79. Bertero MG, Gonzales B, Tarricone C, Ceciliani F, & Galizzi A (1999) Overproduction and characterization of the *Bacillus subtilis* anti-s factor FlgM. *J Biol Chem* 274(17):12103-12107.

80. Caramori T, Barilla D, Nessi C, Sacchi L, & Galizzi A (1996) Role of FlgM in s^D-dependent gene expression in *Bacillus subtilis*. *J Bacteriol* 178(11):3113-3118.

81. Sorenson MK, Ray SS, & Darst SA (2004) Crystal structure of the flagellar s/anti-s complex s^{28}/FlgM reveals an intact s factor in an inactive conformation. *Mol Cell* 14(1):127-138.

82. Mukherjee S & Kearns DB (2014) The Structure and Regulation of Flagella in *Bacillus subtilis*. *Annu Rev Genet*.

83. Leifson E (1960) Atlas of bacterial flagellation. *Atlas of bacterial flagellation.*

84. Kusumoto A*, et al.* (2006) Regulation of polar flagellar number by the *flhF* and *flhG* genes in *Vibrio alginolyticus*. *J Biochem* 139(1):113-121.

85. Campos-Garcia J, Najera R, Camarena L, & Soberon-Chavez G (2000) The *Pseudomonas aeruginosa motR* gene involved in regulation of bacterial motility. *FEMS Microbiol Lett* 184(1):57-62.

86. Dasgupta N, Arora SK, & Ramphal R (2000) *fleN*, a gene that regulates flagellar number in *Pseudomonas aeruginosa*. *J Bacteriol* 182(2):357-364.

87. Huitema E, Pritchard S, Matteson D, Radhakrishnan SK, & Viollier PH (2006) Bacterial birth scar proteins mark future flagellum assembly site. *Cell* 124(5):1025-1037.

88. Balaban M & Hendrixson DR (2011) Polar flagellar biosynthesis and a regulator of flagellar number influence spatial parameters of cell division in *Campylobacter jejuni*. *PLoS Pathog* 7(12):e1002420.

89. Aizawa SI & Kubori T (1998) Bacterial flagellation and cell division. *Genes Cells* 3(10):625-634.

90. Ping L (2010) The asymmetric flagellar distribution and motility of *Escherichia coli*. *J Mol Biol* 397(4):906-916.

91. Gonzalez-Pedrajo B*, et al.* (1997) Structural and genetic analysis of a mutant of *Rhodobacter sphaeroides* WS8 deficient in hook length control. *J Bacteriol* 179(21):6581-6588.

92. Kim YK & McCarter LL (2000) Analysis of the polar flagellar gene system of *Vibrio parahaemolyticus*. *J Bacteriol* 182(13):3693-3704.

93. Stewart BJ & McCarter LL (2003) Lateral flagellar gene system of *Vibrio parahaemolyticus*. *J Bacteriol* 185(15):4508-4518.

94. Altarriba M*, et al.* (2003) A polar flagella operon (*flg*) of *Aeromonas hydrophila* contains genes required for lateral flagella expression. *Microb Pathog* 34(5):249-259.

95. Canals R*, et al.* (2006) Analysis of the lateral flagellar gene system of *Aeromonas hydrophila* AH-3. *J Bacteriol* 188(3):852-862.

96. Kawagishi I, Maekawa Y, Atsumi T, Homma M, & Imae Y (1995) Isolation of the polar and lateral flagellum-defective mutants in *Vibrio alginolyticus* and identification of their flagellar driving energy sources. *J Bacteriol* 177(17):5158-5160.

97. Shinoda S & Okamoto K (1977) Formation and function of *Vibrio parahaemolyticus* lateral flagella. *J Bacteriol* 129(3):1266-1271.

98. Shimada T, Sakazaki R, & Suzuki K (1985) Peritrichous flagella in mesophilic strains of *Aeromonas*. *Jpn J Med Sci Biol* 38(3):141-145.

99. Tarrand JJ, Krieg NR, & Dobereiner J (1978) A taxonomic study of the Spirillum lipoferum group, with descriptions of a new genus, *Azospirillum* gen. nov. and two species, *Azospirillum lipoferum* (Beijerinck) comb. nov. and *Azospirillum brasilense* sp. nov. *Can J Microbiol* 24(8):967-980.

100. McClain J, Rollo DR, Rushing BG, & Bauer CE (2002) *Rhodospirillum centenum* utilizes separate motor and switch components to control lateral and polar flagellum rotation. *J Bacteriol* 184(9):2429-2438.

101. Merino S, Shaw JG, & Tomas JM (2006) Bacterial lateral flagella: an inducible flagella system. *FEMS Microbiol Lett* 263(2):127-135.

102. Bubendorfer S, Koltai M, Rossmann F, Sourjik V, & Thormann KM (2014) Secondary bacterial flagellar system improves bacterial spreading by increasing the directional persistence of swimming. *Proc Natl Acad Sci USA* 111(31):11485-11490.

103. Schuhmacher JS*, et al.* (2015) MinD-like ATPase FlhG effects location and number of bacterial flagella during C-ring assembly. *Proc Natl Acad Sci USA* 112(10):3092-3097.

104. Sogaard-Andersen L (2013) Stably bridging a great divide: localization of the SpoIIQ landmark protein in *Bacillus subtilis*. *Mol Microbiol* 89(6):1019-1024.

105. Lam H, Schofield WB, & Jacobs-Wagner C (2006) A landmark protein essential for establishing and perpetuating the polarity of a bacterial cell. *Cell* 124(5):1011-1023.

106. Ebersbach G, Briegel A, Jensen GJ, & Jacobs-Wagner C (2008) A self-associating protein critical for chromosome attachment, division, and polar organization in *Caulobacter*. *Cell* 134(6):956-968.

107. Tsokos CG & Laub MT (2012) Polarity and cell fate asymmetry in *Caulobacter crescentus*. *Curr Opin Microbiol* 15(6):744-750.

108. Kirkpatrick CL & Viollier PH (2012) Cell polarity: ParA-logs gather around the Hub. *Curr Biol* 22(24):R1055-1057.

109. Davis BM & Waldor MK (2013) Establishing polar identity in gram-negative rods. *Curr Opin Microbiol* 16(6):752-759.

110. Obuchowski PL & Jacobs-Wagner C (2008) PflI, a protein involved in flagellar positioning in *Caulobacter crescentus*. *J Bacteriol* 190(5):1718-1729.

111. Lutkenhaus J (2012) The ParA/MinD family puts things in their place. *Trends Microbiol* 20(9):411-418.

112. Lutkenhaus J (2007) Assembly dynamics of the bacterial MinCDE system and spatial regulation of the Z ring. *Annu Rev Biochem* 76:539-562.

113. Margolin W (2001) Spatial regulation of cytokinesis in bacteria. *Curr Opin Microbiol* 4(6):647-652.

114. Rowlett VW & Margolin W (2013) The bacterial Min system. *Curr Biol* 23(13):R553-556.

115. Mierzejewska J & Jagura-Burdzy G (2012) Prokaryotic ParA-ParB-*parS* system links bacterial chromosome segregation with the cell cycle. *Plasmid* 67(1):1-14.

116. Reyes-Lamothe R, Nicolas E, & Sherratt DJ (2012) Chromosome replication and segregation in bacteria. *Annu Rev Genet* 46:121-143.

117. Ringgaard S*, et al.* (2014) ParP prevents dissociation of CheA from chemotactic signaling arrays and tethers them to a polar anchor. *Proc Natl Acad Sci USA* 111(2):E255-264.

118. Bange G*, et al.* (2011) Structural basis for the molecular evolution of SRP-GTPase activation by protein. *Nat Struct Mol Biol* 18(12):1376-1380.

119. Leipe DD, Wolf YI, Koonin EV, & Aravind L (2002) Classification and evolution of P-loop GTPases and related ATPases. *J Mol Biol* 317(1):41-72.

120. Bange G & Sinning I (2013) SIMIBI twins in protein targeting and localization. *Nat Struct Mol Biol* 20(7):776-780.

121. Grudnik P, Bange G, & Sinning I (2009) Protein targeting by the signal recognition particle. *Biol Chem* 390(8):775-782.

122. Akopian D, Shen K, Zhang X, & Shan SO (2013) Signal recognition particle: an essential protein-targeting machine. *Annu Rev Biochem* 82:693-721.

123. Carpenter PB, Hanlon DW, & Ordal GW (1992) *flhF*, a *Bacillus subtilis* flagellar gene that encodes a putative GTP-binding protein. *Mol Microbiol* 6(18):2705-2713.

124. Bange G, Petzold G, Wild K, Parlitz RO, & Sinning I (2007) The crystal structure of the third signal-recognition particle GTPase FlhF reveals a homodimer with bound GTP. *Proc Natl Acad Sci USA* 104(34):13621-13625.

125. Green JC*, et al.* (2009) Recruitment of the earliest component of the bacterial flagellum to the old cell division pole by a membrane-associated signal recognition particle family GTP-binding protein. *J Mol Biol* 391(4):679-690.

126. Kojima M*, et al.* (2011) Conversion of mono-polar to peritrichous flagellation in *Vibrio alginolyticus*. *Microbiol Immunol* 55(2):76-83.

127. Kitaoka M*, et al.* (2013) A novel *dnaJ* family gene, *sflA,* encodes an inhibitor of flagellation in marine *Vibrio* species. *J Bacteriol* 195(4):816-822.

128. Kusumoto A*, et al.* (2008) Collaboration of FlhF and FlhG to regulate polar-flagella number and localization in *Vibrio alginolyticus*. *Microbiology* 154(Pt 5):1390-1399.

129. Kusumoto A, Nishioka N, Kojima S, & Homma M (2009) Mutational analysis of the GTP-binding motif of FlhF which regulates the number and placement of the polar flagellum in *Vibrio alginolyticus*. *J Biochem* 146(5):643-650.

130. Jenal U & Shapiro L (1996) Cell cycle-controlled proteolysis of a flagellar motor protein that is asymmetrically distributed in the *Caulobacter* predivisional cell. *EMBO J* 15(10):2393-2406.

131. Correa NE, Peng F, & Klose KE (2005) Roles of the regulatory proteins FlhF and FlhG in the *Vibrio cholerae* flagellar transcription hierarchy. *J Bacteriol* 187(18):6324-6332.

132. Murray TS & Kazmierczak BI (2006) FlhF is required for swimming and swarming in *Pseudomonas aeruginosa*. *J Bacteriol* 188(19):6995-7004.

133. Schniederberend M, Abdurachim K, Murray TS, & Kazmierczak BI (2013) The GTPase activity of FlhF is dispensable for flagellar localization, but not motility, in *Pseudomonas aeruginosa*. *J Bacteriol* 195(5):1051-1060.

134. Pandza S*, et al.* (2000) The G-protein FlhF has a role in polar flagellar placement and general stress response induction in *Pseudomonas putida*. *Mol Microbiol* 36(2):414-423.

135. Shen Y, Chern M, Silva FG, & Ronald P (2001) Isolation of a *Xanthomonas oryzae* pv. *oryzae* flagellar operon region and molecular characterization of *flhF*. *Mol Plant Microbe Interact* 14(2):204-213.

136. Balaban M, Joslin SN, & Hendrixson DR (2009) FlhF and its GTPase activity are required for distinct processes in flagellar gene regulation and biosynthesis in *Campylobacter jejuni*. *J Bacteriol* 191(21):6602-6611.

137. Dasgupta N & Ramphal R (2001) Interaction of the antiactivator FleN with the transcriptional activator FleQ regulates flagellar number in *Pseudomonas aeruginosa*. *J Bacteriol* 183(22):6636-6644.

138. Baraquet C & Harwood CS (2013) Cyclic diguanosine monophosphate represses bacterial flagella synthesis by interacting with the Walker A motif of the enhancer-binding protein FleQ. *Proc Natl Acad Sci USA* 110(46):18478-18483.

139. Yamaichi Y*, et al.* (2012) A multidomain hub anchors the chromosome segregation and chemotactic machinery to the bacterial pole. *Genes Dev* 26(20):2348-2360.

140. Trueba FJ (1982) On the precision and accuracy achieved by *Escherichia coli* cells at fission about their middle. *Arch Microbiol* 131(1):55-59.

141. Bi EF & Lutkenhaus J (1991) FtsZ ring structure associated with division in *Escherichia coli*. *Nature* 354(6349):161-164.

142. Lutkenhaus J & Addinall SG (1997) Bacterial cell division and the Z ring. *Annu Rev Biochem* 66:93-116.

143. Weiss DS (2004) Bacterial cell division and the septal ring. *Mol Microbiol* 54(3):588-597.

144. Wu LJ & Errington J (2004) Coordination of cell division and chromosome segregation by a nucleoid occlusion protein in *Bacillus subtilis*. *Cell* 117(7):915-925.

145. Bernhardt TG & de Boer PA (2005) SlmA, a nucleoid-associated, FtsZ binding protein required for blocking septal ring assembly over Chromosomes in *E. coli*. *Mol Cell* 18(5):555-564.

146. Wu LJ*, et al.* (2009) Noc protein binds to specific DNA sequences to coordinate cell division with chromosome segregation. *EMBO J* 28(13):1940-1952.

147. Adams DW, Wu LJ, & Errington J (2014) Cell cycle regulation by the bacterial nucleoid. *Curr Opin Microbiol* 22:94-101.

148. Adams DW, Wu LJ, & Errington J (2015) Nucleoid occlusion protein Noc recruits DNA to the bacterial cell membrane. *EMBO J* 34(4):491-501.

149. Thanbichler M & Shapiro L (2006) MipZ, a spatial regulator coordinating chromosome segregation with cell division in *Caulobacter*. *Cell* 126(1):147-162.

150. Adler HI, Fisher WD, Cohen A, & Hardigree AA (1967) Miniature *Escherichia coli* cells deficient in DNA. *Proc Natl Acad Sci USA* 57(2):321-326.

151. Dajkovic A, Lan G, Sun SX, Wirtz D, & Lutkenhaus J (2008) MinC spatially controls bacterial cytokinesis by antagonizing the scaffolding function of FtsZ. *Curr Biol* 18(4):235-244.

152. Shen B & Lutkenhaus J (2010) Examination of the interaction between FtsZ and MinCN in *E. coli* suggests how MinC disrupts Z rings. *Mol Microbiol* 75(5):1285-1298.

153. Wu W, Park KT, Holyoak T, & Lutkenhaus J (2011) Determination of the structure of the MinD-ATP complex reveals the orientation of MinD on the membrane and the relative location of the binding sites for MinE and MinC. *Mol Microbiol* 79(6):1515-1528.

154. Lackner LL, Raskin DM, & de Boer PA (2003) ATP-dependent interactions between *Escherichia coli* Min proteins and the phospholipid membrane in vitro. *J Bacteriol* 185(3):735-749.

155. Shen B & Lutkenhaus J (2009) The conserved C-terminal tail of FtsZ is required for the septal localization and division inhibitory activity of MinC(C)/MinD. *Mol Microbiol* 72(2):410-424.

156. Park KT*, et al.* (2011) The Min oscillator uses MinD-dependent conformational changes in MinE to spatially regulate cytokinesis. *Cell* 146(3):396-407.

157. Park KT, Wu W, Lovell S, & Lutkenhaus J (2012) Mechanism of the asymmetric activation of the MinD ATPase by MinE. *Mol Microbiol* 85(2):271-281.

158. Raskin DM & de Boer PA (1999) Rapid pole-to-pole oscillation of a protein required for directing division to the middle of *Escherichia coli*. *Proc Natl Acad Sci USA* 96(9):4971-4976.

159. Marston AL, Thomaides HB, Edwards DH, Sharpe ME, & Errington J (1998) Polar localization of the MinD protein of *Bacillus subtilis* and its role in selection of the mid-cell division site. *Genes Dev* 12(21):3419-3430.

160. Patrick JE & Kearns DB (2008) MinJ (YvjD) is a topological determinant of cell division in *Bacillus subtilis*. *Mol Microbiol* 70(5):1166-1179.

161. Bramkamp M*, et al.* (2008) A novel component of the division-site selection system of *Bacillus subtilis* and a new mode of action for the division inhibitor MinCD. *Mol Microbiol* 70(6):1556-1569.

162. Marston AL & Errington J (1999) Selection of the midcell division site in *Bacillus subtilis* through MinD-dependent polar localization and activation of MinC. *Mol Microbiol* 33(1):84-96.

163. Szeto TH, Rowland SL, Habrukowich CL, & King GF (2003) The MinD membrane targeting sequence is a transplantable lipid-binding helix. *J Biol Chem* 278(41):40050-40056.

164. Karoui ME & Errington J (2001) Isolation and characterization of topological specificity mutants of *minD* in *Bacillus subtilis*. *Mol Microbiol* 42(5):1211-1221.

165. Porter SL, Wadhams GH, & Armitage JP (2011) Signal processing in complex chemotaxis pathways. *Nat Rev Microbiol* 9(3):153-165.

166. Wadhams GH & Armitage JP (2004) Making sense of it all: bacterial chemotaxis. *Nat Rev Mol Cell Biol* 5(12):1024-1037.

167. Amin DN & Hazelbauer GL (2010) The chemoreceptor dimer is the unit of conformational coupling and transmembrane signaling. *J Bacteriol* 192(5):1193-1200.

168. Hazelbauer GL, Falke JJ, & Parkinson JS (2008) Bacterial chemoreceptors: high-performance signaling in networked arrays. *Trends Biochem Sci* 33(1):9-19.

169. Alexander RP & Zhulin IB (2007) Evolutionary genomics reveals conserved structural determinants of signaling and adaptation in microbial chemoreceptors. *Proc Natl Acad Sci USA* 104(8):2885-2890.

170. Briegel A*, et al.* (2009) Universal architecture of bacterial chemoreceptor arrays. *Proc Natl Acad Sci USA* 106(40):17181-17186.

171. Maddock JR & Shapiro L (1993) Polar location of the chemoreceptor complex in the *Escherichia coli* cell. *Science* 259(5102):1717-1723.

172. Vladimirov N & Sourjik V (2009) Chemotaxis: how bacteria use memory. *Biol Chem* 390(11):1097-1104.

173. Hoff WD, van der Horst MA, Nudel CB, & Hellingwerf KJ (2009) Prokaryotic phototaxis. *Methods Mol Biol* 571:25-49.

174. Schweinitzer T & Josenhans C (2010) Bacterial energy taxis: a global strategy? *Arch Microbiol* 192(7):507-520.

175. Alexandre G (2010) Coupling metabolism and chemotaxis-dependent behaviours by energy taxis receptors. *Microbiology* 156(Pt 8):2283-2293.

176. Welch M, Oosawa K, Aizawa S, & Eisenbach M (1993) Phosphorylation-dependent binding of a signal molecule to the flagellar switch of bacteria. *Proc Natl Acad Sci USA* 90(19):8787-8791.

177. Dyer CM, Vartanian AS, Zhou H, & Dahlquist FW (2009) A molecular mechanism of bacterial flagellar motor switching. *J Mol Biol* 388(1):71-84.

178. Sourjik V & Berg HC (2002) Receptor sensitivity in bacterial chemotaxis. *Proc Natl Acad Sci USA* 99(1):123-127.

179. Borkovich KA & Simon MI (1990) The dynamics of protein phosphorylation in bacterial chemotaxis. *Cell* 63(6):1339-1348.

180. Rao CV & Ordal GW (2009) The molecular basis of excitation and adaptation during chemotactic sensory transduction in bacteria. *Contrib Microbiol* 16:33-64.

181. Carpenter PB, Hanlon DW, Kirsch ML, & Ordal GW (1994) Novel aspects of chemotactic sensory transduction in *Bacillus subtilis*. *Res Microbiol* 145(5-6):413-419.

182. Garrity LF & Ordal GW (1995) Chemotaxis in *Bacillus subtilis*: how bacteria monitor environmental signals. *Pharmacol Ther* 68(1):87-104.

183. Szurmant H, Bunn MW, Cannistraro VJ, & Ordal GW (2003) *Bacillus subtilis* hydrolyzes CheY-P at the location of its action, the flagellar switch. *J Biol Chem* 278(49):48611-48616.

184. Szurmant H, Muff TJ, & Ordal GW (2004) *Bacillus subtilis* CheC and FliY are members of a novel class of CheY-P-hydrolyzing proteins in the chemotactic signal transduction cascade. *J Biol Chem* 279(21):21787-21792.

185. Szurmant H & Ordal GW (2004) Diversity in chemotaxis mechanisms among the bacteria and archaea. *Microbiol Mol Biol Rev* 68(2):301-319.

186. Muff TJ, Foster RM, Liu PJ, & Ordal GW (2007) CheX in the three-phosphatase system of bacterial chemotaxis. *J Bacteriol* 189(19):7007-7013.

187. Muff TJ & Ordal GW (2008) The diverse CheC-type phosphatases: chemotaxis and beyond. *Mol Microbiol* 70(5):1054-1061.

188. Porter SL, Wadhams GH, & Armitage JP (2008) *Rhodobacter sphaeroides*: complexity in chemotactic signalling. *Trends Microbiol* 16(6):251-260.

189. Mackenzie C*, et al.* (2001) The home stretch, a first analysis of the nearly completed genome of *Rhodobacter sphaeroides* 2.4.1. *Photosynth Res* 70(1):19-41.

190. Armitage JP & Macnab RM (1987) Unidirectional, intermittent rotation of the flagellum of *Rhodobacter sphaeroides*. *J Bacteriol* 169(2):514-518.

191. Poggio S*, et al.* (2007) A complete set of flagellar genes acquired by horizontal transfer coexists with the endogenous flagellar system in *Rhodobacter sphaeroides*. *J Bacteriol* 189(8):3208-3216.

192. Garcia N*, et al.* (1998) The flagellar switch genes *fliM* and *fliN* of *Rhodobacter sphaeroides* are contained in a large flagellar gene cluster. *J Bacteriol* 180(15):3978-3982.

193. Lee SY*, et al.* (2001) Crystal structure of an activated response regulator bound to its target. *Nat Struct Biol* 8(1):52-56.

194. Dyer CM*, et al.* (2004) Structure of the constitutively active double mutant CheYD13K Y106W alone and in complex with a FliM peptide. *J Mol Biol* 342(4):1325-1335.

195. Schuhmacher JS (2012) Structure and Function of a MinD-like ATPase. Master Thesis (Heidelberg University, Heidelberg).

196. Kirkpatrick CL & Viollier PH (2011) Poles Apart: Prokaryotic Polar Organelles and Their Spatial Regulation. *Cold Spring Harbor Perspectives in Biology* 3(3).

197. Feng L*, et al.* (2007) Genome and proteome of long-chain alkane degrading *Geobacillus thermodenitrificans* NG80-2 isolated from a deep-subsurface oil reservoir. *Proc Natl Acad Sci USA* 104(13):5602-5607.

198. McPherson A (1982) *Preparation and analysis of protein crystals* (John Wiley & Sons).

199. McPherson A & Gavira JA (2014) Introduction to protein crystallization. *Acta Crystallogr F Struct Biol Commun* 70(Pt 1):2-20.

200. Deckert G*, et al.* (1998) The complete genome of the hyperthermophilic bacterium *Aquifex aeolicus*. *Nature* 392(6674):353-358.

201. Nelson KE*, et al.* (1999) Evidence for lateral gene transfer between Archaea and bacteria from genome sequence of *Thermotoga maritima*. *Nature* 399(6734):323-329.

202. Hu Z & Lutkenhaus J (2001) Topological regulation of cell division in *E. coli.* spatiotemporal oscillation of MinD requires stimulation of its ATPase by MinE and phospholipid. *Mol Cell* 7(6):1337-1343.

203. Manne V, Bekesi E, & Kung HF (1985) Ha-ras proteins exhibit GTPase activity: point mutations that activate Ha-ras gene products result in decreased GTPase activity. *Proc Natl Acad Sci USA* 82(2):376-380.

204. Mukherjee A, Dai K, & Lutkenhaus J (1993) *Escherichia coli* cell division protein FtsZ is a guanine nucleotide binding protein. *Proc Natl Acad Sci USA* 90(3):1053-1057.

205. Battye TGG, Kontogiannis L, Johnson O, Powell HR, & Leslie AGW (2011) iMOSFLM: a new graphical interface for diffraction-image processing with MOSFLM. *Acta Crystallographica Section D* 67(4):271-281.

206. Winn MD*, et al.* (2011) Overview of the CCP4 suite and current developments. *Acta Crystallographica Section D* 67(4):235-242.

207. McCoy AJ*, et al.* (2007) Phaser crystallographic software. *Journal of Applied Crystallography* 40(4):658-674.

208. Emsley P & Cowtan K (2004) Coot: model-building tools for molecular graphics. *Acta Crystallographica Section D* 60(12 Part 1):2126-2132.

209. Adams PD*, et al.* (2010) PHENIX: a comprehensive Python-based system for macromolecular structure solution. *Acta Crystallographica Section D* 66(2):213-221.

210. Shiomi D & Margolin W (2007) The C-terminal domain of MinC inhibits assembly of the Z ring in *Escherichia coli*. *J Bacteriol* 189(1):236-243.

211. Stjepanovic G*, et al.* (2011) Lipids trigger a conformational switch that regulates signal recognition particle (SRP)-mediated protein targeting. *J Biol Chem* 286(26):23489-23497.

212. Walker JE, Saraste M, Runswick MJ, & Gay NJ (1982) Distantly related sequences in the alpha- and beta-subunits of ATP synthase, myosin, kinases and other ATP-requiring enzymes and a common nucleotide binding fold. *EMBO J* 1(8):945-951.

213. Koonin EV (1993) A superfamily of ATPases with diverse functions containing either classical or deviant ATP-binding motif. *J Mol Biol* 229(4):1165-1174.

214. Ramakrishnan C, Dani VS, & Ramasarma T (2002) A conformational analysis of Walker motif A [GXXXXGKT (S)] in nucleotide-binding and other proteins. *Protein Eng* 15(10):783-798.

215. Zhao R, Pathak N, Jaffe H, Reese TS, & Khan S (1996) FliN is a major structural protein of the C-ring in the *Salmonella typhimurium* flagellar basal body. *J Mol Biol* 261(2):195-208.

216. Khan S, Zhao R, & Reese TS (1998) Architectural features of the *Salmonella typhimurium* flagellar motor switch revealed by disrupted C-rings. *J Struct Biol* 122(3):311-319.

217. Kawamoto A*, et al.* (2013) Common and distinct structural features of *Salmonella* injectisome and flagellar basal body. *Sci Rep* 3:3369.

218. Egan AJ & Vollmer W (2013) The physiology of bacterial cell division. *Ann N Y Acad Sci* 1277:8-28.

219. Adams DW & Errington J (2009) Bacterial cell division: assembly, maintenance and disassembly of the Z ring. *Nat Rev Microbiol* 7(9):642-653.

220. Tavares JR, de Souza RF, Meira GL, & Gueiros-Filho FJ (2008) Cytological characterization of YpsB, a novel component of the *Bacillus subtilis* divisome. *J Bacteriol* 190(21):7096-7107.

221. Pompeo F, Foulquier E, Serrano B, Grangeasse C, & Galinier A (2015) Phosphorylation of the cell division protein GpsB regulates PrkC kinase activity through a negative feedback loop in *Bacillus subtilis*. *Mol Microbiol*.

222. Fleurie A*, et al.* (2014) Interplay of the serine/threonine-kinase StkP and the paralogs DivIVA and GpsB in pneumococcal cell elongation and division. *PLoS Genet* 10(4):e1004275.

223. Ravikumar V*, et al.* (2014) Quantitative phosphoproteome analysis of *Bacillus subtilis* reveals novel substrates of the kinase PrkC and phosphatase PrpC. *Mol Cell Proteomics* 13(8):1965-1978.

224. Wolfe AJ & Visick KL (2008) Get the message out: cyclic-Di-GMP regulates multiple levels of flagellum-based motility. *J Bacteriol* 190(2):463-475.

225. Hengge R (2009) Principles of c-di-GMP signalling in bacteria. *Nat Rev Microbiol* 7(4):263-273.

226. Jenal U & Malone J (2006) Mechanisms of cyclic-di-GMP signaling in bacteria. *Annu Rev Genet* 40:385-407.

227. Boyd CD & O'Toole GA (2012) Second messenger regulation of biofilm formation: breakthroughs in understanding c-di-GMP effector systems. *Annu Rev Cell Dev Biol* 28:439-462.

228. Mills E, Pultz IS, Kulasekara HD, & Miller SI (2011) The bacterial second messenger c-di-GMP: mechanisms of signalling. *Cell Microbiol* 13(8):1122-1129.

229. Romling U, Galperin MY, & Gomelsky M (2013) Cyclic di-GMP: the first 25 years of a universal bacterial second messenger. *Microbiol Mol Biol Rev* 77(1):1-52.

230. Hoofnagle AN, Resing KA, & Ahn NG (2003) Protein analysis by hydrogen exchange mass spectrometry. *Annu Rev Biophys Biomol Struct* 32:1-25.

231. Eyles SJ & Kaltashov IA (2004) Methods to study protein dynamics and folding by mass spectrometry. *Methods* 34(1):88-99.

232. Garcia RA, Pantazatos D, & Villarreal FJ (2004) Hydrogen/deuterium exchange mass spectrometry for investigating protein-ligand interactions. *Assay Drug Dev Technol* 2(1):81-91.

233. Wales TE & Engen JR (2006) Hydrogen exchange mass spectrometry for the analysis of protein dynamics. *Mass Spectrom Rev* 25(1):158-170.

234. Engen JR & Smith DL (2001) Investigating protein structure and dynamics by hydrogen exchange MS. *Anal Chem* 73(9):256A-265A.

235. Dyson HJ & Wright PE (2004) Unfolded proteins and protein folding studied by NMR. *Chem Rev* 104(8):3607-3622.

236. Katta V & Chait BT (1991) Conformational changes in proteins probed by hydrogen-exchange electrospray-ionization mass spectrometry. *Rapid Commun Mass Spectrom* 5(4):214-217.

237. Lanman J*, et al.* (2003) Identification of novel interactions in HIV-1 capsid protein assembly by high-resolution mass spectrometry. *J Mol Biol* 325(4):759-772.

238. Lanman J*, et al.* (2004) Key interactions in HIV-1 maturation identified by hydrogen-deuterium exchange. *Nat Struct Mol Biol* 11(7):676-677.

239. Pascal BD*, et al.* (2012) HDX workbench: software for the analysis of H/D exchange MS data. *J Am Soc Mass Spectrom* 23(9):1512-1521.

240. Ozin AJ, Claret L, Auvray F, & Hughes C (2003) The FliS chaperone selectively binds the disordered flagellin C-terminal D0 domain central to polymerisation. *FEMS Microbiol Lett* 219(2):219-224.

241. Muskotal A*, et al.* (2006) Interaction of FliS flagellar chaperone with flagellin. *FEBS Lett* 580(16):3916-3920.

242. Auvray F, Thomas J, Fraser GM, & Hughes C (2001) Flagellin polymerisation control by a cytosolic export chaperone. *J Mol Biol* 308(2):221-229.

243. Evdokimov AG*, et al.* (2003) Similar modes of polypeptide recognition by export chaperones in flagellar biosynthesis and type III secretion. *Nat Struct Biol* 10(10):789-793.

244. Galeva A*, et al.* (2014) Bacterial flagellin-specific chaperone FliS interacts with anti-s factor FlgM. *J Bacteriol* 196(6):1215-1221.

245. Titz B, Rajagopala SV, Ester C, Hauser R, & Uetz P (2006) Novel conserved assembly factor of the bacterial flagellum. *J Bacteriol* 188(21):7700-7706.

246. Mukherjee S, Babitzke P, & Kearns DB (2013) FliW and FliS function independently to control cytoplasmic flagellin levels in *Bacillus subtilis*. *J Bacteriol* 195(2):297-306.

247. Evans LD, Poulter S, Terentjev EM, Hughes C, & Fraser GM (2013) A chain mechanism for flagellum growth. *Nature* 504(7479):287-290.

248. Kanjee U, Ogata K, & Houry WA (2012) Direct binding targets of the stringent response alarmone (p)ppGpp. *Mol Microbiol* 85(6):1029-1043.

249. Potrykus K & Cashel M (2008) (p)ppGpp: still magical? *Annu Rev Microbiol* 62:35-51.

250. Dalebroux ZD, Svensson SL, Gaynor EC, & Swanson MS (2010) ppGpp conjures bacterial virulence. *Microbiol Mol Biol Rev* 74(2):171-199.

251. Jain V, Kumar M, & Chatterji D (2006) ppGpp: stringent response and survival. *J Microbiol* 44(1):1-10.

252. Agirrezabala X*, et al.* (2013) The ribosome triggers the stringent response by RelA via a highly distorted tRNA. *EMBO Rep* 14(9):811-816.

253. Wendrich TM, Blaha G, Wilson DN, Marahiel MA, & Nierhaus KH (2002) Dissection of the mechanism for the stringent factor RelA. *Mol Cell* 10(4):779-788.

254. English BP*, et al.* (2011) Single-molecule investigations of the stringent response machinery in living bacterial cells. *Proc Natl Acad Sci USA* 108(31):E365-373.

255. Hogg T, Mechold U, Malke H, Cashel M, & Hilgenfeld R (2004) Conformational antagonism between opposing active sites in a bifunctional RelA/SpoT homolog modulates (p)ppGpp metabolism during the stringent response [corrected]. *Cell* 117(1):57-68.

256. Mechold U, Potrykus K, Murphy H, Murakami KS, & Cashel M (2013) Differential regulation by ppGpp versus pppGpp in *Escherichia coli*. *Nucleic Acids Res* 41(12):6175-6189.

257. Geiger T, Kästle B, Gratani FL, Goerke C, & Wolz C (2014) Two small (p)ppGpp synthases in *Staphylococcus aureus* mediate tolerance against cell envelope stress conditions. *J Bacteriol* 196(4):894-902.

258. Nanamiya H*, et al.* (2008) Identification and functional analysis of novel (p)ppGpp synthetase genes in *Bacillus subtilis*. *Mol Microbiol* 67(2):291-304.

259. Lemos JA, Lin VK, Nascimento MM, Abranches J, & Burne RA (2007) Three gene products govern (p)ppGpp production by *Streptococcus mutans*. *Mol Microbiol* 65(6):1568-1581.

260. Srivatsan A*, et al.* (2008) High-precision, whole-genome sequencing of laboratory strains facilitates genetic studies. *PLoS Genet* 4(8):e1000139.

261. Sprang SR (1997) G protein mechanisms: insights from structural analysis. *Annu Rev Biochem* 66:639-678.

262. Temeles GL, Gibbs JB, D'Alonzo JS, Sigal IS, & Scolnick EM (1985) Yeast and mammalian ras proteins have conserved biochemical properties. *Nature* 313(6004):700-703.

263. Kalbitzer HR, Goody RS, & Wittinghofer A (1984) Electron-paramagnetic-resonance studies of manganese(II) complexes with elongation factor Tu from *Bacillus stearothermophilus*. Observation of a GTP hydrolysis intermediate state complex. *Eur J Biochem* 141(3):591-597.

264. Gilman AG (1987) G proteins: transducers of receptor-generated signals. *Annu Rev Biochem* 56:615-649.

265. Du X, Black GE, Lecchi P, Abramson FP, & Sprang SR (2004) Kinetic isotope effects in Ras-catalyzed GTP hydrolysis: evidence for a loose transition state. *Proc Natl Acad Sci USA* 101(24):8858-8863.

266. Ahmadian MR, Stege P, Scheffzek K, & Wittinghofer A (1997) Confirmation of the arginine-finger hypothesis for the GAP-stimulated GTP-hydrolysis reaction of Ras. *Nat Struct Biol* 4(9):686-689.

267. Stock AM, Robinson VL, & Goudreau PN (2000) Two-component signal transduction. *Annu Rev Biochem* 69:183-215.

268. Capra EJ & Laub MT (2012) Evolution of two-component signal transduction systems. *Annu Rev Microbiol* 66:325-347.

269. Salazar ME & Laub MT (2015) Temporal and evolutionary dynamics of two-component signaling pathways. *Curr Opin Microbiol* 24:7-14.

270. Gass J & Khosla C (2007) Prolyl endopeptidases. *Cell Mol Life Sci* 64(3):345-355.

271. Pausch P*, et al.* (2015) Co-translational capturing of nascent ribosomal proteins by their dedicated chaperones. *Nat Commun* 6:7494.

272. Fülöp V & Jones DT (1999) Beta propellers: structural rigidity and functional diversity. *Curr Opin Struct Biol* 9(6):715-721.

273. Chen CK, Chan NL, & Wang AH (2011) The many blades of the beta-propeller proteins: conserved but versatile. *Trends Biochem Sci* 36(10):553-561.

274. Quisel JD, Lin DC, & Grossman AD (1999) Control of development by altered localization of a transcription factor in *B. subtilis*. *Mol Cell* 4(5):665-672.

275. Marston AL & Errington J (1999) Dynamic movement of the ParA-like Soj protein of *B. subtilis* and its dual role in nucleoid organization and developmental regulation. *Mol Cell* 4(5):673-682.

276. Wu LJ & Errington J (2003) RacA and the Soj-Spo0J system combine to effect polar chromosome segregation in sporulating *Bacillus subtilis*. *Mol Microbiol* 49(6):1463-1475.

277. Dyer CM & Dahlquist FW (2006) Switched or not?: the structure of unphosphorylated CheY bound to the N terminus of FliM. *J Bacteriol* 188(21):7354-7363.

278. Lam KH*, et al.* (2013) Structural basis of FliG-FliM interaction in *Helicobacter pylori*. *Mol Microbiol* 88(4):798-812.

279. Sircar R, Greenswag AR, Bilwes AM, Gonzalez-Bonet G, & Crane BR (2013) Structure and activity of the flagellar rotor protein FliY: a member of the CheC phosphatase family. *J Biol Chem* 288(19):13493-13502.

280. Lewis PJ & Marston AL (1999) GFP vectors for controlled expression and dual labelling of protein fusions in *Bacillus subtilis*. *Gene* 227(1):101-109.

281. Rist W, Jorgensen TJ, Roepstorff P, Bukau B, & Mayer MP (2003) Mapping temperature-induced conformational changes in the *Escherichia coli* heat shock transcription factor s^{32} by amide hydrogen exchange. *J Biol Chem* 278(51):51415-51421.

282. Kressler D*, et al.* (2012) Synchronizing nuclear import of ribosomal proteins with ribosome assembly. *Science* 338(6107):666-671.

283. Hope MJ, Bally MB, Webb G, & Cullis PR (1985) Production of large unilamellar vesicles by a rapid extrusion procedure: characterization of size distribution, trapped volume and ability to maintain a membrane potential. *Biochim Biophys Acta* 812(1):55-65.

284. Parlitz R*, et al.* (2007) *Escherichia coli* signal recognition particle receptor FtsY contains an essential and autonomous membrane-binding amphipathic helix. *J Biol Chem* 282(44):32176-32184.

285. Zeigler DR*, et al.* (2008) The origins of 168, W23, and other *Bacillus subtilis* legacy strains. *J Bacteriol* 190(21):6983-6995.

Appendix

7.1 Supporting Tables

Table S1. Crystallographic table

	*Gt*FlhG-monomer	*Gt*FlhG-dimer
Data collection		
Space group	P $2_12_12_1$	P 2_1
Cell dimensions		
a, *b*, *c* (Å)	63.87	51.25
	89.36	72.56
	111.88	65.62
α, β, γ (°)	90.00	90.00
	90.00	93.73
	90.00	90.00
Energy (keV)	12.6616	
Resolution (Å)	51.96 – 2.80	41.8 – 1.90
	(2.95 – 2.80)	(2.00 – 1.90)
R_{merge}	0.136 (0.47)*	0.058 (0.247)*
$I / \sigma I$	11.7 (5.2)	12.0 (5.8)
Completeness (%)	100 (100)	99.2 (99.4)
Redundancy	5.1 (5.2)	3.9 (3.9)
Refinement		
Resolution (Å)	47.4 – 2.80	29.84 – 1.90
No. reflections	15916	36165
R_{work}/R_{free} (%)	17.7/22.8	22.1/26.0
No. atoms		
Protein	3952	3743
Ligand	0	38
Water	57	246

R.m.s deviations		
Bond lengths (Å)	0.008	0.008
Bond angles (°)	1.228	1.229
Ramachandran (%)		
Preferred	96.64	96.90
Allowed	3.12	2.69
Outliers	0.20	0.41

Table S2. Proteins found in the pull down experiments of GST-*Sp*HubP$_{102-580}$

Protein	Additionl information	Coverage
50S ribosomal protein L1		54 %
50S ribosomal protein L2		34 %
50S ribosomal protein L3		25.5 %
30S ribosomal protein S2		16.5 %
ArcA	response regulator	19.3 %
putative signalling transduction protein	WP_011788148	18.6 %
Methyltransferase	Sputcn32_1759	10 %
phage shock protein A, PspA		24 %

Table S3. List of oligonucleotides. The oligonucleotides listed below were used for molecular cloning in this work.

Oligonucleotide	Product	RE	Sequence (5' to 3')
YlxH Geo D61A F	FlhG D60A	-	ttgctggctcgatatggccatcggcatgggcaac
YlxH Geo D61A R	FlhG D60A	-	gttgcccatgccgatggccatatcgagccagcaa
GtYlxH-K36Q-F	FlhG K36Q	-	ggggtgggccagtcgaacgtttcgc
GtYlxH-K36Q-R	FlhG K36Q	-	gcgaaacgttcgactggcccacccc
GtYlxH-Y173D-F	FlhG Y173D	-	catgaccgacgcggatgccatgatgaaatatatg
GtYlxH-Y173D-R	FlhG Y173D	-	catatatttcatcatggcatccgcgtcggtcatg
GtYlxH-K177E-F	FlhG K177E	-	cgtatgccatgatggaatatatgcacgctg
GtYlxH-K177E-R	FlhG K177E	-	cagcgtgcatatattccatcatggcatacg
GtYlxH-R199E-F	FlhG R199E	-	cgccggcaaggaggaggaagggtatgaag
GtYlxH-R199E-R	FlhG R199E	-	cttcataccttcctcctccttgccggcg
GtYlxH-Y202D-F	FlhG Y202D	-	ggagcgggaaggggatgaagtttttgagcgg
GtYlxH-Y202D-R	FlhG Y202D	-	ccgctcaaaaacttcatccccttcccgctcc
GtYlxH-R207E-F	FlhG R207E	-	ggtatgaagtttttgaggagctgaagcacgtcaccg
GtYlxH-R207E-R	FlhG R207E	-	cggtgacgtgcttcagctcctcaaaaacttcatacc
GtYlxH-H210L-F	FlhG H210L	-	gagcggctgaagctcgtcaccggtcg
GtYlxH-H210L-R	FlhG H210L	-	cgaccggtgacgagcttcagccgctc
GtYlxH-R214E-F	FlhG R214E	-	gaagcacgtcaccggtgagtttttaaacaaagatattg
GtYlxH-R214E-R	FlhG R214E	-	caatatctttgtttaaaaactcaccggtgacgtgcttc
GtYlxH-F215S-F	FlhG F215S	-	cacgtcaccggtcggtctttaaacaaagatattgcg
GtYlxH-F215S-R	FlhG F215S	-	cgcaatatctttgtttaaagaccgaccggtgacgtg
Gt_YlxH_R234G_F	FlhG R234G	-	gatcggacggtcgctggcgcggttgtcagccaaacgc
Gt_YlxH_R234G_R	FlhG R234G	-	gcgtttggctgacaaccgcgccagcgaccgtccgatc

GeoFliY-Nco-F	FliY	NcoI	ttaaccatgggcaatgatggaatgttgtcgc
GtFliM-C2-NcoIF	FliM	NcoI	ttaaccatgggtgcccaattgccgattgtcgc
GtFliM-dN-NcoI	FliM ΔN25	NcoI	ttaaccatgggcgcggaagaactaaaaaaggaagagg
GtFliM-BamHI-R	FliM	BamHI	ttaaggatccttattcatcataactttcttcgccc
SpFliM1-Pci-F	FliM1	PciI	ttaaacatgtctgatttattaagccaagacg
SpFliM2-Xho6H-R	FliM2	XhoI	ttaactcgagttaatggtgatggtgatggtggccaatgtcgttctcc
SpFliN1-Pci-F	FliN1	PciI	ttaaacatgtctacagaagatacgggcg
SpFliN2-Nco-F	FliN2	NcoI	ttaaccatgggcaggagaacgacattgg
BsFlhG_full_ApaI	FlhG	ApaI	ttaagggcccatggtgcagatgaacagatatg
BsFlhG_500_ApaUP	FlhG	ApaI	ttaagggccccagctcgatcagagaaaatgg
BsFlhG_DOWN_NS	FlhG	EcoRI	ttaagaattccccgccagccctcctcattaaaaaagaag
GeoYlxH-MTS-F	FlhG-MTS	NcoI	ttaaccatggcgccgcagcgggagg
GeoYlxH-MTS-R	FlhG-MTS	BamHI	ttaaggatccttacctttctaggaaaagttggcg

Restriction enzyme is abbreviated with RE.

Table S4. List of plasmids. The plasmids listed below were used in the scope of this work.

Vector	Product	Org.	RE	Tag
pET24d	FlhG	*Gt*	NcoI/BamHI	N-His
pET24d	FlhG D60A	*Gt*	NcoI/BamHI	N-His
pET24d	FlhG K36Q	*Gt*	NcoI/BamHI	N-His
pET24d	FlhG Y173D	*Gt*	NcoI/BamHI	N-His
pET24d	FlhG K177E	*Gt*	NcoI/BamHI	N-His
pET24d	FlhG R199E	*Gt*	NcoI/BamHI	N-His
pET24d	FlhG Y202D	*Gt*	NcoI/BamHI	N-His

pET24d	FlhG R207E	*Gt*	NcoI/BamHI	N-His
pET24d	FlhG H210L	*Gt*	NcoI/BamHI	N-His
pET24d	FlhG R214E	*Gt*	NcoI/BamHI	N-His
pET24d	FlhG F215S	*Gt*	NcoI/BamHI	N-His
pET24d	FlhG R234G	*Gt*	NcoI/BamHI	N-His
pGAT3	FlhG	*Gt*	NcoI/XhoI	N-GST; N-His
pET24d	FliM	*Gt*	NcoI/BamHI	C-His
pET24d	FliM ΔN25	*Gt*	NcoI/BamHI	C-His
pET16b	FliM ΔN25	*Gt*	NcoI/BamHI	C-His
pET24d	FliY	*Gt*	NcoI/BamHI	C-His
pET16b	FliY	*Gt*	NcoI/BamHI	no His
pET16b	FliY ΔN25	*Gt*	NcoI/BamHI	no His
pET24d	MinC	*Gt*	NcoI/BamHI	N-His
pSG 1164	FlhG	*Bs*	ApaI/EcoRI	YFP-fusion
pGAT3	GpsB	*Bs*	NcoI/BamHI	N-GST; N-His
pGAT3	GpsB 1-24	*Bs*	NcoI/BamHI	N-GST; N-His
pGAT3	GpsB 1-70	*Bs*	NcoI/BamHI	N-GST; N-His
pGAT3	GpsB 21-98	*Bs*	NcoI/BamHI	N-GST; N-His
pET24d	CheY	*Bs*	NcoI/BamHI	N-His
pET24d	FlhG	*Sp*	NcoI/XhoI	N-His
pGAT3	FlhG	*Sp*	NcoI/XhoI	N-GST; N-His
pET24d	FliM1	*Sp*	PciI/BamHI	C-His
pET24d	FliM2	*Sp*	NcoI/XhoI	C-His
pET24d	FliN1	*Sp*	PciI/BamHI	no His
pET24d	FliN2	*Sp*	NcoI/BamHI	no His

pET24d	FlrA	*Sp*	NcoI/BamHI	N-His
pET24d	FlrA-DNA-bind.	*Sp*	NcoI/BamHI	N-His
pET24d	FlrA-FleQ-domain	*Sp*	NcoI/BamHI	N-His
pGEX	GST-HubP 369-1097	*Sp*	-	N-GST; C-His

Restriction enzyme is abbreviated with RE.

Table S5. List of *B. subtilis* strains used in this work.

PY79	PY79; wild-type	(285)
Jss01	PY79 *flhG-yfp* (Cm^R)	this study
Jss02	PY79 *flhG-yfp* (Cm^R) *amyE::fliM-cfp* ($Spec^R$)	this study

7.2 $^{1}H/^{2}H$ Exchange data

7.2.1 $^{1}H/^{2}H$ exchange data for FlhG and FliY

Deuterium uptake of FlhG alone and in FlhG/FliY after 30 s exchange.

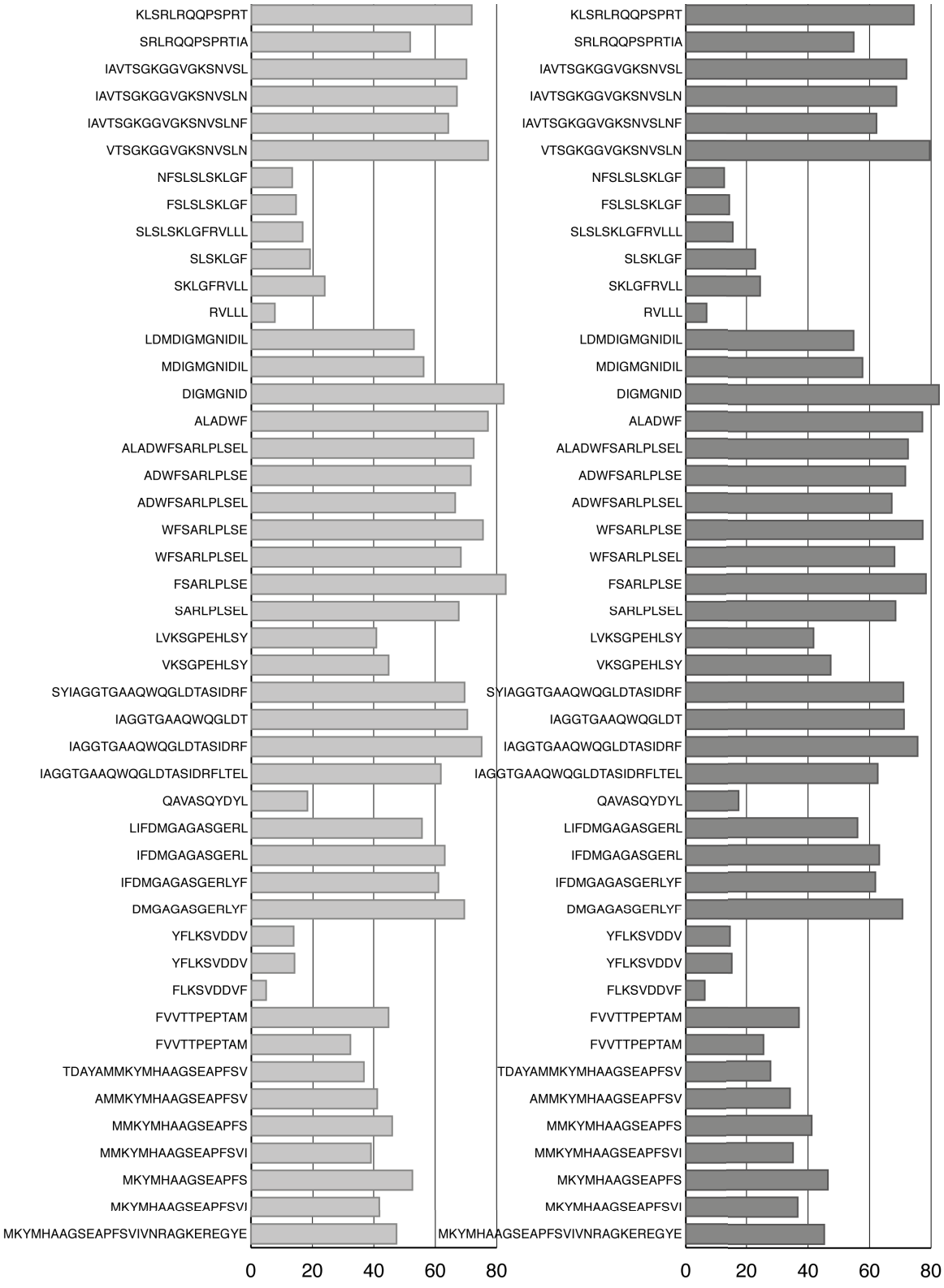

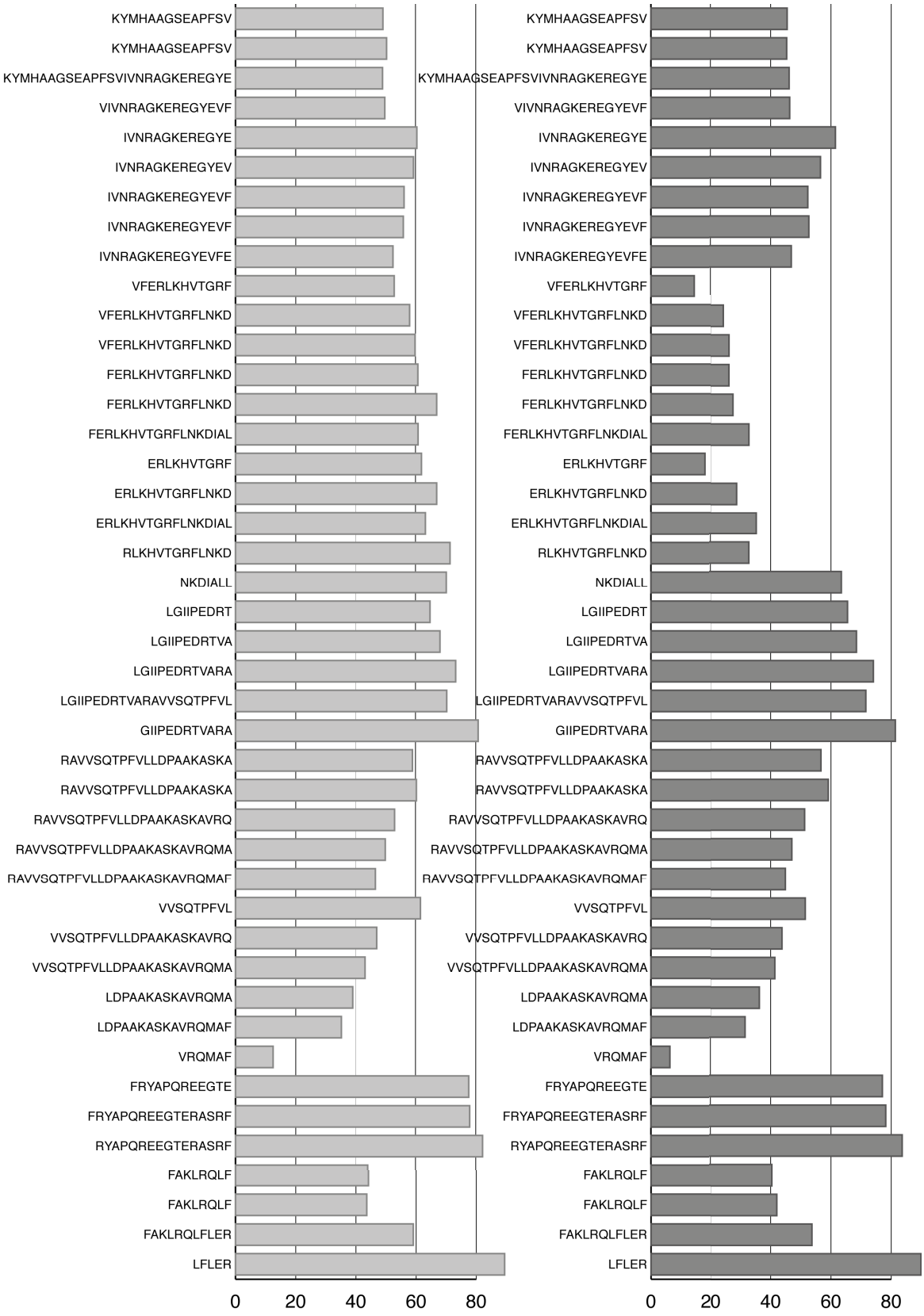
KYMHAAGSEAPFSV
KYMHAAGSEAPFSV
KYMHAAGSEAPFSVIVNRAGKEREGYE
VIVNRAGKEREGYEVF
IVNRAGKEREGYE
IVNRAGKEREGYEV
IVNRAGKEREGYEVF
IVNRAGKEREGYEVF
IVNRAGKEREGYEVFE
VFERLKHVTGRF
VFERLKHVTGRFLNKD
VFERLKHVTGRFLNKD
FERLKHVTGRFLNKD
FERLKHVTGRFLNKD
FERLKHVTGRFLNKDIAL
ERLKHVTGRF
ERLKHVTGRFLNKD
ERLKHVTGRFLNKDIAL
RLKHVTGRFLNKD
NKDIALL
LGIIPEDRT
LGIIPEDRTVA
LGIIPEDRTVARA
LGIIPEDRTVARAVVSQTPFVL
GIIPEDRTVARA
RAVVSQTPFVLLDPAAKASKA
RAVVSQTPFVLLDPAAKASKA
RAVVSQTPFVLLDPAAKASKAVRQ
RAVVSQTPFVLLDPAAKASKAVRQMA
RAVVSQTPFVLLDPAAKASKAVRQMAF
VVSQTPFVL
VVSQTPFVLLDPAAKASKAVRQ
VVSQTPFVLLDPAAKASKAVRQMA
LDPAAKASKAVRQMA
LDPAAKASKAVRQMAF
VRQMAF
FRYAPQREEGTE
FRYAPQREEGTERASRF
RYAPQREEGTERASRF
FAKLRQLF
FAKLRQLF
FAKLRQLFLER
LFLER
0
20
40
60
80
KYMHAAGSEAPFSV
KYMHAAGSEAPFSV
KYMHAAGSEAPFSVIVNRAGKEREGYE
VIVNRAGKEREGYEVF
IVNRAGKEREGYE
IVNRAGKEREGYEV
IVNRAGKEREGYEVF
IVNRAGKEREGYEVF
IVNRAGKEREGYEVFE
VFERLKHVTGRF
VFERLKHVTGRFLNKD
VFERLKHVTGRFLNKD
FERLKHVTGRFLNKD
FERLKHVTGRFLNKD
FERLKHVTGRFLNKDIAL
ERLKHVTGRF
ERLKHVTGRFLNKD
ERLKHVTGRFLNKDIAL
RLKHVTGRFLNKD
NKDIALL
LGIIPEDRT
LGIIPEDRTVA
LGIIPEDRTVARA
LGIIPEDRTVARAVVSQTPFVL
GIIPEDRTVARA
RAVVSQTPFVLLDPAAKASKA
RAVVSQTPFVLLDPAAKASKA
RAVVSQTPFVLLDPAAKASKAVRQ
RAVVSQTPFVLLDPAAKASKAVRQMA
RAVVSQTPFVLLDPAAKASKAVRQMAF
VVSQTPFVL
VVSQTPFVLLDPAAKASKAVRQ
VVSQTPFVLLDPAAKASKAVRQMA
LDPAAKASKAVRQMA
LDPAAKASKAVRQMAF
VRQMAF
FRYAPQREEGTE
FRYAPQREEGTERASRF
RYAPQREEGTERASRF
FAKLRQLF
FAKLRQLF
FAKLRQLFLER
LFLER
0
20
40
60
80

Deuterium uptake of FlhG alone and in FlhG/FliY after 60 s exchange.

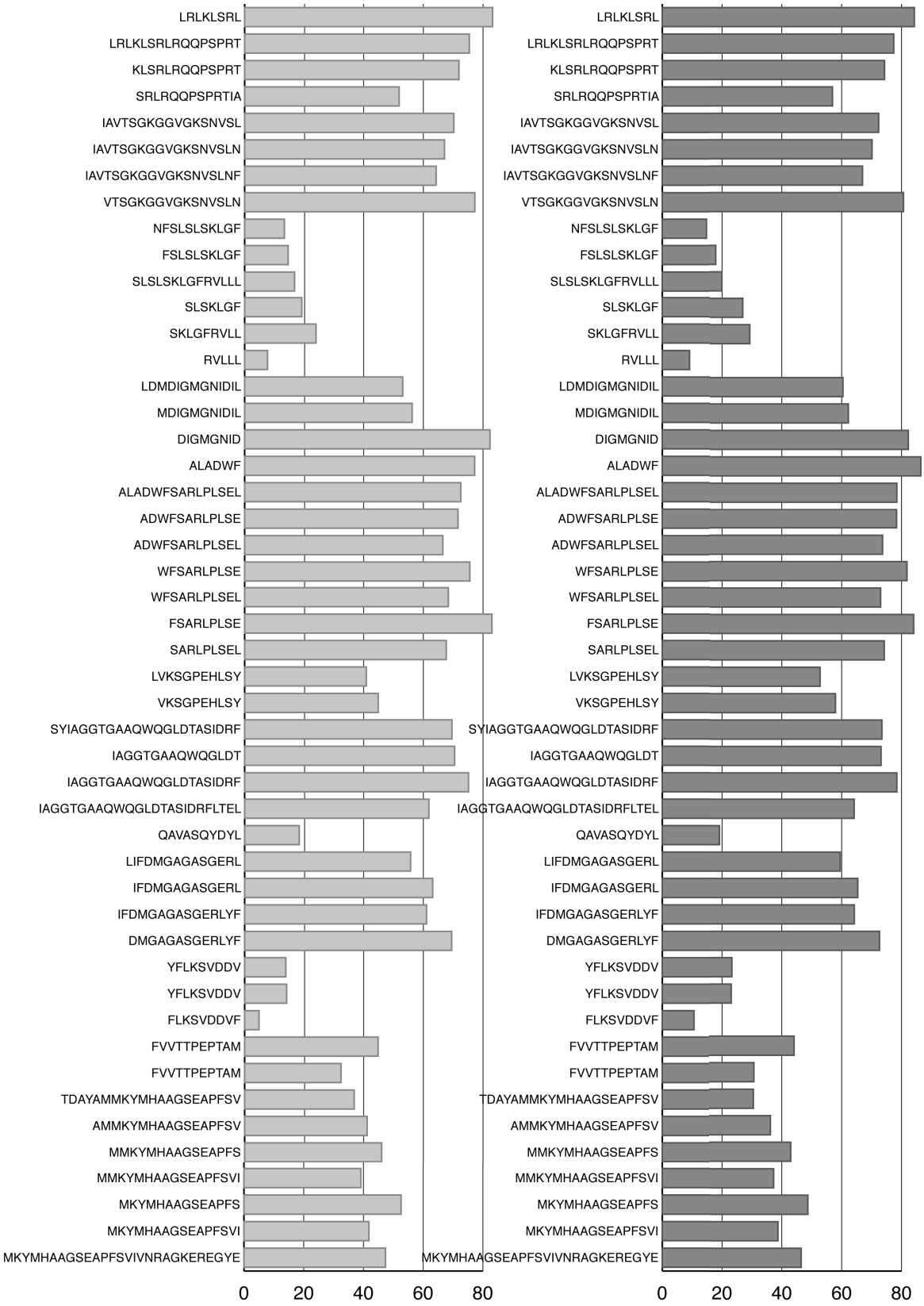

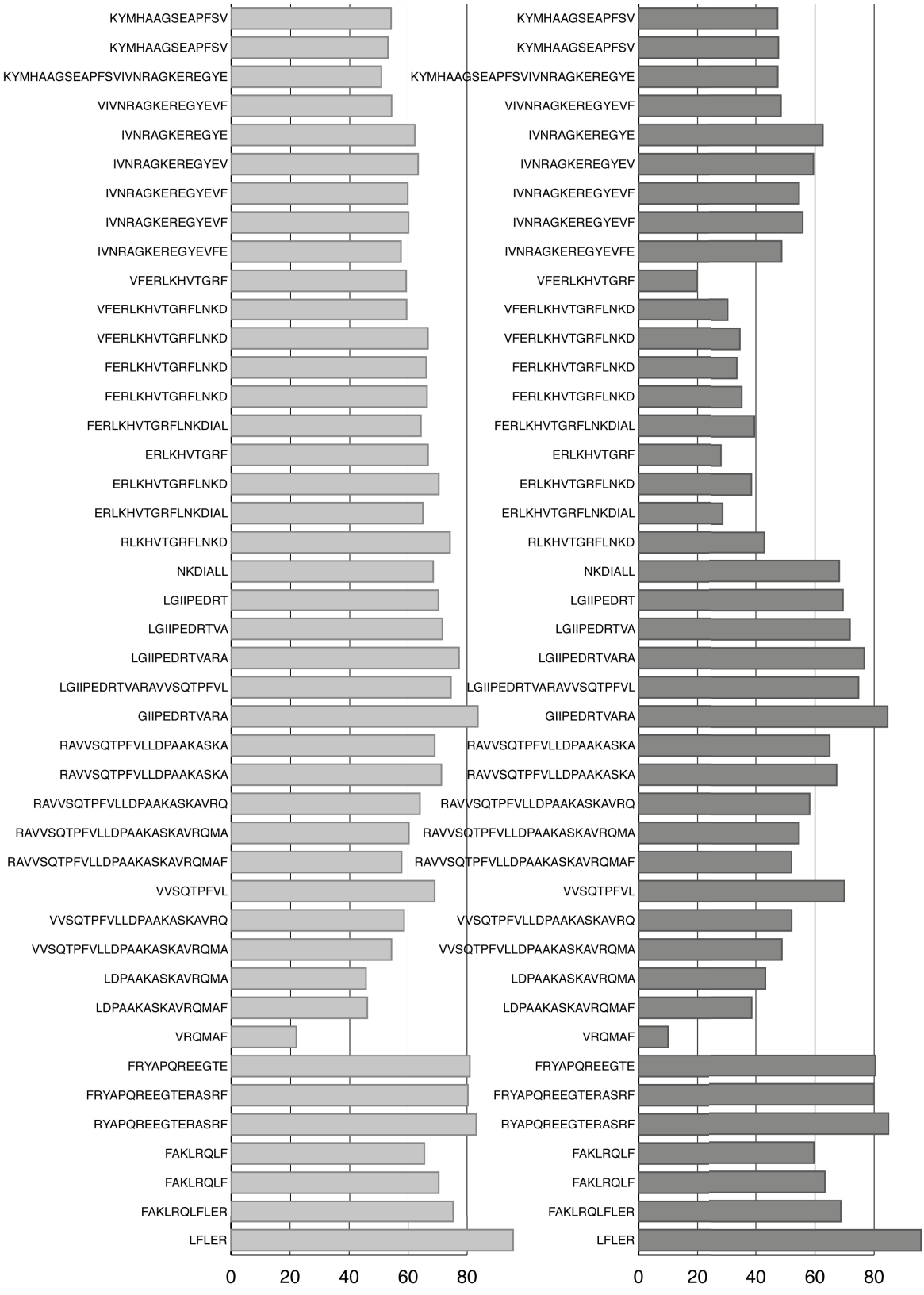
KYMHAAGSEAPFSV
KYMHAAGSEAPFSV
KYMHAAGSEAPFSVIVNRAGKEREGYE
VIVNRAGKEREGYEVF
IVNRAGKEREGYE
IVNRAGKEREGYEV
IVNRAGKEREGYEVF
IVNRAGKEREGYEVF
IVNRAGKEREGYEVFE
VFERLKHVTGRF
VFERLKHVTGRFLNKD
VFERLKHVTGRFLNKD
FERLKHVTGRFLNKD
FERLKHVTGRFLNKD
FERLKHVTGRFLNKDIAL
ERLKHVTGRF
ERLKHVTGRFLNKD
ERLKHVTGRFLNKDIAL
RLKHVTGRFLNKD
NKDIALL
LGIIPEDRT
LGIIPEDRTVA
LGIIPEDRTVARA
LGIIPEDRTVARAVVSQTPFVL
GIIPEDRTVARA
RAVVSQTPFVLLDPAAKASKA
RAVVSQTPFVLLDPAAKASKA
RAVVSQTPFVLLDPAAKASKAVRQ
RAVVSQTPFVLLDPAAKASKAVRQMA
RAVVSQTPFVLLDPAAKASKAVRQMAF
VVSQTPFVL
VVSQTPFVLLDPAAKASKAVRQ
VVSQTPFVLLDPAAKASKAVRQMA
LDPAAKASKAVRQMA
LDPAAKASKAVRQMAF
VRQMAF
FRYAPQREEGTE
FRYAPQREEGTERASRF
RYAPQREEGTERASRF
FAKLRQLF
FAKLRQLF
FAKLRQLFLER
LFLER
0
20
40
60
80
KYMHAAGSEAPFSV
KYMHAAGSEAPFSV
KYMHAAGSEAPFSVIVNRAGKEREGYE
VIVNRAGKEREGYEVF
IVNRAGKEREGYE
IVNRAGKEREGYEV
IVNRAGKEREGYEVF
IVNRAGKEREGYEVF
IVNRAGKEREGYEVFE
VFERLKHVTGRF
VFERLKHVTGRFLNKD
VFERLKHVTGRFLNKD
FERLKHVTGRFLNKD
FERLKHVTGRFLNKD
FERLKHVTGRFLNKDIAL
ERLKHVTGRF
ERLKHVTGRFLNKD
ERLKHVTGRFLNKDIAL
RLKHVTGRFLNKD
NKDIALL
LGIIPEDRT
LGIIPEDRTVA
LGIIPEDRTVARA
LGIIPEDRTVARAVVSQTPFVL
GIIPEDRTVARA
RAVVSQTPFVLLDPAAKASKA
RAVVSQTPFVLLDPAAKASKA
RAVVSQTPFVLLDPAAKASKAVRQ
RAVVSQTPFVLLDPAAKASKAVRQMA
RAVVSQTPFVLLDPAAKASKAVRQMAF
VVSQTPFVL
VVSQTPFVLLDPAAKASKAVRQ
VVSQTPFVLLDPAAKASKAVRQMA
LDPAAKASKAVRQMA
LDPAAKASKAVRQMAF
VRQMAF
FRYAPQREEGTE
FRYAPQREEGTERASRF
RYAPQREEGTERASRF
FAKLRQLF
FAKLRQLF
FAKLRQLFLER
LFLER
0
20
40
60
80

Deuterium uptake of FliY alone and in FlhG/FliY after 30 s exchange.

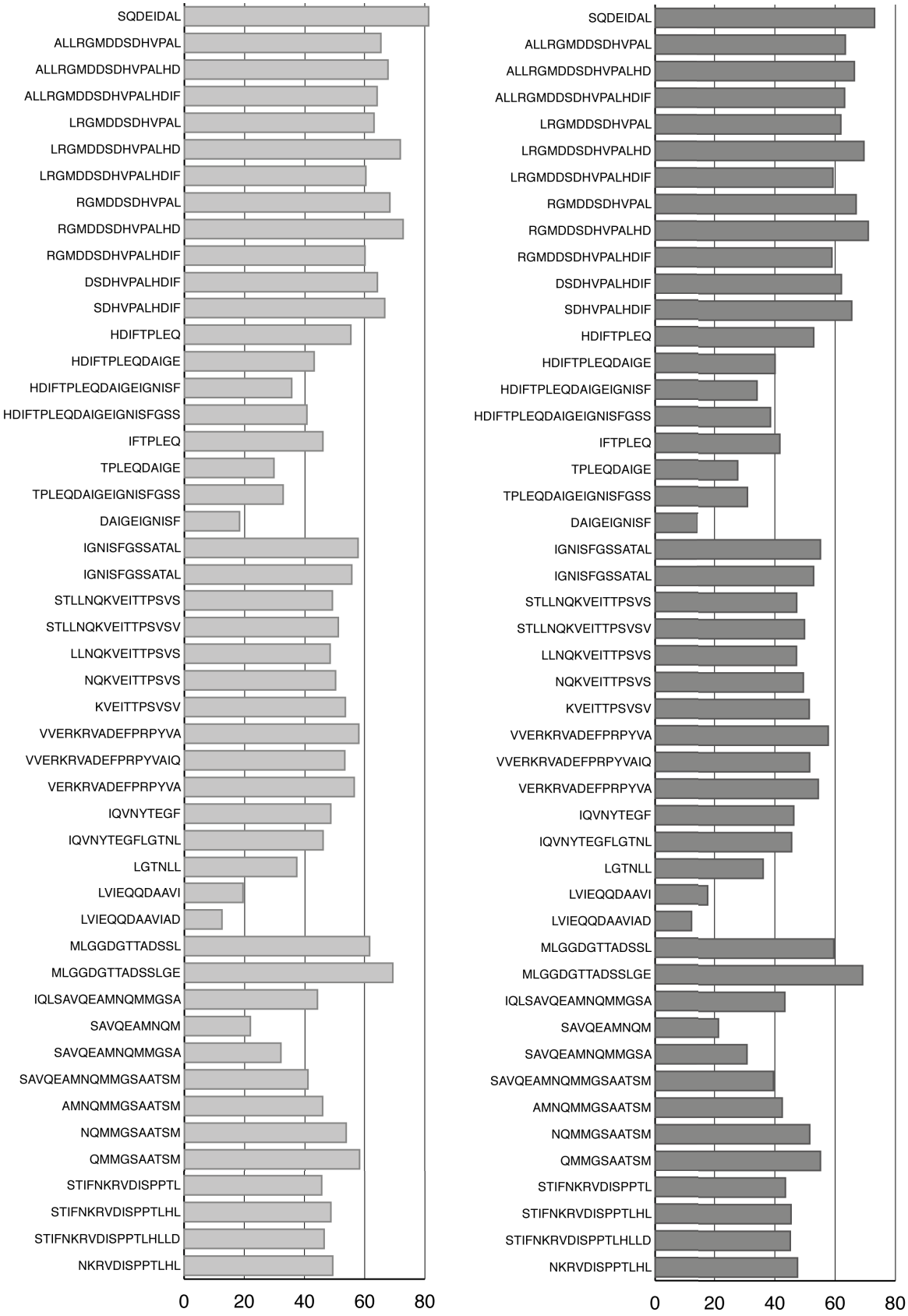

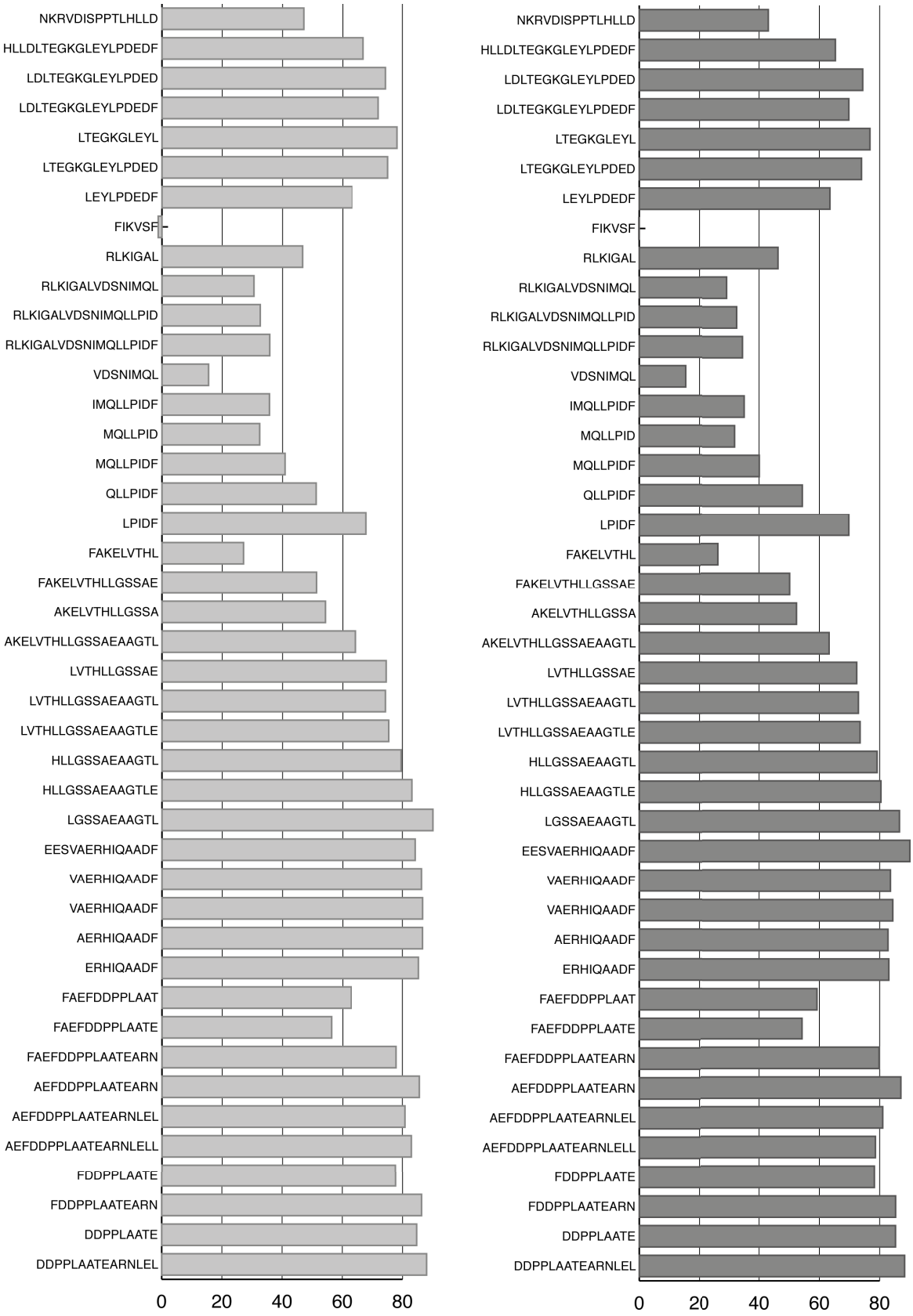
NKRVDISPPTLHLLD
HLLDLTEGKGLEYLPDEDF
LDLTEGKGLEYLPDED
LDLTEGKGLEYLPDEDF
LTEGKGLEYL
LTEGKGLEYLPDED
LEYLPDEDF
FIKVSF
RLKIGAL
RLKIGALVDSNIMQL
RLKIGALVDSNIMQLLPID
RLKIGALVDSNIMQLLPIDF
VDSNIMQL
IMQLLPIDF
MQLLPID
MQLLPIDF
QLLPIDF
LPIDF
FAKELVTHL
FAKELVTHLLGSSAE
AKELVTHLLGSSA
AKELVTHLLGSSAEAAGTL
LVTHLLGSSAE
LVTHLLGSSAEAAGTL
LVTHLLGSSAEAAGTLE
HLLGSSAEAAGTL
HLLGSSAEAAGTLE
LGSSAEAAGTL
EESVAERHIQAADF
VAERHIQAADF
VAERHIQAADF
AERHIQAADF
ERHIQAADF
FAEFDDPPLAAT
FAEFDDPPLAATE
FAEFDDPPLAATEARN
AEFDDPPLAATEARN
AEFDDPPLAATEARNLEL
AEFDDPPLAATEARNLELL
FDDPPLAATE
FDDPPLAATEARN
DDPPLAATE
DDPPLAATEARNLEL
0
20
40
60
80
NKRVDISPPTLHLLD
HLLDLTEGKGLEYLPDEDF
LDLTEGKGLEYLPDED
LDLTEGKGLEYLPDEDF
LTEGKGLEYL
LTEGKGLEYLPDED
LEYLPDEDF
FIKVSF
RLKIGAL
RLKIGALVDSNIMQL
RLKIGALVDSNIMQLLPID
RLKIGALVDSNIMQLLPIDF
VDSNIMQL
IMQLLPIDF
MQLLPID
MQLLPIDF
QLLPIDF
LPIDF
FAKELVTHL
FAKELVTHLLGSSAE
AKELVTHLLGSSA
AKELVTHLLGSSAEAAGTL
LVTHLLGSSAE
LVTHLLGSSAEAAGTL
LVTHLLGSSAEAAGTLE
HLLGSSAEAAGTL
HLLGSSAEAAGTLE
LGSSAEAAGTL
EESVAERHIQAADF
VAERHIQAADF
VAERHIQAADF
AERHIQAADF
ERHIQAADF
FAEFDDPPLAAT
FAEFDDPPLAATE
FAEFDDPPLAATEARN
AEFDDPPLAATEARN
AEFDDPPLAATEARNLEL
AEFDDPPLAATEARNLELL
FDDPPLAATE
FDDPPLAATEARN
DDPPLAATE
DDPPLAATEARNLEL
0
20
40
60
80

Deuterium uptake of FliY alone and in FlhG/FliY after 60 s exchange.

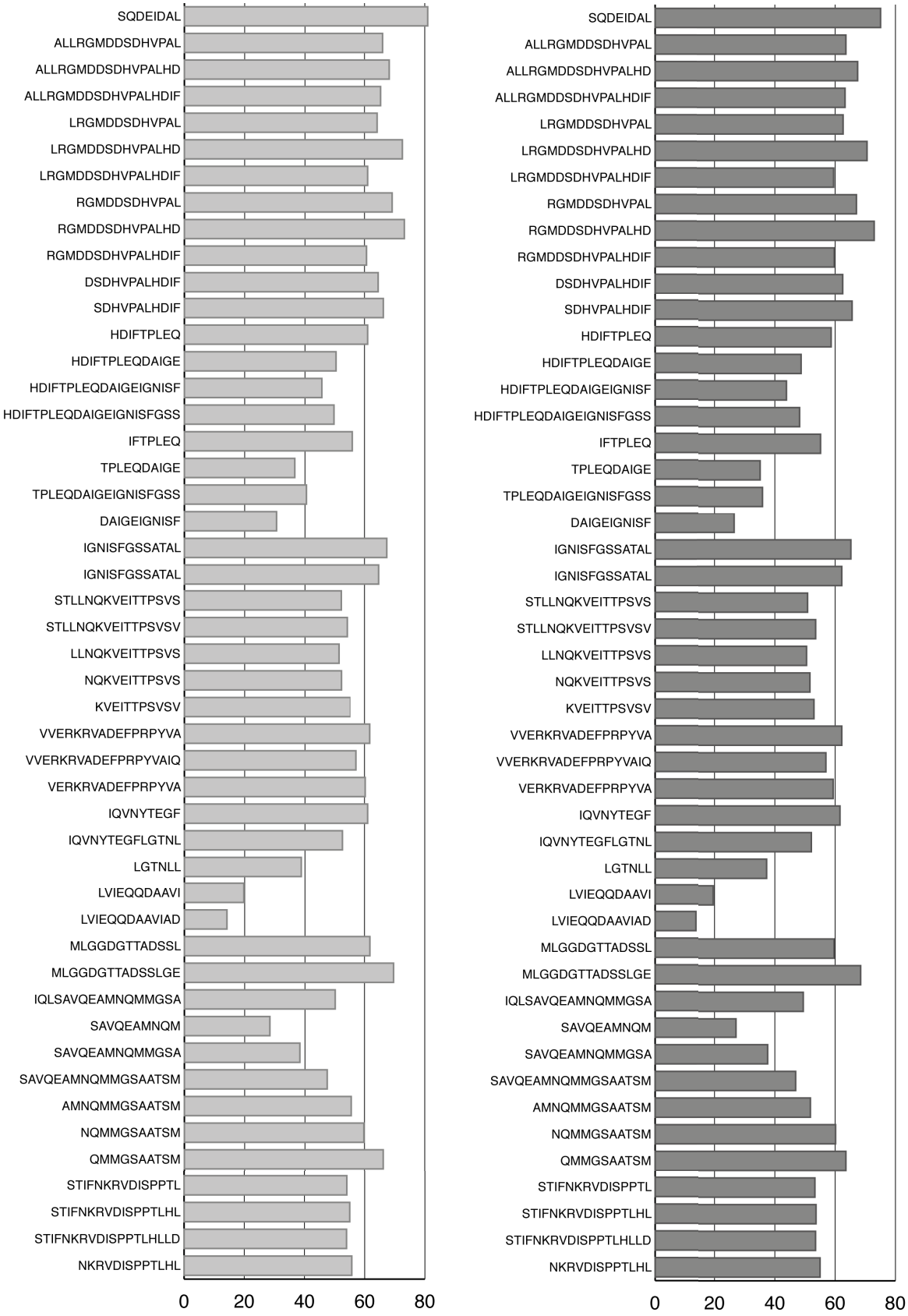

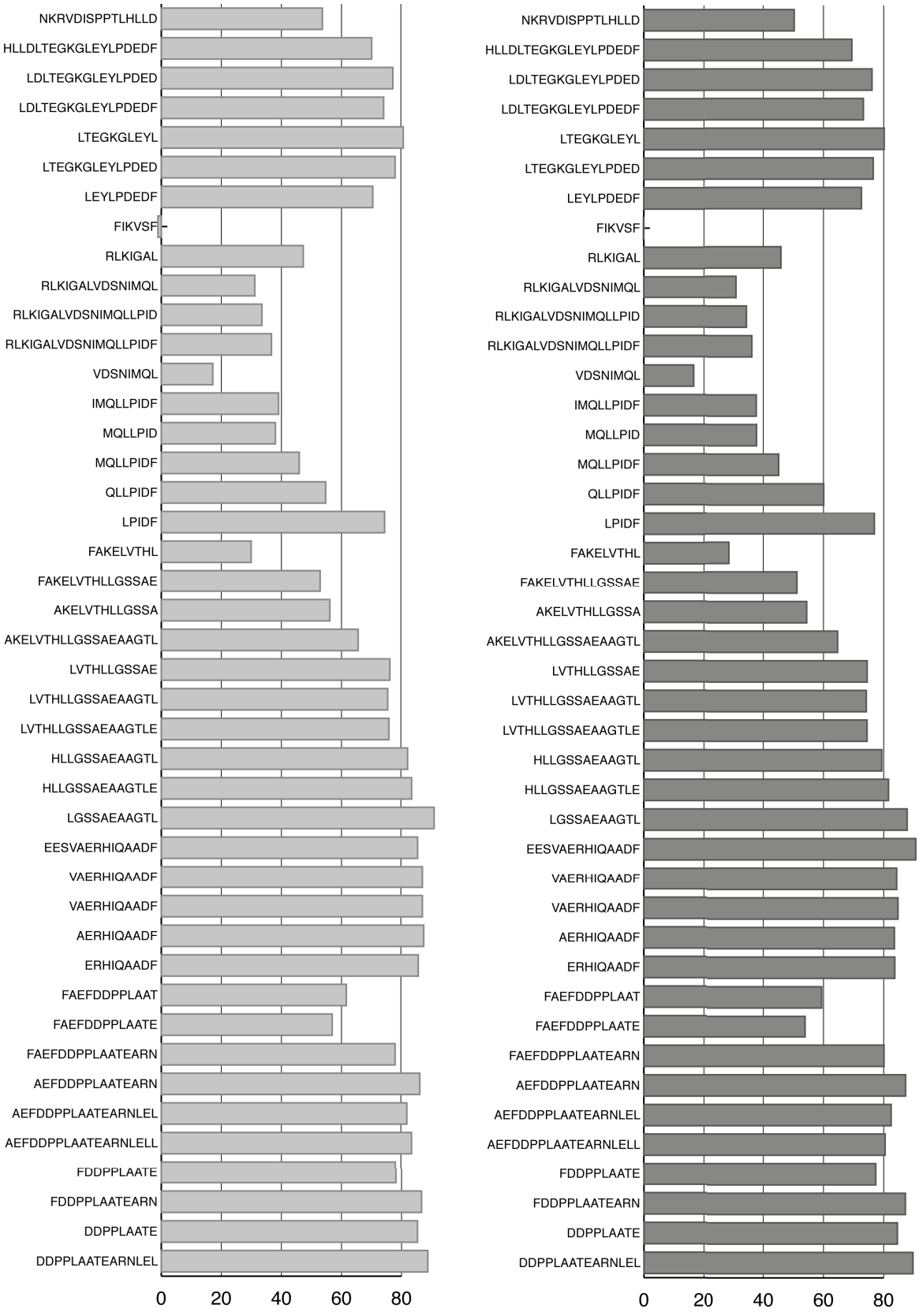
NKRVDISPPTLHLLD
HLLDLTEGKGLEYLPDEDF
LDLTEGKGLEYLPDED
LDLTEGKGLEYLPDEDF
LTEGKGLEYL
LTEGKGLEYLPDED
LEYLPDEDF
FIKVSF
RLKIGAL
RLKIGALVDSNIMQL
RLKIGALVDSNIMQLLPID
RLKIGALVDSNIMQLLPIDF
VDSNIMQL
IMQLLPIDF
MQLLPID
MQLLPIDF
QLLPIDF
LPIDF
FAKELVTHL
FAKELVTHLLGSSAE
AKELVTHLLGSSA
AKELVTHLLGSSAEAAGTL
LVTHLLGSSAE
LVTHLLGSSAEAAGTL
LVTHLLGSSAEAAGTLE
HLLGSSAEAAGTL
HLLGSSAEAAGTLE
LGSSAEAAGTL
EESVAERHIQAADF
VAERHIQAADF
VAERHIQAADF
AERHIQAADF
ERHIQAADF
FAEFDDPPLAAT
FAEFDDPPLAATE
FAEFDDPPLAATEARN
AEFDDPPLAATEARN
AEFDDPPLAATEARNLEL
AEFDDPPLAATEARNLELL
FDDPPLAATE
FDDPPLAATEARN
DDPPLAATE
DDPPLAATEARNLEL
0
20
40
60
80

7.2.2 $^{1}H/^{2}H$ exchange data of flagellin/FliS and FliW

Deuterium uptake of FliS in flagellin/Flis and flagellin/FliS/FliW after 60 s exchange.

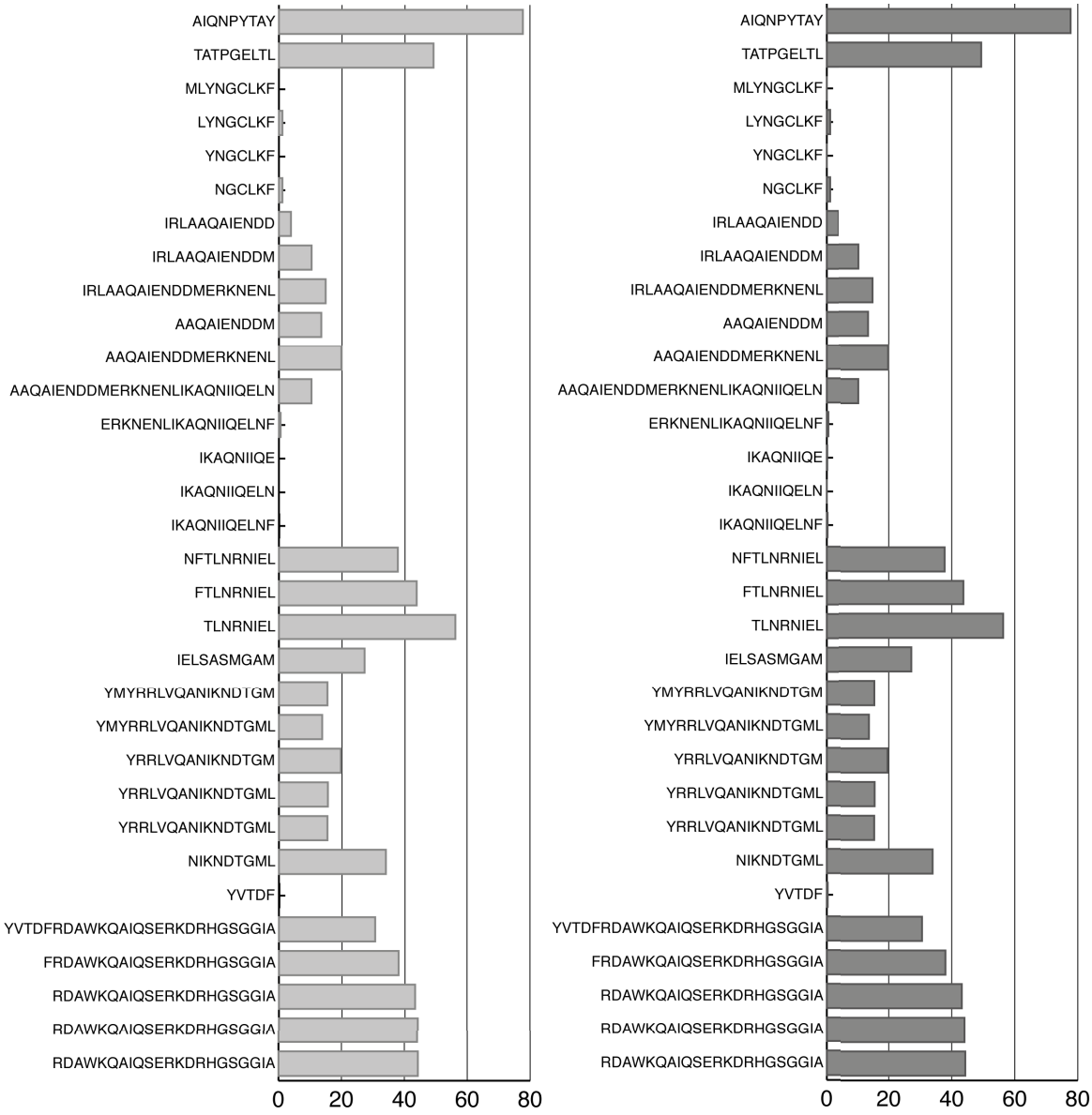

Deuterium uptake of flagellin in flagellin/Flis and flagellin/FliS/FliW after 60 s exchange.

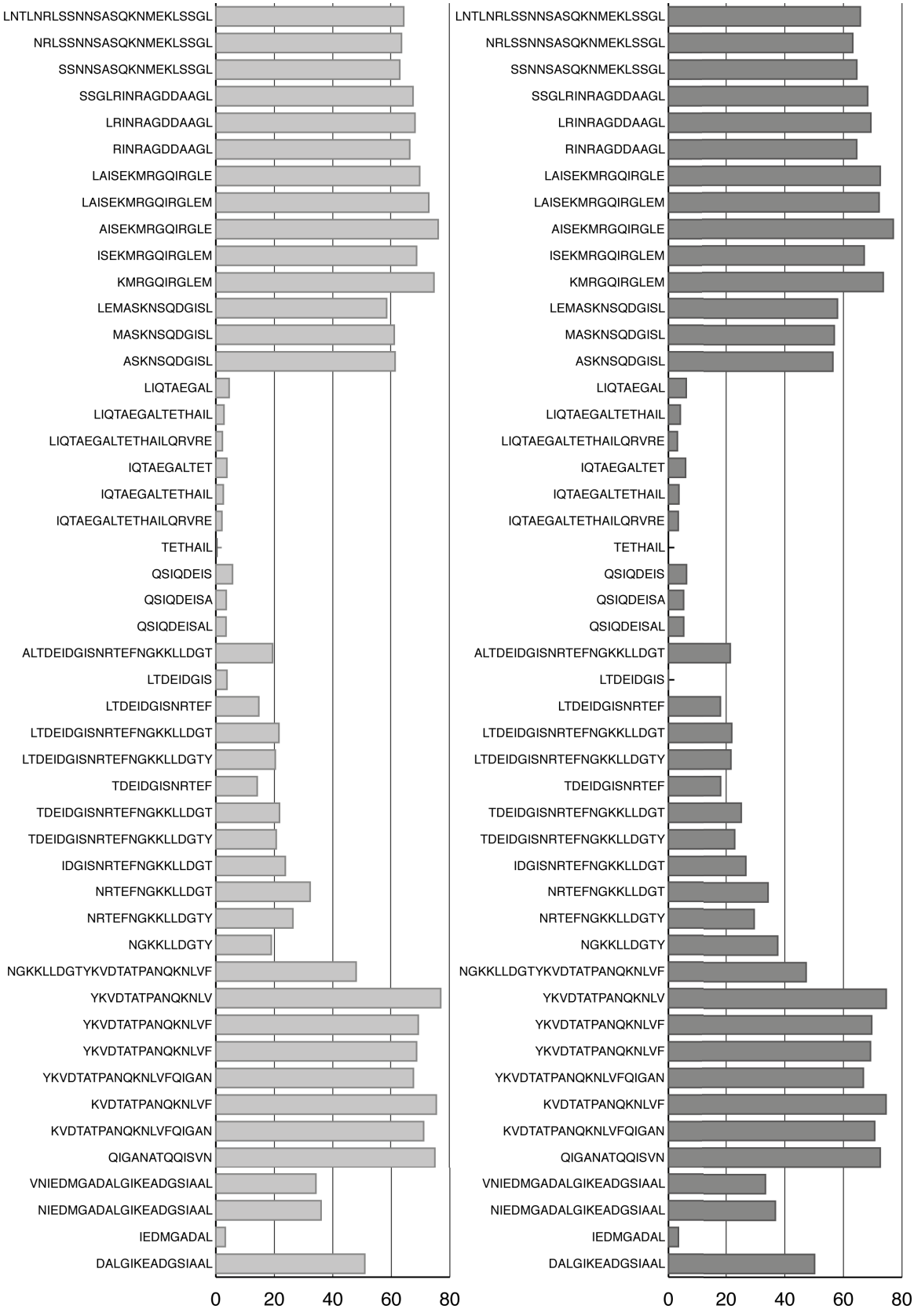

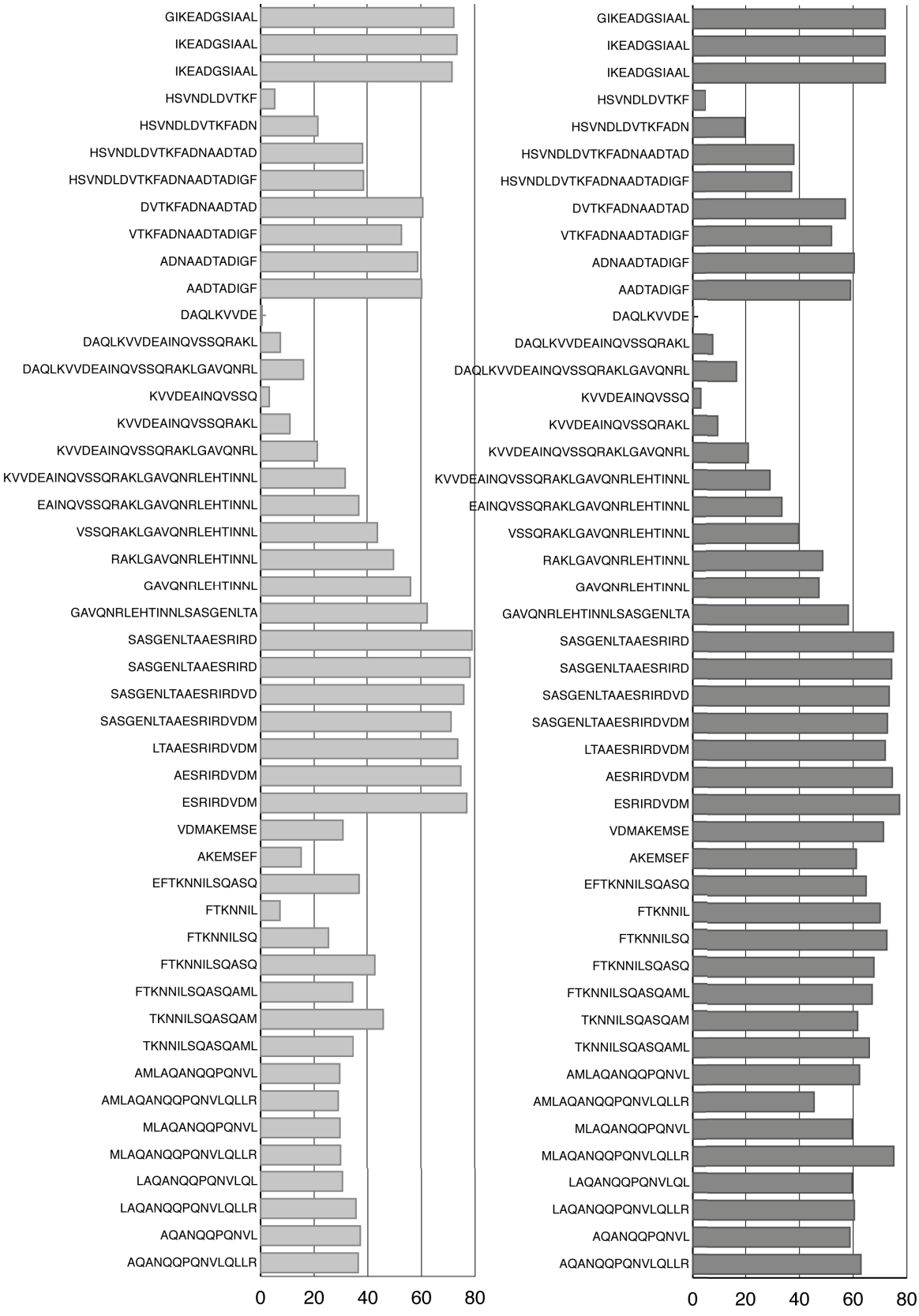
GIKEADGSIAAL
IKEADGSIAAL
IKEADGSIAAL
HSVNDLDVTKF
HSVNDLDVTKFADN
HSVNDLDVTKFADNAADTAD
HSVNDLDVTKFADNAADTADIGF
DVTKFADNAADTAD
VTKFADNAADTADIGF
ADNAADTADIGF
AADTADIGF
DAQLKVVDE
DAQLKVVDEAINQVSSQRAKL
DAQLKVVDEAINQVSSQRAKLGAVQNRL
KVVDEAINQVSSQ
KVVDEAINQVSSQRAKL
KVVDEAINQVSSQRAKLGAVQNRL
KVVDEAINQVSSQRAKLGAVQNRLEHTINNL
EAINQVSSQRAKLGAVQNRLEHTINNL
VSSQRAKLGAVQNRLEHTINNL
RAKLGAVQNRLEHTINNL
GAVQNRLEHTINNL
GAVQNRLEHTINNLSASGENLTA
SASGENLTAAESRIRD
SASGENLTAAESRIRD
SASGENLTAAESRIRDVD
SASGENLTAAESRIRDVDM
LTAAESRIRDVDM
AESRIRDVDM
ESRIRDVDM
VDMAKEMSE
AKEMSEF
EFTKNNILSQASQ
FTKNNIL
FTKNNILSQ
FTKNNILSQASQ
FTKNNILSQASQAML
TKNNILSQASQAM
TKNNILSQASQAML
AMLAQANQQPQNVL
AMLAQANQQPQNVLQLLR
MLAQANQQPQNVL
MLAQANQQPQNVLQLLR
LAQANQQPQNVLQL
LAQANQQPQNVLQLLR
AQANQQPQNVL
AQANQQPQNVLQLLR
0
20
40
60
80
GIKEADGSIAAL
IKEADGSIAAL
IKEADGSIAAL
HSVNDLDVTKF
HSVNDLDVTKFADN
HSVNDLDVTKFADNAADTAD
HSVNDLDVTKFADNAADTADIGF
DVTKFADNAADTAD
VTKFADNAADTADIGF
ADNAADTADIGF
AADTADIGF
DAQLKVVDE
DAQLKVVDEAINQVSSQRAKL
DAQLKVVDEAINQVSSQRAKLGAVQNRL
KVVDEAINQVSSQ
KVVDEAINQVSSQRAKL
KVVDEAINQVSSQRAKLGAVQNRL
KVVDEAINQVSSQRAKLGAVQNRLEHTINNL
EAINQVSSQRAKLGAVQNRLEHTINNL
VSSQRAKLGAVQNRLEHTINNL
RAKLGAVQNRLEHTINNL
GAVQNRLEHTINNL
GAVQNRLEHTINNLSASGENLTA
SASGENLTAAESRIRD
SASGENLTAAESRIRD
SASGENLTAAESRIRDVD
SASGENLTAAESRIRDVDM
LTAAESRIRDVDM
AESRIRDVDM
ESRIRDVDM
VDMAKEMSE
AKEMSEF
EFTKNNILSQASQ
FTKNNIL
FTKNNILSQ
FTKNNILSQASQ
FTKNNILSQASQAML
TKNNILSQASQAM
TKNNILSQASQAML
AMLAQANQQPQNVL
AMLAQANQQPQNVLQLLR
MLAQANQQPQNVL
MLAQANQQPQNVLQLLR
LAQANQQPQNVLQL
LAQANQQPQNVLQLLR
AQANQQPQNVL
AQANQQPQNVLQLLR
0
20
40
60
80

Deuterium uptake of FliW in flagellin/Flis and flagellin/FliS/FliW after 60 s exchange.

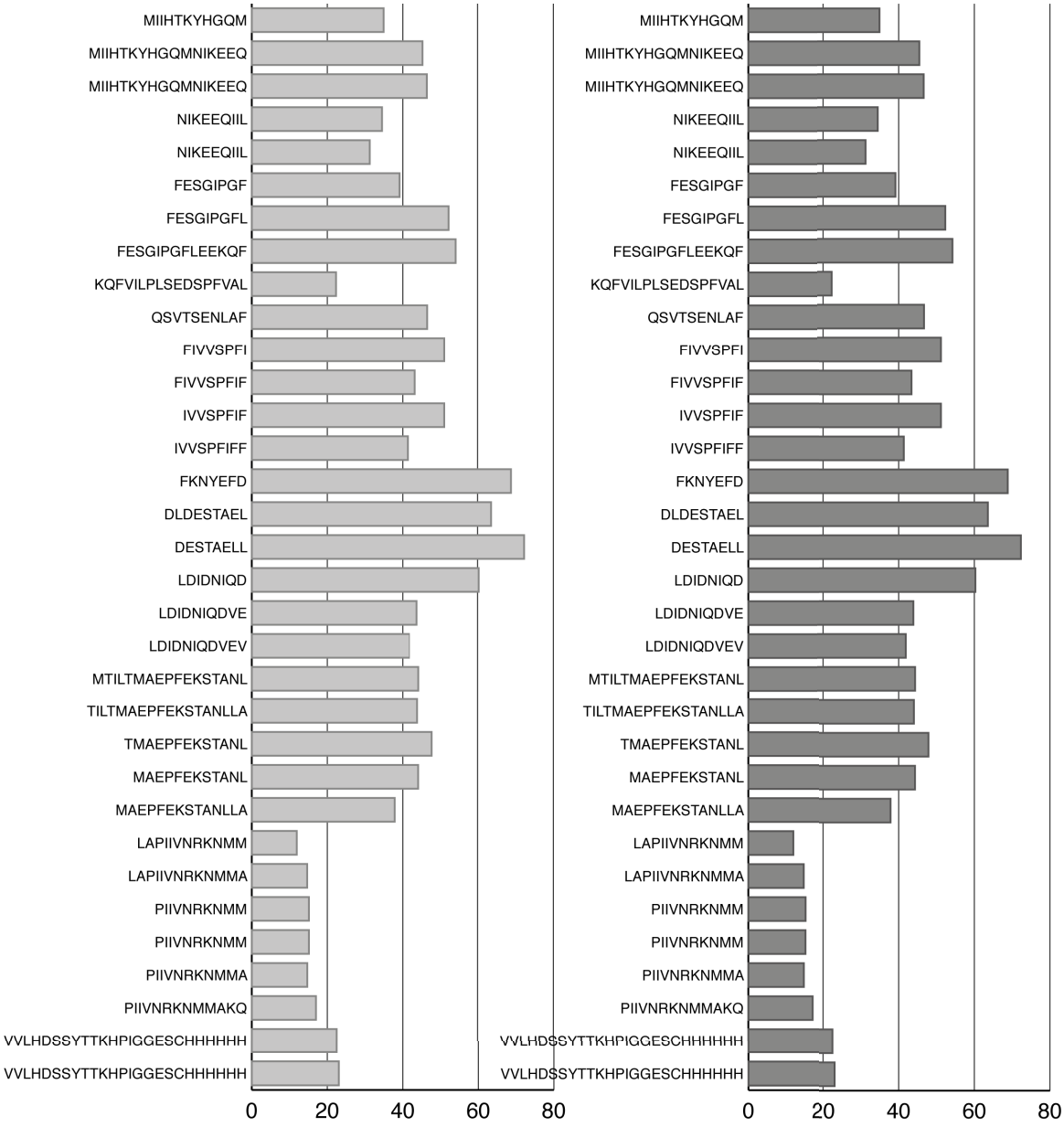

7.2.3 $^{1}H/^{2}H$ exchange data of SAS1

Deuterium uptake of SAS1 apo after 30 s exchange.

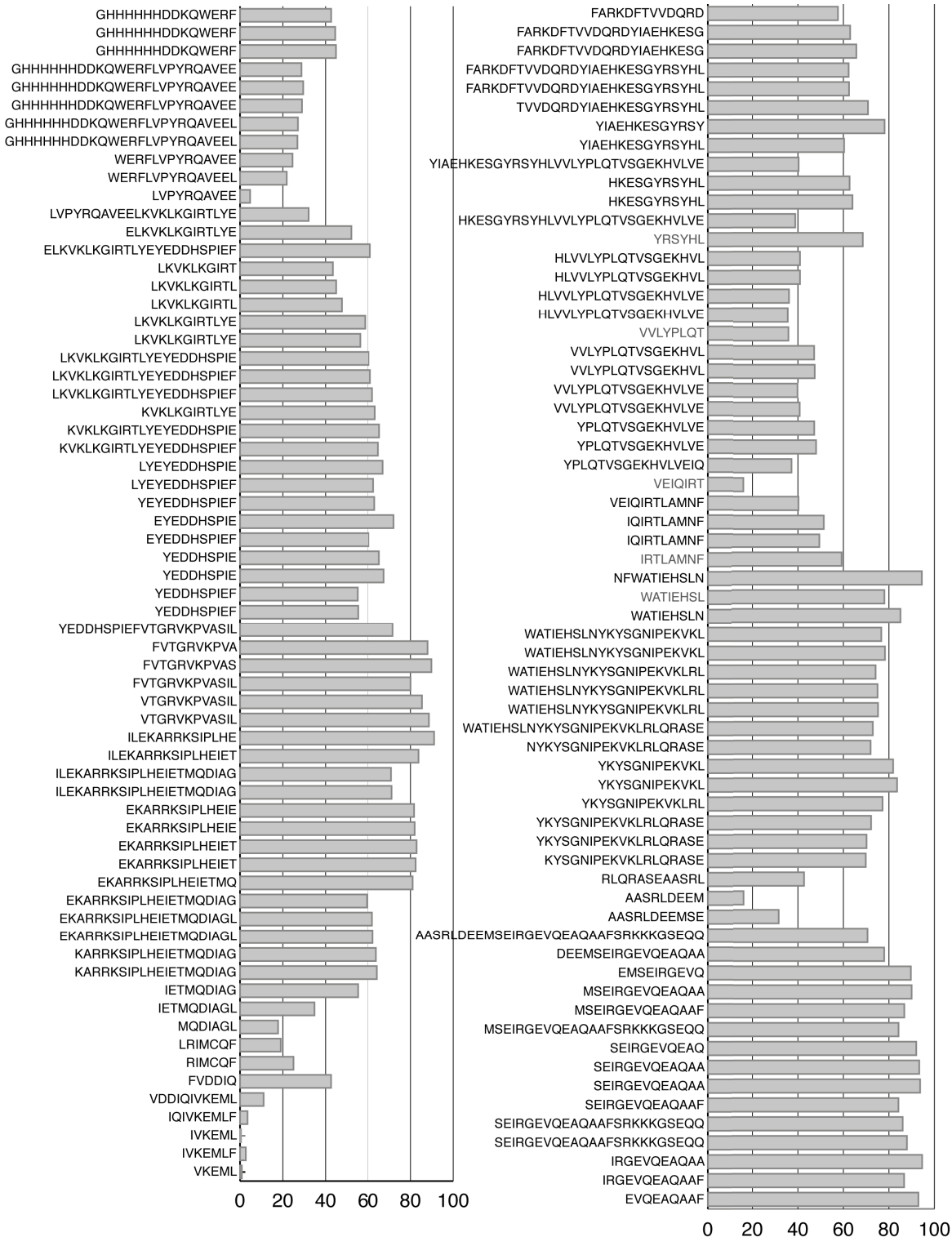

Deuterium uptake of SAS1 in the presence of GDP after 30 s exchange.

Deuterium uptake of SAS1 in the presence of GTP after 30 s exchange.

Deuterium uptake of SAS1 in the presence of AMPCPP after 30 s exchange.

Deuterium uptake of SAS1 in the presence of AMPCPP and GDP after 30 s exchange.

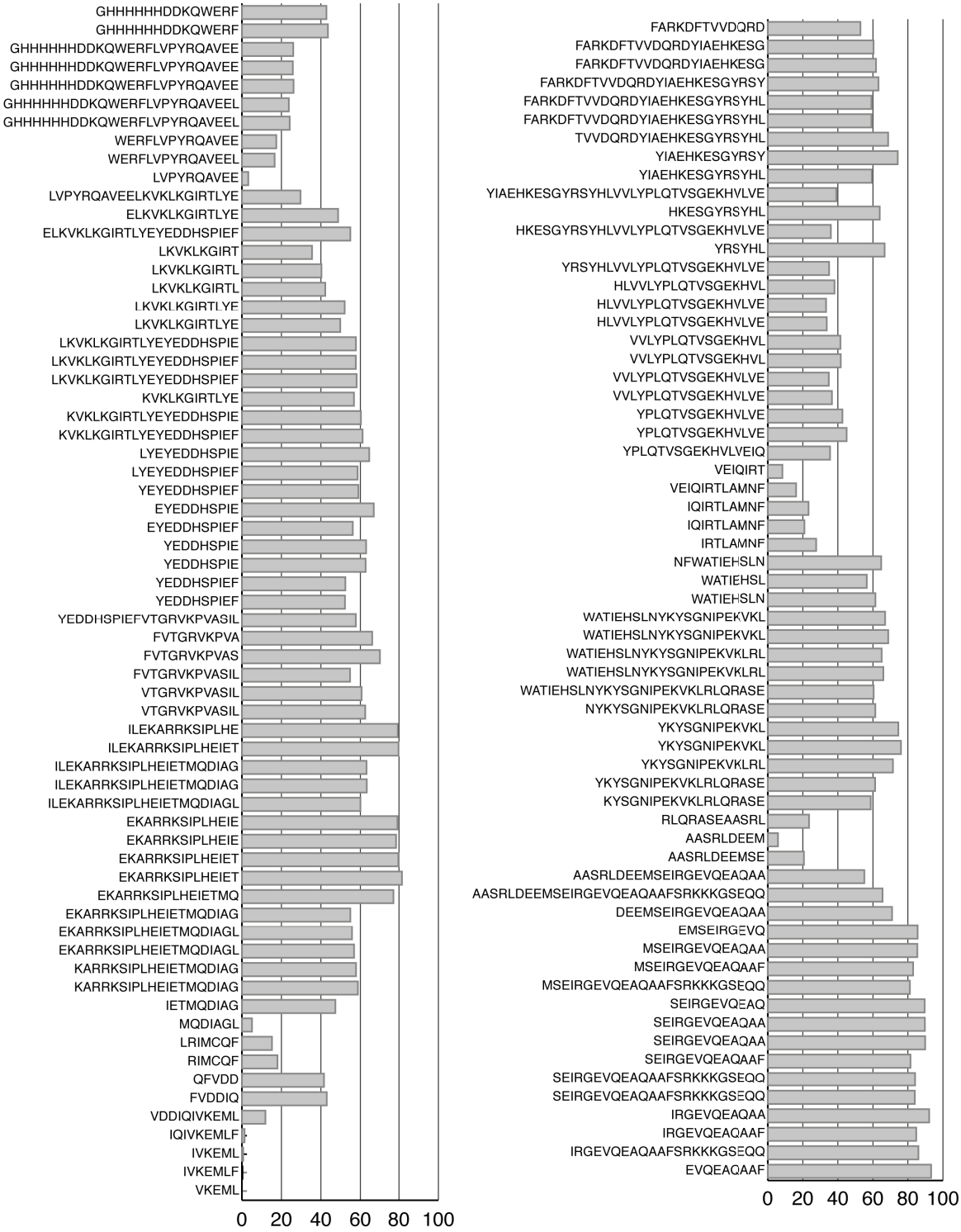

Deuterium uptake of SAS1 in the presence of AMPCPP GTP after 30 s exchange.

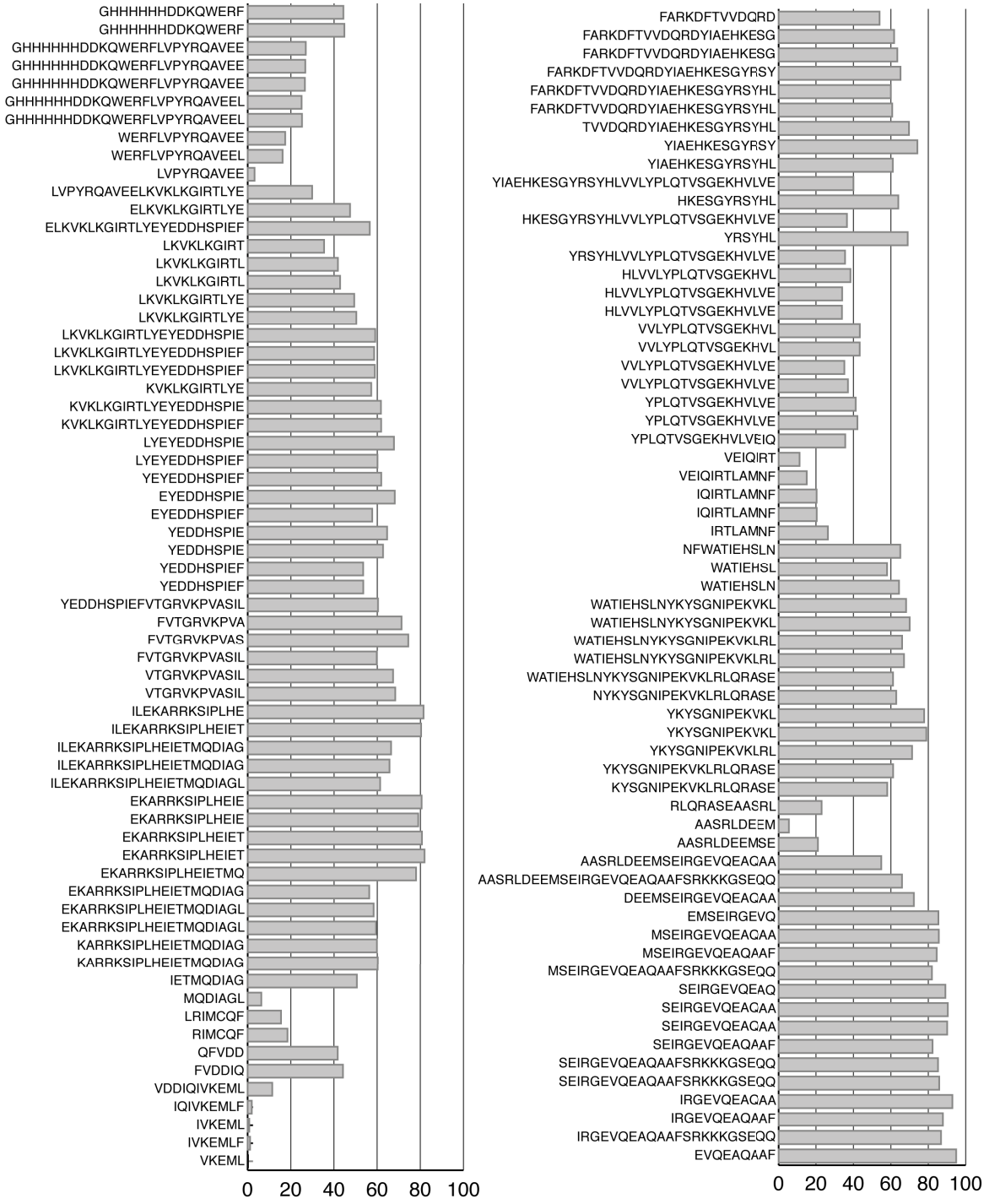

Deuterium uptake of SAS1 in the presence of ATP and GDP after 30 s exchange.

Deuterium uptake of SAS1 in the presence of ATP and GTP after 30 s exchange.